UNIVERSITY OF SOUTHAMPTON

FACULTY OF ENGINEERING AND APPLIED SCIENCE

ENGINEERING SCIENCES

Thesis submitted for the degree of Doctor of Philosophy

FINITE ELEMENT AND ANALYTICAL MODELLING OF ROUGHNESS INDUCED FATIGUE CRACK CLOSURE

by Matthew Roger Parry

February 2001

UNIVERSITY OF SOUTHAMPTON

ABSTRACT

FACULTY OF ENGINEERING AND APPLIED SCIENCE

ENGINEERING SCIENCES

Doctor of Philosophy

FINITE ELEMENT AND ANALYTICAL MODELLING OF ROUGHNESS INDUCED FATIGUE CRACK CLOSURE

by Matthew Roger Parry

The incidence of roughness induced fatigue crack closure has been studied by finite element and analytical modelling. Results of the finite element model under constant amplitude show: (1) an increasing effect of crack deflection angle on crack closure levels, consistent with the simple geometrical model of Suresh & Ritchie, and (2) little dependence of crack closure levels on the value of the ratio of asperity size to the crack tip plastic zone above a certain critical value. From the finite element model results an important new mechanism to explain the origin of roughness induced crack closure has been proposed, arising from the residual shear deformation of the asperities. This new mechanism has been considered in relation to the conventional description of roughness induced crack closure, in which a global shear offset of the fracture surfaces is required. In particular, problems with the conventional roughness induced crack closure mechanism have been discussed.

An analytical model based on the proposed closure mechanism has been constructed using standard fracture mechanics expressions. The results of the analytical model are shown to be consistent with the finite element results. The model is considered particularly valuable in: (1) showing that the novel micromechanistic understanding derived from the finite element modelling is consistent with well established fracture mechanics descriptions of crack behaviour, and (2) providing a simple analytical description of RICC, without introducing any arbitrary crack shear parameters. The model has been shown to be consistent with the experimental crack closure behaviour typically exhibited by damage tolerant aluminium aerospace alloys.

Both the finite element and analytical modelling techniques have been extended to consider the effect of crack deflection on variable amplitude fatigue crack growth. From the results of the finite element models, the ratio of the asperity size to the scale of overload plasticity has been shown to be a critical factor. Mechanistic explanations for this behaviour have been presented, based on the relative effect of a given overload induced global fracture surface offset with varying asperity size. An investigation into the effects of crack closure on the near-tip conditions has confirmed the importance of closure on the fatigue crack driving force, particularly when occurring close to the crack tip.

Contents

Acknowledgements

I would like to express my gratitude to Dr Ian Sinclair for his dedicated and excellent supervision of this work. My thanks go also to Dr Tim Austin for his co-supervision in the initial stage of the work, and to Dr Stavros Syngellakis for taking on the co-supervisory role part way through the project, and for his supervision of the numerical modelling aspects of the work.

I would like to thank Airbus UK for the financial support that this work has received, and in particular Dr Richard Collins for his interest in this work. I am also grateful for the interest shown in the work by Jean-Christophe Ehrstrom and Tim Warner of Pechiney CRV.

To all my colleagues in the Materials Research Group I express my thanks for their friendship and support. In particular, this work has benefited greatly from many useful discussions with Yigeng Xu, Dr Julien Boselli and Mark Joyce, to whom I am grateful.

Lastly, I would like to thank my parents, friends and family for all their support, and of course Janet and Anna, for everything.

Nomenclature

$\%OL$	overload ratio
a	crack length
a^*	distance from previous crack deflection
A'	cyclic strength coefficient
a_0	initial crack length
A_{band}	area of slip band plane
ACR	adjusted compliance ratio
ACR_n	normalised adjusted compliance ratio
A_{truss}	cross sectional area of truss element
B	specimen thickness
b	undeflected length of the crack
C	Paris law scaling constant
CCP	centre cracked panel
C_i	compliance of uncracked body
C_o	compliance above opening load
COD	crack opening displacement
C_{oi}/C_{si}	normalising factor for adjusted compliance ratio
$CRSS$	critical resolved shear stress
C_s	secant compliance
$CTOD$	crack tip opening displacement
$CTOD_{max}$	maximum crack tip opening displacement
$CTOD_{res(BL)}$	residual crack tip opening displacement of the baseline cycle
$CTOD_{res(OL)}$	residual crack tip opening displacement of the overload cycle
$CTSD_{max}$	maximum crack tip sliding displacement
$CTSD_{res}$	residual crack tip sliding displacement
da/dN	crack growth rate
$da/dN_{(BL)}$	crack growth rate under baseline loading
d_n	material constant
E	Young's modulus
E'	$E/(1-\nu^2)$
F	stress intensity factor geometry correction factor
FD	finite difference
FE	finite element

f_{ij}	dimensionless function
G	energy release rate; shear modulus
G_c	critical energy release rate
H	slope of the plastic portion of stress-strain curve
h	effective residual displacement of the asperity
$h_{(analytical)}$	residual deformation of asperity evaluated from analytical model
$h_{(FE)}$	residual deformation of asperity evaluated from FE model
HRR	Hutchinson-Rice-Rosengren (crack tip field)
I_n	integration constant
J	J-integral
K	stress intensity factor
K^*_{max}	threshold condition for crack growth
k_I	local mode I stress intensity factor
$k_{I(deflected)}$	local mode I stress intensity factor at the tip of a deflected crack
k_{2max}	maximum local mode II stress intensity factor
K_c	critical stress intensity factor
K_{cl}	closure stress intensity factor
K_I	mode I stress intensity factor
$K_{I(deflected)}$	mode I stress intensity factor at the tip of an undeflected crack
$K_{I\,max}$	maximum mode I stress intensity factor
K_{II}	mode II stress intensity factor
K_{IImax}	maximum mode II stress intensity factor
K_{max}	maximum stress intensity factor
K_{min}	minimum stress intensity factor
K_{OL}	overload stress intensity factor
K_{op}	opening stress intensity factor
K_M^p	mixed mode plastic stress intensity factor
L	crack deflection length
l	distance behind the crack tip
l_c	characteristic length associated with crack tip plasticity
L_e	element size
LEFM	linear elastic fracture mechanics
m_{open}	gradient of compliance curve for an open crack
M^e	far-field elastic mixity
M^p	near-tip plastic mixity
N	number of cycles

n	strain hardening exponent
N_d	number of delay cycles
n_f	cyclic strain hardening exponent
N_{fi}	number of cycles to failure at $\Delta\sigma_i$
n_i	number of cycles in constant amplitude block i
PICC	plasticity induced crack closure
r	cylindrical polar co-ordinate
R	ratio of minimum to maximum applied stress intensity factor
r_c	cyclic plastic zone size
RICC	roughness induced crack closure
r_p	monotonic plastic zone size
$r_{p(BL)}$	baseline plastic zone size
$r_{p(OL)}$	overload plastic zone size
s	arc length
SENB	single edge notched bend specimen
T	non-singular 'T-stress'; applied tractions
U	ratio of effective to applied stress intensity factor range
U_{BL}	crack tip driving force for a crack under baseline loading
$U_{contact}$	crack tip driving force based on crack face contact
U_{CTOD}	crack tip driving force based on crack tip opening displacements
$u^{LOAD\ POINT}$	displacement at point at which load is applied
U_{OL}	crack tip driving force for a crack which has undergone an overload
u_x	mode II displacement of fracture surfaces
u_y	displacement of crack flank
$\dot{u}$	displacement increments
U_ε	crack tip driving force based on crack tip strain
V	displacement geometry correction factor
w	strain energy density
W	specimen width
Δa	crack growth increment
$\Delta CTOD$	cyclic crack tip opening displacement
$\Delta CTOD_{BL}$	cyclic crack tip opening displacement of the baseline cycle
$\Delta CTOD_{OL}$	cyclic crack tip opening displacement of the overload cycle
$\Delta CTSD$	cyclic crack tip sliding displacement
ΔK	stress intensity factor range
$\Delta K_{(BL)}$	baseline stress intensity factor range

ΔK^*_{th}	threshold condition for crack growth
ΔK_{app}	applied stress intensity factor range
ΔK_{eff}	effective stress intensity factor range
$\Delta K_{eff(BL)}$	effective stress intensity factor range for a crack under baseline loading
$\Delta K_{eff(OL)}$	effective stress intensity factor range for a crack which has undergone an overload
$\Delta\delta_0$	cyclic crack tip opening displacement
$\Delta\varepsilon$	uniaxial strain amplitude
$\Delta\varepsilon_{22}$	tensile crack tip strain range
ε_{ii}^{pl}	tensile plastic strain component
$\dot{\varepsilon}_{ii}$	strain increments
$\Delta\sigma$	uniaxial stress range
$\Delta\sigma_i$	constant stress amplitude
Γ	curve enclosing a crack tip
α	proportionality constant; constraint factor
β	constant of proportionality; biaxiality ratio; scaling factor (residual asperity offset); plane strain crack opening constraint factor
χ	ratio of mode II to mode I displacement which occurs during unloading
δ	crack opening displacement
δ^*	reduced crack opening displacement due to mode II displacement of fracture surfaces
δ_0	crack tip opening displacement at maximum load
δ_{cl}	reduced crack opening due to crack flank shear
δ_{offset}	offset displacement
δ_R	crack tip plastic stretch
ε_0	strain at σ_0
ε_{ij}	strain tensor/component
$\tilde{\varepsilon}_{ij}$	dimensionless function
κ	elastic constant
λ	constant representing relative strength of slip band; fraction of the plastic zone
ν	Poisson's ratio
θ	cylindrical polar co-ordinate; crack deflection angle
σ	remote uniaxial stress

σ_0	yield stress
σ_{ij}	stress tensor/component
σ_{max}	maximum stress in load cycle
$\tilde{\sigma}_{ij}$	dimensionless function
τ_0	critical shear stress
ξ	$K_{max(OL)}/K_{max(BL)}$

1 Introduction

The damage tolerant design philosophy was introduced into the aerospace industry in 1978 as a response to the perceived limitations of the fail-safe and safe-life design approaches [Swift, 1996], and remains the design philosophy in use today for many aspects of airframe engineering. Under this philosophy an understanding of the fatigue crack growth rate in a material is used to predict the growth of a fatigue crack from an initial flaw size to a critical length, with an inspection program then being designed such that fatigue cracks are detected before the critical length is attained. As such, alloys exhibiting low fatigue crack growth rates are clearly desirable if inspection intervals are to be maximised [Lawson *et al*, 1999]. An understanding of the factors which affect the fatigue crack growth rates of aerospace alloys is therefore valuable in the design of lifing algorithms, and in the selection and optimisation of the alloys themselves.

Factors which affect the fatigue crack growth rates in aerospace aluminium alloys are complex, but are commonly categorised into; (a) intrinsic factors, in which aspects of the alloy composition and microstructure have a direct influence on the cyclic strain behaviour actually occurring at the crack tip and subsequent fatigue damage, and; (b) extrinsic factors, whereby crack growth resistance is developed due to 'shielding' of the crack tip from the full range of remotely applied cyclic loading due to processes occurring either in the crack wake, or ahead of the crack tip. The relative importance of intrinsic and extrinsic fatigue crack growth resistance is highly dependent upon the active growth mode and loading conditions.

Stage I type crack growth, which commonly occurs in the early stages of fatigue crack propagation, is generally considered to involve the formation of new crack surface by the shear decohesion along a slip band [e.g. Slavik & Gangloff, 1996]. Such slip band cracking generally occurs under conditions where deformation is localised to a small number of active slip systems. In terms of alloying influence on such behaviour, the principal hardening mechanism in underaged commercial aluminium alloys is the formation of shearable precipitates through ageing [e.g. Vasudevan & Suresh, 1985]. When deformation of these alloys occurs such precipitates lead to marked concentration of strain on individual slip systems [Brechet *et al*, 1987]. This propensity for strain localisation may promote stage I cracking at loading levels well above the crack growth threshold [Sinclair & Gregson, 1994, Liu *et al*, 1999]. Given that the active slip plane will of necessity be deflected from the nominal mode I crack growth plane, and that crystallographic textures may permit slip band

growth across several grains at a time, large, regular deflection patterns of crack growth may occur. As such, extrinsic contributions to fatigue crack growth resistance may be important, with the crack tip shielding mechanisms of crack deflection and roughness induced crack closure (RICC) then being active [Venkateswara Rao & Ritchie, 1992].

When the region at a crack tip undergoing plastic strains extends to encompass many grains, many slip planes may become active, and the crack growth mode may then change toward stage II, which can be visualised as a process of simultaneous or alternating shear on two or more slip planes, producing crack growth in the nominal mode I growth plane [Laird, 1979]. The resulting fatigue crack paths are generally more planar and RICC is not widely considered to have a strong effect. However, extrinsic contributions to fatigue crack growth resistance may still occur through the process of plasticity induced crack closure (PICC).

Given the incidence of different crack shielding mechanisms and their complex dependence on materials and loading parameters, it can be seen that an increased quantitative understanding of the origins and effects of both RICC and PICC, and their potential interactions, may be beneficial to the implementation of alloy design for optimum fatigue performance, as well as the design of accurate damage tolerant life prediction methodologies. However, despite the numerous experimental and modelling studies of crack closure which have been reported over the last 30 years, significant controversy and uncertainty of the importance of the crack closure mechanisms remains. For example, Vasudevan and co-workers [Vasudevan *et al*, 1992, Louat *et al*, 1993] have suggested that the actual influences of closure on crack growth are dramatically lower than many works in the literature suggest, and propose alternative explanations to observed crack growth phenomena. An extensive body of experimental evidence and theoretical analysis does however exist to support the dependence of fatigue crack growth on closure phenomena [Newman & Elber, 1988, McClung & Newman, 1999].

Several quantitative and semi-quantitative models of RICC exist within the literature, although they are generally rather simplified. Furthermore, interactions between different closure mechanisms are largely ignored. As such, the present work seeks to extend the current understanding of RICC, focusing on geometrical and micromechanical closure effects, through the implementation of finite element (FE) and analytical modelling techniques. The use of FE techniques in the investigation of fracture mechanics is well developed [Liebowitz & Moyer, 1989, Rice & Tracey, 1973]. In particular, the details of many FE studies of crack closure occurring as a result of fatigue crack propagation are available in the literature. In the present work, the existing FE techniques have been

extended to consider deflected crack propagation in an elastic-plastic material, under constant and variable loading histories. Whilst employing numerical modelling methods, the results are interpreted micromechanistically, with a number of analytical fracture mechanics models being developed to validate and extend the understanding derived from the finite element work.

2 Literature review

Fatigue in metals has been studied extensively in the past 100 years, and various excellent reviews on the subject are available. The review of the literature presented here is focussed for the purposes of the work. As such for a review of the various basic aspects of fatigue research the reader is directed elsewhere. Specifically, for an overview of the historical development of the study of fatigue, the reader is directed to the work of Schutz [1996], Paris, [1998] and Miller [1991]. For details regarding the mechanics and metallurgy concerning fatigue crack initiation and growth, the reader is directed to the texts of Laird [1979], Rice [1967], Miller [1993], Lawson *et al* [1999] and Suresh [1991]. Lastly, for an overview of the implementation of fatigue based research in the design of aluminium aerospace structures the reader is referred to the work of Gangloff *et al* [1994], and Swift [1996].

2.1 Basic concepts of fracture mechanics

An understanding of fracture mechanics concepts is essential in the study of fatigue. In this section a basic review of some of the concepts is presented. In particular, various terms are introduced which are useful in describing the behaviour of cracks under small scale yielding conditions.

2.1.1 Energy balance approach

The first quantitative analysis of the effect of cracks or flaws on the fracture stress of a material was presented by Griffith [1921], for brittle materials. It was proposed that in a cracked body under stress, fracture would occur if the rate of release of elastic strain energy due to crack propagation was equal to the rate of increase in elastic surface energy caused by the formation of the new crack surface. This approach was extended to the fracture of ductile materials by Irwin [1948], by the inclusion of a term to account for the work done in plastic deformation accompanying crack growth. From this approach, the energy release rate G, which represents the elastic energy per unit crack area that is available for crack extension can be defined, which can be considered as a driving force for crack growth. As such, the resistance of a material to fracture can be characterised through a critical value of energy release rate, G_c, a measure of fracture toughness.

2.1.2 The stress intensity approach

The use of the energy balance approach was found to be limited due to difficulties in measuring the work done in plastic deformation of the material during crack growth. A significant advance in the theory of fracture came with the advent of the stress intensity approach. From the Westergaard [1939] solution for the stresses ahead of a crack tip, Irwin [1957] showed that the elastic stresses σ_{ij}, ahead of a crack under a remote uniaxial stress σ, could be written as an infinite power series, as,

$$\sigma_{ij} = \frac{K}{\sqrt{2\pi r}} f_{ij}(\theta) + higher\ order\ terms \qquad (2.1)$$

where r, θ, are the cylindrical polar co-ordinates of a point with respect to the crack tip, $f_{ij}(\theta)$ is a dimensionless function of θ, and K, is the stress intensity factor which gives the magnitude of the elastic stress field, and is a function of crack length, the applied stress, and the specimen geometry. The higher order terms of the power series are commonly ignored. From the principle of virtual work it was demonstrated that the stress intensity factor was related to the energy release rate as,

$$G = \frac{K^2}{E'} \qquad (2.2)$$

where $E' = E$ for plane stress, $= E/(1-\nu^2)$ for plane strain, and ν is Poisson's ratio. Hence, a critical stress intensity factor K_c can be defined which is equivalent to G_c, and which is a measure of the fracture toughness. The stress intensity approach has the advantage that K is a function of the applied stress, the crack length and component geometry only, all of which can be directly quantified.

Three modes of loading can be applied to a crack and are defined as mode I (opening), mode II (in-plane shear) and mode III (out-of-plane shear), as illustrated in Figure 2.1. A crack loaded in tension normal to the crack plane can be described by the mode I stress intensity factor,

$$K_I = \sigma\sqrt{\pi a}\, F, \qquad (2.3)$$

where F is a function of the crack and component geometry, and a is the crack length. Solutions for F in many different geometries have been produced either analytically or through finite element methods.

Equation 2.1 is only valid for a perfectly sharp crack within an elastic body. In a ductile material there will be some degree of crack blunting, and inelastic deformation at the tip. However if the zone within which the inelastic deformation exists is small compared to the

area over which the singularity term in Equation 2.1 holds (called the region of K-dominance) then this is considered a meaningful description of the crack tip conditions. This is known as the small scale yielding condition, forming the basis for "linear elastic fracture mechanics" (LEFM) as applied to metals. An assumption of similitude is then made, such that the behaviour of a crack for any size, shape, or loading condition can be described fully in terms of K values alone.

In the power series which describes the crack tip stress field (Equation 2.1) the first term exhibits a $1/\sqrt{r}$ singularity, the second term is independent of r, the third term is proportional to $\sqrt{r}$, and so on. Classical fracture mechanics theory commonly ignores all but the first term, resulting in a single parameter description of the crack tip fields. However, at the crack tip the second term in the expansion remains finite and may have a significant influence. When written to include this second term in the series expansion, the elastic stresses at the tip of a crack are given by [e.g. Larsson & Carlsson, 1973]

$$\sigma_{ij} = \frac{K}{\sqrt{2\pi r}} f_{ij}(\theta) + \begin{bmatrix} T & 0 & 0 \\ 0 & 0 & 0 \\ 0 & 0 & vT \end{bmatrix}, \tag{2.4}$$

where T is a non-singular, constant stress term acting in the x-direction (which induces a stress vT in the z-direction in plane strain, where v is the Poisson ratio). This so-called T-stress can have a significant effect on the plastic zone shape and the stresses within the plastic zone [Bilby *et al*, 1986, Betegon & Hancock, 1991]. However, for closure free, long fatigue crack growth under small scale yielding conditions the T-stress is generally not critical.

2.1.3 Characterising cyclic loading and fatigue crack growth

The use of the stress intensity factor to correlate fatigue crack growth was introduced by Paris *et al* [1961], based on empirical observations. This concept was met with initial resistance, given that fatigue (which was known to be controlled by local plastic strains) was not considered to be able to be related to a purely elastic parameter [see Paris, 1998]. However, as the understanding of ability of the stress intensity factor to characterise crack tip plasticity under small scale yielding grew, the concept became widely accepted, with fatigue crack growth rates commonly being expressed through the so-called 'Paris law',

$$\frac{da}{dN} = C(\Delta K)^m, \tag{2.5}$$

where $\Delta K = K_{max} - K_{min}$ is the stress intensity factor range, K_{max} and K_{min} are the minimum and maximum stress intensity factors which arise due to the cyclic loading, a is the crack

length, N is the number of load cycles, and C and m are scaling constants dependent on the material, the microstructure, the load frequency, the test environment and $R = K_{min}/K_{max}$, the loading ratio. It is important to note that Equation 2.5 is not valid for all values of ΔK, with the relationship between $log\, da/dN$ and $log\, \Delta K$ generally exhibiting a sigmoidal shape. The central range of the crack growth curve for which this relationship approximately holds is termed the Paris regime.

2.1.4 Crack tip plasticity

As noted above, in a ductile material a zone of plastically deformed material will form under the action of an applied far-field tensile load at the tip of a crack. Irwin [1960] derived a first order estimate of the scale of deformation under plane stress conditions by using the elastic analysis to estimate the elastic plastic boundary, to give an approximate plastic zone size,

$$r_p = \frac{1}{\pi}\left(\frac{K_I}{\sigma_0}\right)^2, \tag{2.6}$$

where r_p is the diameter of the (assumed circular) plastic zone directly ahead of the crack tip, and σ_0 is the yield stress. Dugdale's strip yield model [1960] of a crack in an elastic perfectly plastic thin plate, (i.e. plane stress conditions), assumes that the plastic zone forms as slender region ahead of the crack tip. Based on the balance of stresses about the crack tip this analysis estimates the extent of the plastic zone to be,

$$r_p = \frac{\pi}{8}\left(\frac{K_I}{\sigma_0}\right)^2 \tag{2.7}$$

which makes the Dugdale approximation about 20% greater than the Irwin approximation.

In thick sections, the highly stressed material near the crack tip tries to contract in the through thickness direction, but is constrained by the surrounding material. This constraint promotes a triaxial stress state, with plane strain conditions existing in the mid-thickness. From the Tresca criterion, yielding can be expected to occur when the maximum shear stress is equal to a critical value, τ_0. Under plane stress conditions this gives,

$$\begin{aligned} &\sigma_{22} - \sigma_{33} = 2\tau_0 = \sigma_0 \\ &\Rightarrow \quad \sigma_{22} = \sigma_0 \end{aligned} \tag{2.8}$$

where the σ_{22} is the stress normal to the crack plane, and σ_{33} is the stress in the through thickness direction (=0). Under plane strain conditions, the Tresca criterion gives,

$$\begin{aligned} &\sigma_{22} - \sigma_{11} = 2\tau_0 = \sigma_0 \\ &\Rightarrow \quad \sigma_{22} = \sigma_0 + \sigma_{11} \end{aligned} \tag{2.9}$$

where σ_{11} is the stress in the crack growth direction ($\neq 0$). That is for yielding to occur under plane strain conditions the tensile stress must be raised to a higher level than under plane stress conditions. To account for this effect, a plane strain constraint factor is commonly included, such that the plane strain plastic zone sizes are commonly given as,

$$r_p = \frac{1}{3\pi}\left(\frac{K_I}{\sigma_0}\right)^2, \text{ based on the Irwin analysis,} \tag{2.10}$$

and

$$r_p = \frac{\pi}{24}\left(\frac{K_I}{\sigma_0}\right)^2, \text{ based on the Dugdale analysis.} \tag{2.11}$$

Approximations to the shape of the plastic zone can be arrived at by considering a specific yield criteria from plasticity theory, and determining the contour around the crack tip along which the stress is equal to the yield stress. No account of the redistribution of stresses above the yield stress is made in this procedure, and as such this method is approximate. From the von Mises criterion the plastic zone shape can be shown to be given by

$$\begin{aligned} \frac{r(\theta)}{r_p} &= \frac{3}{4}\sin^2\theta + \frac{1}{2}(1-2\nu)^2(1+\cos\theta), && \textit{under plane strain,} \\ \frac{r(\theta)}{r_p} &= \frac{1}{2} + \frac{3}{4}\sin^2\theta + \frac{1}{2}\cos\theta, && \textit{under plane stress.} \end{aligned} \tag{2.12}$$

These plastic zone shapes are shown in Figure 2.2.

Under cyclic loading conditions reverse plastic flow at the crack tip will occur during unloading. The extent of this cyclic plastic zone was estimated by Rice [1967], using a simple superposition argument. By considering a crack loaded to K_{max}, it can be seen that if the stress intensity is reduced by ΔK, the effective yield stress of material undergoing compressive yielding may be considered to be $2\sigma_0$ since the stress in the material in the cyclic plastic zone must go from $+\sigma_0$ to $-\sigma_0$ as unloading occurs. Hence the diameter of the cyclic plastic zone is given by,

$$\begin{aligned} r_c &= \frac{1}{3\pi}\left(\frac{\Delta K}{2\sigma_0}\right)^2, && \textit{for plane strain,} \\ r_c &= \frac{1}{\pi}\left(\frac{\Delta K}{2\sigma_0}\right)^2, && \textit{for plane stress.} \end{aligned} \tag{2.13}$$

i.e. equivalent to Equations 2.6 & 2.10, but with the yield stress doubled. As such the cyclic plastic zone is approximately one quarter of the monotonic plastic zone for $R = 0$.

2.1.5 Crack tip opening displacement

The crack tip opening displacement (*CTOD*) provides a measure of the blunting at an initially sharp crack due to plastic deformation. As the degree of blunting gives a fairly direct indication of the maximum deformation conditions at the crack tip the *CTOD* can be used to characterise the behaviour of cracks in ductile materials. From the analysis of Irwin it is possible to produce an expression for the *CTOD* under plane stress as,

$$CTOD = \frac{4}{\pi}\frac{K_I^{\,2}}{\sigma_0 E}, \tag{2.14}$$

where E is Young's modulus and ν is Poisson's ratio. A similar expression for the *CTOD* under plane stress can be found from the Dugdale model,

$$CTOD = \frac{K_I^{\,2}}{\sigma_0 E}, \tag{2.15}$$

which is approximately 20% smaller than the Irwin approximation. Under plane strain, a wide variety of expressions have been reported for *CTOD* based on experimental, analytical and numerical investigations (e.g. see McMeeking, [1977]), such as that of Rice [1973], which gives,

$$CTOD = 0.5\frac{K_I^{\,2}}{\sigma_0 E}. \tag{2.16}$$

Under cyclic loading, Rice's model of reversed plastic flow can be used to show that the change in *CTOD* on going from K_{max} to K_{min} under plane stress conditions may be given as,

$$\Delta CTOD \approx \frac{\Delta K^2}{2\sigma_0 E} \tag{2.17}$$

and similarly under plane strain conditions,

$$\Delta CTOD \approx 0.5\frac{\Delta K^2}{2\sigma_0 E}. \tag{2.18}$$

2.1.6 The *J*-integral

If the extent of plastic deformation at the crack tip becomes large enough, the use of LEFM becomes invalid, and another way of characterising the behaviour of the crack must be found. The Griffith/Irwin energy balance approach was extended by Rice [1968] for the case of a non-linear elastic material. Consider a crack of length a, in a body bounded by a curve Γ, subject to applied tractions T, as shown in Figure 2.3. The energy release rate J due to crack advance was shown by Rice [1968] to be given by a path independent line integral which encircles the crack tip,

$$J = \int_{\Gamma}\left(wdy - T \cdot \frac{\partial u}{\partial x} ds \right) \tag{2.19}$$

where w is the strain energy density given by $w = \int_0^{\varepsilon_{ij}} \sigma_{ij}\varepsilon_{ij}$, which is valid for any (linear or non-linear) unique relationship between the stresses (σ_{ij}) and the strains (ε_{ij}), x and y are distances as shown in Figure 2.3, and s is the arc length along the contour. Hence, J can be used to give the energy release rate due to crack advance for a monotonically loaded material undergoing plastic deformation at the crack tip, by equating the elastic-plastic stress-strain behaviour to that of a non-linear elastic material. As such, J can be considered to be a parameter of crack driving force. However, a clear restriction on the use of J to describe elastic-plastic behaviour exists in that no unloading can occur, since the stress-strain behaviour of the non-linear elastic and elastic-plastic materials would no longer be equivalent.

The J-integral was shown to characterise the crack tip conditions in a non-linear material under proportional loading by Hutchinson [1968] and Rice & Rosengren [1968]. At the crack tip, plastic strains dominate and can be approximated through a power-law relationship as,

$$\frac{\varepsilon}{\varepsilon_0} = \alpha\left(\frac{\sigma}{\sigma_0}\right)^n \tag{2.20}$$

where $\varepsilon_0 = \sigma_0/E$, α is a dimensionless constant and n is the strain hardening exponent. It was shown that path independence of J required the stress and strain fields to be given by,

$$\begin{aligned} \sigma_{ij} &= \sigma_0\left(\frac{J}{\alpha\sigma_0\varepsilon_0 I_n r}\right)^{1/(n+1)} \tilde{\sigma}_{ij}(\theta, n) \\ \varepsilon_{ij} &= \alpha\varepsilon_0\left(\frac{J}{\alpha\sigma_0\varepsilon_0 I_n r}\right)^{n/(n+1)} \tilde{\varepsilon}_{ij}(\theta, n) \end{aligned} \tag{2.21}$$

where I_n is an integration constant that depends on n, r and θ are polar co-ordinates with respect to the crack tip, and $\tilde{\sigma}_{ij}$ and $\tilde{\varepsilon}_{ij}$ are dimensionless functions of θ and n. The stress and strain fields given by Equation 2.21 are known as the HRR fields (after Hutchinson, Rice and Rosengren). It can be seen that J defines the amplitude of the stress and strain singularity in the region of non-linear deformation at the crack tip analogous to the stress intensity factor characterisation of the elastic singularity.

2.1.7 Crack tip conditions under small scale yielding

The stress fields at the tip of a crack under small scale yielding conditions are illustrated schematically in Figure 2.4. In the outer region the stresses are dominated by the elastic singularity and are proportional to $r^{-1/2}$. The region is called the zone of *K*-dominance. Well inside the plastic zone (typically 20-25% of r_p, see the FE analyses of McMeeking, [1977] and McMeeking & Parks, [1979]) the stresses are dominated by the plastic singularity and the HRR solution is approximately valid. As such the stresses are proportional to $r^{(-1/(n+1))}$, with the region being called the zone of *J*-dominance. Closer to the tip (approximately 2-3 *CTOD*) large deformations occur and the HRR solution loses validity. This is known as the large strain zone. The diameter of this inner region may also be affected by microstructural considerations e.g. grain size or particle spacing which may influence near-tip plastic deformation.

Under small scale yielding conditions, the crack tip conditions are uniquely characterised by both *K* and *J*, despite the fact that neither the *K*-field or the *J*-field exist all the way to the crack tip. For a linear elastic material *J* reduces to the strain energy release rate *G*, hence the two parameters can be related as,

$$J = \frac{K^2}{E'}. \tag{2.22}$$

2.1.8 Mixed-mode crack tip fields

The near tip stress and strain fields for a crack undergoing mixed-mode I and II loading in a non-linear elastic material were shown by Shih [1974] to be analogous to the HRR fields for a mode I crack. i.e.

$$\begin{aligned} \sigma_{ij} &= \sigma_0 \, K_M^p \, r^{-1/(n+1)} \, \tilde{\sigma}_{ij}\left(\theta, n, M^p\right) \\ \varepsilon_{ij} &= \alpha\varepsilon_0 \left(K_M^p\right)^n r^{-n/(n+1)} \, \tilde{\varepsilon}_{ij}\left(\theta, n, M^p\right) \end{aligned} \tag{2.23}$$

where K_M^p is a mixed-mode plastic stress intensity factor, and M^p is the near-tip plastic mode-mixity parameter. These parameters can be related to the *J*-integral and K_I and K_{II} under small scale yielding conditions as,

$$J = \frac{1}{E'}\left(K_I^{\,2} + K_{II}^{\,2}\right) = \frac{\alpha\sigma_0^{\,2}}{E} I_n\left(M^p\right)\left(K_M^p\right)^{n+1} \tag{2.24}$$

For the case where K_I and K_{II} are known, in order to be able to fully describe the near-tip fields, the relationship between the elastic far-field mode-mixity $M^e = \frac{2}{\pi} tan^{-1}\left|\frac{K_I}{K_{II}}\right|$ and M^p must be found. This relationship was determined by Shih [1974] by a finite element analysis. This then allowed the elastic-plastic boundaries to be plotted for varying M^e and n, as shown in Figure 2.5.

2.2 Fatigue crack closure

2.2.1 Overview

In Section 2.1.3 it was indicated that the stress intensity factor range, ΔK, may be used to characterise fatigue crack growth. It is however valuable to consider a fatigue crack in a specimen undergoing fully reversed tension-compression cyclic loading (i.e. $R = -1$). During the tensile portion of the load cycle ($\sigma > 0$), it can be assumed that the crack will open and be subjected to damaging plastic strains at the crack tip, leading in some way to growth of the fatigue crack. During the compressive portion of the load cycle ($\sigma < 0$), it is reasonable to assume that the crack flanks will come into contact and transmit the compressive stress across their faces. As such, it would appear that the tensile portion of the loading cycle is the only effective portion, in terms of leading to fatigue crack propagation. This line of reasoning is of course a simplification, given that the compressive part of the load cycle has been clearly seen to have an influence on fatigue crack propagation, in terms of cyclic plastic deformation, and re-sharpening of the crack tip [e.g. see Suresh, 1991]. Indeed, fatigue cracks can initiate and grow under purely compressive cyclic loading [Suresh, 1985*a*]. However under tension-tension or tension-compression cyclic loading, the tension portion of the loading cycle can be expected to be the dominant factor in subsequent fatigue damage.

It has also been found that crack faces can be in contact at tensile applied loads, and the term crack closure has been coined to describe any of the physical processes which lead to such premature crack face contact. The discovery of crack closure is usually attributed to Elber [1970], who indicated that premature crack face contact can occur during unloading due to the presence of previously plastically deformed material in the crack wake. Elber suggested that the resultant driving force for crack growth was reduced, and that an effective stress intensity factor range,

$$\Delta K_{eff} = K_{max} - K_{cl}, \tag{2.25}$$

could be defined, where K_{max} is the maximum applied stress intensity factor, and K_{cl} is the stress intensity factor at which crack face contact occurs. The crack growth rate (da/dN) can then be expressed through a modified Paris law (see Equation 2.5) as,

$$\frac{da}{dN} = C(\Delta K_{eff})^m \tag{2.26}$$

where C and m are scaling constants, dependent on the material, the environment and the load conditions. Hence the assumption that the stress intensity factor range at the crack tip

uniquely determines the behaviour of a fatigue crack under small scale yielding conditions was shown not to hold in all cases, i.e. loading and deformation history may influence current crack tip conditions. This approach implies that the crack tip is entirely isolated from the applied stresses on the point of first contact of the crack faces during unloading. However it has been suggested that the contribution to crack tip fatigue damage on going from K_{cl} to K_{min} is not insignificant [Donald, 1997]. As such Equations 2.25 and 2.26 may overestimate the effects of crack closure. A significant body of experimental and modelling evidence does however exist to illustrate the merit of the crack closure concept (e.g. see Newman & Elber, 1988, McClung & Newman, [1999]).

The closure mechanism identified by Elber has subsequently become known as plasticity induced crack closure (PICC). Other mechanisms by which crack shielding (i.e. any process that tends to reduce crack tip driving force) can occur have been identified and are summarised by Ritchie [1988]. Briefly, they include

- crack deflection, whereby the stress intensity factor at a crack tip is reduced by deviation away from the plane of maximum opening stress,
- zone shielding mechanisms, such as transformation toughening effects seen in steels undergoing a strain induced martensitic transformation, and
- contact shielding mechanisms, whereby premature crack face contact can arise from a range of processes, including the presence of corrosion products on the crack surface (oxide induced crack closure) or interference between crack surface asperities arising from deflected crack growth, (RICC), or indeed plasticity induced closure as noted above.

In terms of aerospace aluminium alloys, PICC and RICC are generally recognised to be the most consistently significant closure processes (depending on the alloy and load conditions). The following sections will consider the mechanisms by which PICC and RICC occur, the effect which they have on fatigue crack growth, and various models which have been constructed to quantify these effects.

2.2.2 Closure Mechanisms

2.2.2.1 PICC

Consider a crack in a ductile material under a far-field tensile cyclic load. At the crack tip the material will undergo a tensile plastic deformation on application of the load. During

unloading, a degree of reverse plastic deformation will occur, however a residual tensile plastic deformation of the crack tip material will exist, i.e. the crack has become blunted. When the crack propagates this residually strained material will be transferred into the crack wake, thereby reducing the crack opening displacement and leading to the possibility of premature crack closure, termed PICC. This mechanism is illustrated schematically in Figure 2.6(a).

Plastic deformation of metallic materials occurs with no change in volume, hence under plane stress a residual tensile deformation of the material must be associated with a contraction in the through thickness direction. Under plane strain there can by definition be no strain in the through thickness direction, hence the origin of the plane strain PICC is not as clear. From the literature at various mechanisms by which plane strain PICC could occur can be found:

- Residual plastic strain in the through thickness direction, equal and opposite to the elastic strain in this direction, giving a total through thickness strain of zero, whereby tensile strain in the loading direction comes about through the discrepancy in the Poisson contraction due to elastic and plastic deformation. See Fleck & Newman, [1988] for details).
- A residual shear or rotation of material in the wake towards the crack tip, leading to contact of the crack faces immediately behind the crack tip, as described by Sehitoglu & Sun, [1991] and Riemelmoser & Pippan, [1998], and illustrated schematically in Figure 2.7.
- Changes in the shape of asperities in the crack wake due to previous plastic deformation, leading to non-matching fracture surfaces and premature closure, proposed by Pippan *et al* [1994] and illustrated schematically in Figure 2.8.
- Incomplete relief of residual compressive stresses ahead of the crack tip, as put forward by Ritchie *et al* [1989].

It should be noted that the origin of the residual compressive stresses is the elastic constraint of material near the crack tip in which a residual tensile strain exists, hence this suggestion by Ritchie *et al* [1989] does not in any way explain the origin of the residual strain under plane strain conditions.

There is no conclusive evidence as to what the relative importance of the various mechanisms are in leading to PICC. FE simulation [Sehitoglu & Sun, 1991] has shown the first two mechanisms to operate, with the residual rotation of material towards the crack tip apparently

more significant. This mechanism has also been described through dislocation based [Pippan & Riemelmoser, 1998] and mechanics based [Riemelmoser & Pippan, 1998] approaches, however it has been criticised by other researchers [Vasudevan *et al*, 1994] as leading to only a very small closure effect.

2.2.2.2 RICC

Consider a crack growing along a deflected crack path. If a permanent shear deformation of the crack faces occurs the crack faces will no longer match upon unloading, leading to premature crack closure, termed RICC. This mechanism is illustrated schematically in Figure 2.6(b). The possibility that crack roughness could lead to premature crack closure was first identified by Walker & Beevers [1979], who studied fatigue crack growth in titanium samples. Whilst PICC effects were apparently absent, contact was seen to occur at discrete points behind the crack tip as a result of deflected crack growth and residual shear of the crack flanks. Corroboration of these findings were made by Minakawa & McEvily [1981], Blom *et al* [1983] and Ritchie & Suresh [1982] who introduced the term RICC. In order for RICC to occur, a combination of crack path deflection and a residual shear offset of the fracture surfaces is clearly required. The source of the crack deflection can be failure along grain boundaries, slip bands, secondary phases, precipitates, etc. At the tip of a deflected crack mixed mode loading conditions will exist, which may then lead to a residual plastic shear offset of the fracture surfaces on unloading.

Under near threshold fatigue conditions, plastic deformation can be localised to bands of intense shear ahead of the crack tip. Crack growth may then occur by shear decohesion of the active slip plane (i.e. through stage I crack growth as described previously), and so the crack path will follow well defined crystallographic directions, which commonly leads to highly faceted fracture surfaces. Under such conditions, environmental interactions with material at the crack tip have been suggested to enhance the irreversibility of shear displacements, and hence the magnitude of any RICC [Suresh *et al*, 1984, Carter *et al*, 1984].

The mechanism of RICC has been used to explain the dependence of near-threshold crack growth rates on ageing condition, specifically in 7X75 aluminium alloys, although the principles are more general [Lafarie-Frenot & Gasc, 1983, Suresh *et al*, 1984, Carter *et al*, 1984]. For underaged microstructures, the shearability of the strengthening precipitates by dislocations was found to lead to a highly inhomogeneous slip distribution and crystallographic crack growth, as described by Hornbogen & Zum Gahr, [1976]. This resulted in lower crack growth rates, due to the operation of RICC. In the overaged microstructure, the strengthening precipitates are non-shearable, with dislocation looping or

bypassing of the precipitates believed to occur. This was found to lead to a wavy slip pattern causing a much smoother fracture surface, with an associated drop in closure levels due to the lack of RICC.

2.2.3 Quantification of crack closure effects

From Equations 2.25 and 2.26 it can be seen that the fatigue crack growth rate is dependent on the closure stress intensity factor K_{cl}. Hence quantitative fatigue understanding is dependent on meaningful determination of K_{cl}. It is then important to understand how K_{cl} varies with the loading parameters, material properties, microstructure and environment.

There are a variety of methods which can be used to experimentally determine K_{cl}. The most common are based on direct observation of the crack tip (either by using a microscope mounted on the loading stage, or by examining surface replicas), or by monitoring the change in various physical properties of the specimen such as crack opening displacement (*COD*), strain at various points in the specimen, electrical conductivity, or acoustic properties. For example, by monitoring the variation of the displacement of the crack faces with applied load, the point in the unloading cycle at which crack closure occurs can be inferred by identifying the onset of non-linearity in the resulting compliance curve. A schematic illustration of an idealised compliance curve is shown in Figure 2.9. Initially, a reduction in applied stress σ from σ_{max} leads to a linear reduction in crack opening δ (region A-B in Figure 2.9). The slope of the compliance curve in this region is equal to that of an identical specimen with a saw-cut of same length as the fatigue crack, indicating that the fatigue crack is open all the way up to the tip. In the region B-C the slope of the compliance curve increases as σ is reduced, implying that the open length of the fatigue crack is reducing (i.e. progressive closure of the crack is occurring). In the final region C-D the slope becomes constant again, and equal to the slope of an identical but uncracked specimen, implying that complete crack closure has occurred. In reality, the change in the slope through the unloading cycle may be small, and the determination of the onset of closure (i.e. the position of point B) may be subject to a large degree of uncertainty.

It should be noted that there will be an inherent variation in the results that are produced by the various techniques for determining closure. The methods based on direct observation will give the closure point at the surface, while the methods based on specimen compliance will generally give a nominal closure point for the specimen as a whole (or for the mid-section for the case of push rod compliance gauges, for example). An historical element of experimental

variability is introduced due to the lack of rigorous, standard methods for the analysis of compliance curves. In general, offset compliance techniques have been used, i.e. a linear relationship is fitted to the upper part of the compliance curve for which the crack is open, which is then subtracted from the observed compliance for the entire load cycle, thus amplifying the difference between the open and closed crack compliance. There is subjectivity in defining the upper part of the compliance curve and the closure point, leading to variability in the analysis of a given set of results. Indeed, the results of a round-robin study of crack closure measurement and analysis have shown a large dependence of crack closure level on measurement technique, analysis technique, and laboratory for nominally identical tests (in terms of material, specimen type, loading and crack length) [see Phillips, 1989, 1993]. This is reflected by the large scatter of closure data in the literature. Objective treatments of analysing compliance curves do exist [e.g. Allison *et al*, 1988, Xu *et al*, 2000*b*] but they have not been uniformly adopted by the closure community.

Despite this variability in results, there are some well defined trends that can be identified in closure behaviour [McClung, 1991, 1994], which can be rationalised by considering the variation of the asperity height, plastic wedge thickness, and *COD* with the loading parameters. With decreasing stress intensity levels, monolithic alloys generally exhibit increasing asperity size. At low *R*-ratios *COD* values will be low, and hence RICC effects can be considerable. At higher K_{max}, RICC effects diminish as asperity sizes typically reduce and the *COD* increases. However, the magnitude of the residual plastic strain of the material in the crack wake leading to PICC (i.e. the thickness of the plastic 'wedge') can be shown to increase with K_{max} in proportion with the *COD* (e.g. see the model of Budiansky & Hutchinson [1978] which is considered in detail in the next section). Hence PICC levels can be expected to be independent of K_{max}. With increasing *R* the increasing values of *COD* will lead to a reduction in closure. However, the wedge thickness increases with increasing *R* as reverse yield contributions diminish. Hence closure can still be a factor for relatively high *R*-ratios. As K_{max} is further increased, such that small scale yielding conditions no longer apply, loss of elastic constraint will cause closure levels to tend to zero.

2.3 Analytical models of fatigue crack closure

From the previous section, it can be seen that crack closure effects are widely considered to have a significant influence on fatigue crack growth behaviour. As such, accurate modelling of these effects, whether they arise from PICC or RICC, is desirable in terms of the implementation of damage tolerant design. To this end, various analytical models of closure effects have been developed.

2.3.1 Analytical models of PICC

The earliest analytical model of PICC was developed by Budiansky & Hutchinson [1978]. The model considers a long crack under far-field mode I loading such that small scale yielding conditions exist at the crack tip. The Dugdale [1960] model (applicable to plane stress conditions) is used to describe the crack tip deformation of a stationary crack i.e.

$$r_p = \frac{\pi}{8}\left(\frac{K}{\sigma_0}\right)^2, \text{ and } \delta_0 = \frac{K}{E\sigma_0}, \tag{2.27}$$

where δ_0 is the *CTOD* at maximum load. With the origin of the Cartesian co-ordinate system at the crack tip,

$$\frac{\delta}{\delta_0} = g\left(\frac{x}{r_p}\right), \text{ where } g(\xi) = \sqrt{1-\xi} - \frac{\xi}{2}log\left|\frac{1+\sqrt{1-\xi}}{1-\sqrt{1-\xi}}\right| \tag{2.28}$$

where δ/δ_0 describes the variation of the plastic stretch for $0 \le x \le r_p$ (i.e. ahead of the crack tip) and the opening of the crack for $x < 0$ (i.e. in the crack wake). On unloading to $K_{min} = 0$ it can be shown that the residual plastic strain in the region $0 \le x \le (r_p/4)$ (i.e. within the plastic zone) and the residual crack opening is given by,

$$\frac{\delta}{\delta_0} = g\left(\frac{x}{r_p}\right) - \frac{1}{2}g\left(\frac{4x}{r_p}\right) \tag{2.29}$$

For steady state fatigue crack growth a plastic stretch of magnitude $\delta_R/2$ is assumed to be appended to the crack faces. Using the standard complex Muskhelishvili potentials with the appropriate boundary conditions it can be shown that for $R = 0$, $\delta_R/\delta_0 \approx 0.86$, i.e. the residual stretch behind the crack tip is 86% of the maximum crack tip opening displacement. Upon unloading it is found that contact of the crack faces will occur at a location very close to the tip at $K_{cl}/K_{max} = 0.483$. Closure at the crack tip itself occurs very shortly after the point of first contact. On reloading, the crack is found to open fully at $K_{op}/K_{max} = 0.557$ (i.e. K_{op} was

found to be slightly higher than K_{cl}). A similar analysis performed for positive values of R was shown to give good agreement with Elber's experimentally estimated formula,

$$\frac{K_{cl}}{K_{max}} = 0.5 + 0.1R + 0.4R^2 \qquad (2.30)$$

The analytical model justified the use of a closure-based effective stress intensity factor range ΔK_{eff} in correlating crack growth rates for different R-ratios, in that a relation of the form

$$\delta_0 - \delta_R = \beta \frac{\Delta K_{eff}^{\ 2}}{E\sigma_0} \qquad (2.31)$$

was found to hold. Given that the crack growth rate in a material can reasonably be expected to be a function of the cyclic stretch δ_0 - δ_R, the value of ΔK_{eff} should provide a valid description of crack driving force.

A conceptually similar model was constructed by Newman [1981] using what has become known as a discretised strip yield or Dugdale model. In the model the near-tip region is broken down into a series of rigid-perfectly plastic bar elements, with the intact elements ahead of the tip capable of carrying tensile and compressive stresses, and the broken elements behind the tip capable of carrying compressive stresses only. The crack opening stresses are calculated by numerically solving the displacement and compatibility equations for the system of connected elements. A constraint factor α is used to elevate the tensile flow stress of the elements ahead of the crack tip to account for the effect of stress state on crack tip plastic deformation. Under plane stress conditions $\alpha = 1$ (i.e. the flow stress is unchanged) and for plane strain conditions $\alpha = 3$ (i.e. the stress in the crack tip elements must reach three times the nominal flow stress for plastic deformation to occur). This representation of plane strain constraint is an approximation given that the Dugdale model is valid for plane stress conditions. However the use of the constraint factor for plane strain conditions has been validated [e.g. see Newman, 1998] through a comparison of the crack surface displacements and crack opening stresses predicted by the strip yield model to those calculated from a three dimensional FE analysis of fatigue crack growth and closure in a finite thickness plate [Blom *et al*, 1990]. By splitting the crack tip region into discrete elements in this way, variations in closure which occur due to a decrease in through thickness constraint or due to loading transients can be studied. The latest version of this modelling approach is implemented as FASTRAN III [Newman, 1999]. When adequate fitting via selection of the constraint factor to relevant experimental data is performed for constant amplitude loading conditions, reasonably accurate predictions of the growth rate response under more complex loading histories can be obtained [Newman, 1997, 1998, Harter, 1999]. However there are also situations where load transient interactions are poorly represented by the model [Collins,

1999, Zapatero *et al*, 1997]. For example the work of Zapatero *et al* [1997] demonstrates a high sensitivity to the constraint factor used in the model, as well as a variability of the quality of the results dependent upon the particular load history used. The FASTRAN model is also limited in that it clearly makes no allowance for the influence of other closure mechanisms (e.g. RICC, oxide induced crack closure) which may be important under particular loading conditions. The ability of this model to predict reasonable crack growth rate response in some situations does however illustrate the importance of the concept of crack closure to damage tolerant design.

2.3.2 Analytical models of RICC

Numerous attempts have been made to model RICC effects [e.g. Beevers *et al*, 1984, Carlson & Beevers, 1985, Evans & Hutchinson, 1989, Ravichandran, 1990, Mendelsohn *et al*, 1995, Chen *et al*, 1996, Garcia & Sehitoglu, 1997]. The earliest model of RICC is that of Suresh & Ritchie [1982], who used a simple geometrical model of a deflecting crack to derive an expression for the closure stress intensity factor due to RICC as,

$$\frac{K_{cl}}{K_{max}} = \sqrt{\frac{\delta_{cl}}{\delta_0}} = \sqrt{\frac{\chi \tan\theta}{1 + \chi \tan\theta}}, \qquad (2.32)$$

where δ_{cl} is the reduced crack opening displacement due to crack flank shear, δ_0 is the initial (unsheared) crack opening displacement, θ is the crack deflection angle and χ is the ratio of the mode II to the mode I displacement that occurs during unloading, illustrated in Figure 2.10. By choosing to relate K to $\sqrt{\delta}$, Suresh & Ritchie [1982] imply that closure is caused by contact in the near-tip region, where plastic strains dominate. Experimental evidence of RICC [e.g. Walker & Beevers, 1979, Suresh & Ritchie, 1982] has shown closure occurring remote from the crack tip, hence in this situation it may be appropriate to relate K to δ in a linear fashion (i.e. dominated by elastic crack opening behaviour).

In keeping with the basic link between surface geometry and closure levels, Wasen *et al* [1988] proposed an empirical relationship between K_{cl} and the standard deviation of asperity heights (related to grain size), based on experimental observations of ferritic steels, with deflection angles not being considered to be an important factor (c.f. the model of Suresh & Ritchie [1982] in which asperity height is not considered to be a factor but deflection angle is critical). Wang *et al* [1998] have argued that the model of Suresh & Ritchie [1982] is geometrically oversimplified, and that the empirical relationship of Wasen *et al* [1988] contains no information on the applied load or the asperity shape. Hence, they have extended these statistical and geometric approaches by incorporating a dislocation-based model to

estimate fracture surface mismatch. However the predictive power of this model is limited due to the inclusion of unknown proportionality constants, which must be fitted to experimental results. Similarly, the χ parameter used in the model of Suresh & Ritchie [1982] is essentially a fitting parameter.

2.4 Finite element models of fatigue crack closure

2.4.1 Overview

Initial attempts to model PICC using the finite element method were presented independently by Newman & Armen [1975] and Ohji *et al* [1974]. Using an essentially arbitrary crack growth algorithm and continuum plasticity theory, a finite element model of a cracked plate was constructed. Contact of the crack faces was modelled using spring elements to enforce the varying boundary conditions along the line of the crack. It was predicted that the crack faces come into contact under tensile far field loads in agreement with experimental observations. Although these analyses were limited to a small number of crack growth increments, steady-state closure levels were predicted under plane stress conditions in reasonable agreement with experimental results. In particular, the effects of variable amplitude loading histories and R-ratio were investigated. Similar models have subsequently been used by many researchers to investigate closure under different stress states and loading conditions [e.g. McClung & Sehitoglu, 1989, Ogura *et al*, 1977, Blom & Holm, 1985, Fleck & Newman, 1988, McClung *et al*, 1991, Sehitoglu & Sun, 1991, Llorca & Sanchez-Galvez, 1990, Wei & James, 2000, Socie, 1977, Nakamura *et al*, 1983, Ashbaugh *et al*, 1997, Ritchie *et al*, 1987, Lalor & Sehitoglu, 1988, Fleck, 1986, Biner *et al*, 1994]. It is apparent from the various numerical models which have been presented in the literature that there are several important issues, such as mesh sufficiency and the attainment of a steady-state crack closure level, which must be addressed to produce meaningful finite element models of the crack closure process. A summary of these issues is presented here.

2.4.2 Mesh sufficiency

By examining results from Newman [1976] and comparing them to their own results, McClung & Sehitoglu [1989] highlighted the existence of a false peak in the variation of closure levels with applied load which occurs due to insufficient mesh refinement. At some load level for a given mesh, the mesh will be too coarse to pick up the reverse yielding at the crack tip upon unloading. Thus the forward plasticity contributions at the tip will be artificially high leading to artificially high closure levels. Through parametric investigation McClung & Sehitoglu [1989] suggested that a ratio of ten elements to the plastic zone radius for first order quadrilaterals at $R = 0$ was sufficient.

2.4.3 Crack closure stabilisation

It is also important to allow stabilised crack closure levels to be produced (i.e. the crack closure level does not vary significantly from one cycle to the next). That is, the crack must propagate far enough to develop a significant plastic wake and ensure that the crack tip is outside of the stress field of the initial notch or pre-crack. The imposition of a baseline cyclic load on a perfectly sharp precrack (as is the case in the FE model approach) is analogous to a low-to-high step load history. Experimental observations of closure under such variable amplitude fatigue loading conditions [see Skorupa, 1998] are not conclusive in terms of affected distance, but suggest that quasi-steady state behaviour may be achieved sooner than for single overloads situations (where a steady-state closure level will typically be reached when the crack has grown through three to four overload plastic zone sizes following a transient [e.g. Ward-Close & Ritchie, 1988]). Hence, a criterion based on crack growth through a small number of crack tip plastic zones would appear to be suitable for numerical closure models. McClung & Sehitoglu [1989] have identified the requirement of sufficient crack advance based on FE model behaviour, and suggest that growth of the fatigue crack through the plastic zone at the initial crack length to be adequate. Certainly FE closure results which are presented where the crack has been grown through less than a single plastic zone may not be truly representative of actual steady state crack closure response.

2.4.4 Nodal release point

The effect of the point in the load cycle at which the crack tip node is released during FE crack growth modelling has been investigated by McClung & Sehitoglu [1989]. Schemes that have been used in the literature include (i) release at maximum load, after Newman & Armen [1975], (ii) release at minimum load, after Ohji *et al* [1974], (iii) release at some point in the unloading cycle, e.g. Lalor & Sehitoglu [1988], Nicholas *et al* [1988], or (iv) release at the point at which the crack tip stresses just become tensile [Ogura *et al* 1977]. It has been argued [e.g. Ashbaugh *et al,* 1997, Dougherty *et al,* 1997] that release at or near maximum load is more physically realistic, and hence more appropriate. But, as McClung & Sehitoglu [1989] point out, the crack growth scheme is essentially arbitrary in these models, using crack growth increments many orders of magnitude greater than physically observed crack growth rates. The crack growth algorithms are merely designed to produce a model of a crack with a physically realistic plastic wake. Hence, the criteria for selection of a nodal release scheme should not be based on comparison to the actual mechanics of fatigue crack growth, but rather on the effect the crack propagation scheme has on crack tip plasticity and crack

opening displacements. That being said, McClung & Sehitoglu [1989] found only small variations in crack closure levels and crack tip deformation, using the first three schemes listed above (for plane stress loading outside the small scale yielding regime). Releasing the crack tip node immediately following maximum load was found to give the most consistent performance and was the suggested choice of the authors.

2.4.5 Effect of the constitutive model

The majority of the closure analyses in the literature utilise constitutive models based on a bilinear stress-strain curve, with the material either displaying elastic-perfectly plastic behaviour or undergoing hardening upon plastic deformation governed by an isotropic or kinematic hardening rule. The advantages of this approach lie in the ease with which this constitutive model can be implemented within the analysis. The bilinear stress-strain curve is also a fair representation of the response to cyclic loading of some materials e.g. medium carbon steels [Landgraf, 1979]. However, there are some aspects of cyclic plasticity that these simple bilinear models cannot replicate such as cyclic ratchetting (the accumulation of plastic strain over time under stress controlled non-zero mean stress fatigue conditions) and mean stress relaxation (the tendency of the mean stress to go to zero under strain controlled non-zero mean strain fatigue conditions). There are also many materials for which the bilinear stress-strain curve is a poor representation of the cyclic stress-strain behaviour e.g. aluminium 2024-T4 [Mitchell, 1979]. Attempts to overcome these limitations have been undertaken [McClung & Sehitoglu, 1989, Ashbaugh *et al*, 1997] by the use of a power law hardening constitutive model, based on the Ramberg-Osgood relationship

$$\frac{\Delta\varepsilon}{2} = \frac{\Delta\sigma}{2E} + \left(\frac{\Delta\sigma}{2A'}\right)^{1/n_f} \tag{2.33}$$

where $\Delta\varepsilon$ is the uniaxial strain amplitude, $\Delta\sigma$ is the uniaxial stress range, E is Young's modulus, A' is the cyclic strength coefficient and n_f is the cyclic strain hardening exponent. By relating the cyclic stress and strain in this way the actual material behaviour can be more closely approximated. There are however significant drawbacks to this method. The implementation of this constitutive model within the numerical analysis is not as straight forward as that of the bilinear model, and accurate calibration of the material parameters is required. Given that this model does include the possibility of stress relaxation effects, the rate of stress relaxation can become important. All the numerical models of closure are run over many orders of magnitude less cycles than an actual fatigue test, and hence there is a discrepancy in the rates of crack growth in the model and the real system. This will lead to unrealistic stress relaxation rates in the model. The results of the study by McClung &

Sehitoglu [1989] into the choice of constitutive model are not conclusive. At $R = 0$, the power law model was found to yield higher closure levels compared to the bilinear model. This is confirmed in the findings of Ashbaugh *et al* [1997]. It is suggested that this is a consequence of the differences in the onset of flow in the power-law and bilinear constitutive models. It is noted that both forms of modelling can compare well with experimental results under different loading conditions and for different materials. For example the closure levels gained from using the power law hardening model were found to be in good agreement with the experimental results of Lankford *et al* [1984] for high maximum stress levels, whereas the bilinear model agreed well with the experimental data of Elber [1970], taken at lower maximum stress levels. Another approach which can be readily implemented in many finite element codes is the use of a multi-linear stress-strain curve, as used by Dougherty *et al* [1997] and Ritchie *et al* [1987]. That is, the shape of the cyclic stress-strain curve can be implemented into the model by specifying the explicit dependence of the yield stress on increasing plastic strain. There does not appear to be any rigorous investigation on how the closure levels produced from models using this construction compare to those using the bilinear stress-strain relationship.

2.4.6 Effect of specimen geometry

The effect of specimen geometry on the observed closure levels was investigated by Fleck & Newman [1988] and Fleck [1986]. Plane strain FE analyses were conducted for centre cracked panel (CCP) and single edge notched bend (SENB) specimens. The results of these analyses showed an influence of specimen geometry on the closure behaviour. Specifically, closure was found not to occur in the bend specimen for $R \geq 0$, whereas transient closure was observed in the CCP specimen, due to residual crack flank deformation at the location of the pre-crack tip (This transient closure effect is discussed in more detail in the next subsection). These results were explained in terms of the influence of the T-stress, which arises from the second term in the power series representing the elastic crack tip stress field, and is a uniform stress in the x-direction (for a crack parallel to the x-axis, with mode I loading applied in the y-direction). The relationship between the T-stress and K for a cracked body under mode I loading can be expressed through the biaxiality ratio, β, as

$$T = \beta \frac{K}{\sqrt{\pi a}} \tag{2.34}$$

For a CCP specimen $\beta \approx -1$ for small values of a/W, where a is the crack length and W is the specimen width, and for the SENB specimen β increases with a/W and is positive for $a/W >$ 0.35. To understand the role of the T-stress on PICC first consider a fatigue crack under

small scale yielding, $T = 0$, plane strain conditions. At the crack tip, the material will have undergone a tensile plastic strain in the y-direction, ε_{yy}^{pl}, and a compressive plastic strain in the x-direction, ε_{xx}^{pl}. The magnitude of crack closure on subsequent crack propagation will be dependent on the magnitude of ε_{yy}^{pl}. If the CCP specimen is now considered for loading such that a significant (negative) T-stress exists (acting in the x-direction), it is clear that the compressive strain ε_{xx}^{pl} will be enhanced, thus enhancing ε_{yy}^{pl} and the level of crack closure. For the SENB specimen, for $a/W > 0.35$, the T-stress will be positive thus reducing the magnitude of ε_{xx}^{pl} and constraining ε_{yy}^{pl}. This will reduce the magnitude of PICC. It is interesting to note that a similar analysis undertaken by Fleck [1986] for plane stress conditions showed no sensitivity to specimen geometry, where tensile deformation in the y-direction causes a through thickness contraction ε_{zz}^{pl}, and the changes of ε_{xx}^{pl} induced by changes of the T-stress have no effect. This analysis was performed on the limit of applicability of LEFM, and a diminishing effect of specimen geometry with decreasing loading level would be expected as the T-stress becomes negligible compared to the singular crack tip stresses. Effects of specimen geometry were also investigated by McClung [1994] for plane stress conditions, at loading levels at and outside the limit of small scale yielding. Different closure levels were predicted in the specimen geometries modelled (CCP, SENB, and single edge notched tension specimens), when plotted against σ/σ_0, where σ is the far-field applied stress. However, the closure levels in the different specimens were found to be in much better agreement when plotted against $F\sigma/\sigma_0$, where F is the specimen geometry factor for the stress intensity factor. Only at high loading levels were T-stress effects considered to be a factor.

2.4.7 Modelling PICC under plane strain

As noted in Section 2.2.2.1, the issue of PICC under plane strain conditions has been the subject of some debate [e.g. see Pippan & Riemelmoser, 1998, Riemelmoser & Pippan, 1998, Ritchie *et al*, 1989, Vasudevan *et al*, 1994]. Under plane stress, through-thickness contraction is a clear source of the 'extra material' required for crack closure to occur. Under plane strain conditions through-thickness contraction is zero by definition, and this has led various authors to argue that PICC cannot occur under these conditions [Louat *et al*, 1993, Minakawa *et al*, 1986]. However, there are experimental data to suggest that PICC can occur under plane strain conditions [Fleck & Smith, 1982, Bray *et al*, 1992]. This was first investigated through the use of numerical models by Ogura *et al* [1977] and Blom & Holm

[1985]. The results of Blom & Holm in particular showed stabilised closure levels in agreement with experimental results from a study of Al 2024, whereas the results of Ogura *et al* would not satisfy the mesh refinement criteria of McClung & Sehitoglu [1989], and so may be regarded as questionable. Fleck & Newman [1988] argued that PICC in plane strain was due to an artificial 'wedge' of material forming near the pre-crack tip used in the modelling process. It was argued that if the crack was allowed to grow far away from this wedge, then its influence would diminish such that closure levels would go to zero, i.e. plane strain PICC essentially being a transient effect caused by unrepresentative residual strains at the pre-crack. This however is in apparent contradiction with more recent studies [McClung *et al*, 1991, Sehitoglu & Sun, 1991, Llorca & Sanchez-Galvez, 1990, Wei & James, 2000], which have shown plane strain closure levels in the region of 0.2 to 0.3 K_{max}, for $R = 0$, under small-scale yielding conditions. The origin of this closure has in some cases been shown to be a contraction of material in the in-plane transverse direction, (i.e. parallel to the crack plane). This is consistent with the analytical descriptions of plane strain closure subsequently put forward by Pippan & Riemelmoser [1998]. However, fundamental to the closure levels reported in the literature are the ways in which the closure point is defined. Newman & Armen's [1975] initial approach was to monitor the behaviour of the first node behind the tip, and to define the closure point as the point in the load cycle at which the displacement of the node immediately behind the crack tip from the crack symmetry plane becomes zero. This approach has been adopted in many subsequent analyses in the literature. However, Fleck & Newman [1988] showed that in plane strain analyses the node immediately behind the crack tip may be affected by unrealistic residual strains close to the tip (arising from the crack extension process). In particular, the contact behaviour of the first node behind the tip can be very different form the rest of the nodes behind the crack tip, regardless of the mesh size, (i.e. exhibiting clear mesh dependency). Hence, it was suggested that closure at the first node behind the tip should not be taken as the definition of the closure point. Attempts to identify crack closure points based on nodal contact are of course subject to the essentially nominal scale of mesh refinement used, and attempts have been made [Socie, 1977, Nakamura *et al*, 1983] to avoid such definitions by examining instead changes in specimen compliance (cf. experimental closure determination methods). However, no comparisons between the closure points determined by the compliance method and by the behaviour of nodes behind the crack tip were apparently made. Overall there does not appear to be any standard definition of the closure point in finite element analyses. For example, although McClung & Sehitoglu [1989] adopted the criterion of the closure at the second node behind the crack tip, the original criterion of closure at the first node behind the crack tip is used in a later paper by Sehitoglu & Sun [1991].

2.4.8 Numerical models incorporating crack deflection

Llorca [1992] used the finite difference (FD) technique to demonstrate the effect of periodic and irregular crack deflection on crack closure levels. In the FD technique, the response of the elastic-plastic solid is governed by the linear momentum theorem, the energy balance and the constitutive equations of the material. The continuum body is discretised into a mesh of nodes and elements (as in FE), and the calculation is broken down into a number of time steps. In each step the loads acting on the nodes are used to determine the nodal accelerations, which are then integrated over time to obtain velocities and displacements. From the displacements the strains can be computed, and from the constitutive response of the material the stresses can be found. By integrating the stresses, the residual loads on each node can be determined. This information is then carried forward into the next time step and the calculation progresses. In the Llorca analysis, the time increment is selected such that it is less than the time taken for information to pass between the two closest nodes (based on pressure wave speed). This necessitates a simulated fatigue test frequency of 5000 Hz (i.e. far greater than standard experimental practice). It is claimed that dynamic effects in the model are small and do not effect the results. The study is an extension of an earlier FD analysis of PICC [Llorca & Sanchez-Galvez, 1990], where the meshing criteria defined by McClung & Sehitoglu [1989] for FE analyses were used to ensure accurate modelling of crack tip plasticity. In the Llorca model of RICC, it is stated that the effects of plasticity on RICC are almost negligible, and that the source of closure can be expected to be the displacements of the crack surfaces in the wake. Hence the meshing criteria of McClung & Sehitoglu is not adhered to. Instead a minimum criterion of four elements to the crack branch length is selected. In fact due to the low loading used in the model (K_{max} increases from 0.64 to 1 MPa$\sqrt{m}$) and the large crack tip element sizes (typically 10 μm), the ratio of element size to plastic zone size is at best 10:1 (cf. the ratio of 1:10 suggested by McClung & Sehitoglu). Contact of the crack faces was modelled in a similar manner to the FE models discussed previously. The results of the analysis showed that RICC was strongly dependent on deflection angle, in keeping with the geometrical model of Suresh & Ritchie [1982], with no effect of deflection length for the range studied. Closure was found to be discontinuous (i.e. occurring at discrete locations in the crack wake, concentrated at the turning point of the crack). When the deflection angle was allowed to vary from one deflected section to the next, significant increases in the crack closure levels were found. The origin of RICC in the model was considered to be the changing ratio of the mode I to mode II displacements around the crack tip due to variations in the crack length and geometry. That is, the mode I and II displacements which occur around the tip during the loading cycle are not identical to the

displacements which occur during unloading, due to the intervening propagation of the crack tip. As such, a residual displacement of the crack faces is predicted, leading to non-mating crack surfaces and RICC. From a physical standpoint this proposed mechanism can be criticised on two points. Firstly, in a near-threshold fatigue crack the increment of crack growth per cycle can be expected to be very small, hence the change in the ratio of mode I to II displacements from the loading to unloading cycle due to crack propagation can be expected to be infinitesimal. Secondly, the mechanism as described would lead to residual deformation of a purely elastic crack, which is clearly not sensible. In fact permanent deformation of the crack faces and hence RICC can only arise from plastic deformation. Given that this aspect of the model behaviour is clearly not accurately represented, the validity of the model predictions must be considered as questionable.

2.5 Fatigue crack growth under variable amplitude loading

The preceding discussion is essentially related to fatigue crack growth response under constant amplitude loading. The study of fatigue under constant amplitude loading provides valuable insights into the mechanics of the crack growth process. However, the majority of components in aerospace applications, and indeed many other engineering situations, undergo variable amplitude loading. Unfortunately, the insights gained through the study of constant amplitude fatigue cannot be simply extrapolated to variable amplitude conditions. It is therefore important to study and understand the effects of variable amplitude loading in order to implement an accurate damage tolerant design philosophy under such conditions.

The effects of excursions from constant amplitude loading (i.e. overloads and underloads) were noted experimentally by Schijve & Broek [1962], who showed that significant crack growth retardation occurred following the application of a tensile overload. Results were also presented which showed an acceleration in growth rate following a compressive overload [e.g. Topper & Yu, 1985]. These two results show the inadequacy of the simple concepts of damage accumulation, which predict precisely the opposite results: for example, the Palmgren-Miner rule [Palmgren, 1924, Miner, 1945] states that

$$\sum_{i=1}^{m} \frac{n_i}{N_{fi}} = 1, \tag{2.35}$$

where n_i is the number of cycles corresponding to the ith block of constant amplitude $\Delta\sigma_i$ in a sequence of m blocks, and N_{fi} is the number of cycles to failure at $\Delta\sigma_i$. Clearly, N_{fi} will decrease with increasing $\Delta\sigma_i$, hence the rule predicts that an overload will reduce the remaining fatigue life and an underload will extend it (relative to a baseline load). The Palmgren-Miner rule is formulated to predict the fatigue life of a nominally defect free specimen. Hence, this discrepancy between the prediction of the Palmgren-Miner rule and the experimental overload effects noted above illustrates the differing effects that load transients may have on the crack initiation and crack growth stages.

Given the importance of variable amplitude loading to the aerospace and many other industries, a great deal of research into its effects has subsequently been performed. In particular, much attention has been focused on the effects of a single tensile overload. By restricting attention to this simple case, insights into the mechanistic origins of the fatigue crack growth retardation may be easily identified, and it is this aspect of variable amplitude fatigue behaviour which will be focussed on here. This clearly has limitations given that

significant interaction effects of load transients have been found to occur in reality. For example, the application of an load sequence which contains underloads and overloads tends to reduce the post-overload retardation compared to a load sequence containing only overloads, however the effect is strongly dependent upon the order in which the load transients occur [Zhang *et al*, 1987]. As such, whilst studies of single overload effects may increase baseline understanding of variable amplitude fatigue crack growth, they are in fact somewhat removed from real service loading conditions.

2.5.1 General experimental trends

Application of a single tensile overload during baseline cycling typically leads to transient fatigue crack growth rates as schematically illustrated in Figure 2.11, (which also shows the nomenclature which is used in describing the application and effect of an overload). In general, the application of an overload will be followed by a brief acceleration in crack growth rate. This is followed by a period of prolonged retardation leading either to crack arrest, or an eventual return to the baseline crack growth rate once a minimum in *da/dN* has been passed.

The effect on the fatigue crack growth rate of a single overload will vary depending on a wide variety of mechanical and microstructural parameters. Typically, large values of the overload ratio, *%OL*, will lead to an increased number of delay cycles, N_d, and a more pronounced retardation [e.g. Robin *et al*, 1983, Ward-Close & Ritchie, 1988, Venkateswara Rao & Ritchie, 1988]. Increasing values of the load ratio *R*, tend to limit retardation, and decrease the distance between the application of the overload and the point of minimum *da/dN*. This behaviour has been noted in both steels [Damri & Knott, 1991] and aluminium alloys [Tsukuda *et al*, 1995]. For high values of *R* (= 0.65), immediate retardation has been recorded [Shin & Hsu, 1993] i.e. the delay in retardation commonly seen at lower *R* was found not to occur. The reported evidence on the effect of $\Delta K_{(BL)}$ on overload behaviour is inconsistent. Various authors [e.g. Reynolds, 1992, Venkateswara Rao & Ritchie, 1988, Bray *et al*, 1992, Ward-Close & Ritchie, 1988] have shown for a variety of materials that plots of N_d vs. $\Delta K_{(BL)}$ exhibit a U-shaped curve, i.e. that the effect of the overload is at a minimum at some intermediate value of $\Delta K_{(BL)}$, and the retardation increases for values of $\Delta K_{(BL)}$ towards the threshold and towards unstable fracture. However, the results of Shin & Hsu [1993] show the opposite trend for a stainless steel, while the results of Shuter & Geary [1996] show a steadily decreasing effect of an overload with increasing $\Delta K_{(BL)}$.

2.5.2 Explanations of post-overload fatigue crack growth retardation

A variety of mechanisms have been proposed to account for the observed brief acceleration and subsequent prolonged retardation of a fatigue crack following a tensile overload. It is generally considered that no one mechanism can account entirely for the post-overload behaviour, and that several mechanisms will generally act concurrently (see Suresh [1991], Skorupa [1999]).

2.5.2.1 Plasticity induced crack closure

In section 2.2.2, the way in which PICC leads to fatigue crack growth retardation under constant amplitude loading was discussed. It has been argued [Elber, 1970, 1971] that this mechanism is also able to account for the post-overload effects on the crack growth rate. On application of the overload, crack blunting will occur. Hence, the baseline crack closure level will be reduced (and the effective stress intensity factor range and the crack growth rate will be increased) thus accounting for the initial acceleration of the crack. However, the overload also produces a zone of material ahead of the crack which has undergone a large tensile plastic stretch. So, as the crack propagates this stretched material moves into the crack wake, forming a 'wedge', and leading to enhanced levels of PICC compared to the baseline level. This then accounts for the delayed retardation of the crack. As mentioned above, immediate retardation has been found to occur for high R-ratios [Shin & Hsu, 1993], consistent with the fact that PICC is not necessarily the only mechanism operating. As the crack grows away from the wedge of plastically stretched material, its influence on the near tip strain field, and hence fatigue crack growth rate may be expected to diminish, and crack growth rates return to their baseline level. Experimental evidence suggested for overload-induced PICC includes the loss of striations on the fracture surface ahead of the position of the crack tip at the time of application of the overload (suggesting that fracture surface contact and abrasion have occurred [e.g. Kumai & Higo, 1996, Ward-Close & Ritchie, 1988]) and direct measurement using a push-rod compliance gauge [Fleck, 1988]. It has also been noted [Nayeb-Hashemi *et al*, 1983] that under mode III conditions, where closure due to contact shielding mechanisms such as PICC is not an issue, crack growth retardation does not occur following an overload. Whilst crack closure is widely considered [e.g. Skorupa, 1999, Geary, 1992] to provide the primary contribution to post-overload retardation effects, there are incidences in the literature where closure alone cannot apparently explain the observed da/dN *vs.* ΔK_{eff} relationships [Suresh, 1983, Kim & Shin, 1999] (although the significant degree of uncertainty that accompanies closure measurement is an important consideration). As such, it is important to consider other proposed mechanisms of overload-induced retardation.

2.5.2.2 Crack tip blunting

Christensen [1959] suggested that on application of an overload, a previously sharp fatigue crack will become blunted. Thus the crack will behave like a notch, leading to a retardation as the crack re-initiates and propagates away from the notch stress field. However, whilst crack tip blunting can undoubtedly occur, post-overload crack arrest has been reported for an apparently sharp crack tip [Lankford & Davidson, 1976]. Furthermore, blunting has also been observed following the application of an underload, but with an accompanying acceleration in crack growth rate [Fleck, 1985]. As such, crack blunting is not considered to contribute to post-overload retardation, and may in fact be considered to reduce crack tip closure levels immediately following the overload, thereby contributing to the brief acceleration in the fatigue crack growth rate typically observed.

2.5.2.3 Residual compressive stresses

At the tip of a fatigue crack, residual compressive stresses will exist due to the elastic constraint of previously plastically deformed material. Following the application of an overload, the zone of compressive stress has been shown experimentally to increase in size [Allison, 1979], and it has been suggested that these compressive stresses will retard the crack growth [e.g. Wheeler, 1972, Willenborg *et al*, 1971]. Whilst the compressive stresses will clearly lower the local (crack tip) load ratio, without resorting to crack closure arguments, it is not clear why these stresses would affect ΔK_{eff}, and hence the crack growth rate. Furthermore, the largest residual stresses will occur directly ahead of the crack tip, and thus immediate retardation would be expected. Experiments have also shown [Suresh, 1983] that the retardation effect may last even when the crack has propagated through the zone of compressive stress, further casting doubt on the predominance of this mechanism.

2.5.2.4 Strain hardening

It has been proposed [Jones, 1973] that the strain hardening of the material ahead of the crack tip, due to application of an overload, will contribute to the crack growth retardation, through reduced opening of the crack tip, and experimental data which supports this suggestion has been presented [Knott & Pickard, 1977]. It is widely considered however, that this mechanism alone cannot account for the observed retardation following an overload. For instance, overload retardation is observed in metallic glasses [Chaki & Li, 1984], which do not exhibit any strain hardening behaviour, indicating that strain hardening is not a necessary condition. Results have been presented [Petit *et al*, 1988] showing that the degree of overload retardation for an aluminium alloy was enhanced in the underaged state, where the material exhibits high strain hardening, compared to the overaged state, where the strain

hardening is much lower. However, variations also occurred in the crack morphology, suggesting that the increased retardation could be due to increased crack roughness.

2.5.2.5 Crack deflection and branching

Deflection and/or branching of the fatigue crack have been noted experimentally following the application of an overload [Suresh, 1983, Shuter & Geary, 1996, Ward-Close & Ritchie, 1988, Bray *et al*, 1992, Venkateswara Rao & Ritchie, 1988]. Whilst in some cases this is only a surface effect [Bray *et al*, 1992, Venkateswara Rao & Ritchie, 1988], in others the branching may occur throughout the entire specimen thickness. Given that the stress intensity factor of a deflected or branched crack is reduced compared to a straight crack of the same projected length [Kitagawa *et al*, 1975], crack growth rate is retarded.

A further contributory factor to crack retardation is the possibility of the reactivation of near-threshold crack growth mechanisms [Suresh, 1983]. For instance, if the crack tip ΔK_{eff} is sufficiently reduced subsequent to the application of an overload, it is possible that fatigue crack growth will occur through stage I type (crystallographic) propagation, even though the far-field stress intensity factor range may be well above the threshold. This may then lead to the operation of near-threshold retardation mechanisms such as oxide and roughness induced crack closure, thus magnifying the effect of the overload.

2.5.3 Rationalising the experimentally observed trends

In section 2.5.1, the trends that are generally seen on application of an overload, and how these vary with changes in the loading parameters were discussed. By considering the proposed mechanisms for post-overload retardation discussed in section 2.5.2 (in particular PICC), it is possible to rationalise these trends.

It has already been seen how PICC arguments can explain the initial brief acceleration, the prolonged retardation and the return to baseline crack growth rates following an overload. PICC can also be used to explain the dependence of the retardation on overload ratio, *%OL*. Clearly, for higher *%OL*, the size of the wedge of plastically deformed material in the wake will be greater, leading to a greater reduction in crack growth rate, and an increased number of delay cycles. That is, the predicted variation of PICC effects are consistent with those seen experimentally.

The effect of PICC can clearly be expected to diminish with increasing R, as the increase in crack opening can be expected to be greater then the increase in the thickness of the plastic

wedge (see Budiansky & Hutchinson [1978] for details, discussed in section 2.3.1). Hence, the experimentally observed reduction in number of delay cycles, onset of retardation, and magnitude of retardation, with increasing R are also consistent with the PICC mechanism.

The variation in retardation behaviour with baseline stress intensity factor range, $\Delta K_{(BL)}$, characterised (in most instances, but not all) by a U-shaped plot of the number of delay cycles, N_d, against $\Delta K_{(BL)}$, has been explained by the concept of competing closure mechanisms. Ward-Close & Ritchie [1988] and Venkateswara Rao & Ritchie [1988] proposed that for low $\Delta K_{(BL)}$, near-threshold crack growth will promote crack roughness, which associated with low levels of crack opening will mean that RICC mechanisms will be operative. At intermediate values of $\Delta K_{(BL)}$, RICC will decrease, leading to reduced post-overload retardation. However, for higher values of $\Delta K_{(BL)}$, retardation effects will again increase as the stress state ahead of the crack tip becomes more plane stress in character, and PICC effects are thus increased. A schematic illustration of this behaviour is shown in Figure 2.12. A different explanation for this behaviour was put forward by McEvily & Yang [1990], based solely on PICC. Near the threshold the crack growth rate, and hence N_d, will be highly sensitive to changes in $\Delta K_{(BL)}$ due to the steep gradient of the da/dN vs ΔK_{eff} curve, i.e. a slightly lower $\Delta K_{(BL)}$ may mean a much greater N_d. The rise towards unstable fracture is again attributed to the development of plane stress PICC.

2.5.4 FE models of overload-induced closure

From the earliest FE models of PICC, it was clear that the modelling procedure could be readily extended to investigate load transient effects. Newman & Armen [1975] and Ohji *et al* [1974, 1975] applied simple block loading histories in their FE models to yield closure behaviour in qualitative agreement with experimental observations. Due to considerations of processing time, the overload ratios and the number of crack growth increments were required to be small, hence in-depth analysis of load transient effects was not possible.

Following on from these early models, the FE investigation of variable amplitude closure effects has received comparably less attention in the general scientific literature than constant amplitude closure. However, the general trend of a brief acceleration followed by prolonged retardation following a single overload has been reported by various researchers from both two dimensional [Zhang *et al*, 1992, Ellyin & Wu, 1999, Dougherty *et al*, 1997, Pommier & Bompard, 2000, Fleck & Shercliff, 1989] and three dimensional models [Chermahini *et al*, 1988, Zhang, 1999]. However, quantitative agreement with experimental data has not always

been achieved. For instance Dougherty *et al* [1997] report good quantitative agreement between constant amplitude tests in a steel and their FE model, with FE values of K_{cl}/K_{max} for various ΔK levels typically being within 5% of experimental values. Significant discrepancies are reported however for single overload conditions, with the FE model predicting greater shielding and for a longer duration than was found in the experimental results. This highlights either the limitations of the modelling process, or the importance of multiple mechanisms in post-overload fatigue crack retardation. Pommier & Bompard [2000] highlight the role of factors which influence the cyclic plastic deformation behaviour on overload-induced closure. In particular, materials exhibiting a Bauschinger effect were shown to be far less resistant to variable amplitude fatigue loading than materials which isotropically harden. This is attributed to the dependence of the residual stresses at the crack tip on the cyclic plastic behaviour, which effects the development of the overload plastic zone. Fleck & Shercliff [1989] used FE techniques to show that overload induced closure operates under plane strain conditions. Closure was shown to be dependent upon the deformation of material at the overload location, leading to discontinuous contact behind the crack tip when the crack had propagated some distance from the overload location. This discontinuous closure behaviour was also noted experimentally, and was considered to be responsible for the actual growth rate recovery being faster than that predicted by the closure response, i.e. ΔK_{eff} based on discontinuous closure away from the near-tip region was found to overestimate the actual shielding of the near-tip material. In an attempt to avoid the problems of relating discontinuous post-overload closure to the crack driving force, a ΔK_{eff} definition based on the sign of the stress at the crack tip was implemented by Ellyin & Wu [1999]. It was argued that crack closure would not necessarily prevent further crack growth if the crack tip was still under tension, nor would crack opening necessarily lead to crack propagation if the crack tip was still under compression. Hence ΔK_{eff} was defined as that portion of the load cycle for which the crack tip node was under tension. In terms of removing the definition of ΔK_{eff} from crack face contact to a more micromechanical based criterion, this approach can be criticised for two reasons. Firstly, fatigue crack propagation is fundamentally a cyclic strain based phenomenon [Laird, 1979, Rice, 1967]. Hence a 'true' micromechanical characterisation of crack driving force should be based on the cyclic strain range within the crack tip process zone. Secondly from a modelling standpoint, use of the stress at the crack tip node is suspect given that the crack tip in the FE model is sharp by definition, thus implying a stress singularity. However the elements used in the analyses are not capable of representing this behaviour (exhibiting either constant stress or linear stress variation), and confidence in the very near-tip solution is not justifiable. This is not an issue

for the credibility of the model as a whole, given that the plastic deformations away from the very near-tip region which lead to crack closure may still be accurately modelled.

2.6 Crack closure concepts under reconsideration

In the last ten years the existence and significance of crack closure has come under question. Donald [1997] presented experimental evidence which suggested that crack closure does not entirely isolate the crack tip. Specifically sub-millimetre strain gauges were mounted on the specimen surfaces directly in the line of the fatigue crack, allowing the elastic strain range close to the crack tip to be measured. By considering that the crack driving force should be proportional to the entire elastic crack tip strain range (and not just that portion above the crack closure point), and noticing that a significant contribution to elastic crack tip strain occurred below K_{cl}, Donald [1997] proposed that ΔK_{eff} should be based on the ratio of the measured strain magnitude to that which would have occurred in the absence of closure. This was referred to as the compliance ratio technique, and will clearly lead to lower levels of crack tip shielding than conventional closure measurement. From an experimental point of view this clearly has the advantage that the identification of K_{cl} (subject to large variability arising from experimental technique and the processing of the data) is not necessary. An adjustment to this technique, called the adjusted compliance ratio (ACR) aimed at making the measurement independent of strain gauge location, was also presented which entails subtracting the compliance prior to the initiation of the crack, C_i, from the secant compliance, C_s, and the compliance above the opening load, C_o, (see Figure 2.13), which (with the inclusion of a normalising factor) gives,

$$ACR_n = \frac{C_{oi}}{C_{si}} \frac{C_s - C_i}{C_o - C_i}, \tag{2.36}$$

where ACR_n is the normalised adjusted compliance ratio and C_{oi}/C_{si} is the normalising factor based on the ratio of the values of C_o and C_s prior to the initiation of the crack. The normalising factor is included to account for bias in the compliance measurements due to noise or non-linearity. The driving force of the crack is then given as,

$$\Delta K_{eff} = ACR_n \, \Delta K_{app} \tag{2.37}$$

Apparent experimental justification of this technique has been presented [Donald, 1997, Donald & Phillips, 1999, Bray & Donald, 1999, Donald & Paris, 1999] in which correlation of crack growth rates for different R ratios was claimed to be better using the ACR technique than for the standard crack closure technique. However the comparison is dependent upon the high degree of experimental variability in the compliance based closure data [Phillips, 1989, 1993]. Furthermore a fundamental physical basis for the ACR technique has not been demonstrated. For instance, it could be suggested that basing the technique on the elastic

crack tip strain range is suspect, given that fatigue crack growth can be expected to be controlled by cyclic plastic strain in the crack tip process zone.

Vasudevan and co-workers [Vasudevan *et al*, 1992, 1994, Louat *et al*, 1993] presented dislocation based models to show that PICC effects were apparently non-existent and RICC effects were much smaller than those normally estimated from specimen compliance. The authors implied that the variation of the crack growth rate and threshold with the loading parameters was an intrinsic material property. A 'unified approach' was proposed where fatigue crack growth was considered to be controlled by two crack tip driving forces, ΔK leading to cyclic plastic damage, and K_{max} leading to crack tip rupture. Similarly two thresholds ΔK^*_{th} *and* K^*_{max} were proposed which were considered to be necessary conditions for fatigue crack growth. This line of thinking runs counter to the widely held view in the fatigue community that closure *"must be considered to understand or treat many fatigue crack growth problems, although closure may not be an issue in all problems and does not always provide a complete explanation of crack growth behaviour"* [McClung, 1999]. The work of Vasudevan and co-workers received opposition from McEvily & Ritchie [1998], who illustrated widespread experimental evidence which ran counter to the unified approach. Further opposition was presented by Riemelmoser & Pippan [1999*a*] in which a similar dislocation based analysis to that presented by Vasudevan and co-workers [Louat *et al*, 1993] was in fact shown to exhibit PICC. The difference in the analyses was attributed by Riemelmoser & Pippan [1999a] to a mistake in the reasoning of Louat *et al* [1993]. Specifically, the findings of the dislocation based analyses of Vasudevan and co-workers can be summarised by the statement "*Dislocation flow for the crack is similar to removing matter from the crack and distributing it in the volume ahead of the crack tip. This can only result in opening of the crack*" [Sadananda & Vasudevan, 1998]. They use this reasoning to claim that PICC does not occur, and attribute shielding of the crack tip to the dislocation stress field effect ahead of the crack tip. It is further claimed that earlier results from Weertman [1992] support this conclusion. Riemelmoser & Pippan [1999*b*] do not dispute the claim that crack tip dislocations can only lead to opening of the crack, and cite FE analyses which clearly show non-closure of stationary cracks, as well as their own dislocation based analyses which show the same behaviour. However by moving the crack tip forward with respect to a previous arrangement of crack tip blunting dislocations, premature crack face contact is shown to occur. Riemelmoser & Pippan also dispute the claim that the work of Weertman supports the non-closure conclusion as it does not consider a propagating crack. Vasudevan and co-workers refute the FE evidence for crack closure by claiming that "*If [PICC] exists, [the FE models] should have seen it for a stationary plastic crack as well*" [Sadananda &

Vasudevan, 1998]. This is clearly at odds with the suggested mechanism of PICC [Elber, 1970, 1971] in which the propagation of the fatigue crack into the crack tip plastic zone is a critical aspect.

Notwithstanding the above, the proponents of the unified approach have however continued with their ideas, with the concept receiving strong support in papers presented at the recent conference on *Fatigue Damage in Structural Materials II, Hyannis, USA, 1998*, and being extended to compression-tension [Vasudevan & Sadananda, 1999] and variable amplitude fatigue regimes [Sadananda *et al*, 1999]. The two models of crack driving force, i.e. that based on $\Delta K_{eff} = U\Delta K_{app}$, and that based on ΔK and K_{max}, were shown to be mathematically compatible by Krenn & Morris [1999]. As such, it was suggested by these authors that attention should be focussed on understanding the physical micromechanisms occurring at the crack tip during fatigue crack growth rather than analysis of the global crack driving force or far-field estimates of closure. To this end, sophisticated analysis techniques such as the high resolution computed tomography carried out by Stock and co-workers [Guvenilir & Stock, 1998, Guvenilir *et al*, 1999], where in situ observations of contacting fatigue crack surfaces in the interior of metallic specimens have been made possible, and the high resolution strain measurements made possible by synchotron radiation [Sinclair & Buffiere, 2000], may yield significant insights into the micromechanics of the crack closure process.

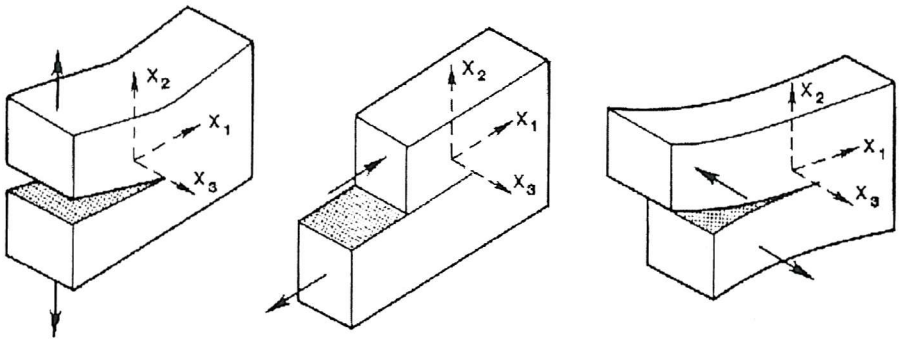

Mode I (opening mode)

Mode II (in-plane shear mode)

Mode III (out-of-plane shear mode)

Figure 2.1. The three modes of loading that can be applied to a crack.

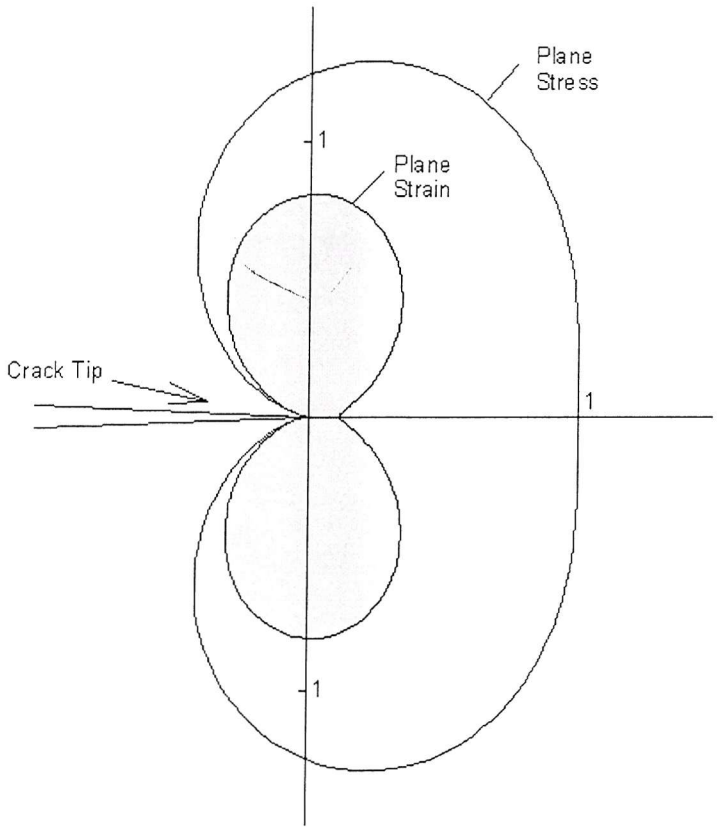

Figure 2.2. Plastic zone shapes predicted by the von Mises criterion.

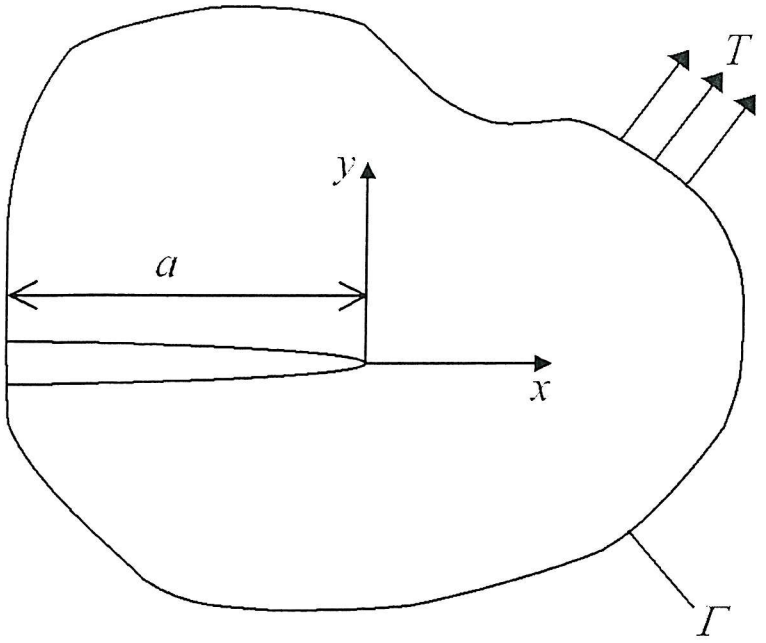

Figure 2.3. A two dimensional body bounded by a curve, Γ.

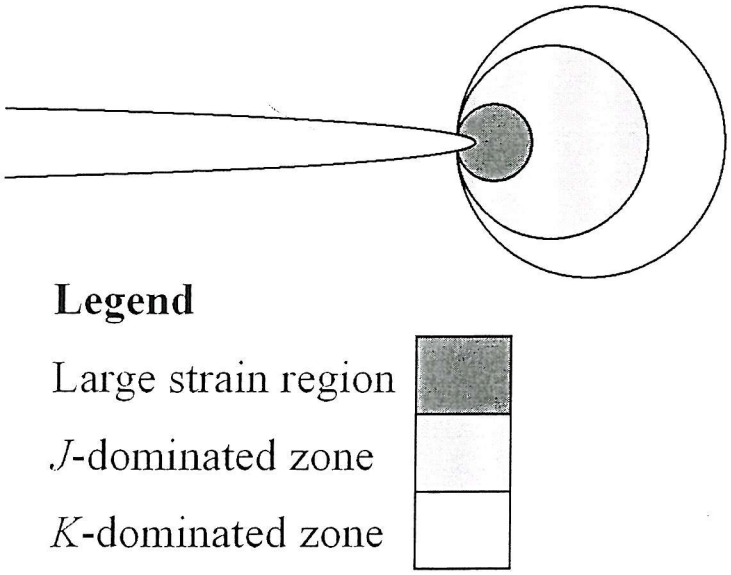

Figure 2.4. Schematic illustration of the crack tip stress fields under small scale yielding conditions. After Anderson [1995].

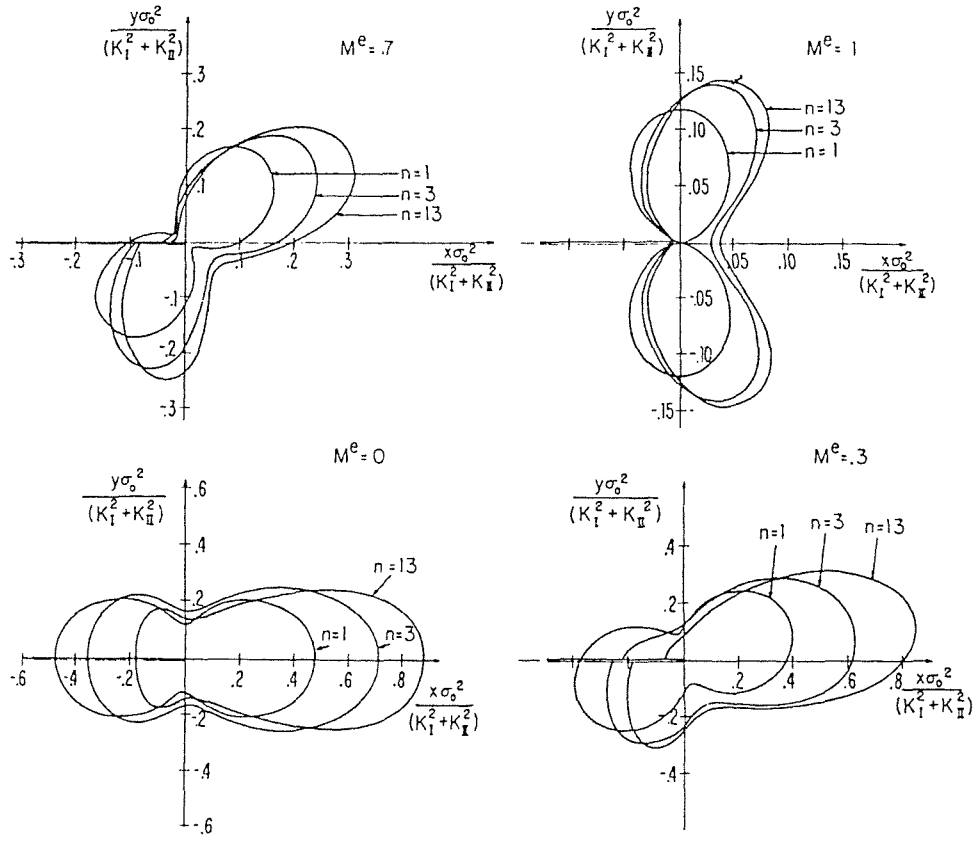

Figure 2.5. Elastic-plastic boundaries for small-scale yielding in plane strain, from Shih, [1974].

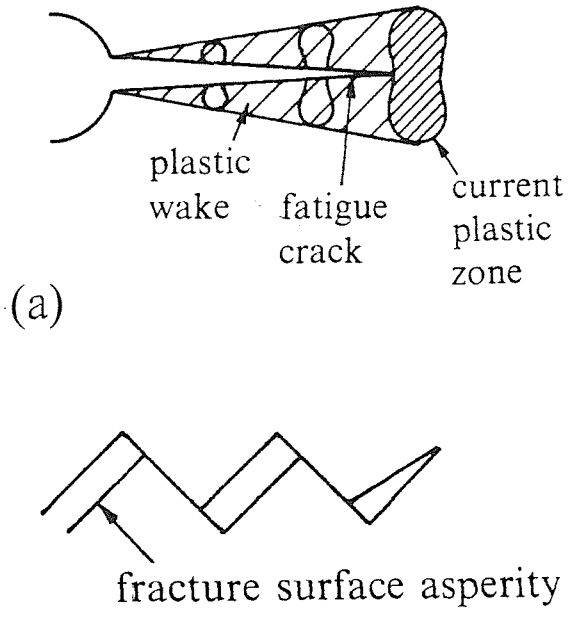

Figure 2.6 Schematic illustration of the retardation of a fatigue crack due to (a) plasticity induced crack closure, and (b) roughness induced crack closure. From Suresh, [1991].

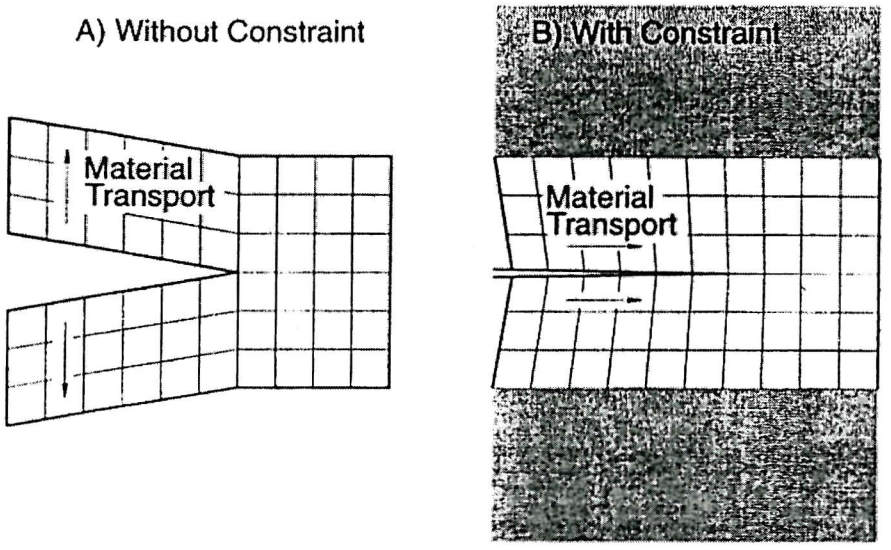

Figure 2.7. Placticity induced crack closure caused by plastic shear deformation in the wake. In (A) the deformation is unconstrained. Addition of the elastci constraint in (B) leads to rotation of the material towards the crack tip, and the possibility of crack closure.

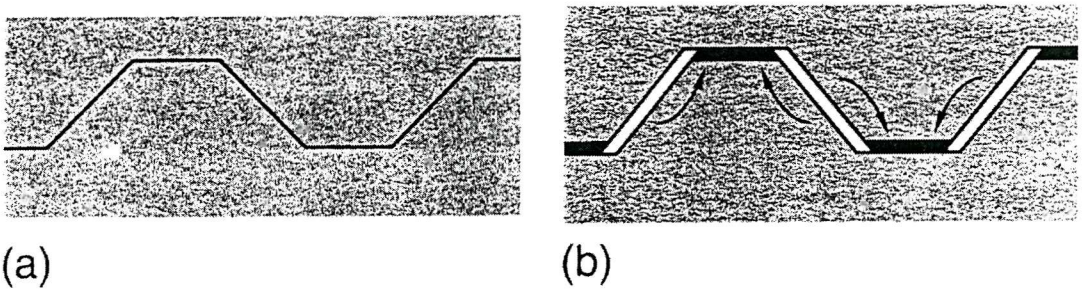

Figure 2.8. Schematic representation of a rough crack: (a) illustrates the perfect fitting of the crack flanks in the absence of plastcity, (b) shows the crack flanks where plastic deformation has caused a reduction of the width of the asperities and an increase in their height, leading to a residual plastic wedge. From Pippan & Riemelmoser, [1998].

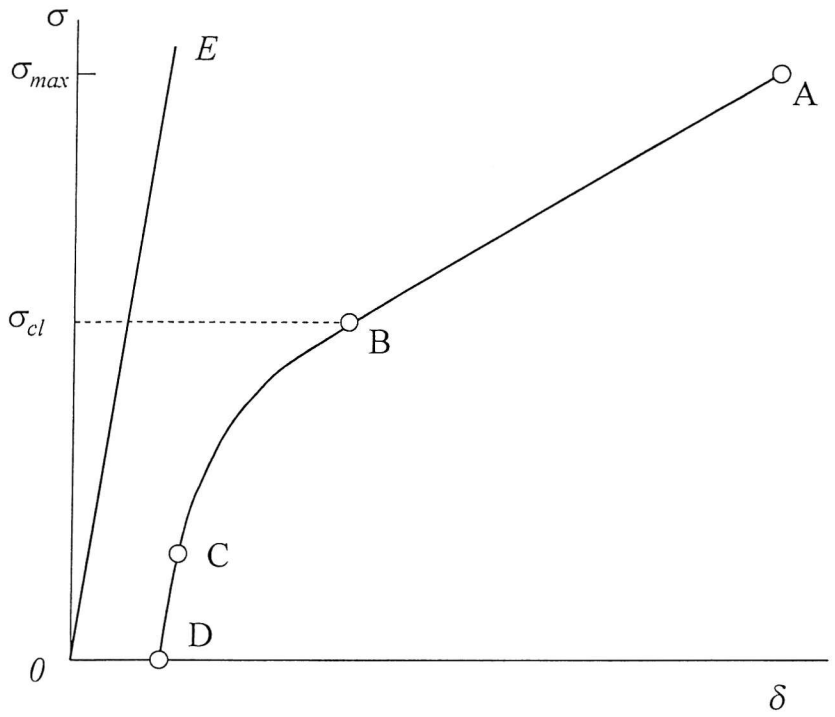

Figure 2.9. Schematic illustration of an idealised compliance curve.

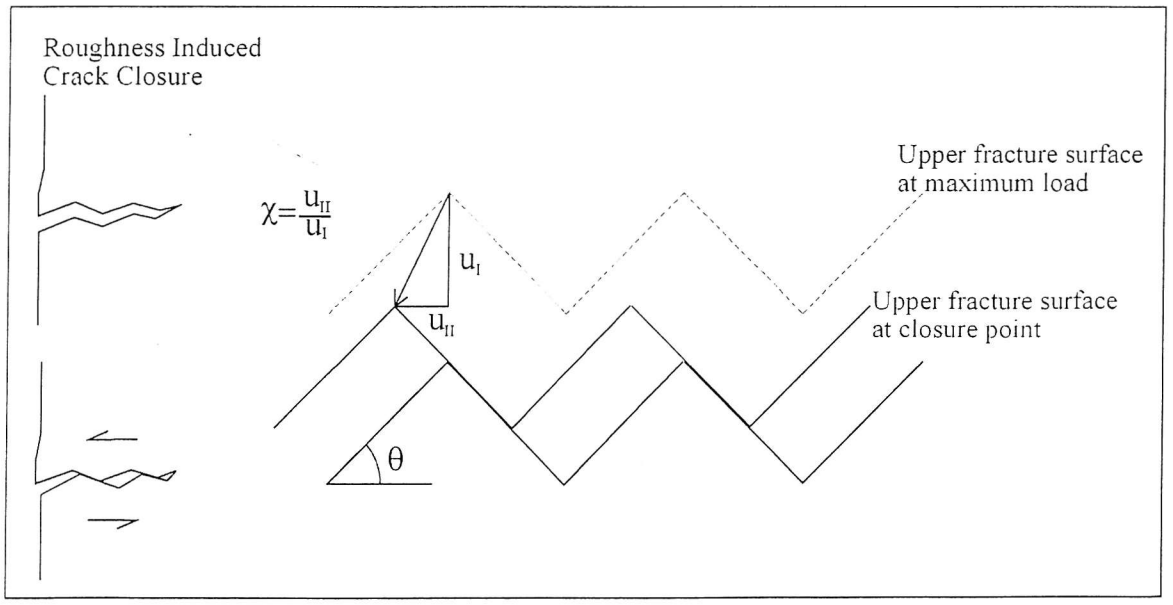

Figure 2.10 Detail of the geometrical model of roughness induced crack closure of Suresh & Ritchie [1982].

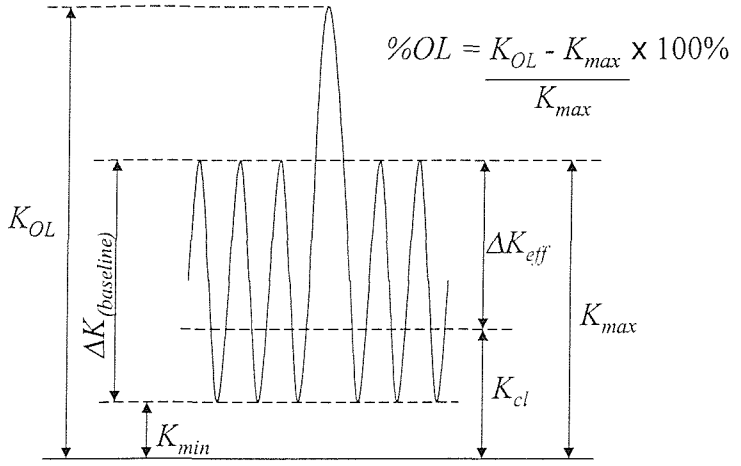

(a)

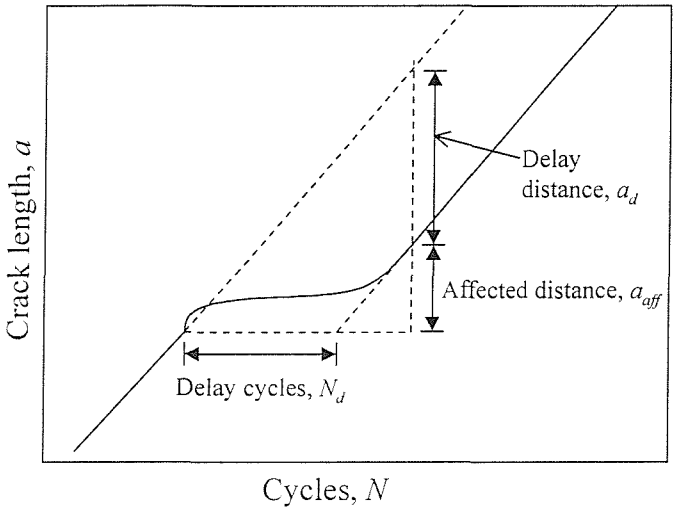

(b)

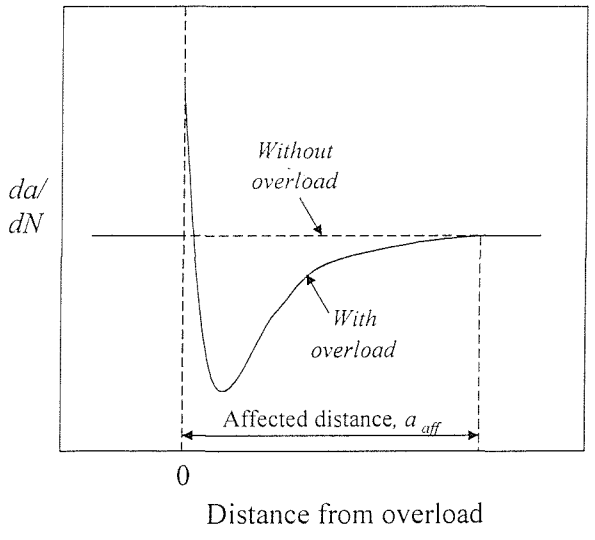

(c)

Figure 2.11 Illustration of the effect of a single spike overload, showing (a) nomenclature, (b) crack length vs number of cycles, and (c) growth rate vs crack length behaviour. After Venkateswara Rao & Ritchie, [1988].

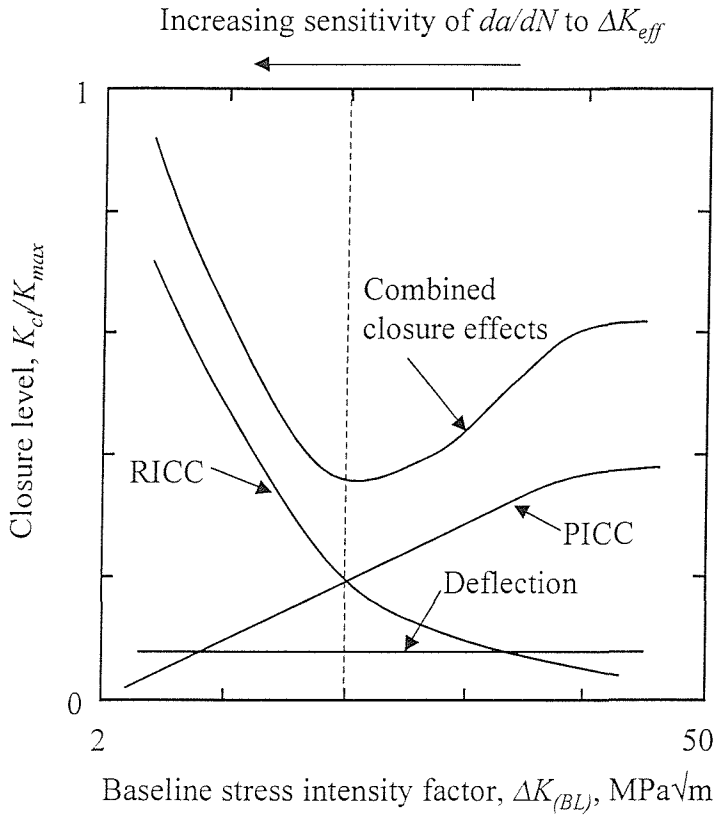

Figure 2.12. Schematic illustration of the variation in crack closure with baseline stress intensity factor range $\Delta K_{(BL)}$,

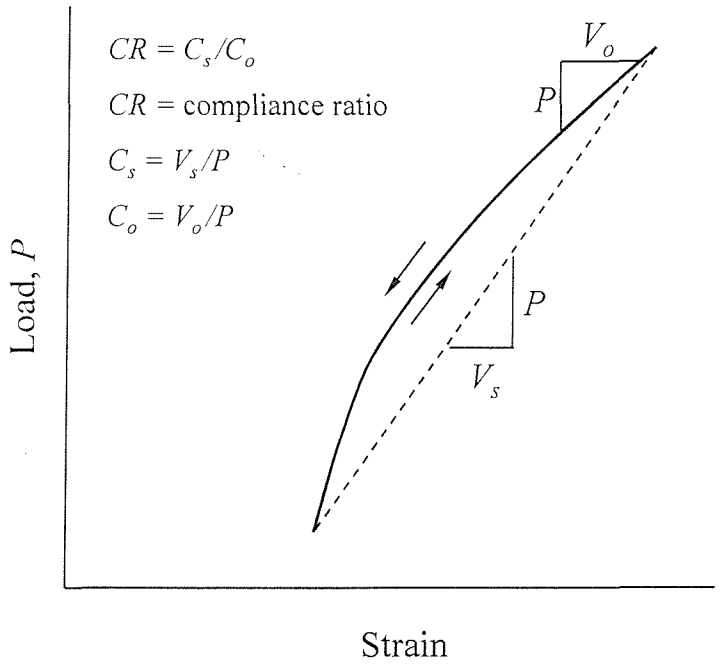

Figure 2.13. Schematic illustration of the use of the compliance ratio technique to quantify crack driving force based on the variation of near-tip elastic strain with applied load.

3 FE modelling of RICC under constant amplitude loading

3.1 Overview

In this chapter, details of the FE models which have been constructed to investigate the phenomenon of RICC are presented. Specifically, the scope of this work is the examination of crack closure arising from a combination of residual plastic deformation and crack deflection, during long fatigue crack growth, under constant amplitude, small-scale yielding conditions, in a damage tolerant aerospace aluminium alloy.

This work builds upon the existing FE models of fatigue crack closure (for undeflected crack growth) presented in the literature. In order to do this, techniques which have previously been implemented in closure specific FE codes, have been incorporated into the general purpose FE code ABAQUS. Extensive verification of the model behaviour has been carried out, along with a detailed investigation of the definition of the closure point. Some additional results of interest, including those relating to the influence of slip bands on RICC, are also presented.

3.2 Design of the model

3.2.1 Material and loading issues

The aim of the modelling work was to investigate closure behaviour which is typically exhibited in damage tolerant aerospace alloys (e.g. 2024-T351, 2124-T351) in the near-threshold fatigue regime. The materials properties chosen to represent this type of alloy were, elastic modulus $E = 74$ GPa, Poisson ratio $\nu = 0.33$, yield stress $\sigma_0 = 370$ MPa [Ritchie *et al*, 1987].

Given that the phenomena of interest occur under small-scale yielding conditions, it can be assumed that there will be minimal influence of specimen geometry. The conventional centre cracked plate (CCP) specimen geometry and the necessary boundary conditions are easily implemented in the FE code, and hence this specimen format was selected. The dimensions chosen were width $W = 75$ mm, initial half crack length $a_0 = 7.6$ mm, and thickness $B = 7.5$ mm.

Given the widely acknowledged role of RICC in plane strain near-threshold crack growth, such loading conditions were of particular interest. As such, ΔK levels of the order of 3-5 MPa$\sqrt{m}$ were primarily investigated (for R-ratios of ~ 0), subject to mesh density considerations (see below).

3.2.2 Crack geometry issues

Any attempt to represent a typical fatigue fracture surface, which includes microscopic roughness, in a FE model will require a certain number of approximations. In order to reduce the complexity of the fracture geometry, a simple zigzag geometry was chosen, where both the crack deflection angle θ, and the length of the crack deflection L (see Figure 3.1 for the definition of these parameters), had constant values. Furthermore, the crack was assumed to deflect only in the plane normal to the thickness direction. That is, the crack exhibited the same deflection angle at all points through the thickness, and hence could be represented as a simple two dimensional model.

Both θ and L (or in fact L/ l_c, where l_c is a characteristic length associated with the plastic deformation in the crack tip region) have been identified as important parameters in the

phenomenon of RICC [Suresh, 1985*b*]. As such, an investigation of the dependence of RICC exhibited by the model on these parameters was considered appropriate. To this end, initial analyses were performed for crack deflection angles of 0°, 30°, 45° and 60°: the length of the deflected section was generally set to 20 μm (exceptions are identified in the text), and the ratio of L/l_c was varied through changes in the applied load. It will be shown in Section 3.2.3 that the element size is dictated by the loading. Hence analyses of large crack deflections for low loading levels can be computationally expensive. As such, the chosen deflection length represents a balance between computational efficiency and the maintaining of a realistic crack morphology. Once the basic model behaviour was established, further model analyses were run where the restrictions of constant deflection angle or length were removed. No attempts were made to model the effects of through-thickness crack deflection.

3.2.3 Implementation

Two-dimensional meshes representing the specimens with embedded deflected cracks as described above were constructed using the commercial pre-processor MSC/PATRAN. These were then implemented as FE models in ABAQUS/Standard 5.8 [ABAQUS, 1998]. The model assumes symmetric crack growth, hence symmetry considerations allowed one half of the specimen to be modelled for deflected crack growth (one quarter for the undeflected crack models). The material properties described above were implemented, with a simple linear kinematic hardening model being assumed ($H = 0.07\,E$, where H is the slope of the plastic line on the stress-strain plot)[1]. As the plastic zone size for the specified loading range can be expected to be much smaller than the specimen thickness, plane strain conditions were assumed.

Up to 10000 first order isoparametric quadrilateral elements (i.e. 4 noded quadrilaterals) were used to discretise one half of the CCP specimen (up to 5000 elements in the quarter model). These elements utilise the selectively reduced-integration technique, which helps to prevent mesh locking and provides an accurate solution in incompressible or nearly incompressible cases, see [Nagtegaal, 1974; ABAQUS, 1998]. There is no particular benefit in using second order elements (i.e. 8 noded quadrilaterals) as the choice of element size is governed by the crack tip plastic zone size, and hence the use of higher order elements will not permit any reduction in mesh density. Typical meshes are illustrated in Figure 3.2.

[1] It may be noted that a number of the results presented here were repeated for isotropic hardening with no significant effect on behaviour being identified.

In modelling closure, plasticity at the crack tip is of particular interest. Special singular crack tip elements were not used in this work. Instead, a fine mesh was employed at the crack tip: in this respect McClung & Sehitoglu's recommendations [1988] (see Section 2.4) for modelling plasticity induced crack closure at $R = 0$ using first order quadrilateral elements were adhered to. As such the maximum element dimension at the crack tip corresponded to one tenth of the plastic zone size, r_p, at maximum load. Under plane strain conditions the Dugdale approximation [1960] gives,

$$r_p = \frac{\pi}{24}\left(\frac{K_{Imax}}{\sigma_0}\right)^2 \tag{3.1}$$

If ΔK is set to 4.6 MPa$\sqrt{m}$, (i.e. to a near threshold stress intensity factor range for a damage tolerant aluminium alloy), and σ_0 is as detailed above, then the plastic zone size will be approximately 20 μm. Hence by setting the crack tip element size to 1 μm, McClung & Sehitoglu's criterion is clearly met. The independence of the model with respect to element size is demonstrated in Section 3.2.4.2.

A procedure for incremental crack propagation was developed along the lines of similar studies in the literature [Newman & Armen, 1975; McClung & Sehitoglu, 1989]. Pairs of opposite nodes along the crack line were initially connected by two (very short) linear spring elements. The first spring element had no stiffness in compression but was very stiff in tension. The second spring element was very stiff in compression, but had no stiffness in tension. Crack propagation was simulated by removing the tension spring element at the crack tip node at maximum load. This allowed the crack to grow one element dimension as the original crack tip nodes were no longer constrained in tension. This process is illustrated schematically in Figure 3.3. The compression springs only acted normal to the crack faces, hence, in common with previous FE analyses of crack closure (e.g. McClung & Sehitoglu, [1989]), friction effects during contact of the crack surfaces were not considered here.

Closure of the crack was determined by monitoring the forces in the compression spring elements behind the tip, in conjunction with the specimen compliance (i.e. plotting the normalised applied stress intensity factor, K/K_{max}, versus displacement, δ, or strain) at various locations analogous to the clip/strain gauges used in experimental closure determination, i.e. at the crack mouth, just behind the crack tip, and on the back face of the specimen. The offset compliance method was used to aid closure determination, i.e. a line fit was made to the upper linear part of the compliance curve which was then subtracted from the observed compliance for the entire load cycle (mathematically, if m_{open} is the gradient of that section of the compliance curve for which the crack is open, then $\delta_{offset} = \delta - m_{open} K/K_{max}$). The

sensitivity of this method depends on the number of decrements in the unloading cycle. Typically, the specimen was unloaded by decrements of one tenth of the applied load, until closure was considered imminent (based on preliminary model runs). Further unloading was then performed using decrements of 0.025 to 0.01 of the applied load.

3.2.4 Verification of model behaviour

To establish confidence in the model results, verification of the model behaviour was undertaken. In particular, the ability of the model to accommodate plane strain plastic deformations, and the response of the model to variations in formulation was investigated. The primary model output which was used as an indicator of model behaviour was the crack face displacements. These are clearly critical to the predicted closure levels, and are an immediate measure of the response of the model to variations in formulation.

3.2.4.1 Incompressible deformation issues

A factor which has arisen in the literature concerning the modelling of plane strain PICC is the accurate modelling of plane strain plastic deformations [McClung *et al*, 1991] (see Section 3.3.1). Nagtegaal [1974] showed that standard first-order isoparametric elements can often produce inaccurate solutions for elastic-plastic material behaviour, under plane strain conditions. Briefly, in a regular mesh of 4-noded rectangular parametric elements, the displacement increments, $\dot{u}$, are of the form,

$$\dot{u} = \begin{Bmatrix} \dot{u}_x \\ \dot{u}_y \end{Bmatrix} = \boldsymbol{a} + \boldsymbol{b}x + \boldsymbol{c}y + \boldsymbol{d}xy, \qquad (3.2)$$

where x and y are Cartesian co-ordinates and $\boldsymbol{a}$, $\boldsymbol{b}$, etc. are vectors expressed in terms of the nodal co-ordinates and velocities. Plastic (i.e. incompressible) deformation under plane strain requires,

$$\dot{\varepsilon}_{xx} + \dot{\varepsilon}_{yy} = \frac{\partial \dot{u}_x}{\partial x} + \frac{\partial \dot{u}_y}{\partial y} = 0 \qquad (3.3)$$

where $\dot{\varepsilon}_{xx}$ and $\dot{\varepsilon}_{yy}$ are the strain increments in the x and y directions. This requires,

$$\boldsymbol{d} = 0, \qquad \boldsymbol{b} + \boldsymbol{c} = 0.$$

Hence, $\dot{\varepsilon}_{xx}$ and $\dot{\varepsilon}_{yy}$ are forced to be constant throughout all elements of the mesh. Clearly this is not a realistic constraint. However, modifications to the FE formulation can be implemented to eliminate the artificial constraint on the elements, and allow numerically accurate solutions. In ABAQUS, this is achieved through the selectively reduced-integration technique, whereby reduced integration is used for volumetric strain, and full integration for the deviatoric strain.

Over-constraint of the elements, in the manner described, manifests itself in the failure of the FE model to exhibit a limit load during fully plastic deformation of a perfectly plastic material. Hence, the prediction of the correct limit load can be used as a verification of the elements ability to correctly represent plastic plane strain deformation. For the CCP specimen, as used in the analyses, the limit load is given as twice the yield stress in shear on the net section (i.e. the uncracked ligament) [e.g. see Anderson, 1995]. In Figure 3.4, the load-deflection curve predicted by the FE solution, for identical model geometry, boundary conditions, and FE formulation as used in the closure analyses, and with elastic-perfectly plastic material behaviour, is shown in comparison to the analytically predicted limit load, where $u^{LOAD\ POINT}$ is the displacement of the point at which the load is applied. The ability of the selectively reduced-integration elements to model the incompressible material behaviour is clearly verified.

3.2.4.2 Effect of element size

Inadequate mesh density in the crack tip region was shown by McClung & Sehitoglu [1988] to lead to spuriously high closure levels, particularly due to the inability of the model to capture reverse crack tip plastic deformation. This led to the formulation of a crack tip element size criterion, which has been adopted in this work, as discussed in section 3.2.3. However, in order to verify that this criterion is adequate for the present model, a set of simple test analyses were performed. Firstly, the analysis was run using the mesh of the undeflected crack (with a ratio of crack tip plastic zone, r_p, to element size, L_e, of 15), and the crack face displacements were recorded at K_{max}, 0.5 K_{max} and K_{min} (= 0). The analysis was then repeated, for twice the crack tip mesh density ($r_p/L_e = 30$). From the results shown in Figure 3.5, it can be seen that the two analyses give very similar crack opening displacements. The only region where the mesh density appears to have any significant effect is for the element immediately behind the crack tip. This mesh dependent behaviour of the near-tip elements is discussed in more detail in section 3.3.1.

3.2.4.3 Effect of spring element stiffness

In the formulation of the model, 'fictitious' spring elements were used to enforce the changing boundary conditions along the line of the crack. The stiffness of these spring elements was set to an arbitrarily high value. However, it is necessary to check that the response of the model is not unduly influenced by changes in the spring element formulation. This is illustrated in Figure 3.6, by means of crack opening displacements, for the standard spring stiffness value of 7.4×10^8 N m^{-1}, and for a spring stiffness of two orders of magnitude more and less. It can be seen that the lower spring stiffness does not adequately enforce the

boundary conditions, and that large positive displacements exist at and ahead of the nominal crack tip. There is no change in behaviour on increasing the spring stiffness from the standard value, indicating that the standard value is indeed sufficient.

3.2.4.4 Effect of the choice of hardening rule

As previously detailed, a kinematic hardening model was selected to give the best approximation to the crack tip strain hardening behaviour. However, strain hardening effects are not considered to be a primary factor in crack closure, and the behaviour of the model should not be strongly dependent upon the choice of hardening rule. Verification of this is shown in Figure 3.7, which shows the crack opening displacement for analyses using kinematic and isotropic hardening, and an analysis using elastic-perfectly plastic material behaviour. It can be seen that the differences in the behaviour is very slight, indicating that the choice of hardening model is not a critical factor.

3.2.4.5 Effect of the point of node release

In the present analysis the point of node release, corresponding to crack propagation, is timed to occur at maximum load. Some variation in closure behaviour has been noted in the literature however [e.g. McClung & Sehitoglu, 1989], when the crack tip node has been released at other points of the load cycle. It has been argued [e.g. Ashbaugh *et al*, 1997] that node release at maximum load is more appropriate, as an approximation to 'real' fatigue crack growth behaviour. However, it must be recognised that the FE model in no way replicates the real crack growth mechanisms (the increment of crack growth per cycle in the near-threshold region is of the order of 10^{-8} - 10^{-6} mm/cycle, compared to the increments of 10^{-3} mm/cycle used in the FE model), and is better thought of merely as a means of translating the zone of crack tip plastic deformation with the crack tip. With this in mind, it is hoped that the point in the load cycle at which the node is released should not have a large influence on the subsequent behaviour. In order to investigate any effects of the nodal release point in the present analysis, separate models were run with nodal release occurring at maximum load (scheme A), at minimum load (B), during the loading step (C), and during the unloading step (D). The subsequent crack profiles are shown in Figure 3.8. Upon first inspection, the predicted crack opening for schemes A and C seem quite different to schemes B and D. This may be explained by considering that at maximum load, schemes B and D are effectively one propagation step behind schemes A and C. During the next load step, the crack profile in schemes B and D will be similar to those of scheme A and C, as indicated by the arrows. That is, unlike the work of McClung & Sehitoglu [1989], no dependence on nodal release point is found. This may be due to the different definitions of crack closure used in the present analysis and that of McClung & Sehitoglu [1989] (see Section 3.3.1).

3.2.4.6 Effect of increment size

In the analysis, the minimum number of increments used in solving any step of the analysis (i.e. loading, debonding and unloading) was set to 10. Given that the problem is inherently non-linear (due to material behaviour and crack face contact considerations), this incremental approach is necessary to be able to accurately solve each step. It is important therefore to verify that the solution is independent of the number of increments used. In Figure 3.9 the crack face displacements are shown for analyses using 5, 10 and 20 increments per step. It can be seen that there is only a very slight increase in predicted crack opening when the number of increments is increased. As such, the chosen minimum number of increments was considered to be sufficient.

3.3 Results and discussion

3.3.1 Straight cracks

In Figure 3.10 the response of the spring elements behind the crack tip and the associated offset compliance plots are shown for an undeflected crack grown under constant applied stress by 100 μm, equivalent to five maximum plastic zone diameters, for plane strain conditions. From Figure 3.10(a) it can be seen that the first spring element behind the crack tip goes into compression (i.e. the crack tip is closed at that point) at 0.25 of the maximum applied stress intensity factor, K_{max}. Compression of spring elements further behind the crack tip does not occur until significantly later in the unloading process (K/K_{max} = 0.07), when the crack becomes closed a short distance (5 to 20 μm) ahead of the pre-crack tip, whilst remaining open closer to the propagated crack tip (see Figure 3.11). By considering Figure 3.10(b), it is evident that closure at the first node behind the crack tip does not affect the overall specimen compliance. However a deviation in this plot occurs at K/K_{max} = 0.07, coinciding with the contact further behind the crack tip. It should be noted that the particular behaviour of the first element behind the tip was eliminated by cycling the crack on reaching the final crack length between maximum and minimum load, without any crack propagation. This cycling of the crack should ensure that the crack tip plasticity is dominated by the loading and not the crack propagation scheme used in the model. After 2 such cycles the first node behind the tip no longer comes into contact at all. However, the remaining contact in the crack wake is relatively unaffected by this procedure, as shown in Figure 3.11.

Assessing the significance of contact at the first node behind the crack tip in relation to results in the literature is difficult, as many authors fail to provide detailed information on the manner of crack face contact in their models [Blom & Holm, 1985, Llorca & Sanchez Galvez, 1990, Ashbaugh *et al*, 1997, Ritchie *et al*, 1987, Lalor & Sehitoglu, 1988]. For those authors who have published this information, the results of Fleck & Newman [1988], Fleck [1986], Biner *et al* [1994] and Wei & James [2000] all indicate that anomalous contact of the first node behind the tip occurs in plane strain models of PICC (anomalous in the sense that only the near-tip element goes into compression on unloading). More physically plausible plane strain PICC behaviour, with nodal contact building up gradually along several nodes behind the crack tip during unloading, has been reported by Sehitoglu & Sun [1991] and McClung *et al* [1991] when using a specific FE code and model formulation. To the authors knowledge, there are no other references which explicitly report such 'zipping up' behaviour

of crack tips due to PICC under plane strain conditions. In rationalising this, McClung *et al* [1991] note that an absence of progressive contact behind the crack tip in FE models may be attributable to element 'locking' problems due to the stress gradients at a plane strain crack tip (i.e. the inability of the FE model to correctly model the incompressible plane strain deformation, as discussed in Section 3.2.4.1): this cannot be considered to be the case in the present work however, as element locking was not detected in the analyses (attributable to the use of selectively reduced-integration elements). The cycling of the quasi-static crack tip (described above) leads to the near-tip strains being dominated by the loading and unloading procedure, as opposed to the crack propagation process. As such, this can be considered to lead to a more realistic representation of the actual fatigue crack tip strains. Given that this procedure eradicates the near-tip closure, the incidence of such closure can be considered to be an artefact of the artificial crack propagation process used, and not a true physical effect. The present work would therefore support the assertion of Fleck [1986, Fleck & Newman, 1988] that very near tip closure effects in plane strain FE models of PICC may be anomalous and should be treated with caution. Whilst the present models remain essentially simplified as a representation of materials behaviour at a real crack tip, it is concluded that previous assertions on the incidence of PICC in plane strain from FE models should not be regarded as proof of its occurrence.

3.3.2 Deflected cracks

The effect of periodic crack deflection on K_{cl}/K_{max} under plane strain loading at $\Delta K = 4.6$ MPa$\sqrt{m}$ can be seen from the plot of the deformed mesh of a 45° deflected crack at $K < K_{cl}$ in Figure 3.12. Closure can be seen to have occurred at discrete points near the asperity tips, with the bulk of the crack remaining open, as noted experimentally by Walker & Beevers [1979]. The response of the spring elements behind the tip and the offset compliance plot is shown in Figure 3.13. The first spring elements that go into compression (i.e. the points of first contact) are those at the tips of previous crack deflections (i.e. at the asperities), which coincides with the onset of non-linearity in the offset compliance. As such it would appear that the discontinuous contact 'problem' and the above discussion on crack closure point definition in undeflected plane strain cracks does not influence the behaviour of the deflected cracks and it is therefore assumed that the deflected crack closure behaviour illustrated in Figure 3.12 is indeed physically realistic. Given the clear build up of crack contact with nonlinearity in compliance, the closure point in these models will be defined in terms in terms of first asperity contact.

From Figure 3.14, which shows the variation in closure levels due to growth along the deflected crack path, it is evident that the closure levels increase strongly with deflection angle. It appears that quasi-stabilised levels of closure are reached when the crack has propagated through the first two deflections. The closure levels are at a maximum immediately following a deflection, and then drop off steadily as the crack tip moves away from the point of deflection.

3.3.2.1 Mechanistic assessment

An important observation from these results is the sense of the shear displacements giving rise to asperity contact. In particular it may be seen that the direction of the relative displacements of the upper and lower fracture surfaces at each asperity tip changes along the crack wake. At point 'A' in Figure 3.12 the lower fracture surface is displaced away from the crack tip (in relation to the upper fracture surface), whilst at point 'B' it is displaced towards the crack tip. It may then be seen that the shear displacements giving rise to closure along the crack wake cannot be 'global' displacements of the upper and lower fracture surfaces due to mixed mode behaviour at the active crack tip. The asperity shear displacements in Figure 3.12 can in fact only arise from local residual strains from the crack propagation process. The asperity displacements and contacts observed in the present models are therefore somewhat different to the conventional representation of RICC (as illustrated by the Suresh model in Figure 3.15). The behaviour of the present models may be rationalised as follows: when a simple deflected crack tip is loaded as shown in Figure 3.16(a), a permanent plastic shear deformation is produced in the direction/sense shown. On unloading, a degree of reverse plasticity will occur, although a net residual deformation will remain in the direction of the original loading (Figure 3.16(b)). As such, the crack tip will be held in a 'compressive' shear (of opposite sense to the loading shear) by the surrounding elastic material when unloading occurs, exactly analogous to the compressive load generated by crack tip plasticity when a simple mode I crack is unloaded. When the crack undergoes a deflection, as shown in Figure 3.16(c), this residual plastic strain/compressive loading may be seen to promote closure on the forward edge of each asperity tip, as identified in Figure 3.12.

To investigate the above process, various simplified models were assessed, see Figures 3.17-3.18. Figure 3.17 illustrates the unloaded condition of a deflected crack where the crack path was simply 'cut' without a propagation process, with the crack then being loaded and unloaded once, with the resultant plastic deformation producing a degree of shear offset along the asperities. The shear is of identical direction for all asperities, consistent with deformation at the tip being the only source of shear offset, but is in fact insufficient for closure to occur due to the associated residual opening displacements (displacements are

greatly magnified in the diagram). In Figure 3.18 the crack has been propagated with loading and unloading only being applied at each crack turning point. For the final crack length shown the crack is simply loaded and unloaded elastically, i.e. no shear offset can be generated at the tip. Closure behaviour is seen to be closely analogous to that in Figure 3.12, confirming the role of residual plastic shear displacements along the crack wake in producing closure. It may be seen that the predominant closure process is in fact closely analogous to plasticity induced closure in mode I loading, although it does rely on crack path roughness to generate the necessary shear displacements. It is important to note that plane stress conditions are not particularly necessary to the asperity contact process shown in Figure 3.16 (i.e. as seen in mode I plasticity induced closure), as the critical deformations are shear in nature and do not require through-thickness contraction for volume conservation.

3.3.3 Mechanistic implications and physical interpretation

In the previous section a new mechanism by which fatigue crack deflection in an elastic-plastic material can lead to crack closure was outlined. In some respects this mechanism can be seen to be similar to that qualitatively described by Pippan *et al* [1994] as a potential origin of PICC under plane strain conditions, in which crack deflection is an essential feature (illustrated schematically in Figure 2.8). This mechanism was considered by Pippan *et al* [1994] to be PICC rather than RICC given that no residual mode II offset is necessary for its operation, although the reliance on surface roughness makes such a distinction clearly moot. In Figure 3.19 experimental observations from Pippan *et al* [1994] which were performed to assess this mechanism are shown. These micrographs show the midsection crack profiles (i.e. specimen cut in half following the fatigue crack growth). It can be seen that crack closure has occurred at the tips of the asperities, with 'cavities' present indicating that plastic flow of the asperity material has occurred. Whilst the present models identify the particular role of shear strains in generating asperity contact, it may be seen that the underlying theme of residual plastic strains giving rise to asperity contact is closely consistent with the qualitative observations of Pippan *et al* [1994].

The present proposed mechanism can be considered in relation to the mechanism by which RICC has conventionally been considered to occur. As has been discussed, the conventional mechanism of RICC relies on a global residual mode II offset of the fracture surfaces to produce crack closure. However the origin and importance of this global mode II displacement requires some consideration. The origin of the offset is generally attributed to the mode II component of irreversible deformation occurring at the crack tip (illustrated schematically in Figure 3.20) [e.g. Minakawa & McEvily, 1981, Ravichandran, 1990]. If this

is the case, the local displacements giving rise to the global mode II displacement can be expected to be of the order of the crack tip opening distance. The distance over which this mode II displacement will have a significant effect on the displacements of the surrounding material can therefore be expected to be of the same order of magnitude as the displacement itself. Any mode II displacement originating from irreversible deformation ahead of the crack tip can be expected to have a relatively local effect, i.e. significantly smaller than typical asperity sizes thought to give rise to RICC. This point is particularly illustrated by the model in Figure 3.17. Under the mechanism of RICC proposed here, mode II displacements exist in the crack wake due to the propagation of the crack through material which has undergone previous plastic deformation. As such the important mode II displacements specifically exist at the crack wake asperities, and do not require the 'translation' of small tip displacements over large distances into what is a predominantly elastically deforming body (i.e. under the near-threshold LEFM conditions of interest here).

Problems associated with generating global mode II displacements from crack tip displacements in real 3 dimensional crack fronts are illustrated in Figure 3.21. As shown, the angle of crack deflection in a real sample will vary through the thickness, with deflections occurring above and below the nominal mode I growth plane. As such, whilst the section of the crack labelled A in Figure 3.21 may favour a global mode II displacement of one sense, the neighbouring section labelled B will lead to a mode II displacement of the opposite sense. As such, the ability of crack tip displacements to produce global offsets at significant distances into the crack wake may be seen to be distinctly constrained.

Experimental evidence has been offered in support of the conventional mechanism of RICC, generally in the form of images of specimen surfaces where fracture surface contact can be seen to have occurred as an apparent result of a global shear offset, e.g. see Figure 3.22. However, these surface representations do not necessarily correspond with the fracture surface displacements in the centre of the specimen. Firstly, in the plane stress region of the crack (i.e. at the specimen surface), the crack is relatively unconstrained and is often deflected in the loading direction (i.e. shear lip formation, see Figure 3.23(a)). Furthermore, there is often a bowing of the crack front in this region, as shown in Figure 3.23(b). These two factors combine to produce distinct local mode II/III displacements in the surface region that may lead to the apparent mismatch of fracture surface asperities. These factors will not be significant for the internal plane strain regions. As such, the existence of a global fracture surface offset at the specimen surface does not necessarily imply the same offset behaviour in the centre of the specimen.

It is interesting to consider the conventional mechanism of RICC in terms of the results of Fitzpatrick *et al* [1996] which show the absence of RICC during deflected fatigue crack growth in PMMA, but significant levels of closure due to deflected crack growth in aluminium alloy 2014-T6. In the PMMA sample the loading conditions are such that plastic deformation does not occur, however the possibility for crack face contact via a shear induced global fracture surface offset is present. In the aluminium alloy sample plastic deformation of crack tip material during fatigue crack growth does occur, and is considered by the authors to be the source of crack closure. The authors use these results to support their own contention that a global displacement of the fracture surfaces (induced by mode II displacements at the crack tip) cannot alone lead to RICC, in keeping with the present analyses.

The manner in which closure occurs in the present FE models is somewhat different from the results of a similar study of RICC by Llorca [1992]. However, it should be noted that the present work does not require the explanation of crack closure put forward by Llorca, whereby a change in the mode mixity from the loading cycle to the unloading cycle arises due to the intervening propagation of the crack, leading to a residual displacement of the crack flanks. This explanation is questionable to some extent, given that in a real near-threshold fatigue crack the increment of crack growth is very small in relation to typical crack deflection distances, and hence the change in mixity during any load/unload cycle may be expected to be negligible.

3.3.4 Quantitative assessment of closure predictions

The dependence on deflection angle of the closure levels may be compared to the simple analytical model of RICC of Suresh & Ritchie [1982] described in Section 2.3.2, for various values of χ, as shown in Figure 3.24 with the FE results being represented by the minimum, maximum, and mean quasi-stabilised closure levels. It can be seen that there is no single value of χ which accurately reflects the dependence on the deflection angle of the present results. However, given that the mechanism by which closure is occurring is governed by shear deformation (independent of whether or not one considers the conventional 'global shear' mechanism or the present 'residual shear' mechanism), the value of χ would itself be expected to be dependent on the crack deflection angle; i.e. the extent of any shear displacements will be dependent on the mode II stress intensity factors at the crack tip, which, under far-field mode I loading, will increase with increasing deflection angle. Values of χ have been evaluated from the FE results, and are shown in Table 1. The data presented

are for the first asperity behind the tip, at which closure occurs first and which can be expected to be the most important asperity in controlling the closure process. It can be seen that the actual values of χ are close to those required to produce comparable closure levels from the Suresh and Ritchie model, and approach the χ value of 0.3 suggested by Suresh and Ritchie for crack growth in high strength Al alloy plate.

In terms of the physical relevance of the present models, it is of course difficult to compare the results to experimental data in the literature given the considerable variability that exists in closure measurement [Phillips, 1989, 1993], and the relatively idealised crack morphology used here. In terms of effecting a comparison, Al-Li alloys are of some interest. In the unrecrystallised plate form, these alloys exhibit strong textures arising from the processing route [Barlat *et al*, 1994], i.e. the crystallographic axes of the grains are grouped closely about certain preferred directions. In Al-Li plate at the mid thickness this is generally a {110}<112> brass type texture, i.e. the rolling plane parallel to a {110} plane, and the rolling direction parallel to a <112> direction. This results in highly anisotropic mechanical properties in the material. The intensity of this texture varies through the plate thickness leading to significant variations in the through-thickness properties. The anisotropy of these Al-Li alloys is further enhanced by mechanical fibering, with unrecrystallised microstructures consisting of coarse pancake shape grains with typical grain dimensions being an order of magnitude greater in the L direction than the S direction. Importantly, these alloys also exhibit a propensity for strain localisation which may promote strong stage I cracking at loading levels well above the crack growth threshold [Sinclair & Gregson, 1994]. The fatigue crack propagation behaviour of these materials is found to be strongly influenced by the orientation of the nominal mode I crack growth plane and direction relative to these slip planes, the grain boundaries and the material texture [Sinclair & Gregson, 1994]. In strongly textured wrought material fatigue crack growth may lead to exceptionally regular crack development e.g. see Figure 3.25, corresponding to crack growth in commercial AA8090 plate [Liu *et al*, 1998]. Work by Liu *et al* [1998] on TL orientation tests in brass textured plate has shown deflection angles to be close to 60° (due to the preferred {111} plane orientations), with corresponding near-threshold closure levels being measured as ~0.7, consistent with similar data in the literature [Venkateswara Rao & Ritchie, 1992]. As such, the K_{cl} predictions of the present FE models may be seen to be relatively low (by approximately 35%, based on peak K_{cl} values in Figure 3.14), although it is important to recognise that: (1) there is still a significant degree of crack path irregularity in Figure 3.25, (2) the effects of through-thickness crack deflection are not addressed in this 2 dimensional model, (3) the present models do not include environmental contributions to crack tip

irreversibility, and (4) the results in Figure 3.14 assume a simple homogeneous plastic deformation mode which clearly differs from the intrinsically heterogeneous slip band behaviour giving rise to the observed crack paths.

3.4 Additional mechanistic assessment

3.4.1 Effect of slip heterogeneity on RICC

In planar slip materials, plastic deformation can be highly localised to bands of intense shear ahead of the crack tip [Brechet *et al*, 1987]. Such behaviour is known to favour extensive stage I type crack growth, as noted in relation to Al-Li alloys in the previous section. The incidence of slip band formation and associated crack growth is very clearly illustrated in Figure 3.26 for a Ni-based superalloy [Reed, 1999]. The marked shear strain concentration of the slip bands may be seen in the offsets in the etched γ' (Ni_3Al) precipitates along the individual slip bands. Given the importance of shear strains in RICC, such behaviour may be of some relevance to the closure process.

As a relatively simple simulation of the presence of slip heterogeneity associated with planar slip bands ahead of a crack tip, the properties of the tension spring elements ahead of the propagating crack tip in the present models were modified to restrain the nodes normal to the line of the crack only, i.e. shear displacement of the nodes could then occur. To restrain the nodes in shear, additional rigid-perfectly plastic truss elements were inserted. By controlling the yield stress of these truss elements, the effective critical resolved shear stress (*CRSS*) along the crack propagation direction was varied. The *CRSS* of the slip band plane of area A_{band} was represented by n truss elements of cross sectional area A_{truss}. Hence an area of A_{band}/n was associated with each truss element. A_{truss} was set to be equal to A_{band}/n, thus the yield stress of the truss element was set equal to the *CRSS* of the plane. To simulate a local strain softening of the material in the slip band (i.e. representing the precipitate shearing process), the yield stress of the truss element was set to $\lambda\tau_0$, where λ is a constant specifying the relative strength of the slip band and bulk material (i.e. $\lambda < 1$, for slip band softening) and τ_0 is the bulk CRSS. The construction of the slip band model is illustrated in Figure 3.27. It should be noted that in this model the geometry of the slip band is defined by the geometry of the predefined crack path (i.e. secondary slip bands are not included), and the single band that extends ahead of the crack tip at any point is constrained to the distance to the next (pre-determined) deflection point.

The influence of such simulated slip bands ahead of the crack tip is shown in Figure 3.28, for a 60° deflected crack after the onset of closure, with the constant λ set to ½, i.e. τ_0 in the slip band is half that of the bulk material. It can be seen that ahead of the crack tip a significant

residual shear offset has developed (c.f. Figure 3.26). The effect that this offset has on the closure levels can be seen by comparison of the predictions of the slip band model to those of the standard models, as shown in Figure 3.29. For the 30° deflected crack the effect of the simulated slip band is fairly small, leading to an 18 % increase in the maximum closure stress. With increasing angle the effect becomes more significant leading to a 40 % increase in closure levels for the 60° deflected crack. In all cases the closure levels return to those of the standard model immediately prior to a deflection. This is due to the active slip band effectively ending at the next deflection point, therefore as the crack approaches the next deflection point the slip band effect is essentially removed by the surrounding constraint. Whilst this represents a quite simple approximation to the presence of a strain softened slip band ahead of a crack tip, it may be seen that there is an increase in closure levels to values which are more consistent with those determined experimentally.

Assessment was also carried out of the dependence of the closure behaviour on the relative strength of the slip band. The analysis was performed for the 45° deflected crack with values of λ ranging from 1 (i.e. the band is effectively as strong as the bulk material) to 0.01 (i.e. the yield stress in the band is just 1 % of that of the bulk material). The results are shown in Figure 3.30 in terms of the mean closure stress intensity factor. It is clear that as the relative strength of the band diminishes there is an increase in the observed closure levels resulting from greater shear offset at the tip. It is important to note that the strain fields associated with a slip band will not be a simple function of the relative yield stress of the slip band and bulk material, but rather are a the result of a complex interaction between precipitate shear and substructure development. The present λ parameter should be seen as an indicator of strain localisation and not as a full physical description of the process.

3.4.2 Asperity size effects

In the results presented in previous sections, the length of the deflected sections of the crack (i.e. the asperity size) and the applied load have been kept constant. Various authors have related apparent closure behaviour in real materials to the scale of fracture surface asperities (e.g. the direct correlation between the standard deviation of asperity height and the closure level, proposed by Wasen *et al* [1988], see Section 2.3.2). The potential effects of a variation in the size of asperity have therefore been directly investigated in a series of FE models. The deflection lengths and loading levels used are detailed in Table 2. All analyses were performed using a crack deflection angle of 45°, with $R = 0$. In Figure 3.31 the predicted closure levels from these models, in terms of maximum, minimum and mean values, are

plotted against normalised deflection lengths, L/r_p. It can particularly be seen that for small relative asperity sizes, the closure levels are low, with little difference between the minimum and maximum values (i.e. the peak/trough behaviour exhibited in Figure 3.14 does not occur). As the relative size of the asperities increases, there is an increase in the closure levels, up to a deflection length of approximately 1.5 r_p, after which the closure levels reach a plateau. This result is consistent with the proposed crack closure mechanism, detailed in section 3.3.2. That is, the extent of the residual asperity deformation, and hence the level of crack closure, is governed by the local shear loading near the points of the crack deflections, and as such is not a strong function of asperity size, (but is a strong function of deflection angle, as previously noted). However, for small values of L/r_p, a decrease in the closure levels is observed. Such behaviour would be consistent with the RICC effects disappearing as the fracture surface tends to an undeflected form as asperities become vanishingly small. Physical interpretation of how closure levels vary when the active crack tip is within the crack tip plastic zone of a prior asperity turning point (i.e. what tends to dominate as L becomes smaller than r_p) is addressed in the following chapter.

It is interesting to consider the present closure results in relation to experimental closure results obtained by Xu *et al* [2000*a*], for fatigue crack growth in aluminium alloy 2024-T351, and an advanced variant 2024A-T351. The observed closure in this study was principally attributed to RICC. The measured closure levels for the two materials are shown in Figure 3.32. Fractographic studies revealed that the larger grained 2024A exhibited considerably larger fracture surface asperities than the 2024. The fact that threshold closure values converge whilst facet size was larger in the 2024A is clearly consistent with the results in Figure 3.31 as L/r_p values become large at threshold for both materials. It is difficult to quantitatively interpret the results in Figure 3.32 for higher ΔK levels, as the extent of facetting drops off more rapidly in the 2024 with increasing ΔK compared to the 2024A, (both are fully facetted at threshold, however).

3.4.3 Variable crack geometry effects

The stereology of realistically representing crack paths in conventional commercial materials is clearly an extensive area of investigation in itself. Whilst a thorough assessment of all possible geometrical parameters is beyond the scope of this thesis, first order investigation of deflection angle and facet size is clearly valuable, particularly in relation to the assertion of Llorca [1992] that variable crack deflection angles along the crack path may lead to greatly increased levels of crack closure.

3.4.3.1 Deflection angle

All of the models discussed so far have utilised constant deflection angles and lengths along the crack path. However, real crack paths do of course exhibit a range of crack deflection angles, and the possibility that increased crack closure levels may arise from such varying crack deflection angles has been suggested [Llorca, 1992]. To investigate such effects , an FE model was constructed for a crack undergoing variable angle crack deflections. The crack path used in this analysis is illustrated schematically in Figure 3.33, and undergoes successive deflections through angles of 45°, 45°, 45°, 30°, 60° and 45°. The resulting closure levels which are produced are shown in Figure 3.34 with the closure levels of the constant deflection angle cracks plotted for comparison. On undergoing the initial 45° deflections, the closure levels in the variable angle case are (obviously) the same as for the constant 45° case, (the slight differences are due to differences in the mesh design and the number of decrements used in the unloading cycle, affecting the sensitivity of the closure detection process). On undergoing the following 30° deflection, the closure level in the variable angle case lies between the constant 30° and 45° cases (i.e. the previous two deflections). On undergoing the 60° deflection, the closure level in the variable angle case lies between the constant 30° and 60° cases. Finally, on undergoing the 45° deflection, the closure level lies between the constant 45° and 60° cases. It is apparent therefore that varying the crack deflection angle does not lead to unduly increased crack closure levels (i.e. crack closure levels are representative of closure behaviour of the recent deflection angles for constant deflection angle models). The particular behaviour of the crack can be explained as follows: when the crack is growing along a deflected path, the crack opening along that section of the crack is a function of the *current* local mixity, and hence a function of the *current* crack deflection angle. However, the residual deformation of the asperity in the wake is governed by the local mixity *prior* to the deflection, and as such is a function of the *previous* crack deflection angle. Hence, it can be seen that it is the two crack deflection angles nearest to the crack tip which determine the crack closure level.

3.4.3.2 Deflection length

An FE model was constructed for a crack undergoing variable length crack deflections: specifically, the crack path used is illustrated schematically in Figure 3.35, and undergoes successive deflections of lengths 10, 30, 10, 10, 30 and 10 μm, through a constant angle of 45°. The resulting closure levels which are produced are shown in Figure 3.36 with the closure levels of the constant deflection length crack plotted for comparison. The closure level of the variable length crack can be seen to be close to that of the constant length crack for the entire length of the crack modelled. As such, the primary conclusion that can be drawn, is that variations in crack deflection lengths along the crack path seem to have no

significant effect on RICC levels. It is interesting to note that the position at which crack face contact first occurs is not always at the first deflection behind the crack tip, as is the case in the constant deflection length crack. For instance, whilst the crack is growing along the second of the long (30 μm) deflected sections, closure occurs first at the point marked C in Figure 3.35, i.e. three deflections behind the crack tip. Hence it appears that the size of the asperity does influence the locations at which closure occurs. The present single model cannot of course be used to identify a comprehensive understanding of variable length effects. Such an assessment, however, may make reference to the behaviour in Figure 3.31, where growth along the small deflections between points C and D in Figure 3.35 is dominated by the prior 30 μm long facet where $L/r_p \sim 1.5$, whilst the two 10 μm facets have $L/r_p \sim 0.5$.

3.5 Summary and conclusions

In this chapter, details of various FE models which have been constructed to investigate the closure behaviour of deflected fatigue cracks under constant amplitude cyclic loading, are presented. In particular;

- Specific issues in the design and implementation of the models have been addressed, and verification of critical aspects of model behaviour has been presented.
- The potentially anomalous near-tip behaviour of plane strain FE models of propagating fatigue cracks has been identified. This has lead to a closure definition based on an overall analysis of specimen compliance and crack face contact, excluding the node immediately behind the crack tip.
- Analyses of deflected cracks show an increasing effect of crack path angle on roughness induced closure levels in keeping with the simple analytical model of Suresh & Ritchie [1982].
- Importantly, the mechanism by which closure occurs has been shown to be more strongly dependent on residual plastic strains in the wake than global shear displacements of the fracture surfaces due to the mixed-mode behaviour at the crack tip.
- The absolute values of the closure levels have been found to be relatively low compared to experimental data, which may be attributed to an absence of environmental irreversibility in the finite element models and the simple two dimensional crack path morphologies that were studied. However, slip band simulations show a significant increasing effect of inhomogeneous deformation on closure levels, improving the apparent accuracy of the modelling results.
- A non-linear, plateauing influence of increasing asperity size on closure behaviour has been identified and correlated with experimental data from the literature. First order investigation of variable two dimensional crack geometries has been carried out, highlighting behaviour that is essentially consistent with the regular crack deflection models.

Deflection angle, degrees	χ at first asperity	χ required to fit Suresh model
30	0.047	0.0225-0.0335
45	0.055	0.0365-0.0885
60	0.27	0.0675-0.170

Table 1. Values of χ evaluated from the finite element results.

Deflection length, L, μm	K_{max}, MPa√m	r_p, μm	L/r_p
5	5.7	25.0	0.20
5	4.4	15.0	0.33
5	3.6	10.0	0.50
20	5.7	25.0	0.80
20	4.4	15.0	1.3
20	3.6	10.0	2.0
100	5.7	25.0	4.0
100	4.6	16.6	6.0

Table 2. Values of deflection lengths and loading levels used in the analysis of the effect of variable asperity size. Plastic zone sizes calculated from the Irwin approximation.

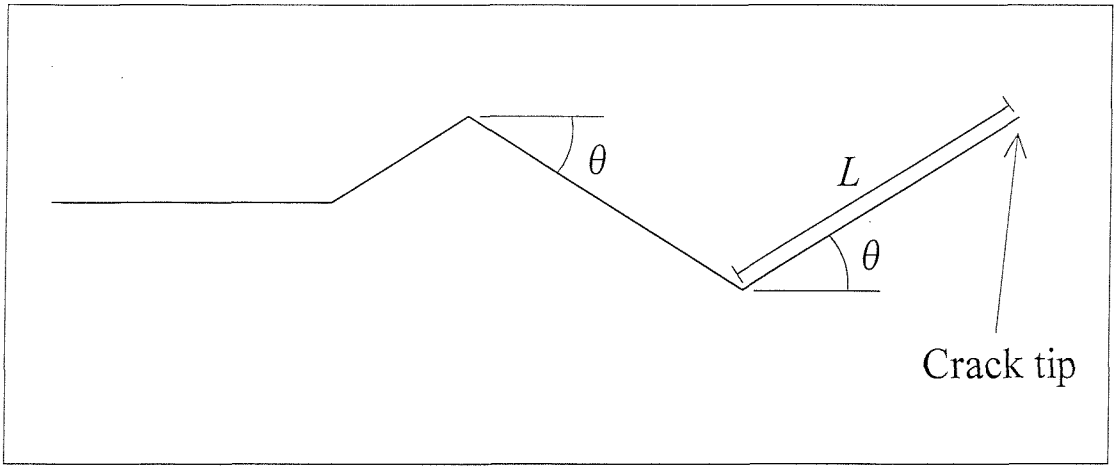

Figure 3.1. Illustration of the definitions of crack deflection angle θ, and deflection length L.

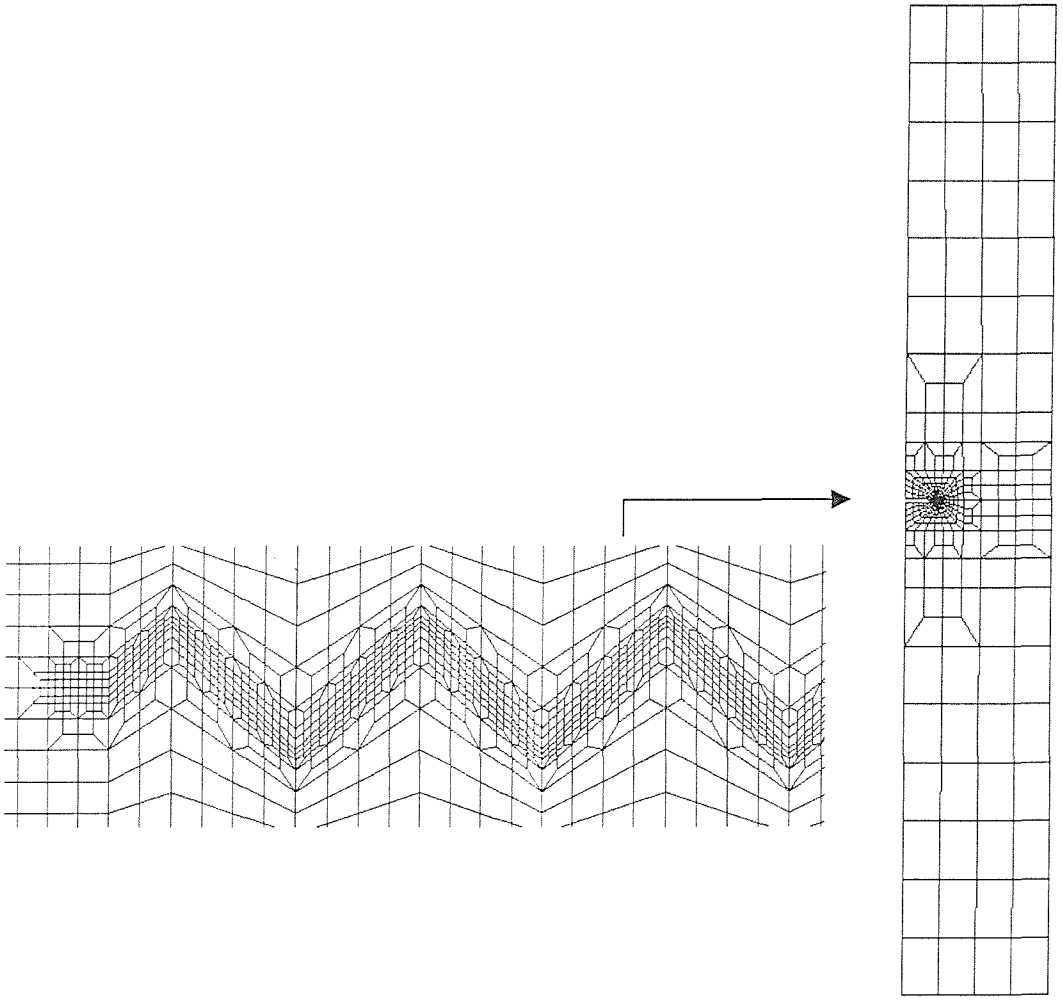

Figure 3.2. Typical mesh used to model deflected fatigue crack growth. Example shows a 45° deflected crack in a standard CCP specimen.

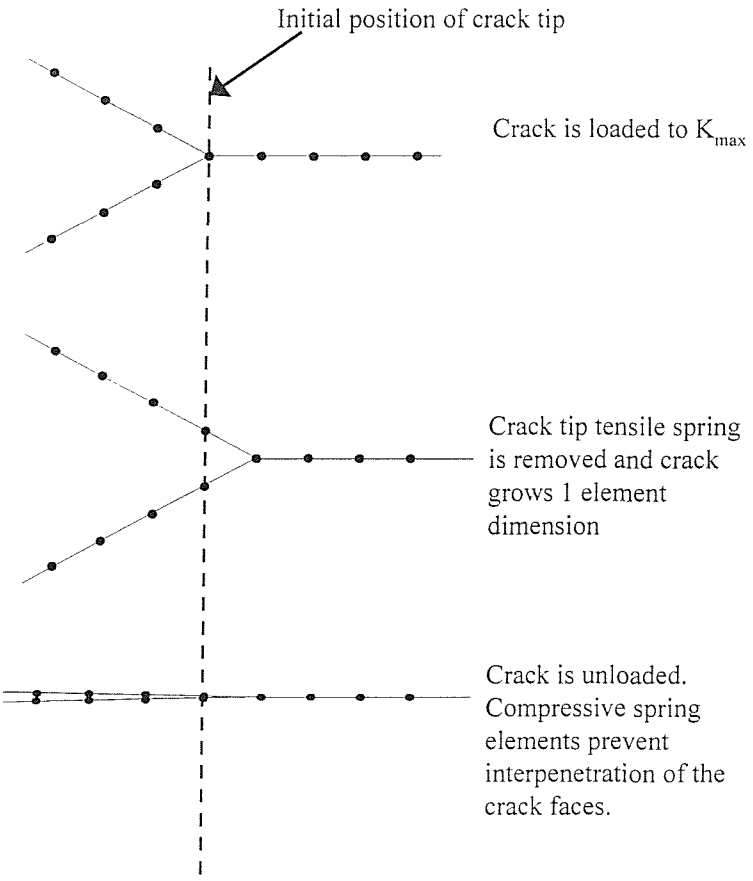

Figure 3.3. Schematic illustration of crack propagation process.

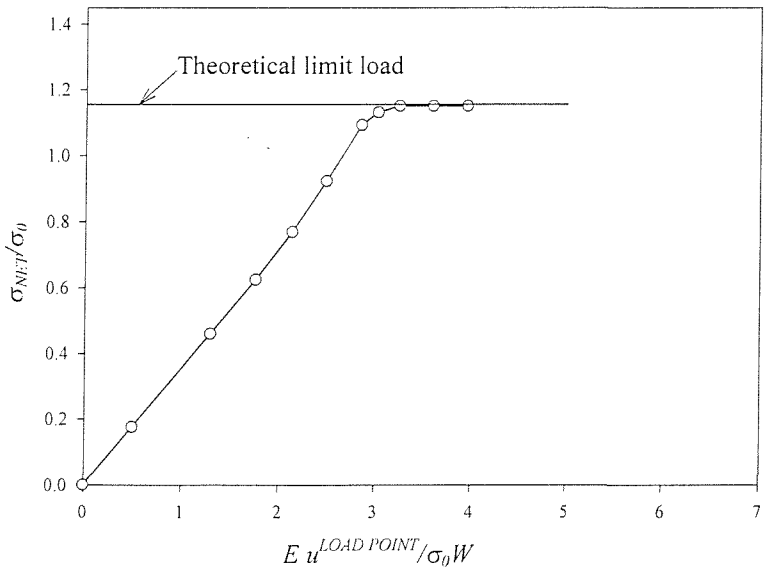

Figure 3.4. Limit load prediction of the finite element model, verifying the ability of the model to accurately represent incompressible deformations.

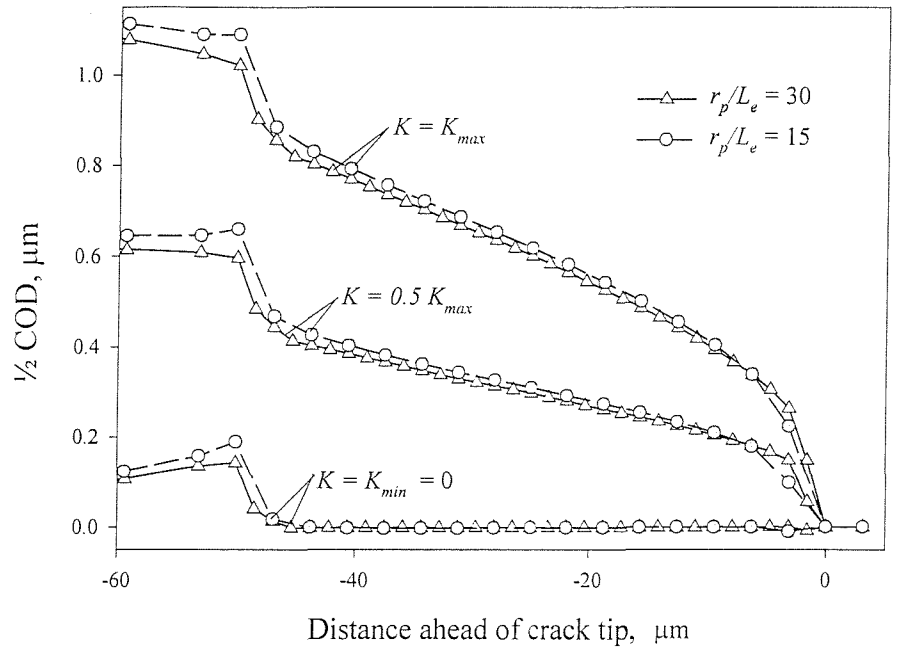

Figure 3.5. Crack opening as a function of mesh density.

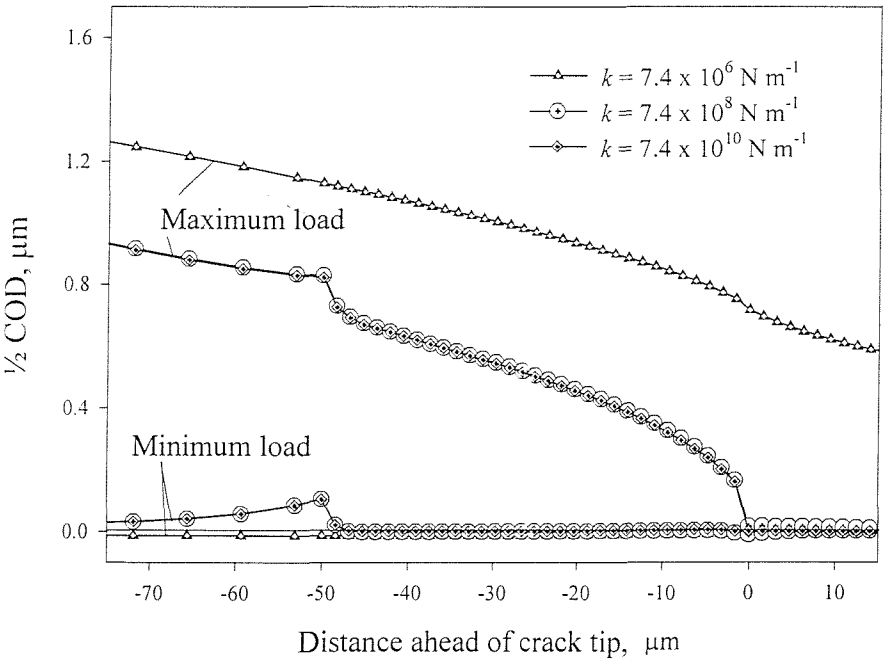

Figure 3.6. Crack opening as a function of spring stiffness, k.

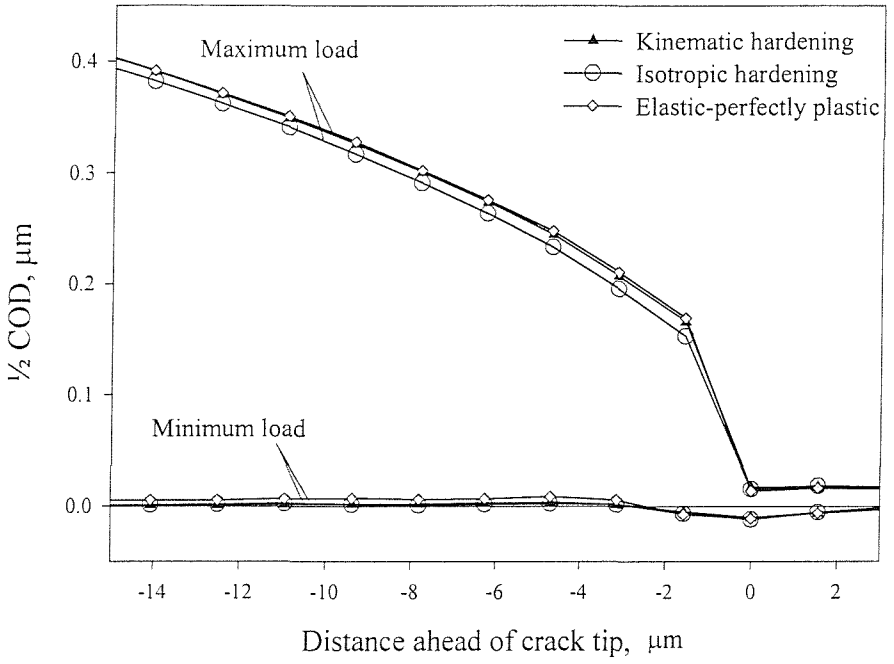

Figure 3.7. Crack opening as a function of hardening rule.

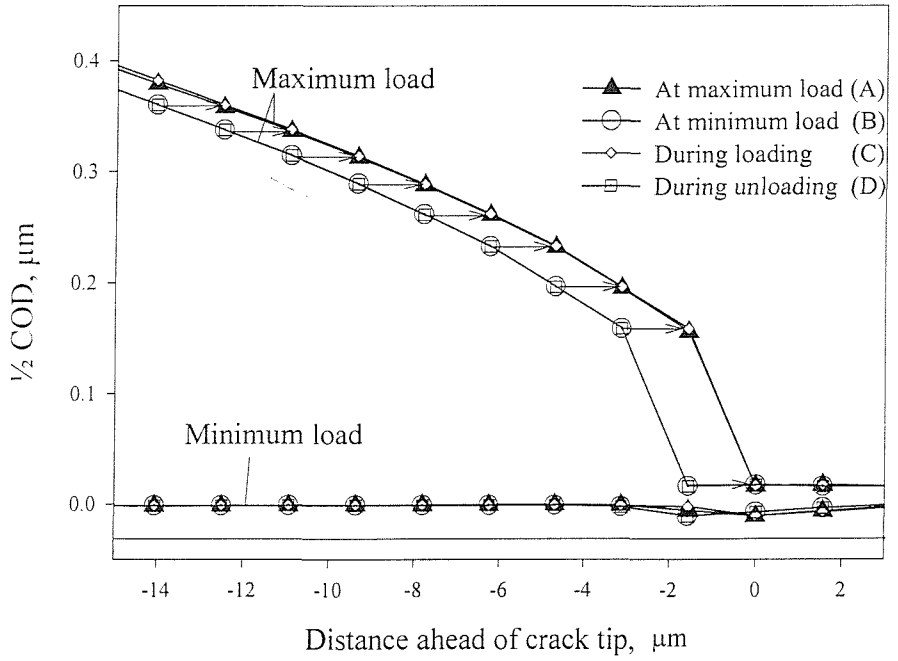

Figure 3.8. Crack opening as a function of the point of node release.

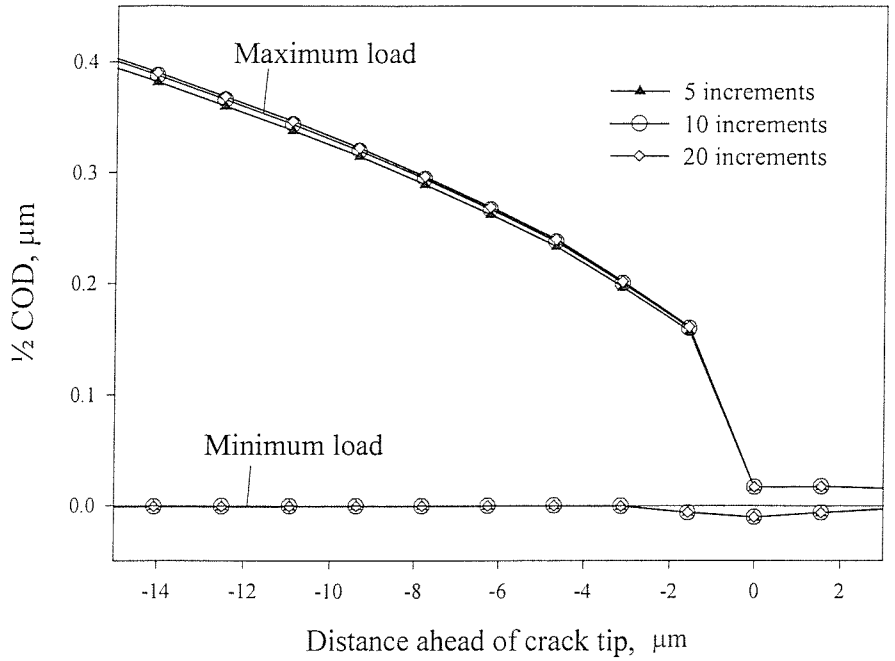

Figure 3.9. Crack opening as a function of the loading increment size.

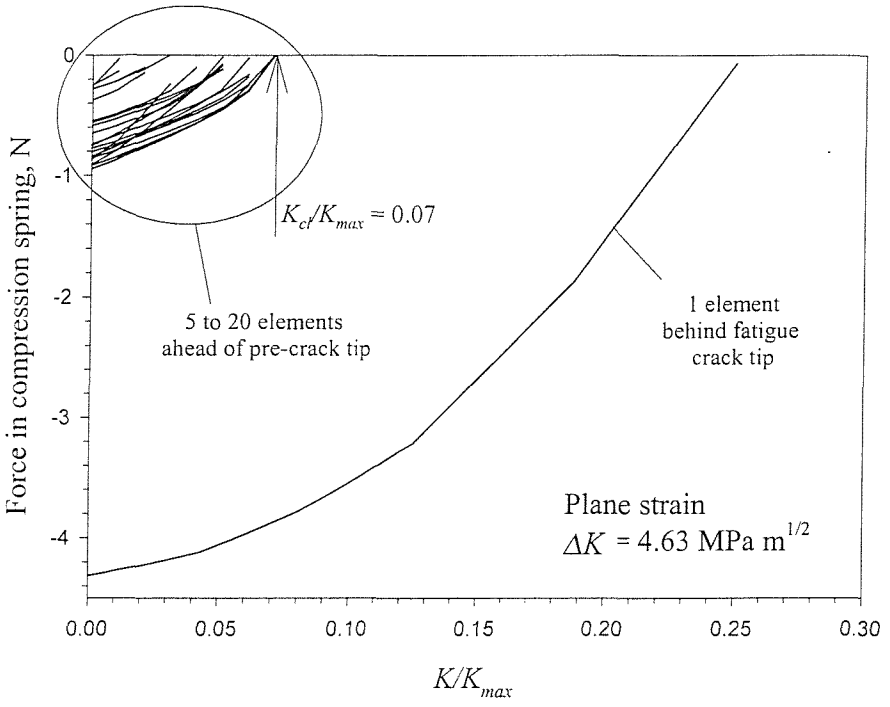

Figure 3.10(a). Response of the spring elements behind the crack tip for an undeflected crack in plane strain.

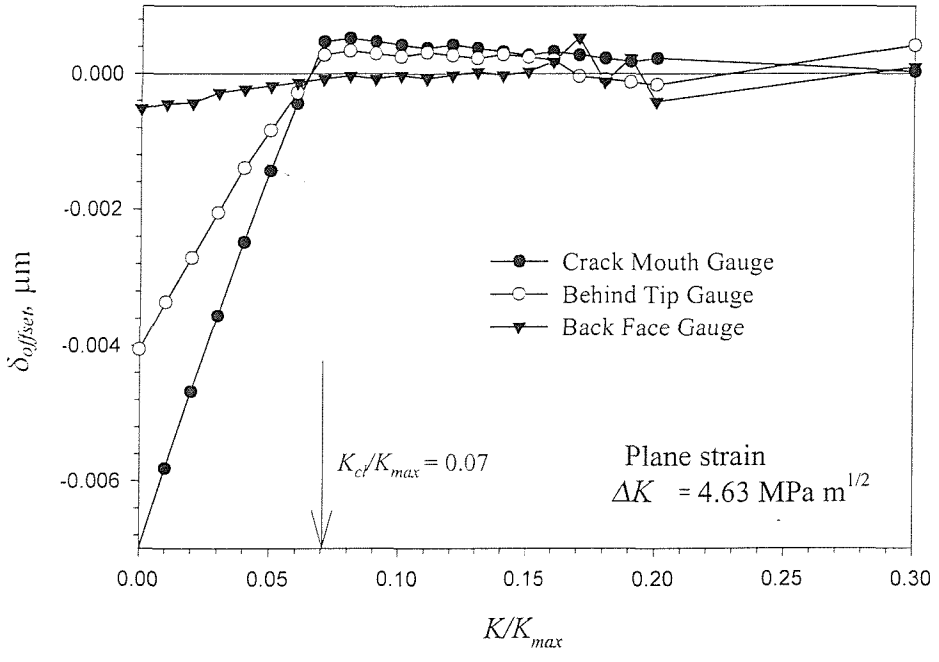

Figure 3.10(b). Offset compliance plot for an undeflected crack in plane strain.

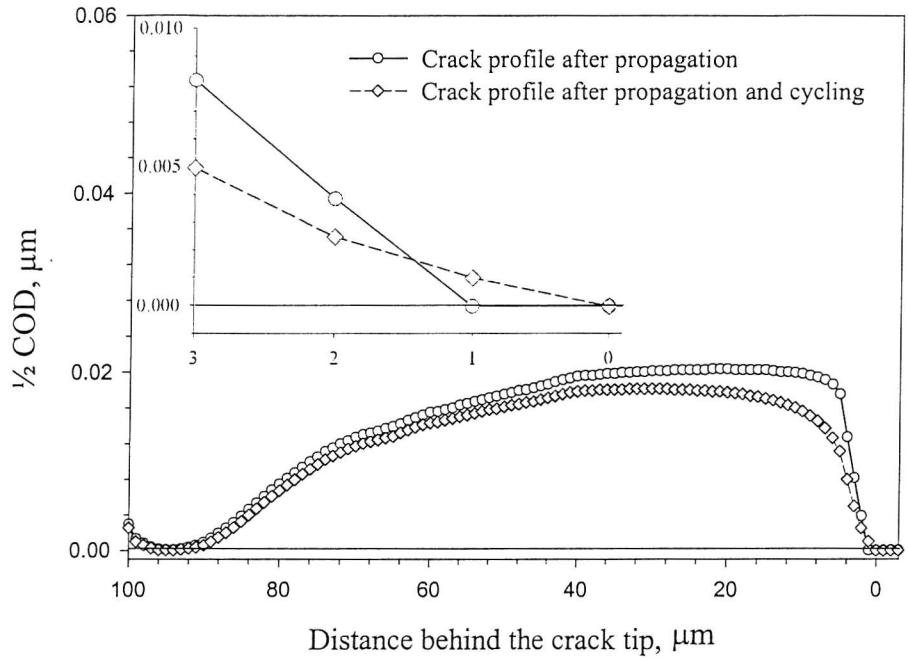

Figure 3.11. Crack profile at $K = K_{cl} = 0.07\ K_{max}$, for a propagated crack, and for a propagated crack with two load/unload cycles applied on reaching the final crack length. Inset shows near tip behaviour.

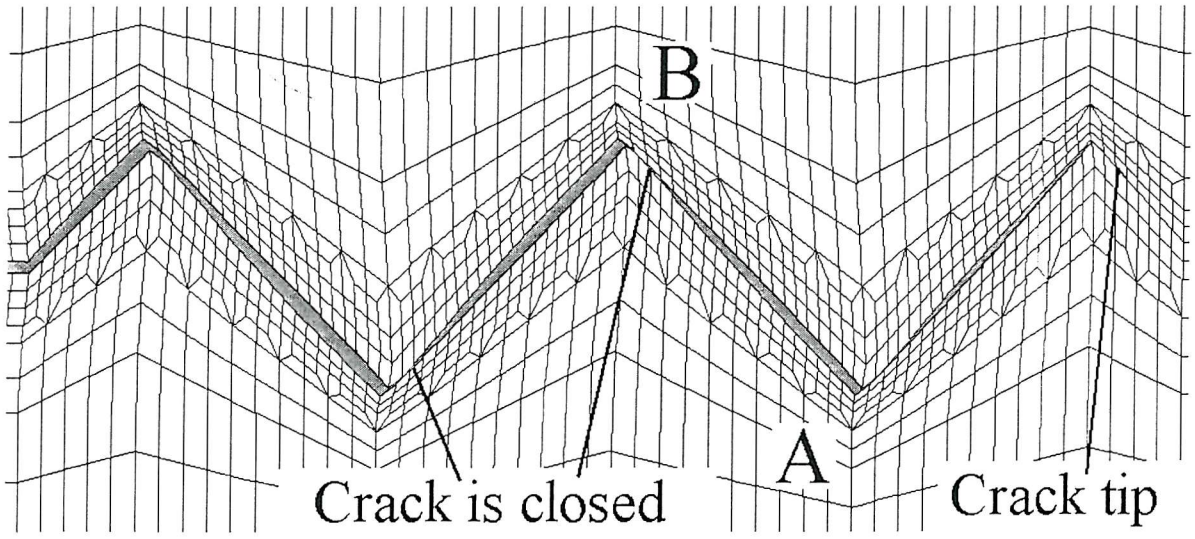

Figure 3.12. Plot of the deformed mesh of a 45° deflected crack at $K = K_{cl}$, exhibiting closure near the tips of the asperities. Displacement magnification x5.

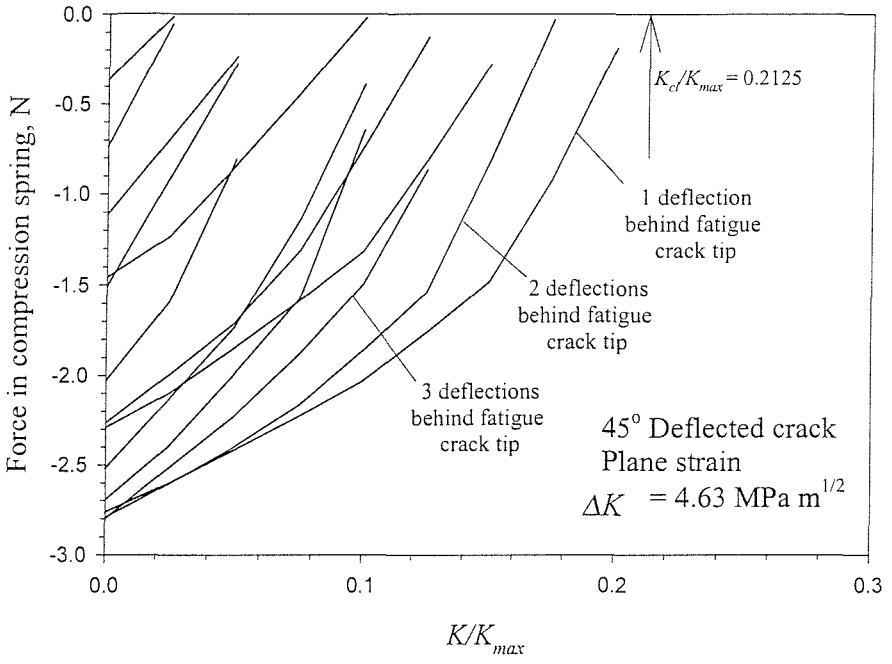

Figure 3.13(a). Response of the compression spring elements behind the crack tip for a 45° deflected crack.

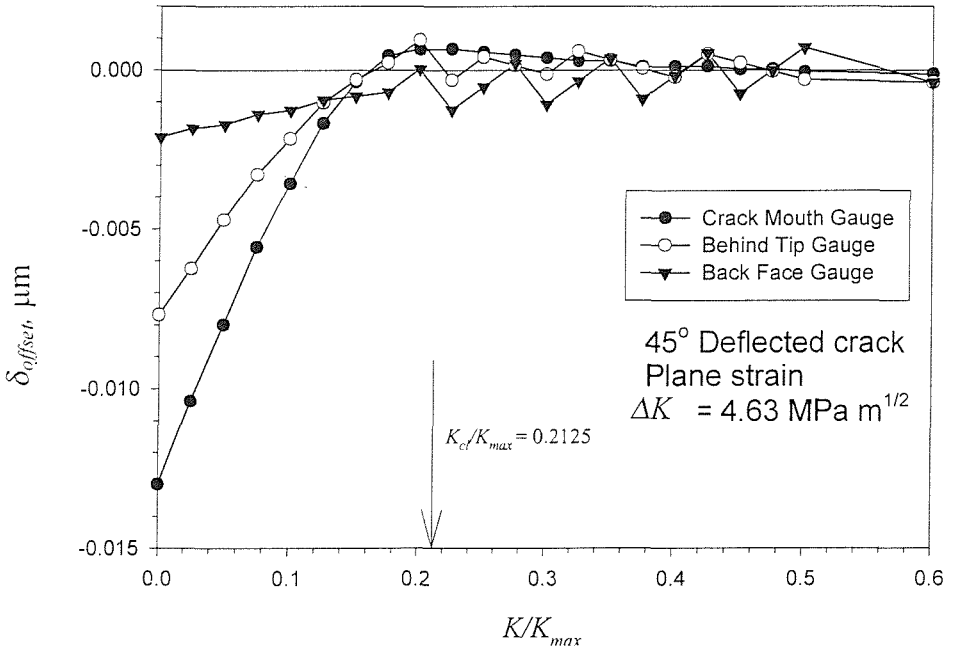

Figure 3.13(b). Offset compliance plot for a 45° deflected crack.

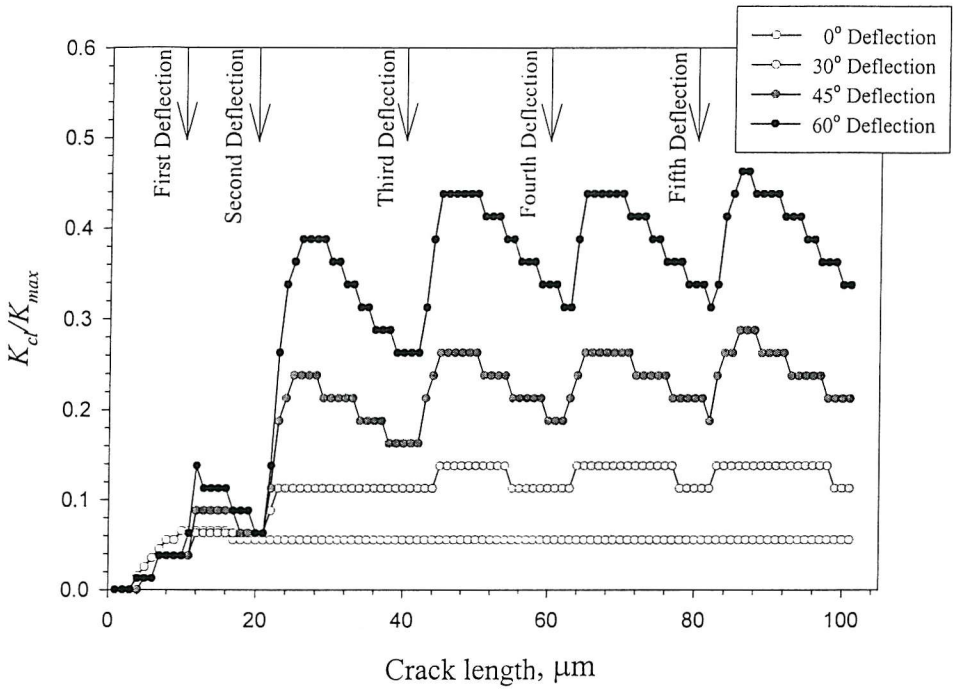

Figure 3.14. Variation of the normalised closure stress intensity factor with crack length for different crack geometries.

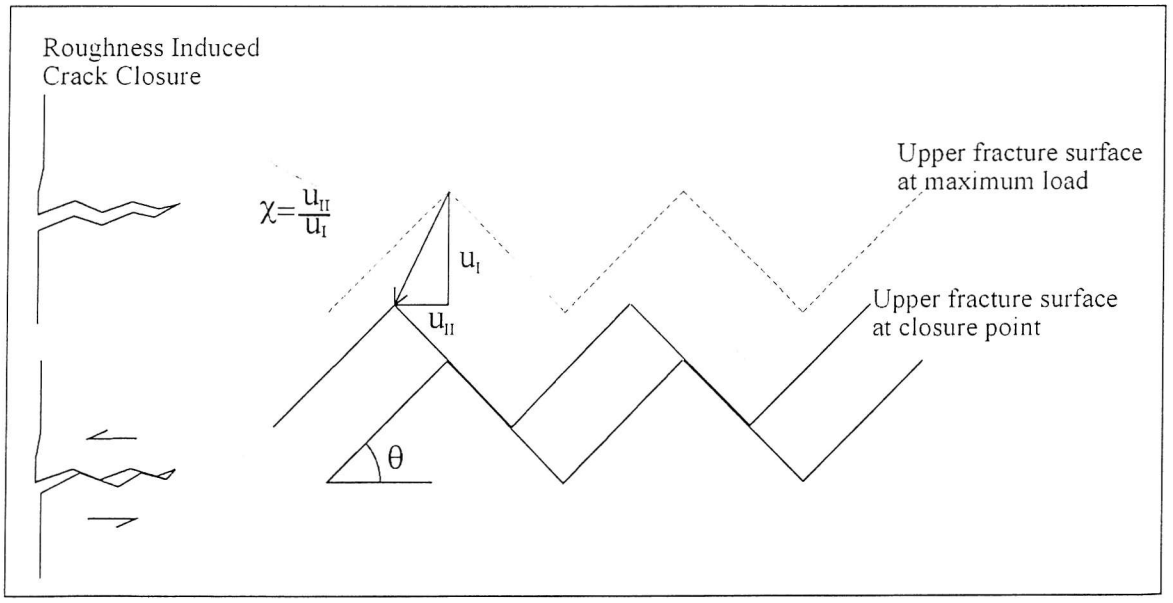

Figure 3.15. Detail of the geometrical model of roughness induced crack closure of Suresh & Ritchie [1982].

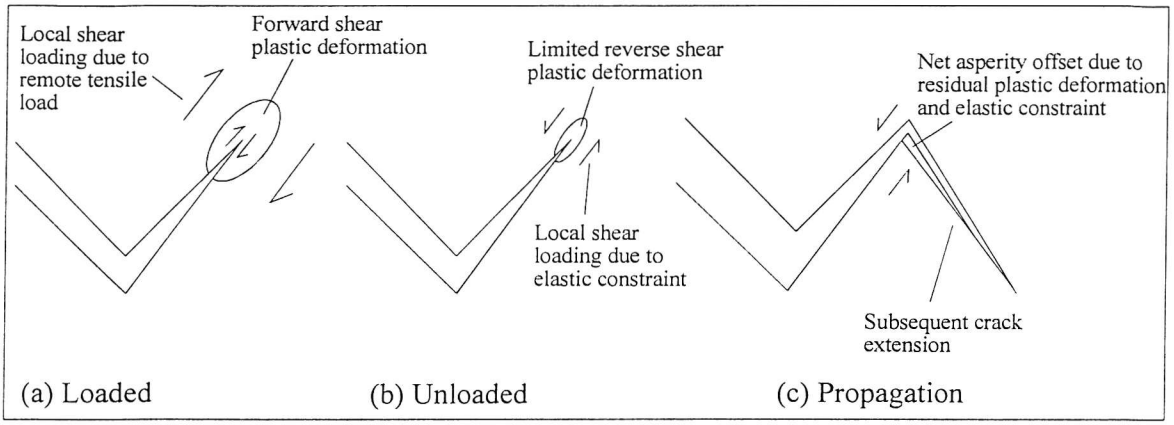

Figure 3.16. Mechanism of crack closure due to residual shear deformation in the crack wake.

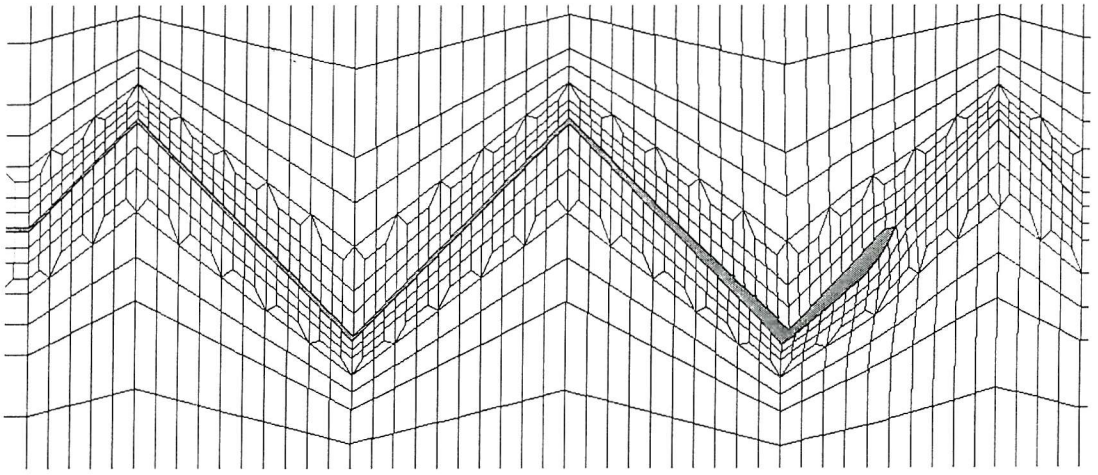

Figure 3.17. Residual deformation of a deflected crack loaded and unloaded once. Displacement Magnification x5.

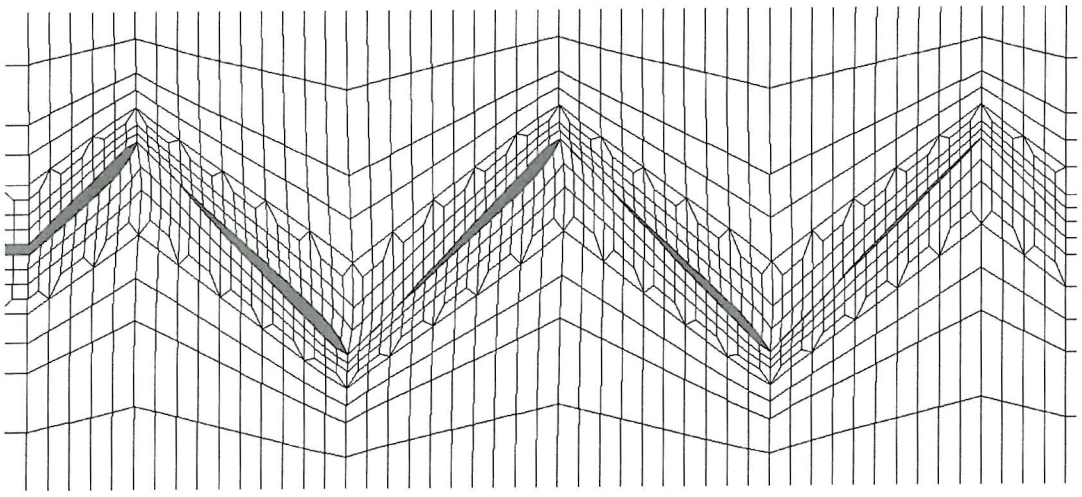

Figure 3.18. Residual deformation of a crack loaded and unloaded at the turning points. Final loading and unloading performed elastically. Displacement Magnification x5.

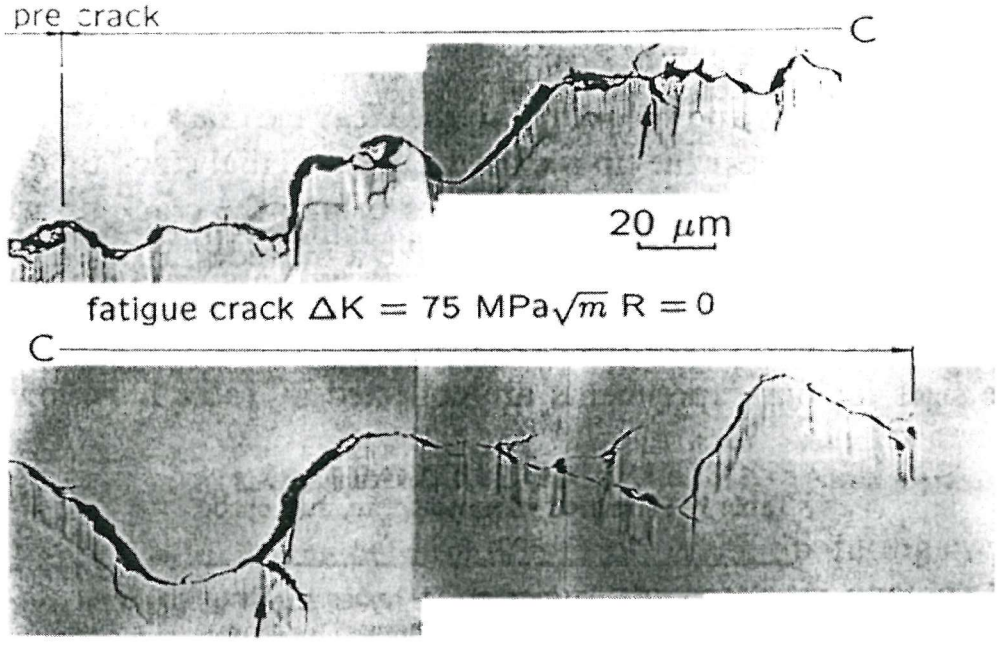

Figure 3.19. Micrograph showing the mid-thickness of a specimen of fatigue cracked SAE 4340 steel.

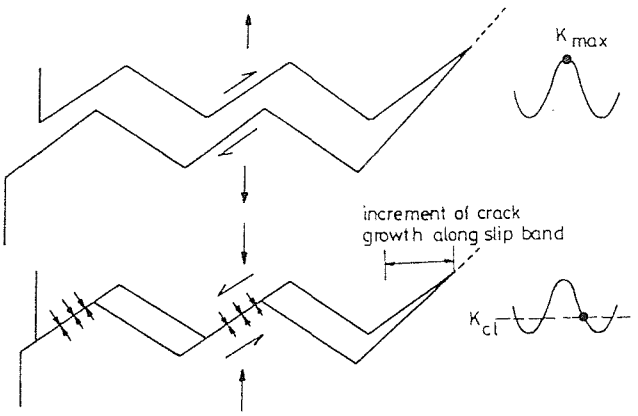

At K_{max}, crack propagation has occurred in the slip band ahead of the crack tip, by a mixture of mode I and mode II opening. Irreversible deformation in the slip band leads to an offset of the fracture surfaces.

At K_{cl}, the fracture surfaces no longer match, and the crack is wedged open, reducing the crack tip stress intensity factor range.

Figure 3.20. The perceived origin of the global shear offset in the conventional mechanism of RICC, from Ravichandran [1990].

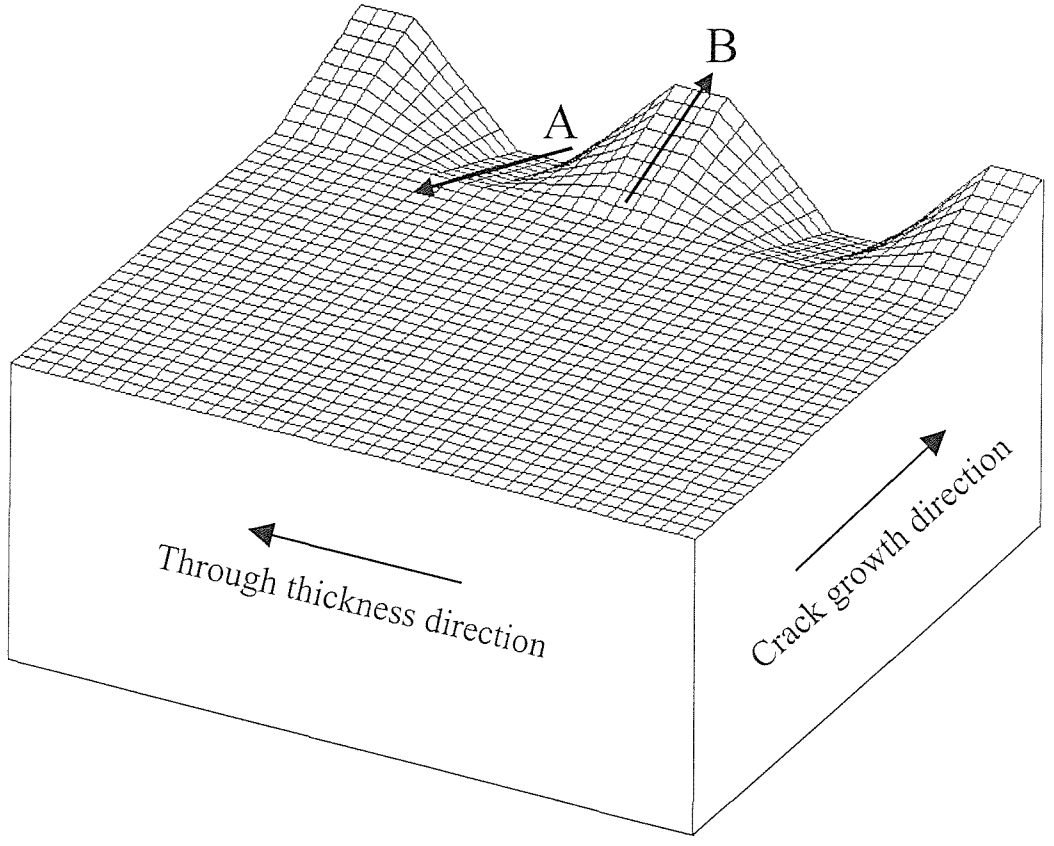

Figure 3.21. Schematic illustration of varying deflections above and below the mode I growth plane in a three dimensional crack front. Points A and B are referred to in the text.

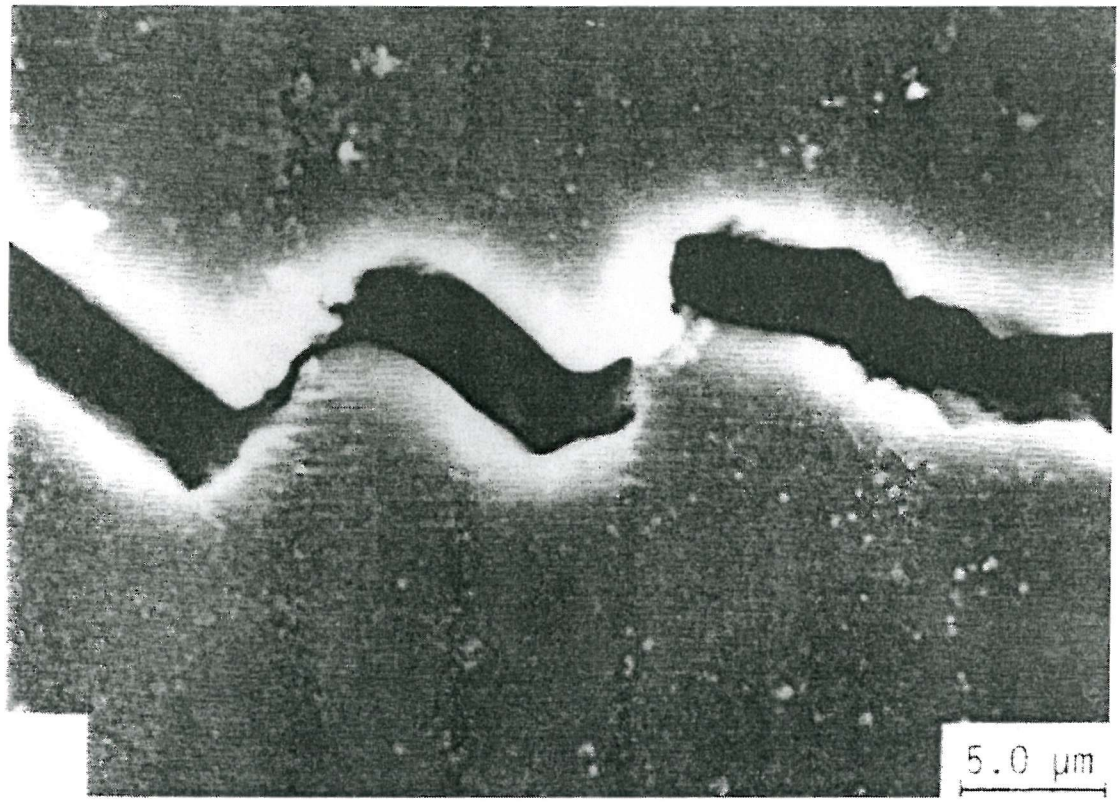

Figure 3.22. Micrograph showing wedging of fracture surface asperities, obtained from the surface of a specimen of 2090-T81 aluminium alloy, from Venkateswara Rao & Ritchie [1991].

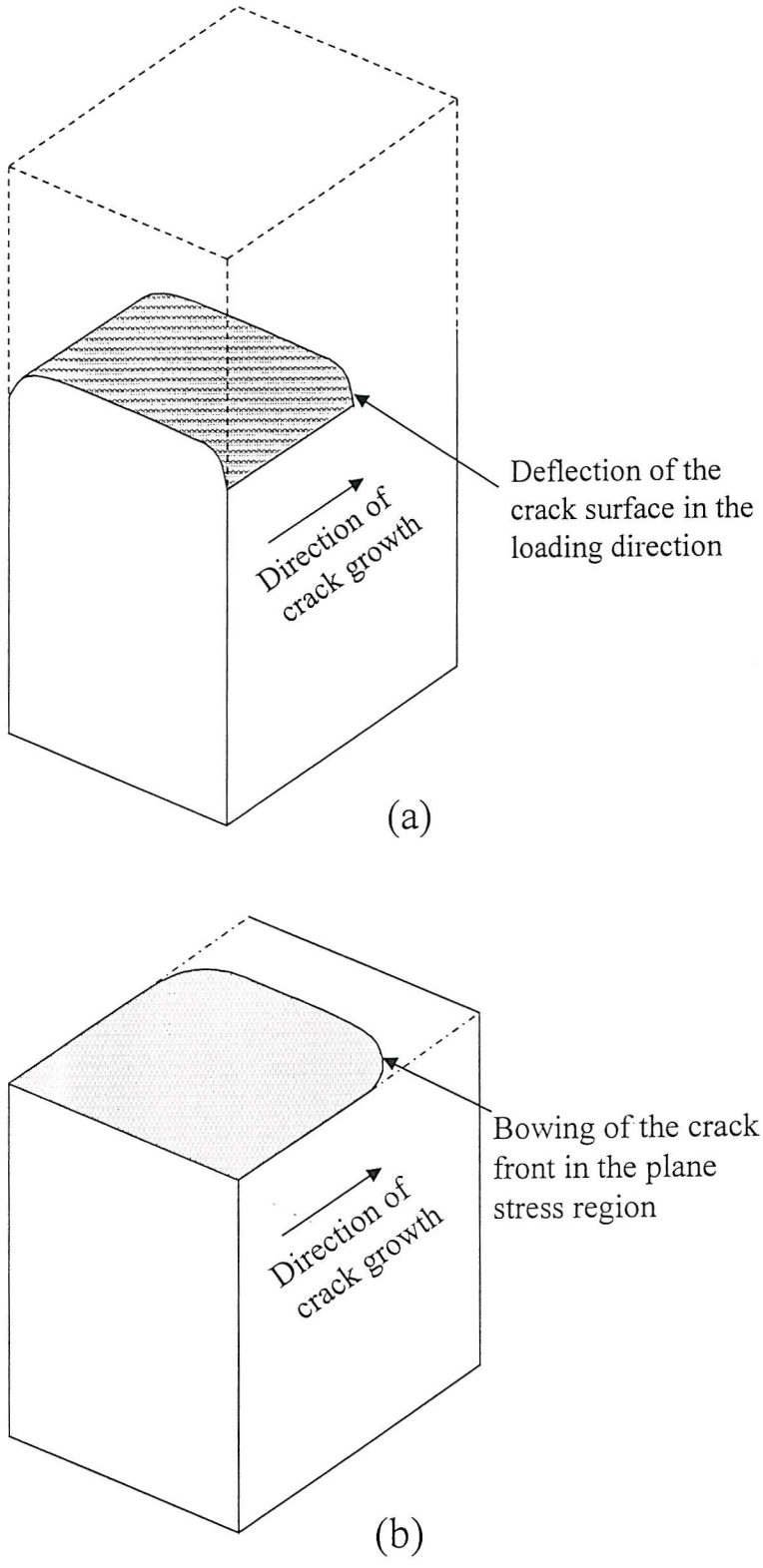

Figure 3.23. Schematic illustration of (a) near surface crack deflection in the loading direction (shear lip), and (b) bowing of the crack front, which is commonly observed near the specimen surfaces.

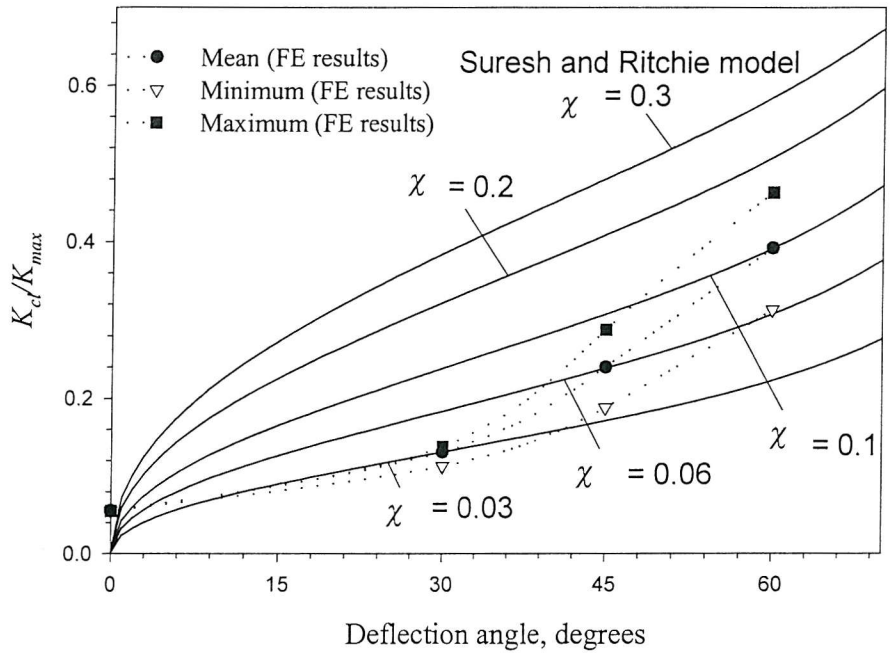

Figure 3.24. Comparison of the present finite element results to the analytical model of Suresh & Ritchie [1982].

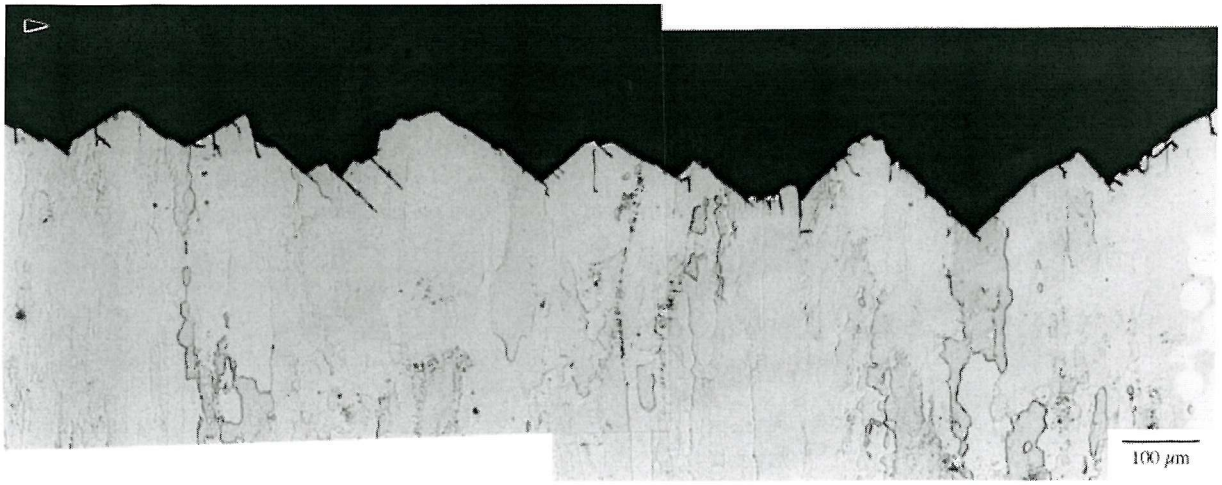

Figure 3.25. Fatigue crack deflection arising from strong crystallographic texture levels in 8090 Al-Li alloy tested in the LT orientation. (Arrow indicates crack growth direction).

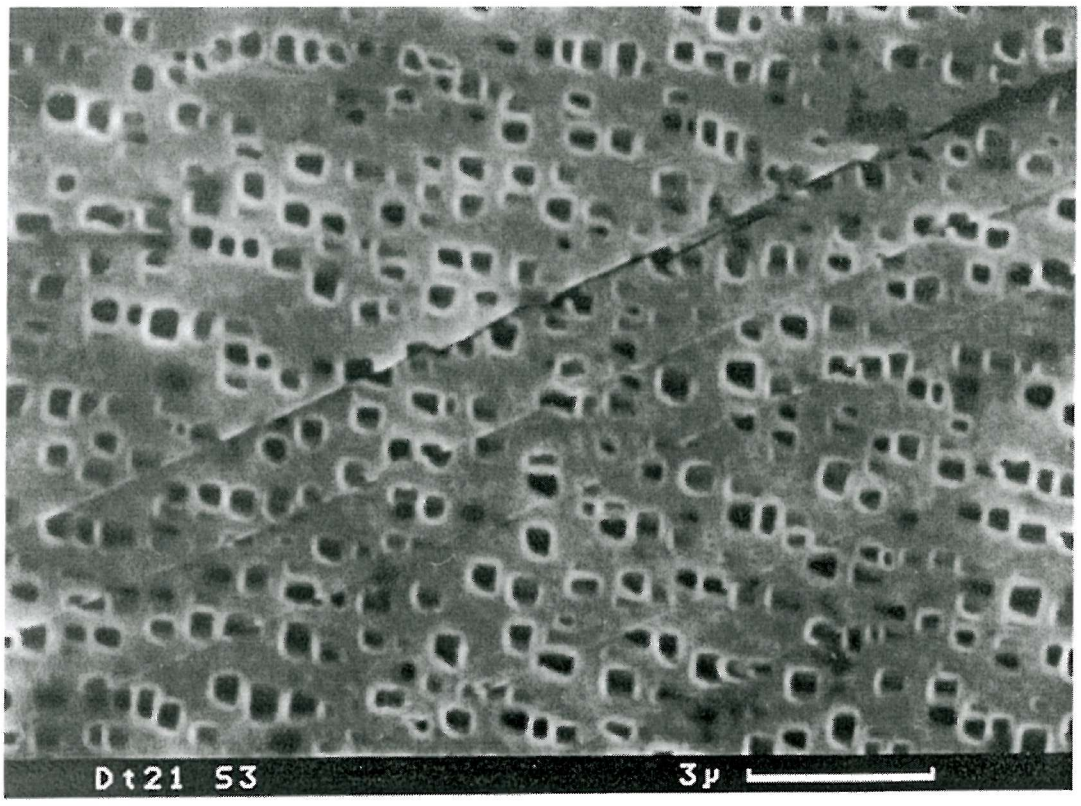

Figure 3.26. Slip band crack growth in a nickel single crystal showing marked shear strain localisation in bands ahead of the propagating crack tip.

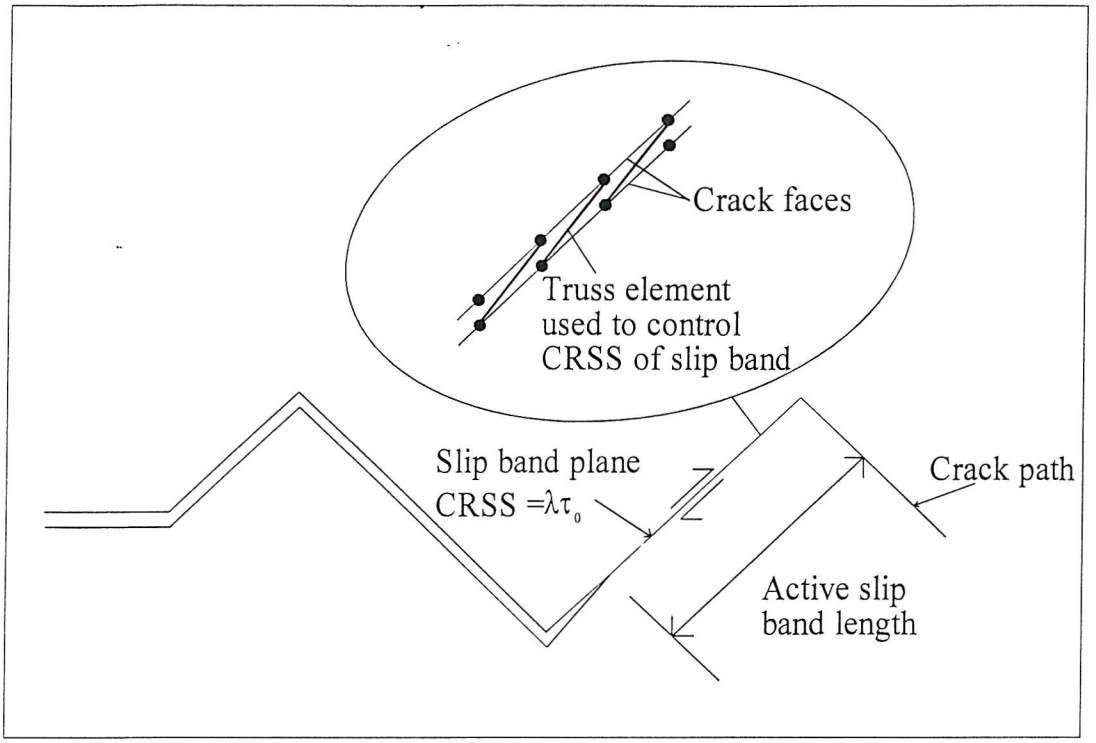

Figure 3.27. Schematic diagram showing the simulation of a slip band ahead of a crack.

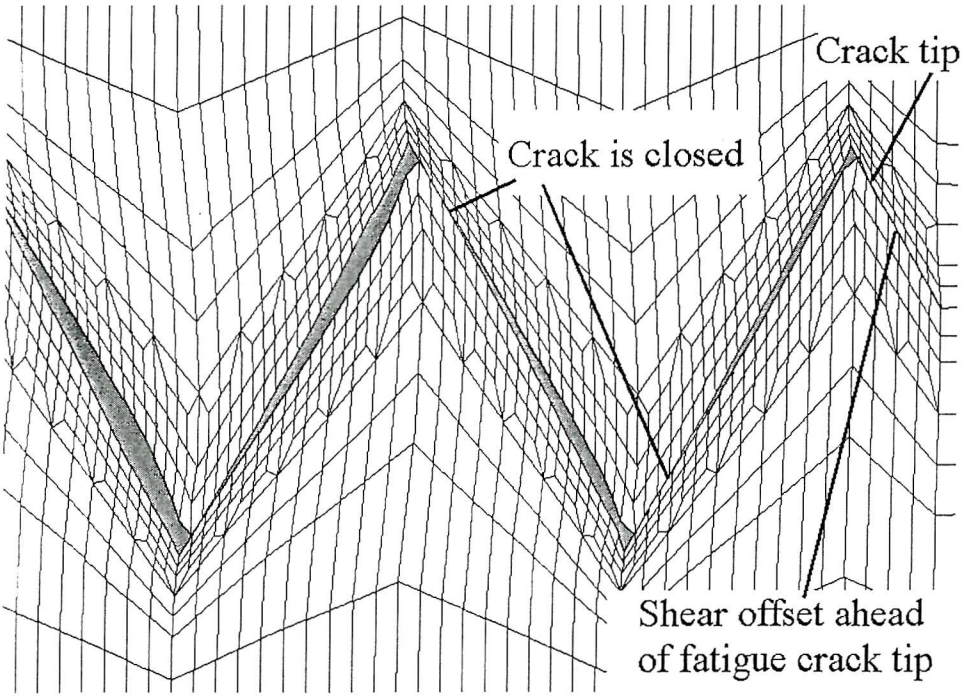

Figure 3.28. Plot of the deformed mesh for a 60° deflected crack with a slip band ahead of the crack tip enhancing the shear offset of the fracture surfaces. Displacement magnification x5.

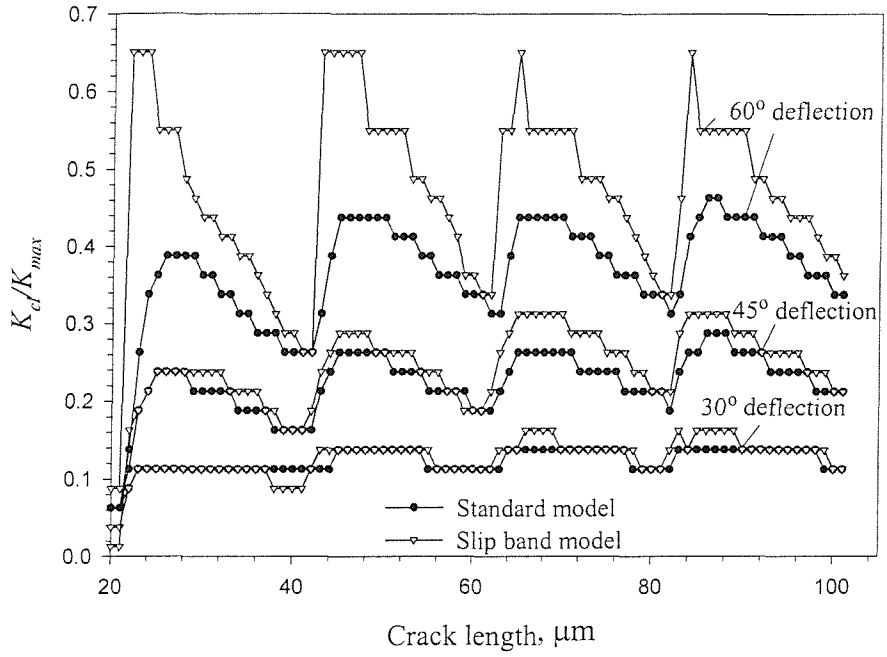

Figure 3.29. Effect of slip localisation on the closure level for deflected crack geometries.

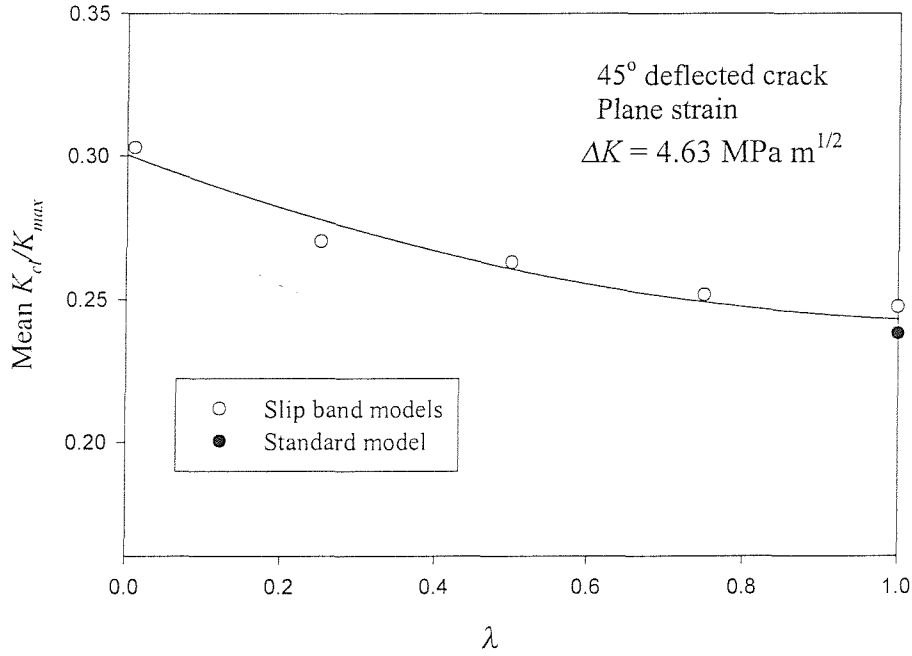

Figure 3.30. Effect of the ratio of slip band yield stress to bulk material yield stress in the mean closure level for a 45° deflected crack.

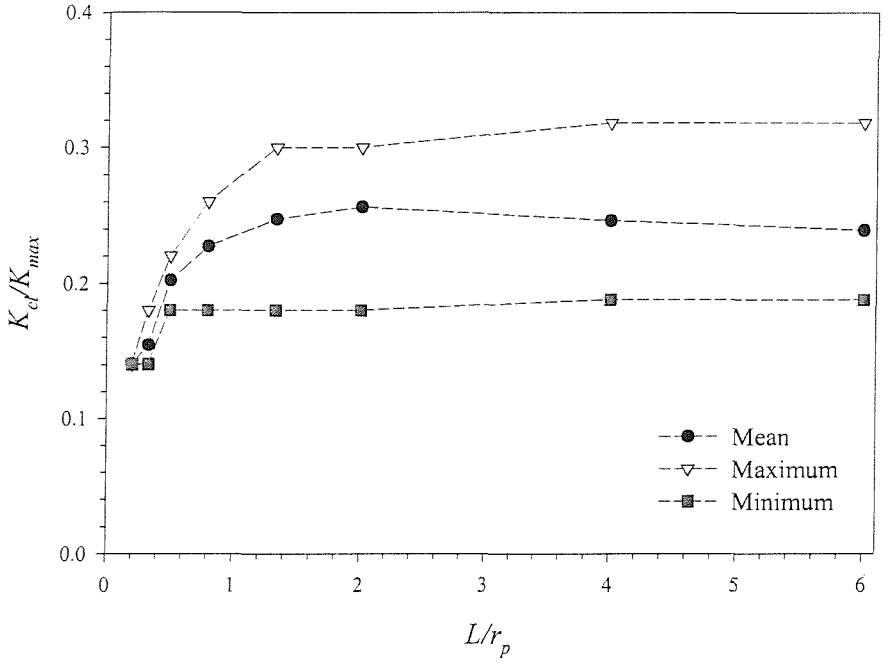

Figure 3.31. Effect of variable relative asperity size.

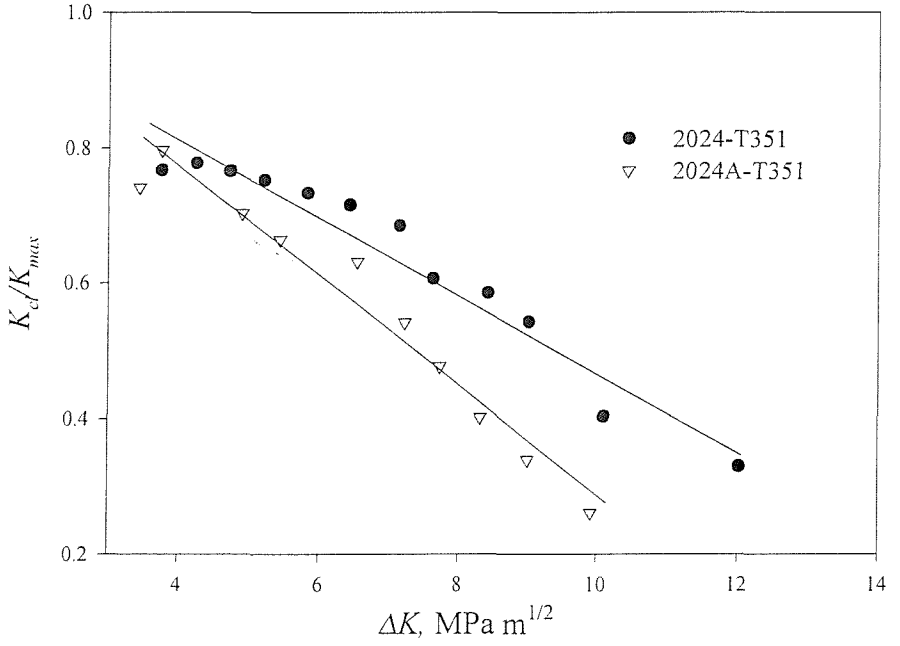

Figure 3.32. Experimental closure data for two 2024-type alloys, replotted from Xu *et al* [2000].

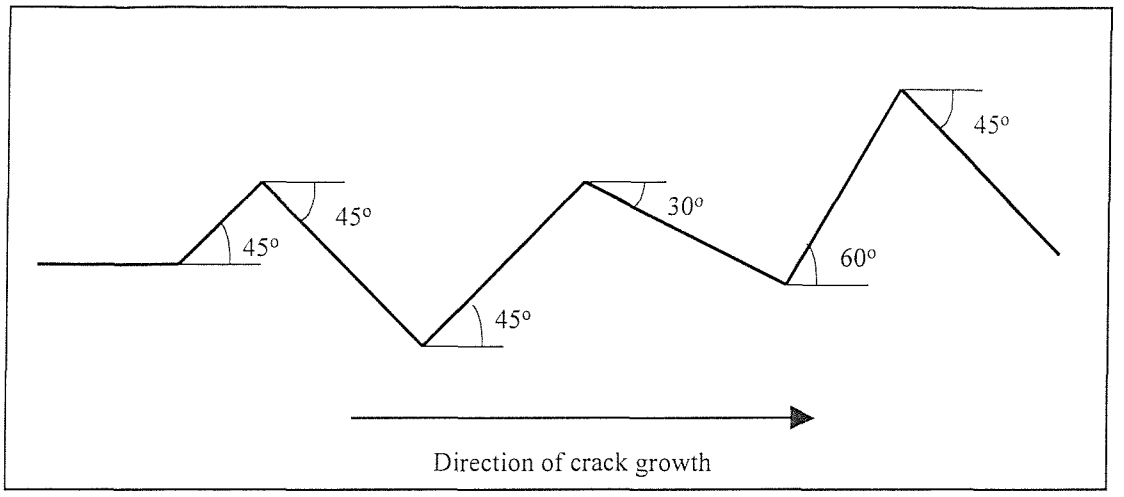

Figure 3.33. Schematic illustration of variable deflection angle crack path.

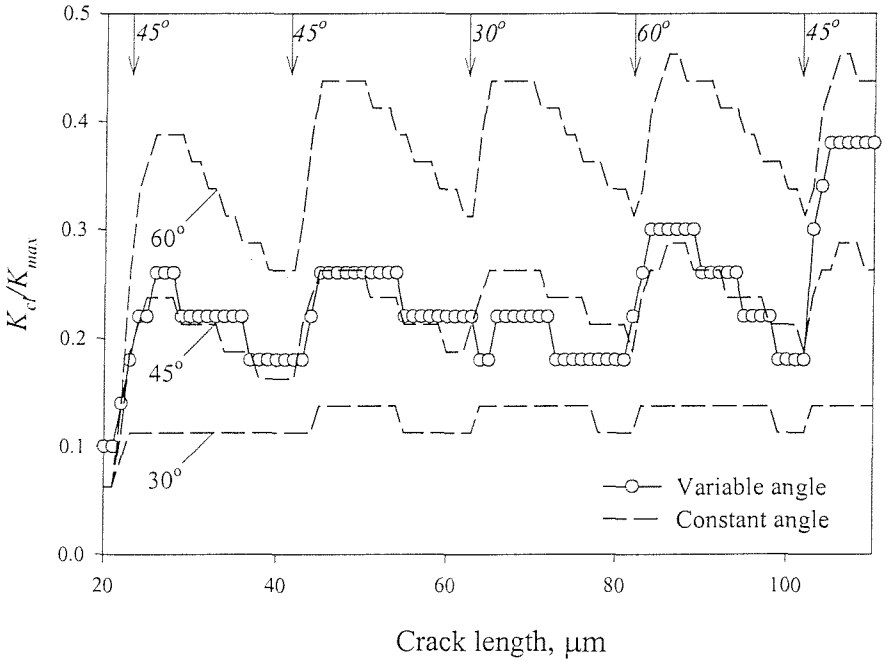

Figure 3.34. Effect of variable deflection angle, with constant angle results plotted for comparison. Arrows at the top of the figure indicate the deflection angle at each deflection for the variable angle model.

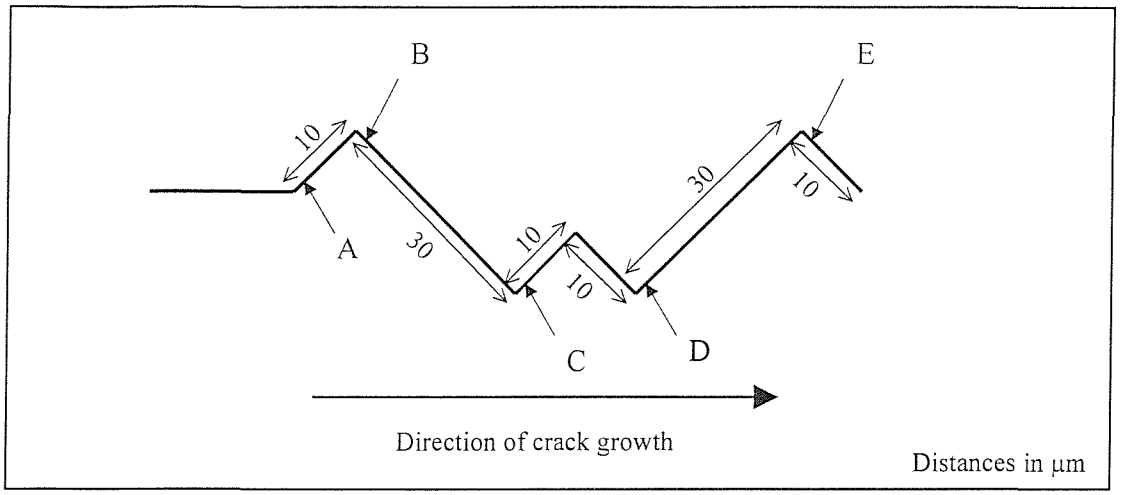

Figure 3.35. Schematic illustration of variable deflection length crack path.

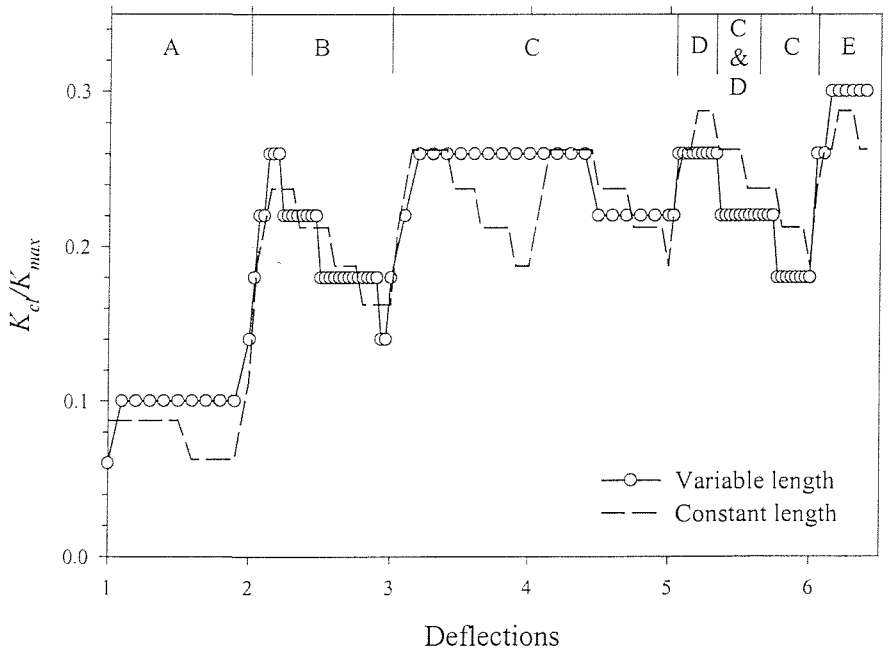

Figure 3.36. Effect of variable deflection length, with constant length result plotted for comparison. Position of initial crack face contact is indicated at the top of the figure, with reference to Figure 3.35.

4 Analytical modelling of RICC

In the previous chapter a mechanism by which crack deflection and associated residual plastic strains may lead to increased levels of crack closure under plane strain conditions was proposed through inspection of the finite element model behaviour. To provide confidence in the mechanism and to extend the applicability of the understanding, a simple analytical model has been developed using standard fracture mechanics expressions.

4.1 Formulation of the model

The mechanism by which crack deflection may lead to crack closure under plane strain conditions, as discussed in detail in Chapter 3, is illustrated in Figure 4.1. As the crack is loaded, a degree of shear plastic shear deformation occurs at the tip of the deflected crack (Figure 4.1(a)). On unloading, the elastic constraint of the surrounding material causes a limited degree of reverse plastic deformation. Hence a degree of residual shear exists in the material surrounding the crack tip (Figure 4.1(b)) analogous to the residual tensile strain that is identified with mode I loading under plane stress conditions. When crack deflection occurs, this residual shear deformation is left in the crack wake, and leads to premature crack face contact on the forward edge of the asperity (Figure 4.1(c)).

The key factors which need to be addressed in producing an analytical model of this process may be identified as: (1) a description of the opening behaviour of the final deflected crack section, and (2) a description of the residual deformation of the asperity in the wake.

4.1.1 Crack opening behaviour

The crack opening profile of a crack of length $2a$, lying in the x-z plane, parallel to the x-axis, in an infinite plate of a linear elastic material, under far-field tension σ, (as shown in Figure 4.2) can be found from the equations of the elastic stress field displacements (e.g. see [Tada *et al*, 1973]). Under plane strain conditions,

$$u_y = \frac{2\sigma}{E}\left(1-\nu^2\right)\sqrt{a^2-x^2}\,, \tag{4.1}$$

where u_y is the elastic displacement of the crack flank in the y-direction at a distance x from the origin, E is the elastic modulus and ν is the Poisson ratio.

Under small-scale yielding conditions, plasticity will develop at the crack tip. As such, the crack will become blunted, and Equation 4.1 will cease to apply in the near-tip region. Consider a fatigue crack which has propagated in a steady manner: material that has previously undergone a residual tensile stretch normal to the crack plane will be found in the crack wake. Hence the opening of the crack will effectively be reduced to accommodate this residual stretch. However, as noted in Chapter 3, the extent of residual deformation due to steady-state fatigue crack growth under plane strain conditions may be relatively small, i.e. plane strain PICC was not found to be significant. As such, provided that the crack length is sufficiently large compared to the extent of crack tip plasticity, Equation 4.1 may be an adequate description of the crack profile of a plane strain fatigue crack in an infinite plate.

For the purposes of the analytical model of RICC an expression for the opening behaviour of a deflected crack tip is required. If the assumption is made that the tensile opening of the final deflected section of the crack (of length a^*) behaves like a small undeflected crack (also of length a^*), with $k_{I(deflected)} = K_{I(undeflected)}$, as shown in Figure 4.3, then an approximation to the opening behaviour of the final deflected section of the crack is,

$$u_y = \frac{2\sigma}{E}\left(1-\nu^2\right)\sqrt{a^{*2}-x^2}\,, \tag{4.2}$$

with the crack opening displacement δ being,

$$\delta = 2u_y = \frac{4k_{I(deflected)}\left(1-\nu^2\right)\sqrt{a^{*2}-x^2}}{E\sqrt{\pi a^*}}\,. \tag{4.3}$$

The value of $k_{I(deflected)}$ is a function of the remote applied K_I and the deflection angle θ. If we make the simplifying assumption that the final deflected section of the crack can be equated to a kink off a straight crack, as shown in Figure 4.4, then as a^*/b is small, k_I is given by the equation for the stress intensity factor at the tip of a pupative kink [Bilby *et al*, 1977], i.e.,

$$k_I = \tfrac{1}{4}\left(3\cos\tfrac{\theta}{2} + \cos\tfrac{3\theta}{2}\right)K_I\,. \tag{4.4}$$

Hence, Equation 4.3 becomes,

$$\delta = \frac{4K_I\left(1-\nu^2\right)\left(3\cos\frac{\theta}{2} + \cos\frac{3\theta}{2}\right)\sqrt{a^{*2}-x^2}}{E\sqrt{\pi a^*}}\,. \tag{4.5}$$

which is a description of the crack opening of the final deflected section of the crack.

4.1.2 Residual deformation of the asperity

The residual shear deformation described at the start of this section leads to an effective displacement h of the asperity, as shown in Figure 4.5. In the first instance this can be thought of as a residual crack tip shear displacement, $CTSD_{res} = h$, from the loading and

unloading that occurred at this point. By considering a Dugdale-type strip yield model under far-field mode II loading, Rice [1967] gives the *CTSD* at maximum load under plane stress as,

$$CTSD_{max} = \frac{(\kappa + 1)K_{II\,max}^{\ 2}}{8G\tau_0}, \tag{4.6}$$

where $\kappa = (3-\nu)/(1+\nu)$, $G = E/(2(1+\nu))$, τ_0 is the critical resolved shear stress, and $K_{II\,max}$ is the maximum far-field mode II stress intensity factor.

If we make the assumption that this is an adequate description of *CTSD* under plane strain (which should be a reasonable assumption given that the constraint which exists for tensile plane strain deformations is not an issue for shear deformations)), then using $\kappa = 3\text{-}4\nu$ (for plane strain), Equation 4.6 becomes,

$$CTSD_{max} = \frac{K_{II\,max}^{\ 2}(1-\nu^2)}{E\tau_0}. \tag{4.7}$$

From the von Mises yield criterion, $\tau_0 = \sigma_0/\sqrt{3}$, hence Equation 4.7 becomes,

$$CTSD_{max} = \frac{\sqrt{3}K_{II\,max}^{\ 2}(1-\nu^2)}{E\sigma_0}. \tag{4.8}$$

Upon unloading, a degree of reversed crack tip sliding will occur. Using Rice's argument [1967] that the yield stress for reverse yielding is effectively twice that for forward yielding (i.e. $\Delta\sigma = +\sigma_0 - (-\sigma_0) = 2\sigma_0$), then the change in *CTSD* (i.e. $\Delta CTSD$) due to a cyclic mode II stress field, characterised by ΔK_{II}, is given by,

$$\Delta CTSD = \frac{\sqrt{3}\Delta K_{II\,max}^{\ 2}(1-\nu^2)}{2E\sigma_0}. \tag{4.9}$$

Hence, $CTSD_{res}$, is given by,

$$\begin{aligned} CTSD_{res} &= CTSD_{max} - \Delta CTSD \\ &= \frac{\sqrt{3}K_{II\,max}^{\ 2}(1-\nu^2)\left(\frac{1}{2} + R - \frac{1}{2}R^2\right)}{E\sigma_0} \end{aligned} \tag{4.10}$$

It should be noted that there is some variability in the expressions for *CTSD* available in the literature. For example Li [1990] gives,

$$CTSD_{max} = \frac{4K_{II\,max}^{\ 2}(1-\nu^2)}{E\tau_0}, \tag{4.11}$$

which is four times that quoted by Rice, whilst by using an effective crack length concept similar to the Irwin approximation to the plastic zone under mode I loading, it can be shown that,

$$CTSD_{max} = \frac{2K_{II\,max}^{\;2}}{E\tau_0}, \tag{4.12}$$

which is approximately 2.2 times that quoted by Rice. In the remainder of the model formulation it is the Rice expression given in Equation 4.7 which is used. The effect of this range of CTSD values is discussed in Section 4.3.

The residual *CTSD* of a crack under a far-field mode II load can be related to the case of a deflected crack, by replacing K_{IImax} with k_{2max}, the local mode II stress intensity factor at the tip of the deflected crack. Using a similar argument as for k_1, k_2 is given by the equation for the local mode II stress intensity factor at the tip of a pupative kink, i.e.,

$$k_2 = \tfrac{1}{4}\left(sin\tfrac{\theta}{2} + sin\tfrac{3\theta}{2}\right)K_I, \tag{4.13}$$

and Equation 4.10 becomes,

$$CTSD_{res} = h = \frac{\sqrt{3}K_{I\,max}^{\;2}\left(1-\nu^2\right)\left(\tfrac{1}{2} + R - \tfrac{1}{2}R^2\right)\left(sin\tfrac{\theta}{2} + sin\tfrac{3\theta}{2}\right)^2}{16E\sigma_0}. \tag{4.14}$$

4.1.3 Estimation of crack closure

From Figure 4.5, it can be seen that the extent of the residual deformation resolved normal to the crack face is $h\,sin\theta$. Hence, closure of the crack will occur when $\delta = h\,sin\theta$. Inserting values for δ and h from Equations 4.5 and 4.14 and rearranging gives,

$$\frac{K_I}{K_{I\,max}} = \frac{K_{cl}}{K_{max}} = \frac{\sqrt{3\pi\,a^*}K_{I\,max}\left(\tfrac{1}{2} + R - \tfrac{1}{2}R^2\right)\left(sin\tfrac{\theta}{2} + sin\tfrac{3\theta}{2}\right)^2 sin\,2\theta}{16\sigma_0\sqrt{a^{*2} - x^2}\left(3cos\tfrac{\theta}{2} + cos\tfrac{3\theta}{2}\right)}, \tag{4.15}$$

where K_{cl}/K_{max} is the normalised closure stress intensity factor. Given that closure occurs at the point of crack deflection it is the crack opening behaviour at $x = 0$ that is of interest, i.e.

$$\frac{K_{cl}}{K_{max}} = \frac{\sqrt{3\pi}K_{I\,max}\left(\tfrac{1}{2} + R - \tfrac{1}{2}R^2\right)\left(sin\tfrac{\theta}{2} + sin\tfrac{3\theta}{2}\right)^2 sin\,2\theta}{16\sigma_0\sqrt{a^*}\left(3cos\tfrac{\theta}{2} + cos\tfrac{3\theta}{2}\right)}, \tag{4.16}$$

or rewriting in terms of $U = (K_{max} - K_{cl})/(K_{max} - K_{min})$,

$$U = \left(\frac{1}{1-R}\right)\cdot\left(1 - \frac{\sqrt{3\pi}K_{I\,max}\left(\tfrac{1}{2} + R - \tfrac{1}{2}R^2\right)\left(sin\tfrac{\theta}{2} + sin\tfrac{3\theta}{2}\right)^2 sin\,2\theta}{16\sigma_0\sqrt{a^*}\left(3cos\tfrac{\theta}{2} + cos\tfrac{3\theta}{2}\right)}\right), \tag{4.17}$$

which is an expression for the extent of shielding arising from crack deflection for a crack under far-field tension.

4.2 Verification of model assumptions

4.2.1 Opening of an undeflected crack

In section 4.1 it was suggested that the elastic opening of a crack (i.e. that predicted by Equation 4.1) is a suitable approximation to the opening of a plane strain fatigue crack grown under constant amplitude cyclic loading. This assumption can be assessed through a comparison of the predicted opening of the FE model of a propagating crack to that predicted by the elastic solution. This comparison is shown in Figure 4.6 (a & b) which shows crack profiles through the unloading cycle for K_{max} = 13.3 MPa$\sqrt{m}$, $R = 0$ (a), and $R = 0.5$ (b). Considering first Figure 4.6 (a) it can be seen that the elastic and FE solutions are reasonably close for all crack lengths and for all values of K/K_{max} in the unloading cycle. It can be seen that at the first node behind the tip the FE solutions are considerably lower than the elastic solutions. However in Chapter 3 it was shown that the displacement of the node immediately behind the crack tip can behave in a spurious manner, and as such the discrepancy between the two solutions at this node is expected. At the second and third nodes behind the tip the opening predicted by the FE model is slightly greater than that predicted by the elastic solution, suggesting that plastic blunting of the crack may be occurring. Further behind the crack tip, the elastic solution generally overpredicts the opening in the FE model. The predicted openings for $R = 0.5$ are shown in Figure 4.6 (b). At this higher R it can be seen that the elastic solution is still a reasonable approximation to the FE prediction of the crack opening, consistently overpredicting to a small extent. However for purposes of the analytical model the approximation of the opening of a plane strain fatigue crack to the elastic crack opening expression seems adequate.

4.2.2 Description of the final deflected section of the crack

In section 4.1.1 the assumption is made that the final deflected section of the crack behaves like a deflection of identical dimension off a straight crack. Furthermore, the assumption is made that the tensile opening of this final deflected section of the crack is equivalent to an undeflected crack of equal length to the deflection. This allows the crack opening displacement to be specified as in Equation 4.5. The accuracy of these two assumptions can be verified by comparing the crack opening predicted by Equation 4.5 with that found for the final deflected section in a FE model of a stationary deflected crack. This is shown in Figure 4.7, for K_{max} = 4.5 MPa$\sqrt{m}$, $\theta = 45^{\circ}$. It can be seen that in the FE solution there is a degree of crack tip blunting which is clearly not accounted for in the elastic solution. Furthermore the

deformation in the FE solution is not entirely symmetric (i.e. some shear deformation has occurred). However the agreement between the two solutions is reasonably good, indicating that the approximations made in the description of the crack tip stress field of the final deflected section of a crack are reasonable.

4.2.3 Crack tip shear displacements

In the formulation of the model it is assumed that there is a residual shear deformation of the asperities and that this can be approximated as a residual *CTSD*. In Figure 4.8 the relative shear displacements of the fracture surfaces at minimum load is plotted. The data are taken from the 45° deflected crack with the crack having propagated through several deflected sections. The plot shows the relative displacement in the x-direction of nodes on the upper fracture surface from the initially matching nodes on the lower fracture surface. It can be seen that a residual mode II offset of the fracture surfaces has arisen from the prior cyclic loading. The relationship between the magnitude of this relative displacement in the overall direction of crack growth (call it x, say) and the effective displacement h of the asperity, can be seen from the geometry of the deflected crack to be $x = h\cos\theta$ (e.g. consider Figure 4.5). From the plot shown in Figure 4.8, at the asperity tips $x/CTOD \sim 0.22$, where *CTOD* is the crack opening displacement (see Section 2.1.5). From Equation 4.14, the predicted normalised offset of the asperity is $h/CTOD \sim 0.20$, i.e. $(h\cos\theta)/CTOD = 0.14$. It can be seen that the residual deformation of the asperities estimated from the residual *CTSD* is of the correct order of magnitude compared to that found in the FE model, with the effective displacement of the asperities in the FE model being approximately 1.6 times greater than that estimated by the residual *CTSD* expression, well within the bounds of the various analytical *CTSD* expressions. i.e. up to a factor of 4 greater than the Rice estimate in Equation 4.6.

4.3 Results and discussion

4.3.1 General behaviour of the model

In Figure 4.9 a comparison is shown between the predictions of the analytical model, plotted as a broken line, and the FE model, for $\theta = 60°$, $K_{I\,max} = 4.6$ MPa$\sqrt{m}$, $R = 0$. The analytical model is plotted using Equation 4.17, i.e. it is based on the elastic crack opening behaviour. The deflections of the crack are at values of $a = 20$, 40, 60 and 80 μm. It can be seen that immediately following a deflection of the crack (i.e. at small values of a^*) the analytical model significantly overestimates the extent of crack closure compared to that found in the FE model. Further away from the points of crack deflection (i.e. at larger values of a^*) the analytical model can be seen to underpredict the extent of crack closure compared to the FE results. The trend of decreasing closure as the crack tip gets further from the point of the deflection can be seen to be well represented however. In fact, the value of h predicted by Equation 4.14 and used in the analytical model was found to be an underestimate of the residual shear deformation of the asperity compared to that found in the FE model. As noted, there is considerable variation in the expressions for the *CTSD* available in the literature. As such, the value of h which is used in the analytical model could be replaced by βh, where β is a scaling factor which accounts for this underestimation. In the present analyses h was found to be 1.6 times greater in the FE model than in the analytical model, i.e. $\beta = 1.6$. Putting this value of β into Equation 4.18 yields much closer agreement to the FE solution as is shown in Figure 4.9 (plotted as the unbroken line). (N.B. The λ factor in Figure 4.9 is discussed in the Section 4.3.2.)

4.3.2 Closure immediately following a deflection

A possible interpretation of the overprediction of crack closure for small a^* (i.e. immediately after the crack undergoes a deflection) may be found from the nature of the shielding process. The shielding of the crack arises due to contact in the wake of material on the crack flanks which has undergone a shear deformation. Contact primarily occurs due to deformed material at the points of the crack deflection. However the crack must propagate some distance ahead of the deformed material in order for the material to move into the crack wake, i.e. a delay in reaching the point of maximum shielding is expected, and shielding is not instantaneous as the formulation of the analytical model implies. This process is clearly analogous to the delay in reaching the point of maximum shielding that occurs following an

overload, which arises given that the material deformed by the overload must move into the crack wake before it can lead to crack closure. The distance over which the crack needs to propagate in order to reach the point of maximum shielding may reasonably be expressed as some fraction λ of the crack tip plastic zone size r_p. There does not appear to be any way of knowing *a priori* what the value of λ should be, but inspection of the FE results suggest a value of 0.4. Hence by ignoring the predictions of the analytical model for $a^* < \lambda r_p$, and replacing it by a simple linear interpolation between the value of U at the point immediately prior to a deflection (i.e. at the maximum value of a^*) and the value of U at $a^* = \lambda r_p$, a much closer representation of the behaviour of the FE model can be achieved, as shown by the plot in Figure 4.9. This linear interpolation can be considered to be a simple representation of the transition in shielding that will occur as the crack tip progresses from the point of crack deflection (i.e. shielding is at a minimum) to the point of maximum shielding some distance ahead.

A second possible explanation for the overprediction of crack closure for small a is as follows: due to the assumptions made in the formulation of the model, Equation 4.17 is only valid for situations where the crack opening profile of the fatigue crack is dominated by elastic behaviour. When the deformed asperity is near the crack tip, plastic blunting of the crack may invalidate this approach, and lead to lower crack closure levels than those predicted by Equation 4.17. Some aspects of this behaviour may be incorporated into the model by utilising a description of the near-tip opening behaviour.

The Dugdale solution [1960] gives an approximation of the near-tip crack opening profile under plane stress, of a stationary crack as,

$$\frac{\delta}{\delta_{0\,max}} = g\left(\frac{x}{r_p}\right), \text{ where } g(\xi) = \sqrt{1-\xi} - \frac{\xi}{2} log\left|\frac{1+\sqrt{1-\xi}}{1-\sqrt{1-\xi}}\right|, \tag{4.18}$$

where δ is the crack opening displacement at a point x behind the crack tip, $\delta_{0\,max}$ is the crack tip opening displacement at maximum load, and r_p is the plastic zone size. This equation is formulated for a plane stress, stationary crack. However, Newman [1981] has shown that by including a factor to account for the constraint of the crack tip material, the Dugdale solution can provide a reasonable description of the opening behaviour of a fatigue crack under plane strain. The necessary modified expressions for $\delta_{0\,max}$ and r_p are,

$$\delta_{0\,max} = 0.5\frac{K_{1\,max}^{\ 2}}{E\sigma_0}, \tag{4.19}$$

$$r_p = \frac{\pi}{24}\left(\frac{K_{I\,max}}{\sigma_0}\right)^2 . \qquad (4.20)$$

At an instantaneous value of $K_I^* < K_{I\,max}$, the instantaneous crack tip opening displacement, δ_0^*, becomes [see Budiansky & Hutchinson, 1978]

$$\delta_0^* = \delta_{0\,max} - \Delta\delta_0$$
$$= 0.5\frac{K_{I\,max}^{\ 2}}{E\sigma_0}\left(\frac{1}{2} + \frac{K_I^*}{K_{I\,max}} - \frac{1}{2}\left(\frac{K_I^*}{K_{I\,max}}\right)^2\right),$$

i.e., $$\frac{\delta_0^*}{\delta_{0\,max}} = \frac{1}{2} + \frac{K_I^*}{K_{I\,max}} - \frac{1}{2}\cdot\left(\frac{K_I^*}{K_{I\,max}}\right)^2 . \qquad (4.21)$$

A zone of reverse plastic deformation will form, of dimension r_c, where

$$r_c = \frac{\pi}{24}\left(\frac{\Delta K}{2\sigma_0}\right)^2 = \frac{\pi}{24}\left(\frac{K_{I\,max} - K_I^*}{2\sigma_0}\right)^2,$$

i.e., $$\frac{r_c}{r_p} = \frac{1}{4}\left(1 - \frac{2K_I^*}{K_{I\,max}} + \left(\frac{K_I^*}{K_{I\,max}}\right)^2\right), \qquad (4.22)$$

and the expression for the crack opening profile at K^* becomes,

$$\frac{\delta^*}{\delta_{0\,max}} = g\left(\frac{x}{r_p}\right) - \left(\frac{1}{2} - \frac{K_I^*}{K_{I\,max}} + \frac{1}{2}\left(\frac{K_I^*}{K_{I\,max}}\right)^2\right) g\left(\frac{4x}{\left(1 - 2\frac{K_I^*}{K_{I\,max}} + \left(\frac{K_I^*}{K_{I\,max}}\right)^2\right) r_p}\right). \qquad (4.23)$$

For the deflected crack, the opening profile can be estimated by using $\delta_{0\,max} = 0.5k_I^{\ 2}/E\sigma_0$, where $k_I = \frac{1}{4}\left(3\cos\frac{\theta}{2} + \cos\frac{3\theta}{2}\right)K_I$, as described earlier.

K_I^* will equal K_{cl} when $\delta^* = h\sin 2\theta$, so using Equation 4.14, closure will occur when,

$$\frac{0.5K_{I\,max}^{\ 2}\left(3\cos\frac{\theta}{2} + \cos\frac{\theta}{2}\right)^2}{16\sigma_0 E}\left\{g\left(\frac{x}{r_p}\right) - \left(\frac{1}{2} - \frac{K_I^*}{K_{I\,max}} + \frac{1}{2}\left(\frac{K_I^*}{K_{I\,max}}\right)^2\right) g\left(\frac{4x}{\left(1 - 2\frac{K_I^*}{K_{I\,max}} + \left(\frac{K_I^*}{K_{I\,max}}\right)^2\right) r_p}\right)\right\}$$

$$= \frac{\sqrt{3}K_{I\,max}^{\ 2}\left(1-\nu^2\right)\left(\frac{1}{2} + R - \frac{1}{2}R^2\right)\left(\sin\frac{\theta}{2} + \sin\frac{3\theta}{2}\right)^2 \sin 2\theta}{16\sigma_0 E}$$

i.e.

$$g\left(\frac{x}{r_p}\right)-\left(\frac{1}{2}-\frac{K_I^*}{K_{I\max}}+\frac{1}{2}\left(\frac{K_I^*}{K_{I\max}}\right)^2\right)g\left(\frac{4x}{\left(1-2\frac{K_I^*}{K_{I\max}}+\left(\frac{K_I^*}{K_{I\max}}\right)^2\right)r_p}\right)$$

$$-\frac{\sqrt{3}\left(1-\nu^2\right)\left(\frac{1}{2}+R-\frac{1}{2}R^2\right)\left(\sin\frac{\theta}{2}+\sin\frac{3\theta}{2}\right)^2\sin 2\theta}{0.5\left(3\cos\frac{\theta}{2}+\cos\frac{\theta}{2}\right)^2}=0 \qquad (4.24)$$

Equation 4.24 can be solved numerically to find values of $K_I^*/K_{I\,max}$ which satisfy this equation for given values of x, ν, R and θ. This is shown in Figure 4.10 (in terms of U) for θ = 45° 60°, ν = 0.33, and R = 0. A β value of 1.6 has been included as above. No plots are shown for θ = 30°, for which the predicted closure level is 0 for all values of x/r_p. Also shown are the predictions of the analytical model based on Equation 4.17, and plotted as in Figure 4.9 with β = 1.6, λ = 0.4. It can be seen that the Dugdale based solution does in fact predict lower closure levels than the elastic solution following the deflection. A transition from the Dugdale-based solution to the elastic solution may be reasonable following a deflection, as the deformed asperity is at first close to the crack tip and within the region where the crack tip is blunted, and then moves further from the tip into the elastic strain dominated region with further crack propagation. As such the lower closure level predictions of the Dugdale based solution can be seen to be qualitatively consistent with the behaviour of the FE models. However, in Figure 4.11 a comparison of the crack openings in the FE model to those predicted by the Dugdale expression is shown for R = 0, from which it can be seen that the Dugdale solution significantly overestimates the opening of the crack, particularly in the near-tip region. As such, whilst near-tip blunting may be a factor in explaining the discrepancy between the closure levels predicted by the FE and elastic analytical models, it can be seen that the attempt to achieve a better approximation to the near-tip opening behaviour through the use of the Dugdale solution is not well founded.

4.3.3 Variation of U with deflection angle

In Figure 4.12 a comparison between the predictions of the analytical and FE models is shown for deflection angles of 60°, 45° and 30°. The plot is focussed on the variation of shielding along a single deflected section (i.e. $0 \le a^* \le 20$ μm), with the analytical model formulated as above with β = 1.6, λ = 0.4, as is the case for all the subsequent plots discussed in this chapter. It can be seen that the agreement between the two solutions is good.

Moreover the values of β and λ which were found to produce a good fit to the FE data for $\theta = 60^\circ$ also provide a good fit for $\theta = 45^\circ$ and 30°.

4.3.4 Variation of U as a function of $K_{I\,max}$

In Figure 4.13, a comparison between the variation of closure with increasing a^* predicted by the analytical and FE models is shown, for $K_{I\,max} = 3.5$, 5.5 and 7.5 MPa$\sqrt{m}$, $R = 0$. The FE analyses were performed using a 45° deflected crack with the length of the deflected section being 36 μm. It can be seen that there are some differences between the closure levels predicted by the analytical and FE models. However, the trend of decreasing U with increasing $K_{I\,max}$ for large a^* predicted by the analytical model is reflected in the FE results (albeit to a significantly lesser extent). The analytical model also predicts that the value of a^* at which the maximum shielding occurs should increase with $K_{I\,max}$, which is also evident in the finite element results for $K_{I\,max} = 7.5$ MPa$\sqrt{m}$ at least.

From Equation 4.17 the model appears to predict that U will decrease linearly with K_{Imax}. This clearly does not agree with the general experimental observation of decreasing closure for increasing ΔK at constant R. However, it is apparent from Figure 4.13 that the minimum value of U, achieved at $a^* = \lambda r_p$, is the same for each value of $K_{I\,max}$. This value can be found by putting $a^* = \lambda r_p$ into Equation 4.17, with r_p given by Equation 4.20, which with the inclusion of the β parameter becomes,

$$U_{min} = \left(\frac{1}{1-R}\right)\cdot\left(1 - \frac{3\sqrt{2}\beta\left(\frac{1}{2}+R-\frac{1}{2}R^2\right)\left(\sin\frac{\theta}{2}+\sin\frac{3\theta}{2}\right)^2 \sin 2\theta}{8\sqrt{\lambda}\left(3\cos\frac{\theta}{2}+\cos\frac{3\theta}{2}\right)}\right). \qquad (4.25)$$

Hence, the value of U_{min} is independent of $K_{I\,max}$ and σ_0, which is consistent with the notion that for small scale yielding conditions, shielding of the fatigue crack arising through plastic deformation should be a function of R but not $K_{I\,max}$ or σ_0, as demonstrated by the analytical model of PICC formulated by Budiansky & Hutchinson [1978]. It should be noted that due to the formulation of the analytical model this statement will not hold for crack geometries where the length of the deflected section $L < \lambda r_p$.

4.3.5 Variation of U with R

In Figure 4.14, a comparison between the analytical model predictions and the finite element results is shown for three R-ratios, for $\theta = 45^\circ$, $K_{I\,max} = 4.6$ MPa$\sqrt{m}$. In general terms, the

agreement between the two solutions is good. The analytical solution overestimates the value of U at low a^* for $R = 0.3$ and $R = 0.6$, but at greater a^* the agreement is very reasonable.

4.3.6 Comparison to experimental results

In Figure 4.15 a plot of the analytical model predictions of the variation of K_{cl}/K_{max} with simultaneous increasing ΔK and decreasing deflection angle is shown. The results of the analytical model are shown as the maximum and average values of K_{cl}/K_{max} that are achieved for the particular values of ΔK and θ that are used. It should be noted that the maximum values of K_{cl}/K_{max} are independent of ΔK. In the formulation of the plot a linear decrease in θ from 65° at $\Delta K = 4$ MPa$\sqrt{m}$ to 25° at $\Delta K = 12$ MPa$\sqrt{m}$ is assumed, with a facet length a^* of 100 μm (i.e. the facet length is greater than λr_p for all values of applied ΔK), and $R = 0.1$. This is an attempt to represent the changes in fracture surface morphology which are commonly observed in damage tolerant aluminium aerospace alloys due to the transition from a faceted crystallographic growth mode at low ΔK to a more planar ductile growth mode at higher ΔK. This is clearly a significant simplification of the actual variation in fracture surface morphology with increasing ΔK given that actual fracture surfaces will generally exhibit asperities of varying shape and size, the morphology of which may vary with changing growth mode. However this can be considered as a first order characterisation of fracture surface roughness. Also shown in Figure 4.15 is a plot of K_{cl}/K_{max} for 2024-T351 [Xu *et al*, 2000*a*] (LT orientation 12 mm thick side-grooved samples in which plane strain conditions prevail, tested at $R = 0.1$). The fatigue crack surfaces in this alloy were found to exhibit a shift from well defined crystallographic features to more ductile crack growth with increasing ΔK as assumed in the plot of the analytical model results. It can be seen that the trend of decreasing K_{cl}/K_{max} with increasing ΔK exhibited by 2024-T351 is well represented by the analytical model (for the maximum K_{cl}/K_{max} levels). However the magnitude of the analytical closure predictions are somewhat low. It should be remembered that the analytical model in its present formulation is essentially fitted to the FE results, which are also somewhat lower than typical experimental RICC levels (see Chapter 3). Possible reasons why the FE (and hence analytical) model results may underestimate the actual experimental results have been discussed previously. As such this underprediction of the experimental results by the analytical model is not surprising. If the value of β used in the analytical expression is increased from 1.6 to 2.2, i.e. an allowance is made for the underprediction of RICC due to the factors outlined above, then a closer fit to the experimental results can be obtained.

4.4 Summary and conclusions

In this chapter details have been presented of an analytical model which has been formulated based on a mechanistic understanding of RICC from Chapter 3. In particular;

- Various simplifications associated with the model formulation have been assessed and validated.
- The model considers growth of the fatigue crack at some distance from the turning points where the residual strain at the asperity has passed fully into the crack wake, allowing a simple elastic expression for the crack opening to be used.
- The model behaviour has been shown to be in good quantitative agreement with FE models, when assessed parametrically.
- The model behaviour has been shown to readily reproduce experimental results when using a simple representation of crack growth mechanisms.
- The model is unique in the literature of analytical RICC models in that the extent of shear offset of the fracture surfaces arises from within the model formulation, and is not defined arbitrarily.

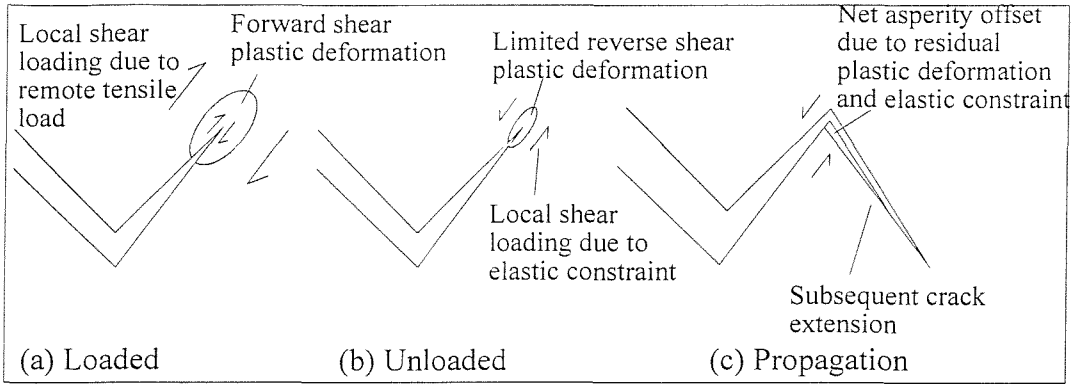

Figure 4.1. Schematic illustration of roughness induced crack closure mechanism.

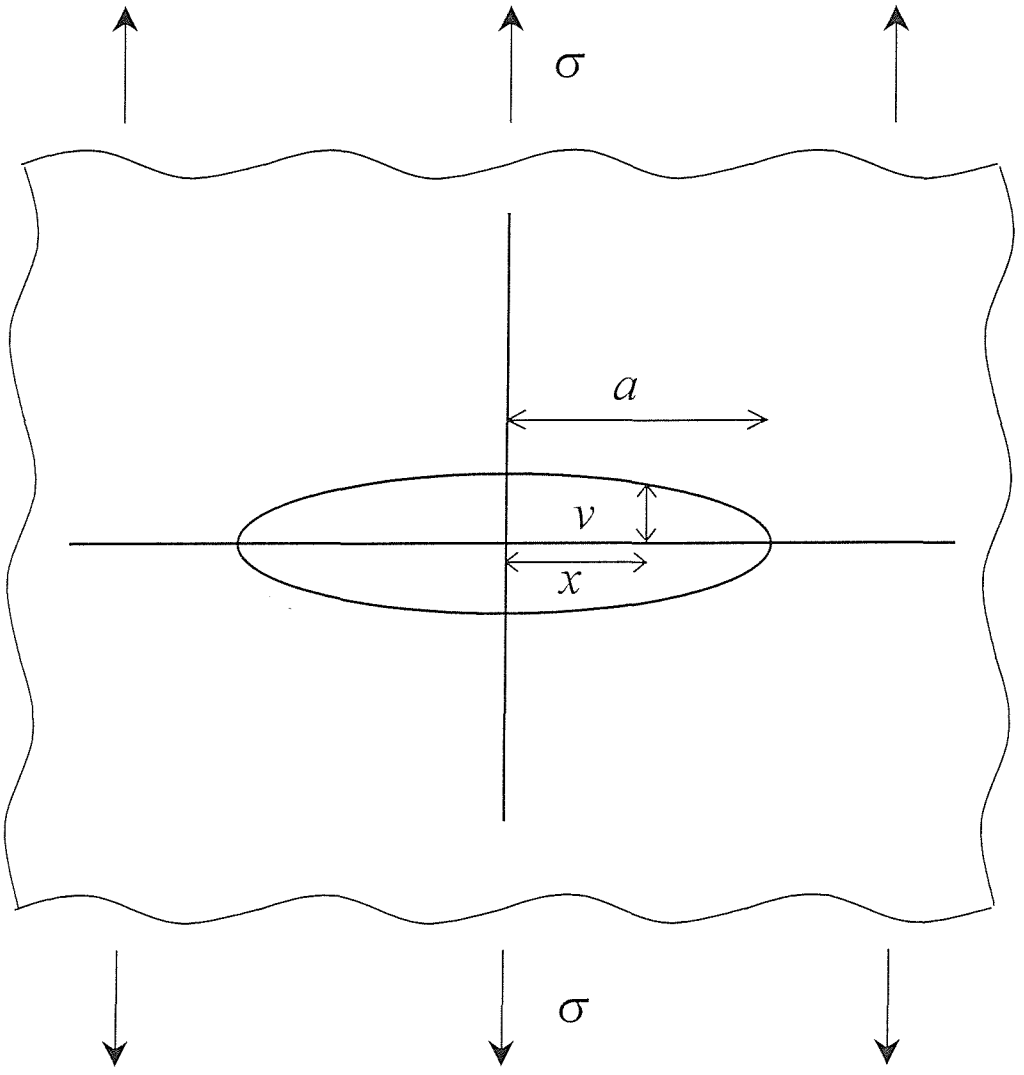

Figure 4.2. A crack in an infinite plate.

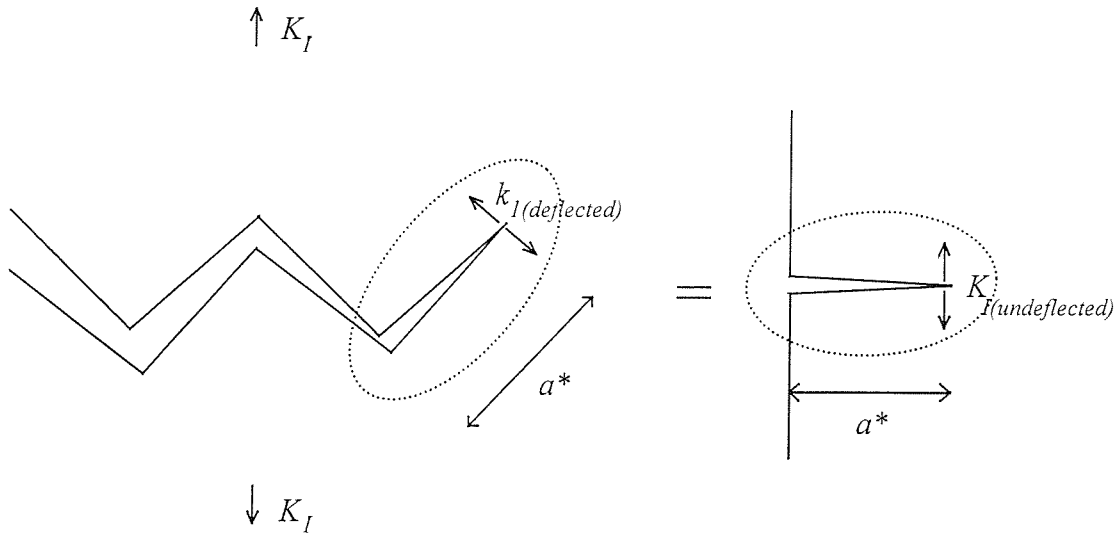

$$k_{1(deflected)} = K_{I(undeflected)}$$

Figure 4.3. Approximation of the final deflected crack section, to a undeflected crack of the same length.

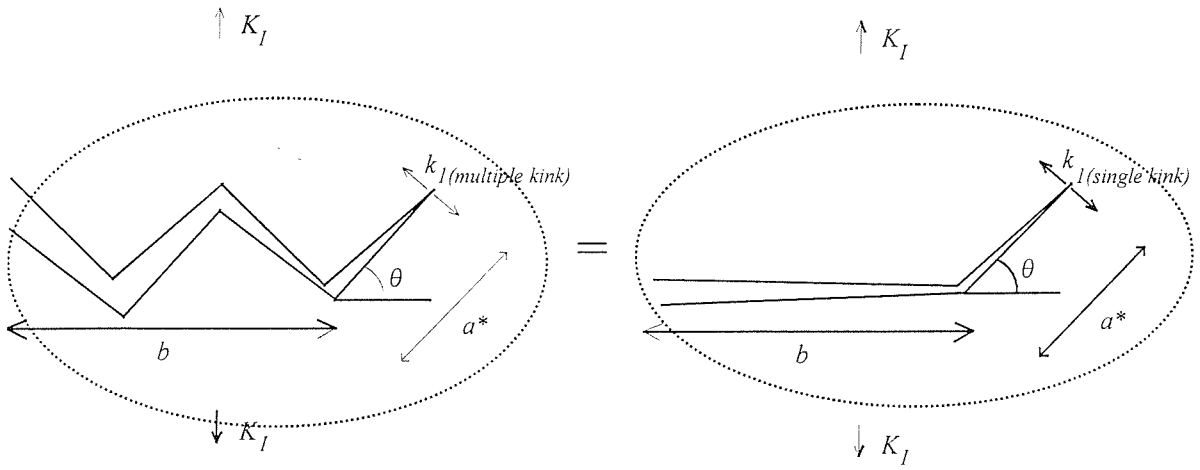

$$k_{1(multiple\ kink)} = k_{1(single\ kink)}$$

Figure 4.4. Approximation of the final deflected crack section, to a single pupative kink (i.e. $a^* << b$) off a straight crack.

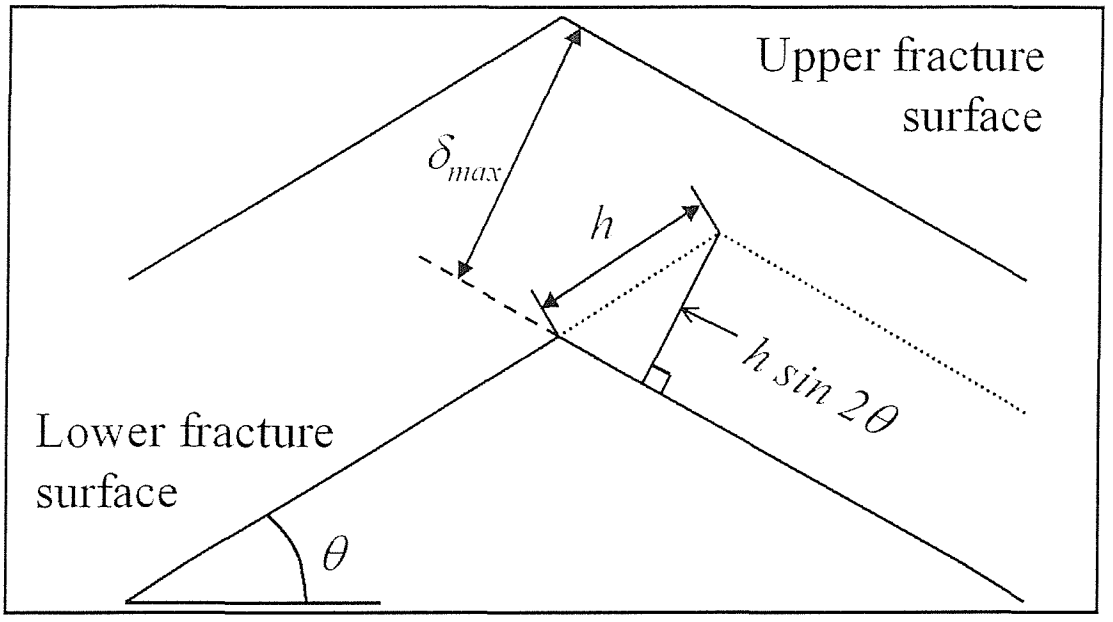

Figure 4.5. Geometry of the crack deflection model.

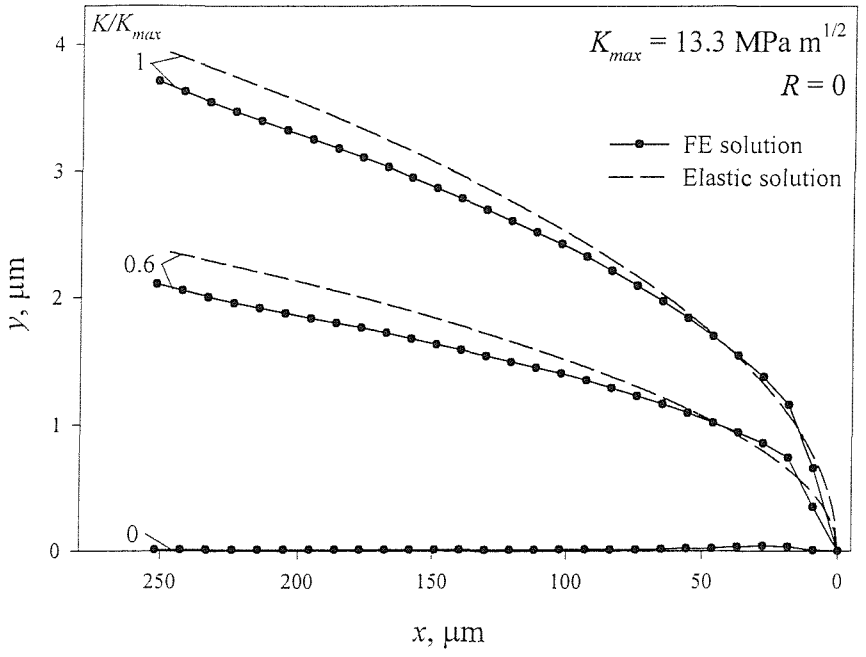

(a)

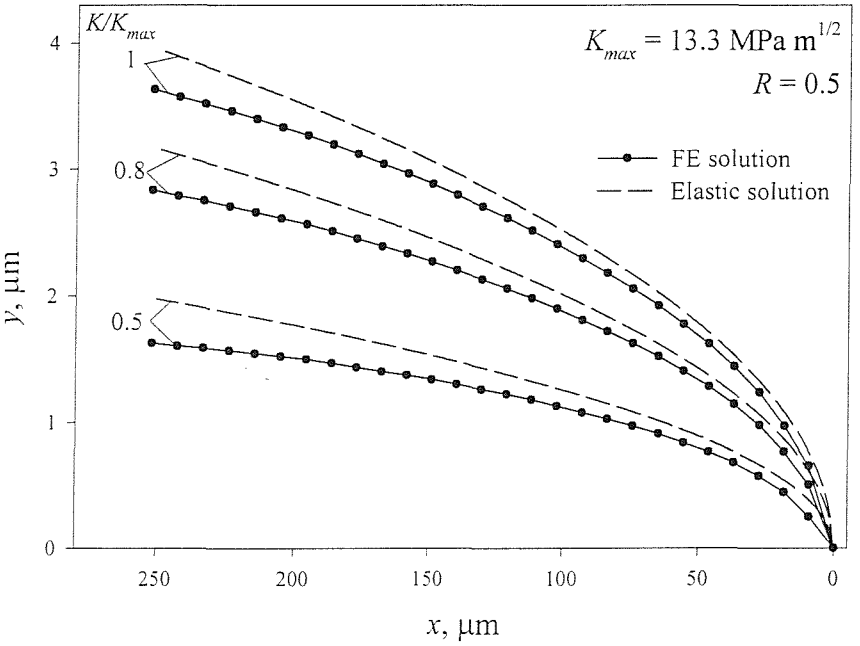

(b)

Figure 4.6. Comparison of the variation of the opening profile of a fatigue crack through the unloading cycle predicted by the FE model to that predicted by the elastic crack opening expression (Equation 4.1). The plots are for K_{max} = 13.3 MPa$\sqrt{m}$, with R = 0 (a) and R = 0.5 (b).

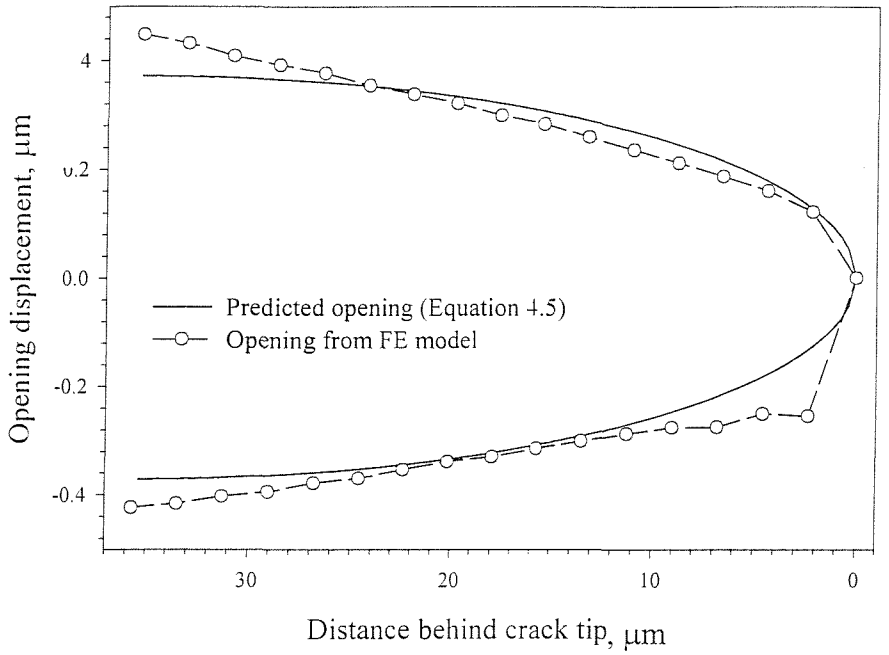

Figure 4.7. Comparison of FE crack opening prediction for the final deflected crack section, with the approximate expression used in the analytical model.

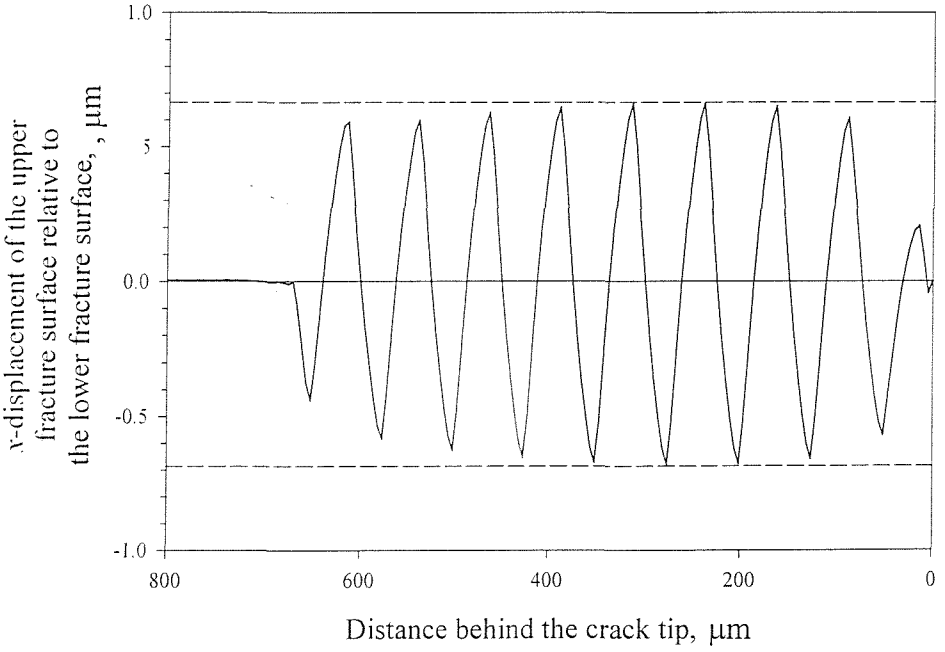

Figure 4.8. Relative shear displacement of the fracture surfaces of a deflected crack at minimum load.

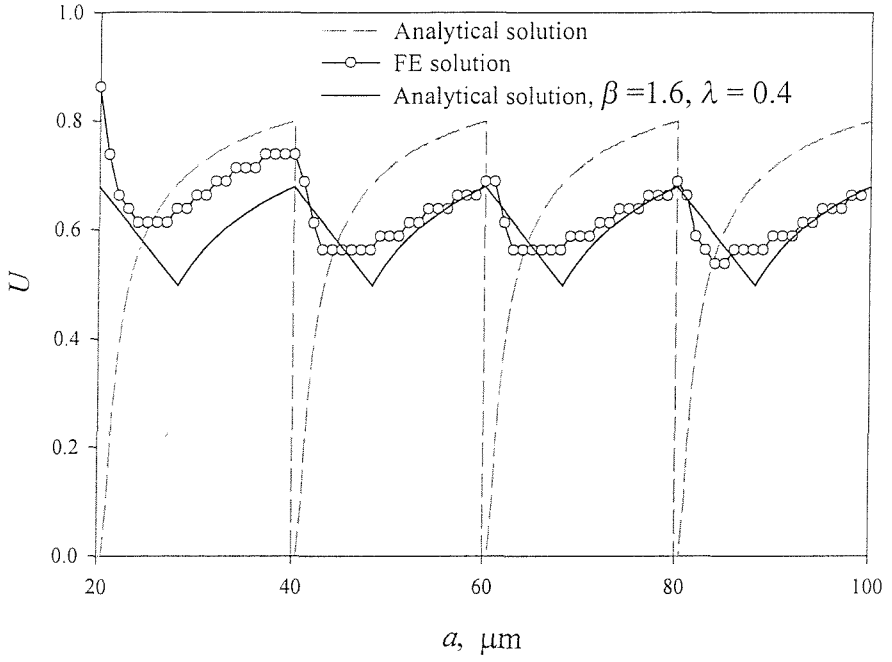

Figure 4.9. Prediction of the analytical model (Equation 4.17) compared to the closure behaviour of the FE model, for a 60° deflected crack, K_{Imax} = 4.6 MPa√m, R = 0.

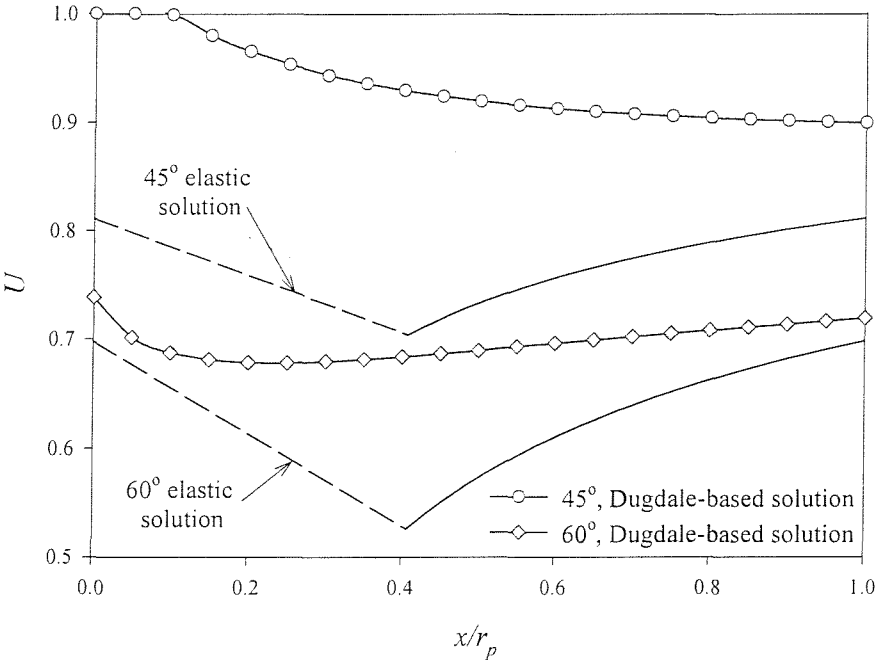

Figure 4.10. Prediction of the Dugdale-based analytical expression (Equation 4.24) which allows for blunting of the crack tip. Also shown is the elastic based model predictions for θ = 45° & 60°, K_{Imax} = 4.6 MPa√m, R = 0.

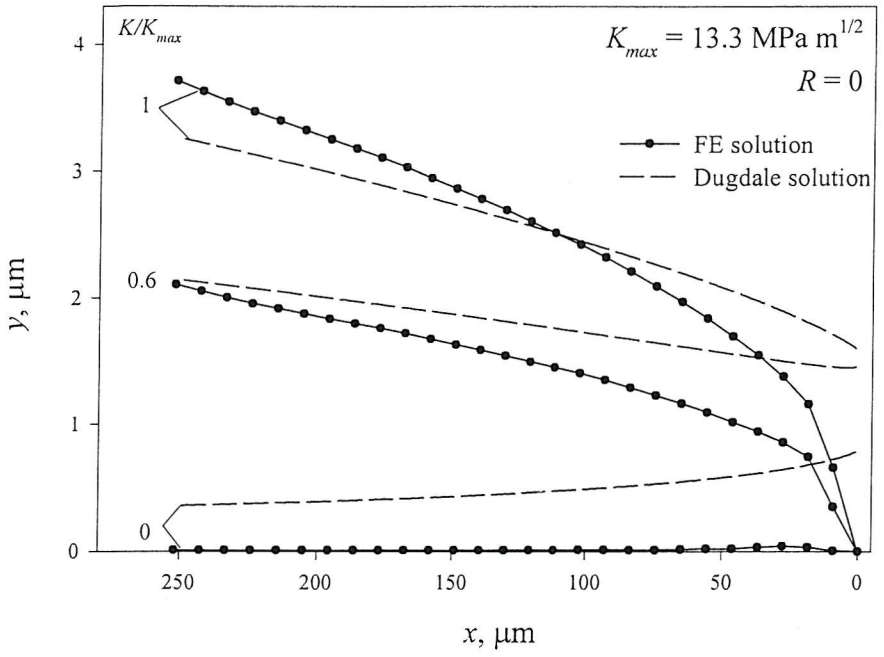

Figure 4.11. Comparison of the variation of the opening profile of a fatigue crack through the unloading cycle predicted by the FE model to that predicted by the Dugdale crack opening expression (Equation 4.23). The plot is for K_{max} = 13.3 MPa√m, with $R = 0$

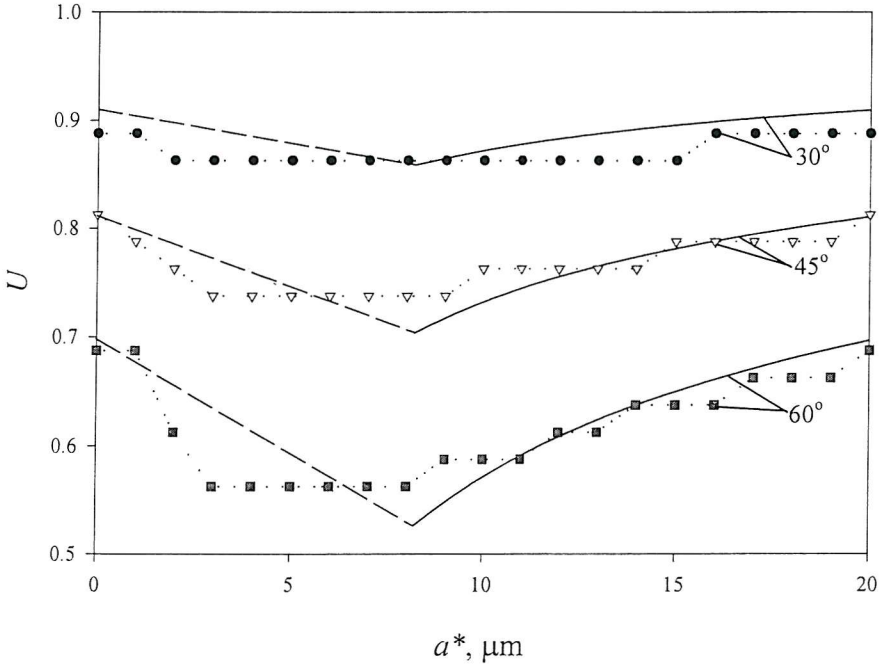

Figure 4.12. U as a function of θ, (K_{Imax} = 4.6 MPa√m, $R = 0$). Comparison of analytical model predictions (solid/dashed line) and finite element results (dotted line) along a single deflected section.

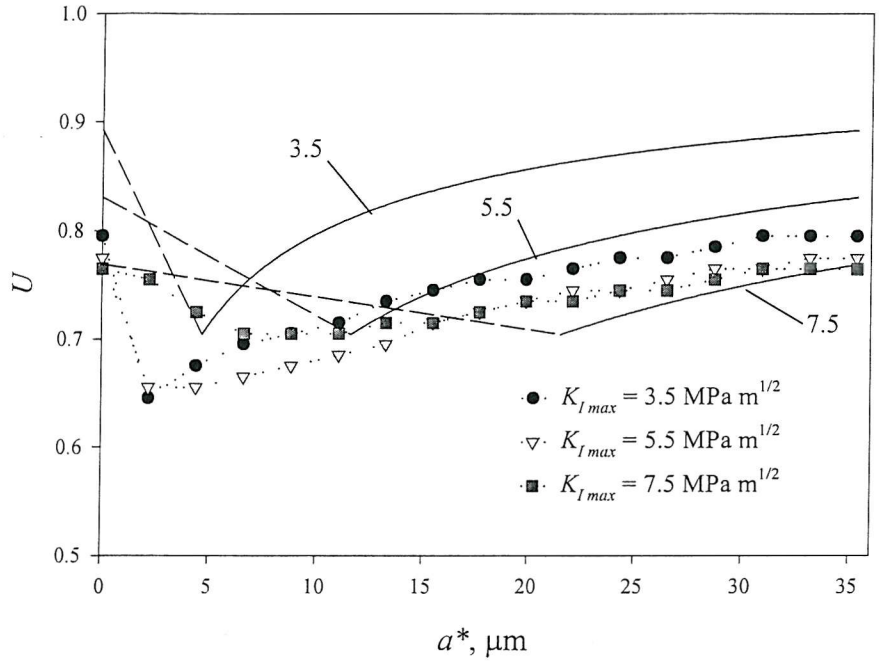

Figure 4.13. U as a function of K_{Imax}, ($R = 0$, $\theta = 45°$). Comparison of analytical model predictions (solid/dashed line) and finite element results (dotted line) along a single deflected section.

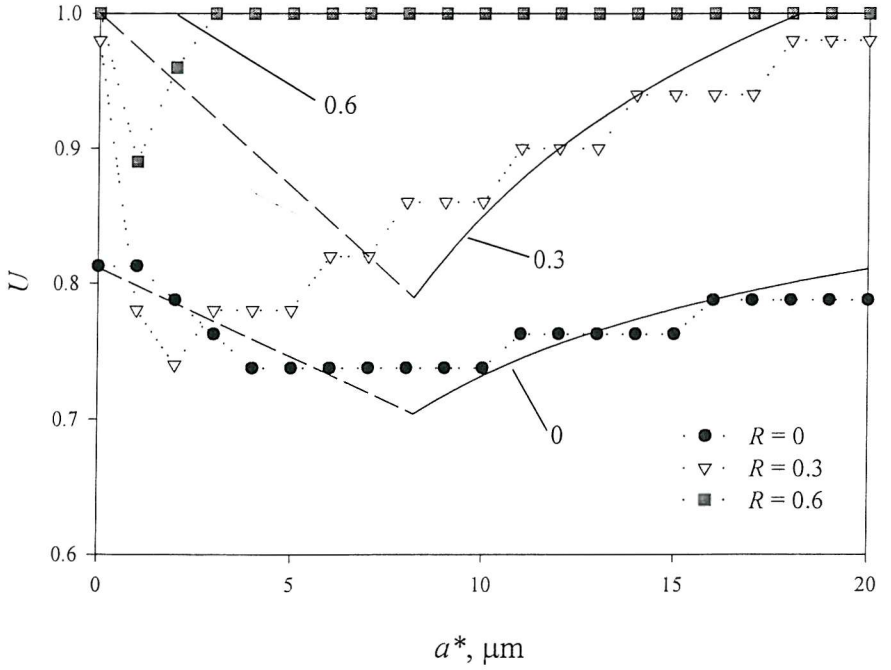

Figure 4.14. U as a function of R, (K_{Imax} = 4.63 MPa√m, $\theta = 45°$). Comparison of analytical model predictions (solid/dashed line) and finite element results (dotted line) along a single deflected section.

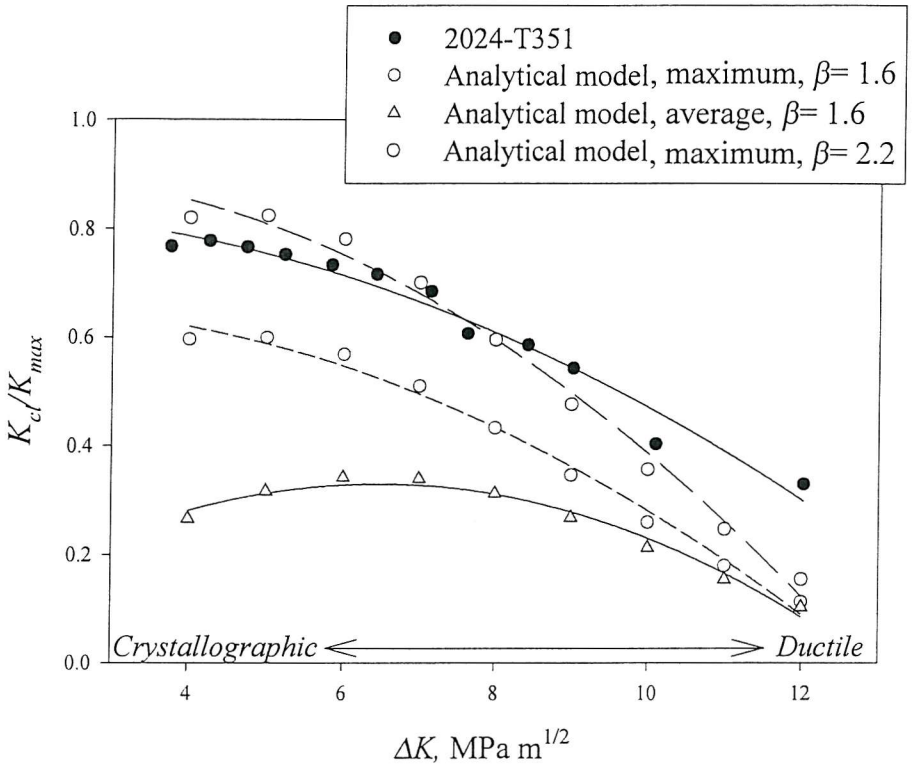

Figure 4.15. Variation of closure level with simultaneous increasing ΔK and decreasing θ, compared to the experimental behaviour of 2024-T351.

5 Modelling RICC under variable amplitude loading

5.1 Overview

In the previous chapters, a mechanism for the retardation in growth rate of a deflected fatigue crack under constant amplitude loading, was identified and investigated. Whilst studies of constant amplitude fatigue crack growth are important in providing baseline data and in investigating the fundamental mechanisms of crack growth, the loading conditions experienced in service by most engineering components and structures are not constant amplitude. Transient excursions from constant amplitude cycling (e.g. overloads and underloads) have been shown to have significant effects on fatigue crack growth rates [e.g. Skorupa, 1998]. Hence the development of a physically sound damage tolerant design philosophy for components undergoing such variable amplitude conditions requires an understanding of the mechanistic origins of load transient effects. As previously discussed, various Al-Li aerospace alloys exhibit highly deflected fatigue crack growth paths, with resulting high levels of RICC being thought to explain the superior constant amplitude fatigue crack growth resistance compared to conventional aerospace alloys (e.g. 2124, 7150) [Venkateswara Rao & Ritchie, 1988]. These Al-Li alloys can also exhibit greater sensitivity to excursions in the load history than the conventional alloys, suggesting that crack deflection may interact with crack tip plastic deformation due to load transients to enhance crack tip shielding. However, no models are available as yet in the literature to explain the processes of RICC under variable amplitude loading. In this chapter, details concerning the application of the FE method to the investigation of this potential interaction between crack deflection and simple single load transients, and the effect these may have on crack growth rates are presented. Based on the results of the FE study, a simple fracture mechanics based model of overload-induced closure in deflected cracks is put forward, and the predictions of this model are discussed.

5.2 Design of the models

The procedure used for the FE modelling of a fatigue crack growing under variable amplitude loading conditions was essentially identical to that used for the modelling of constant amplitude fatigue crack growth, as described in Chapter 3. Based on the availability of experimental data [Xu, 2000] in which a high degree of attention has been paid to the measurement and non-subjective analysis of post-overload crack closure under plane strain conditions, and what were considered to be the parameters of importance based on the current mechanistic understanding of overload induced crack closure, a matrix of basic loading, material and crack geometry combinations was assessed, as shown in Tables 5.1 and 5.2. In order to isolate the potential roughness-plasticity interaction effects, the response of an undeflected crack to single spike overloads was included. This also served to verify the present modelling results against experimental, numerical and analytical modelling results from the literature. The loading parameters of interest were baseline ΔK level ($\Delta K_{(BL)}$), and overload ratio (expressed as a percentage as $\%OL$, see Figure 2.7(a)). In particular, overload ratios of 100% and 150% were selected, for which clear effects on fatigue crack growth rates are seen. Furthermore, single overloads of these ratios are used in the calibration of models of crack growth under spectrum loading, hence their effects are of direct interest to the aerospace industry. Crack geometry aspects included asperity length (L) and the location of overload point in relation to the position of the crack deflection points. In terms of material behaviour, work hardening rate (in terms of the hardening modulus for the bilinear behaviour considered here) was also varied.

5.3 Basic closure behaviour

The general behaviour of the FE models of an undeflected crack subject to a 100% overload is shown in Figure 5.1. The model shown is for $\Delta K_{(BL)}$ = 12 MPa$\sqrt{m}$, R = 0.1, plane strain conditions, with the results being presented in terms of U, the ratio of the effective to applied stress intensity factor range (based on crack face contact), versus normalised post-overload crack extension $\Delta a/r_{p(OL)}$, (where $r_{p(OL)} = \frac{\pi}{24}\left(\frac{K_{OL}}{\sigma_0}\right)^2$ is the overload plastic zone size based on the Dugdale analysis modified for plane strain conditions, and K_{OL} is the value of K applied during the overload cycle)*. It can be seen that on application of an overload (at $\Delta a/r_{p(OL)}$ = 0), the crack driving force drops sharply. This shielding of the crack then reaches a maximum at approximately 0.1-0.3 $\Delta a/r_{p(OL)}$, with U (= $\Delta K_{eff}/\Delta K_{app}$) reaching 0.4 compared to the baseline (pre-overload) level of 1. The shielding of the crack then begins to reduce, with U rising to 0.8 once the crack has propagated through 3 overload plastic zones. The closure response of the model can be seen to replicate two of the three features commonly observed in single-overload tests, i.e. the overall reduction in crack growth rates, followed by a gradual return to baseline levels. However, the baseline value of U for the model is 1 (i.e. baseline closure does not occur for the undeflected crack geometry under plane strain conditions, as discussed in Chapter 3), hence there cannot be any reduction in closure on application of the overload. As such, this aspect of model behaviour is not consistent with the brief crack growth acceleration commonly seen experimentally, which is commonly rationalised in part as a reduction in crack closure level immediately following the application of the overload [Geary, 1992, Skorupa, 1999].

5.3.1 Effect of overload ratio

The effect of overload ratio on the crack closure response in the undeflected crack models is shown in Figure 5.2, for overload ratios ($\%OL$) of 0%, 100% and 150%, for $\Delta K_{(BL)}$ = 12 MPa$\sqrt{m}$, R = 0.1. Crack lengths are normalised by the baseline plastic zone size $r_{p(BL)} = r_{p(OL)} \Big/ \left(\frac{\%OL}{100} + 1\right)^2$. It can be seen that on application of an overload, there is a significant drop in U, followed by a gradual return to baseline behaviour, as in Figure 5.1. The magnitude of the reduction in U increases with increasing overload ratio, being approximately 30% greater for $\%OL$ = 150% compared to 100%. The affected distance (i.e.

the distance for which U is reduced from the baseline value) also increases with increasing $\%OL$. Specifically, a post-overload crack growth distance of approximately 7 $r_{p(BL)}$ is necessary for the shielding to reach half its maximum level following the 100% overload (i.e. U returns from a minimum of 0.4 to 0.7), compared to approximately 14 $r_{p(BL)}$ for the 150% overload (U returns from a minimum of 0.2 to 0.6). Furthermore, the distance to U_{min} (i.e. the distance between the application of the overload and the point of maximum retardation) also increases, being approximately double for 150% compared to 100%. It is apparent that the relationship between the degree of retardation and the extent of crack tip plasticity is not linear, in that a 60% increase in the maximum plastic zone size on going from a 100% to a 150% overload brings about an approximate doubling of the retardation effected distance. The results can be related to the deformed crack profiles which are shown in Figure 5.3. For the 100% and 150% overload models the profiles shown are for cracks which have been grown approximately 4 $r_{p(BL)}$ from the initial precrack, with the overload being applied after 2 $r_{p(BL)}$ of growth. It can be seen that the overload has deformed the crack surfaces, with an increasing degree of blunting of the material behind the overload location, and an increasing wedge of deformed material ahead of the overload location (shaded region), with increasing overload ratio, compared to the 0% overload profile. It is clear that the deformed material ahead of the overload location may contribute significantly to premature closure of the crack upon unloading.

The effect of overload ratio on crack closure response in the deflected crack models ($\theta = 45^{\circ}$, L = 150 μm) is shown in Figure 5.4, for overload ratios of 0%, 100% and 150%, for $\Delta K_{(BL)}$ = 12 MPa$\sqrt{m}$, $R = 0.1$. As previously, crack lengths are normalised by the baseline plastic zone size. Shown for comparison in Figure 5.4 are the crack closure responses of the undeflected crack models for the same loading conditions (dotted lines). On application of the overload in the deflected crack models, U increases immediately to 1 (i.e. effects of constant amplitude RICC are removed), which is consistent with the brief rise in crack growth rates seen experimentally. This increase in U is then followed by a rapid reduction and a gradual return to baseline, which is very similar to the response of the undeflected crack models. Whilst the crack deflection clearly has an influence on the baseline constant amplitude closure behaviour (as discussed in Chapter 3), the effect of the crack deflection on the 100% and 150% overload cases is minimal (for this particular crack geometry). That is, the post-overload crack closure response of the deflected crack is seemingly unmodified by the presence of crack deflection. It can be seen that due to the existence of a baseline closure level for the deflected crack

* It may be noted that generally higher ΔK levels are considered in this chapter compared to Chapter 3, due to the availability of experimental data for comparison purposes [Xu, 2000].

growth, the return to the (higher) baseline closure levels occurs sooner than for the undeflected crack models.

The similarity in crack closure response of the deflected crack models to the undeflected crack models is consistent with the deformed crack profiles shown in Figure 5.5 for the 100% and 150% overloads. It can again be seen that the effect of the overload is to cause blunting of the crack behind the overload location, and a wedge of material ahead of the overload location, leading to premature crack closure. The size of the wedge of material can be seen to increase with increasing overload ratio.

5.3.2 Effect of hardening

The effect of varying the hardening modulus on the closure response of the undeflected crack models is shown in Figure 5.6. It can be seen that as H, the gradient of the plastic portion of the bi-linear hardening curve, is reduced from 0.07 times the elastic modulus E, to 0.035 E there is a small increase in shielding following the application of the overload. This is consistent with the deformed crack profile shown in Figure 5.7. For the profile shown, the crack has grown 2 $r_{p(BL)}$ from the overload location and it can be seen that the lower hardening material exhibits a greater reduction in crack opening ahead of the overload location than the higher hardening material.

This effect is also seen in the closure response of the deflected crack models shown in Figure 5.8. It can be seen that the closure response of the deflected crack is very similar to that exhibited by the undeflected crack, for the different hardening moduli. The slight increase in closure levels with decreasing hardening modulus is consistent with the slightly increased crack flank deformation shown in Figure 5.9 for the lower hardening material.

5.3.3 Effect of baseline loading level

The effect of varying baseline stress intensity factor range on the closure response of the undeflected crack models is shown in Figure 5.10, for 100% overloads from baseline loading of $\Delta K_{(BL)}$ = 12, 8 and 4 MPa$\sqrt{m}$, R = 0.1. The mesh density used in the models is such that the ratio of the maximum crack tip plastic zone size to crack tip element length is constant. The crack lengths have been normalised by the corresponding baseline plastic zones. It can be seen that as $\Delta K_{(BL)}$ is decreased there is a slight decrease in crack closure levels. In Figure 5.11 the crack profiles are shown at maximum load for the different baseline stress intensity

factor ranges, with approximately 12 $r_{p(BL)}$ of post-overload crack growth having occurred in each case. Displacements in the crack growth direction have been normalised by the corresponding baseline plastic zone sizes, and displacements normal to the crack growth direction have been normalised by the maximum crack tip opening displacement under baseline loading conditions, $CTOD_{max} = 0.49\left(K_{max}^2/E\sigma_0\right)$. It can be seen that there is a slight decrease in normalised size of the deformed hump of material in the crack wake, with the humps for $\Delta K_{(BL)}$ of 8 and 4 MPa$\sqrt{}$m being approximately 90% and 80% respectively of the size of the hump for $\Delta K_{(BL)}$ = 12 MPa$\sqrt{}$m. That is, the crack profiles are consistent with the slightly increased closure levels found with increasing $\Delta K_{(BL)}$.

The effect of varying baseline stress intensity factor range on closure response of the deflected crack models is shown in Figure 5.12, for 100% overloads from baseline loading of $\Delta K_{(BL)}$ = 12, 8 and 4 MPa$\sqrt{}$m, R = 0.1. The closure response is shown in terms of actual crack growth distance past the point of application of the overload. Again the closure behaviour is very close to that exhibited by the undeflected crack models (shown by the dotted lines), with significant differences only arising as the cracks return to the baseline closure levels. In Figure 5.13 the crack profiles are shown for the three baseline loading levels at the closure load. It can be seen that as baseline stress intensity factor increases, so does the relative deformation of the crack flanks due to the overload, as well as the opening of the crack.

Mechanistically, closure occurs because the material at the crack tip at the point of application of the overload undergoes a greater plastic deformation than the surrounding material, which undergoes baseline loading. As such, it can be expected that (for small scale yielding conditions) it is the overload ratio that will control the extent of crack closure. Hence the absence of a dependence of overload induced crack closure on the baseline loading is intuitively acceptable, as overload plasticity and crack opening can be expected to increase at the same rate with increasing baseline loading level. As such, the origin of the apparent, small baseline dependence in the FE models is unclear, but could be an artefact of the sensitivity of the model (particularly in relation to determining the point of maximum closure), or be related to compressive plastic deformation of the overload induced wedge (which is not necessarily independent of baseline ΔK, see Section 5.5.4 below).

5.3.4 Effect of deflection length

In Figure 5.14 the effect of a reduction in the projected length of the asperity from 150 μm to 37.5 μm on the crack closure response is shown. Before the application of the overload it can

be seen that the small asperity size crack exhibits a lower baseline shielding level than the large asperity size crack, consistent with the discussion of relative asperity size effects under constant amplitude loading in Chapter 3. Following the application of the overload, there is a significant increase in the magnitude of the reduction in U for the small asperity size crack compared to the large asperity size crack (with U reducing to approximately 0.2 compared to 0.4). This behaviour is somewhat surprising, in that as the size of the asperity is reduced, it could intuitively be expected that the behaviour of the crack would tend to that exhibited by an undeflected crack. Some insight into this result can be gained by considering Figure 5.15, which shows the deformed crack profile of the small asperity size crack at the point in the unloading cycle at which crack contact occurs, after the crack has propagated some distance from the overload location. It can be seen that the crack is propped open by a wedge of residual deformation in the crack wake which extends over 6 to 7 deflected sections. This can be compared to the behaviour of the large asperity size crack, shown in Figure 5.16, where contact occurs only over 1 to 2 deflected sections. It appears that when the deformation due to the overload is such that it extends over several crack deflections, the resulting crack closure is greatly increased. The apparent significance of the size of the deformed wedge due to overload plasticity and the size of the asperities may then be rationalised as follows. When the size of the hump which arises due to the overload is small compared to the length of the deflected section, any global shear of the fracture surfaces which arises from the mode II component of the overload deformation will have little effect on crack closure, with the onset of closure being governed by the mode I deformation and opening. This is illustrated schematically in Figure 5.17. However, when the size of the hump due to the overload is large compared to the length of the deflected section, the presence of any global fracture surface offset can reduce the effective crack opening and hence increase the crack closure levels. This process is analogous to the conventional description of RICC under constant amplitude loading, and is illustrated schematically in Figure 5.18. These conditions are considered further in Section 5.5.

In order to confirm the importance of the size of the asperities relative to the scale of overload plastic deformation a further model was investigated. In this model the projected length of the asperity was kept at 150 μm, but the loading was increased to ΔK = 17 MPa$\sqrt{m}$, R = 0.1, with a 100% overload applied, such that the overload plastic zone was twice the size of the models performed at ΔK = 12 MPa$\sqrt{m}$. The values of $L/r_{p(OL)}$ for the three models (i.e. (1) ΔK = 12 MPa$\sqrt{m}$, L = 150 μm, (2) ΔK = 17 MPa$\sqrt{m}$, L = 150 μm, and (3) ΔK = 12 MPa$\sqrt{m}$, L = 37.5 μm) were thus 0.22, 0.11 and 0.055 respectively, i.e. in the ratio 4:2:1. A comparison between the closure levels in the three models is shown in Figure 5.19 from

which it can be seen that decreasing the ratio of $L/r_{p(OL)}$ leads to a progressive increase in the post overload crack closure levels.

5.3.5 Effect of overload location

The effect of the relative location of the overload to the points of crack deflection on crack closure behaviour is shown in Figure 5.20. Models were run for instances where the overload was applied when the crack tip was at the turning point of the crack, as well as at the 1/4, 1/2 and 3/4 points (see inset of Figure 5.20). It can be seen from Figure 5.20 that the post-overload closure responses are virtually coincident, i.e. the relative location of the overload seems to have little effect on crack closure response. From the crack profiles shown in Figure 5.21 for the above situations, it can be seen that the location of the overload relative to the crack deflections has little significant effect on the deformation or subsequent closure behaviour.

5.4 Near-tip and far-field closure conditions

In the results presented so far, the effect of the overloads has been reported in terms of $U = \Delta K_{eff}/\Delta K_{app}$, where ΔK_{eff} is defined by the first point of crack face contact. It has been suggested (e.g. Donald, [1997]) that crack closure need not entirely isolate the crack tip material during unloading, and that damaging cyclic strains can occur in the crack tip material below the closure load. Certainly the effectiveness of the closure event in isolating the crack tip material from the applied load can be expected to be dependent upon the distance between the crack tip and the point of crack face contact (e.g. see Chen *et al*, 1996). Unlike the constant amplitude models where closure occurs relatively close to the crack tip, the position of crack face contact in the overload models is often far from the tip. As such, the effective ΔK based on crack face contact may not provide an entirely consistent assessment of crack tip driving forces, and a measurement of actual crack tip conditions may be desirable.

In the first instance it may be reasonable to expect that the fatigue crack growth rate in a material is related to some measurement of the cyclic strain suffered by the material at the crack tip, (e.g. see the model of Donahue *et al* [1972] in which fatigue crack growth is related to the cyclic crack tip opening displacement, $\Delta CTOD$, or the model of Antolovich *et al* [1975] in which fatigue crack growth is related to near tip strain amplitude). As such, it is possible to get a more direct measure of the fatigue crack driving force in the model by considering such parameters. An effective U based on $\Delta CTOD$ (U_{CTOD}) may be arrived at by considering that $\Delta CTOD$ may be related to the fatigue crack driving force ΔK_{eff} as [Higo *et al*, 1981],

$$\Delta CTOD = \beta \frac{\Delta K_{eff}^{\ 2}}{2\sigma_0 E}. \tag{5.1}$$

Hence a normalised cyclic crack opening is,

$$\frac{\Delta CTOD_{OL}}{\Delta CTOD_{BL}} = \left(\frac{\Delta K_{eff(OL)}}{\Delta K_{eff(BL)}}\right)^2 = \left(\frac{U_{OL}}{U_{BL}}\right)^2, \tag{5.2}$$

where $\Delta CTOD_{OL}$ is the measured cyclic crack tip opening from the overload model and $\Delta CTOD_{BL}$ is that from an overload free, baseline model. Given that in the straight crack models $U_{BL} = 1$, i.e. there is no baseline closure,

$$\left(\frac{\Delta CTOD_{OL}}{\Delta CTOD_{BL}}\right)^{\frac{1}{2}} = U_{OL} = U_{CTOD}. \tag{5.3}$$

That is, it is reasonable to expect an effective U, which relates the fatigue crack growth rate to the applied ΔK, to vary as the square root of the cyclic crack tip opening displacement which arises under the overload loading history when normalised by the opening from the baseline loading history.

A similar line of reasoning can be used to arrive at an effective U based on the tensile strain range ahead of the crack tip, U_ε. In a material exhibiting a uniaxial constitutive response which can be approximated as,

$$\frac{\varepsilon}{\varepsilon_0} = \alpha\left(\frac{\sigma}{\sigma_0}\right)^n, \tag{5.4}$$

where $\varepsilon_0 = \sigma_0/E$, the strain ε_{ij} at a distance r ahead of the crack tip, provided r is in the zone of J-dominance, is given by the HRR solution [Hutchinson, 1968, Rice & Rosengren, 1968] as,

$$\varepsilon_{ij} = \alpha\varepsilon_0\left(\frac{J}{\alpha\sigma_0\varepsilon_0 I_n r}\right)^{\frac{n}{n+1}} \tilde{\varepsilon}_{ij}(\theta, n), \tag{5.5}$$

where $\tilde{\varepsilon}_{ij}(\theta, n)$ is a dimensionless function of the polar angle θ, strain hardening exponent n, and stress state, I_n is a factor which depends on n, and J is the J-integral [Rice, 1968], a measure of the strength of the crack tip singularity in a non-linear elastic material. The zone of J-dominance for small scale yielding conditions can be expected to extend from the edge of the crack tip process zone, where large deformations invalidate the HRR theory, to a distance of about 20-25% of the monotonic plastic zone size from the crack tip [e.g. see Suresh, 1991]. FE calculations suggest that the lower limit to applicability of the HRR solutions is approximately $3CTOD_{max}$ [McMeeking, 1977]. Hence, provided the measuring location for near-tip strain is at a distance r ahead of the crack tip such that $3CTOD_{max} < r < 0.2\ r_p$, then Equation 5.5 should be valid. For the material properties used, this equates to $0.06 < r/r_p < 0.2$.

Under elastic-perfectly plastic conditions (i.e. $n = \infty$), the strain in the crack tip region is proportional to the J-integral. For plane strain small scale yielding conditions,

$$J = \frac{K^2}{E\left(1-\nu^2\right)} \tag{5.6}$$

where E is Young's modulus and ν is Poisson's ratio. Hence the value of ε_{ij} at a fixed value of r ahead of the crack tip within the region over which the HRR solutions hold is directly related to the value of the elastic stress intensity factor. The cyclic strain range may therefore be written as,

$$\Delta\varepsilon_{ij} \propto \Delta K^2, \tag{5.7}$$

where $\Delta\varepsilon_{ij}$ is the strain range. Hence, the normalised cyclic strain range can be written as,

$$\frac{\Delta\varepsilon_{ij(OL)}}{\Delta\varepsilon_{ij(BL)}} = \left(\frac{\Delta K_{(OL)}}{\Delta K_{(BL)}}\right)^2 = \left(\frac{U_{OL}}{U_{BL}}\right)^2, \tag{5.8}$$

where $\Delta\varepsilon_{ij(OL)}$ is the strain range measured during an overload loading history, and $\Delta\varepsilon_{ij(BL)}$ is that measured during an overload free, baseline loading history. As before, $U_{BL} = 1$ for the undeflected crack models, hence,

$$\left(\frac{\Delta\varepsilon_{ij(OL)}}{\Delta\varepsilon_{ij(BL)}}\right)^{\frac{1}{2}} = U_{OL} = U_{\varepsilon}. \tag{5.9}$$

That is, it is reasonable to expect an effective U, which relates the fatigue crack growth rate to the applied ΔK, to vary as the square root of the cyclic strain range which arises under the overload loading history when normalised by the strain range from the baseline loading history. In fact, the characterisations of crack advance based on ΔJ and $\Delta CTOD$ are essentially equivalent, as the parameters are related as [Shih, 1981],

$$CTOD = d_n \frac{J}{\sigma_0}, \tag{5.10}$$

where d_n is a material parameter. To enable these near-tip parameters to be extracted from the model, a mesh was designed such that for closure free loading at $\Delta K_{(BL)} = 12$ MPa$\sqrt{\text{m}}$, $R = 0.1$, the element size in the near-tip region was equal to 0.5 $CTOD_{max}$, i.e. the second node behind the crack tip was precisely 1 $CTOD_{max}$ behind the tip. $\Delta CTOD$ was then evaluated at the second node behind the tip, and $\Delta\varepsilon_{22}$ was evaluated at the centre of the eleventh element ahead of the crack tip (i.e. approximately 10% of the monotonic plastic zone ahead of the crack tip), thus removing the need to consider the elements immediately adjacent to the crack tip, where inaccuracies in the solution and spurious displacements may occur. The results are presented in Figure 5.22, in terms of values of U_{CTOD}, U_{ε}, and the conventional U based on crack face contact ($U_{contact}$). From Figure 5.22 the following points can be made. Firstly, U_{CTOD} and U_{ε} were found to increase to approximately 1.8 and 1.3 times the baseline level respectively on application of the overload, suggesting that there would be a brief increase in crack growth rates (consistent with general experimental behaviour). This potential growth rate acceleration is not reflected by the contact based results, given that the baseline behaviour is closure free, as previously discussed. Secondly, some implications on the magnitude of post-overload crack driving force can be made. Both the $\Delta CTOD$ and $\Delta\varepsilon_{22}$ based results indicate that the magnitude of post-overload retardation is much less than that suggested by the contact based data, suggesting that crack driving force will drop to 0.7-0.8

of the baseline level, compared to approximately 0.4 for the contact based data. However, some considerations on the validity of the near-tip based characterisations of crack driving force are necessary. The conventional definition of *CTOD* assumes that the measurement is taken at the point where lines going at 45° from the crack tip intercept the crack flanks. This effectively requires the measurement of *CTOD* at 0.5 times the *CTOD* behind the crack tip. In the model the *CTOD* is measured at 1 (nominal, closure free) *CTOD* behind the crack tip, but as the measured *CTOD*s are normalised, Equation 5.3 should still be reasonable, provided that the measured *CTOD* is still dominated by plastic strain. However, following the application of the overload, the reduction in crack driving force causes a reduction in *CTOD*, and as such the (fixed) measuring location becomes further from the crack tip in terms of multiples of (actual) *CTOD*. For example, if the driving force drops to half of the baseline level on application of the overload, then a fixed monitoring location which is initially a single *CTOD* behind the tip will become 4 times the subsequently reduced *CTOD* behind the crack tip, making the plot shown in Figure 5.22 an upper bound to the actual crack driving force behaviour. For the $\Delta\varepsilon_{22}$ based data, the monitoring location is required to be a fixed absolute distance ahead of the crack tip, and so this problem does not occur. However, the reduction in crack driving force will mean that the monitoring location may pass out of the zone of *J*-dominance, thus reducing the validity of the results. Hence, direct quantitative comparison of the results based on $\Delta CTOD$ and $\Delta\varepsilon_{22}$ to the contact based data is perhaps misleading. The results are however interesting in that they do predict the trend of a rapid onset of retardation, reaching a maximum value at approximately 0.5 $r_{p(BL)}$ followed by a gradual return to baseline levels. Extrapolating the $\Delta CTOD$ and $\Delta\varepsilon_{22}$ based data indicates that their return to baseline levels is significantly sooner than the contact based data, consistent with an effective over-prediction of retardation by the contact based data for situations where the crack tip is far from the point of the application of the overload.

A further indication of the effect of the overload on the fatigue crack growth rate can be found by considering the cyclic strain which is suffered by material in the crack tip process zone (i.e. within 3 $CTOD_{max}$ of the crack tip), which can also be determined to some extent from the FE model. It should be remembered that the ability of the simple plasticity model to replicate the large strains found in the crack tip process zone is limited, but some indication of the near-tip behaviour may be found. An understanding of the relationship between crack closure and the crack tip strain can be gained by considering Figure 5.23, which shows the variation of strain at various distances ahead of the crack tip through the loading and unloading cycle at approximately 0.5 $r_{p(BL)}$ past the overload location. The loading history comprises a 100% overload from $\Delta K_{(BL)}$ = 12 MPa$\sqrt{m}$, R = 0.1 baseline loading. K_{cl}/K_{max},

based on crack face contact was found to be 0.67, with closure occurring immediately behind the crack tip. Three strain measuring locations were used: At 0.25, 0.75 and 5 *CTOD* ahead of the crack tip (all values of *CTOD* based on closure free conditions). It can be seen that all the strain responses exhibit a sharp change in slope at K_{cl}. It may be noted that whilst the measuring locations are within the nominal plastic zone, the actual plastic zone is much reduced due to closure and the compressive stresses around the crack tip associated with the overload, and the measuring location at 5 *CTOD* is actually within the elastic region, as evidenced by the fact that the only non-linearity in the load-strain plot arises due to crack face contact. The importance of crack closure on crack driving force can be evaluated by considering the effect that closure has on the crack tip strain. For the measuring location at 0.25 *CTOD* ahead of the crack tip the portion of the loading cycle from K_{cl} to K_{min} accounts for less than 15% of the crack tip strain. For the measuring locations at 0.25 and 5 *CTOD*, the figures are approximately 25% and 50% respectively. Hence a clear dependence on measuring location on the strain behaviour can be seen. It is evident that for measuring locations increasingly close to the crack tip the significance of the portion of the loading cycle $K < K_{cl}$ decreases. As such it appears that defining the crack driving force from crack face contact in the conventional manner should be a good approximation, provided that contact is occurring close to the crack tip (as in this instance). It is interesting to consider this plot in terms of the compliance ratio technique of Donald [1997] (c.f. Section 2.7). The basis of the compliance ratio technique is the consideration that the crack growth rate should be related to the total (elastic) strain range of material near the crack tip, and not just defined by the portion of the loading cycle above K_{cl}. However, Figure 5.23 indicates that using the elastic strain range in this way will considerably underestimate the effect of crack closure on the very near-tip plastic strain, for which crack growth can be reasonably expected to depend.

The contact based closure results presented thus far have been based on the first point of crack face contact during the unloading cycle (ignoring the potentially anomalous behaviour of the first node behind the crack tip, see Chapter 3). For the models subjected to overloads this contact generally occurs near the location of the crack tip at the point when the overload was applied, whereas for overload-free loading, contact occurs in the deflected crack models fairly close to the crack tip. However as has been discussed, the effectiveness in isolating the crack tip material from the full cycle of applied load of crack closure can be expected to diminish as the point of contact becomes further from the crack tip. As such, global specimen closure (that is, the point of first contact, regardless of position) may overestimate the shielding experienced by the crack tip material due to the overload as discussed above. It is possible however to define alternative closure points based on near-tip contact (taken in this case to mean contact on the same deflected section as the current crack tip), and far-field

contact (based on contact due to material deformed by the overload). The plots of near-tip and far-field closure based on these definitions are shown in Figure 5.24, for a 100% overload, $\Delta K_{(BL)}$ = 12 MPa$\sqrt{m}$, R = 0.1. It can be seen that on application of the overload there is a brief period of closure-free crack growth, followed by a rapid increase in shielding as the crack propagates into the zone of plastic deformation due to the overload. At this stage the point of first contact is immediately behind the crack tip and hence the plots based on the two closure definitions are coincident. After the crack has propagated approximately 1 $r_{p(BL)}$ past the overload a crack deflection occurs. At this point, first contact occurs a little way behind the crack tip and props the now deflected crack tip open, such that the near-tip shielding level is greatly reduced. After some further crack propagation the propping open of the final deflected section reduces and the two plots converge. The subsequent near-tip behaviour can be seen to return to baseline loading more rapidly than the far-field closure level. Indeed by the time the crack has propagated through 6-7 $r_{p(BL)}$ the near-tip closure behaviour has returned to that of the baseline whereas the far-field shielding continues to decrease. This implies that the global closure level does over-predict the shielding of the crack tip material as it mainly reflects the far-field behaviour. Hence, measurements of crack closure would ideally be able to discriminate between near-tip and far-field contact. In fact it has been suggested that near-tip and far-field contact can be separated through the identification of distinct linear sections in the offset compliance curves [Paris & Hermann, 1982]. It should be noted that in the work of Paris & Hermann, it is actually the near-tip closure due to the overload, and the far-field baseline closure which are discriminated between in the specimen compliance, whereas in the present model the far-field closure is essentially due to the overload, and the near-tip closure is essentially due to the operation of constant amplitude RICC. An attempt to discriminate between the two closure points in the present model based on offset displacement and strain curves was unsuccessful (see Figure 5.25), even when virtual strain gauges were located near the position of the crack tip at the point of application of the overload, and near the position of the current crack tip (in each case far away enough from the crack tip for plastic strain effects to be absent), in an attempt to increase sensitivity over the conventional compliance measurement via the crack mouth opening gauge. That is, although the onset of far-field closure is clearly picked up by all the gauges, the near-tip closure point is not discernible from the compliance plots alone, and the closure levels based on the onset of non-linearity in specimen compliance are inherently over-predictions of crack tip shielding. It should be considered that the nature of crack face contact is not well represented in the present FE models in terms of frictional contact, which may have implications for the compliance variations following crack face contact in real samples.

5.5 Analytical modelling of overload effects

In this section a simple analytical model of the effect of an overload on crack flank deformation and subsequent crack closure is presented. The model is based on simple fracture mechanics concepts, and is similar to the modelling of RICC presented in Chapter 4. Through this modelling approach, insights into the functional dependence of overload effects have been attained for both undeflected and deflected fatigue crack growth.

5.5.1 Undeflected fatigue crack growth

Consider an undeflected, through-thickness crack in the centre of a plate, of half length a. In Chapter 4 it was argued that the crack flank displacements of a constant amplitude plane strain fatigue crack away from the tip may be approximated by the equation for the elastic stress field displacements [Tada *et al*, 1973], i.e.

$$u_y = \frac{2\sigma}{E}\left(1-\nu^2\right)\sqrt{a^2-x^2}\,, \tag{5.11}$$

where u_y is the elastic displacement of the crack flank in the y-direction at a distance x from the origin, E is the elastic modulus and ν is the Poisson ratio. Differences in the crack flank displacements between the fatigue crack and elastic crack could be expected to arise through plastic blunting in the near-tip region of the fatigue crack, or through the presence of previously plastically deformed of material in the crack wake. However, under plane strain, constant amplitude conditions, any continuous 'wedge' of material on the crack flanks due to previous deformation may be assumed to be small or non-existent.

Following the application of an overload, material which has previously undergone a tensile deformation will be left in the crack wake, as illustrated in Figure 5.26. The profile of the crack can now be considered to be the elastic crack profile, upon which is superimposed a 'hump' due to the overload, (the origin of the hump of material in the crack wake under plane strain is the contraction in the crack growth direction, hence conservation of volume is not violated). The height h of the hump may in the first instance be approximated as,

$$h = CTOD_{res(OL)} - CTOD_{res(BL)}, \tag{5.12}$$

where $CTOD_{res(OL)}$ and $CTOD_{res(BL)}$ are the residual crack tip opening displacements for the overload and baseline cycles,

i.e. $CTOD_{res} = CTOD_{max} - \Delta CTOD$

$$= \beta \frac{K_{max}^{\ 2}}{\sigma_0 E} - \beta \frac{\Delta K^2}{2\sigma_0 E}$$

$$= \frac{\beta}{2\sigma_0 E}\left(K_{max}^{\ 2} + 2K_{min}K_{max} - K_{min}^{\ 2}\right) \tag{5.13}$$

where $CTOD_{max}$ and $\Delta CTOD$ are the maximum and cyclic crack tip opening displacements, β is a constant usually taken as 0.5 for plane strain conditions, K_{max}, K_{min} and ΔK are the maximum and minimum stress intensity factors and stress intensity factor range respectively, and σ_0 is the yield stress. Hence h can be written as,

$$h = \frac{\beta}{2\sigma_0 E}\left(K_{max(OL)}^{\ 2} + 2K_{min}K_{max(OL)} - K_{min}^{\ 2}\right) - \frac{\beta}{2\sigma_0 E}\left(K_{max(BL)}^{\ 2} + 2K_{min}K_{max(BL)} - K_{min}^{\ 2}\right) \tag{5.14}$$

where $K_{max(OL)}$ and $K_{max(BL)}$ are the maximum stress intensity factors of the overload and baseline cycles. This can be rearranged to give,

$$h = \frac{\beta\, K_{max(BL)}^{\ 2}}{2\sigma_0 E}\left(\xi^2 + 2R\xi - 2R - 1\right), \tag{5.15}$$

where $\xi = \frac{K_{max(OL)}}{K_{max(BL)}} = \left(\frac{OL\%}{100} + 1\right)$, and $R = \frac{K_{min}}{K_{max(BL)}}$.

That is, the height of the hump left in the crack wake as a result of the overload is expressed in Equation 5.15 as a function of the baseline loading, the size of the overload and the materials properties. Hence, this expression for the height of the hump due to the overload can now be considered with the expression for the crack flank displacement, Equation 5.11, to produce an expression for post-overload crack closure. By putting $\sigma = K_I / \sqrt{\pi a} F$, where K_I is the applied mode I stress intensity factor, and F is a geometry correction factor, and including the displacement geometry correction factor V, Equation 5.11 becomes,

$$u_y = \frac{2K_I\left(1-\nu^2\right)}{E\sqrt{\pi a}}\sqrt{a^2 - x^2}\,\frac{V}{F}. \tag{5.16}$$

It is the opening at a distance $l = a\text{-}x$ behind the crack tip that is of interest (see Figure 5.26) hence we can write,

$$u_y = \frac{2K_I\left(1-\nu^2\right)}{E\sqrt{\pi a}}\sqrt{2al - l^2}\,\frac{V}{F}. \tag{5.17}$$

Clearly, when $u_y = h$, $\frac{K_I}{K_{max(BL)}} = \frac{K_{cl}}{K_{max}}$,

i.e. $$\frac{2K_I\left(1-\nu^2\right)}{E\sqrt{\pi a}}\sqrt{2al - l^2}\,\frac{V}{F} = \frac{\beta\, K_{max(BL)}^{\ 2}}{2\sigma_0 E}\left(\xi^2 + 2R\xi - 2R - 1\right) \tag{5.18}$$

This can be rearranged to give,

$$\frac{K_I}{K_{max(BL)}} = \frac{K_{cl}}{K_{max}} = \frac{\beta K_{max(BL)}\sqrt{\pi a}}{4\sigma_0 E\left(1-\nu^2\right)\sqrt{2al-l^2}}\frac{F}{V}\left(\xi^2 + 2R\xi - 2R - 1\right) \qquad (5.19)$$

or in terms of $U = \Delta K_{eff}/\Delta K_{app} = K_{max} - K_{cl}/K_{max} - K_{min}$,

$$U = \frac{1}{1-R}\left(1 - \frac{\beta K_{max(BL)}\sqrt{\pi a}}{4\sigma_0 E\left(1-\nu^2\right)\sqrt{2al-l^2}}\frac{F}{V}\left(\xi^2 + 2R\xi - 2R - 1\right)\right). \qquad (5.20)$$

That is, in Equation 5.20, the post-overload crack closure behaviour of an undeflected plane strain fatigue crack is expressed in terms of the baseline loading, the size of the overload, the specimen geometry, the material properties and the distance through which the crack has propagated subsequent to the overload.

5.5.2 Fatigue crack growth along a single deflected section

Based on the concept of overload plasticity being effectively constrained to one deflected crack section (i.e. idealising the behaviour discussed in relation to Figure 5.15), the case of an overload occurring when the crack is growing along a single deflected section, at an angle θ to the nominal mode I crack growth direction, can now be considered, as illustrated in Figure 5.17. The local mode I stress intensity factor, k_I, at the tip of the crack is given by [Bilby *et al*, 1977]

$$k_I = \frac{1}{4}\left(3\cos\frac{\theta}{2} + \cos\frac{3\theta}{2}\right)K_I . \qquad (5.21)$$

As shown above, the size of the hump due to overload plasticity scales with the square of the opening mode stress intensity factor, whereas the elastic opening of the crack increases linearly with the opening mode stress intensity factor. Hence, the effect on crack tip driving force of an overload of given size would be expected to diminish with increasing crack deflection angle (i.e. the size of the overload induced hump decreases more rapidly than the crack opening as K_I is attenuated with increasing crack deflection angle), for the case of a crack growth along a single deflected section. This can be quantified by combining Equations 5.20 and 5.21, to give,

$$U = \frac{1}{1-R}\left(1 - \frac{\beta K_{max(BL)}\sqrt{\pi a}}{16\sigma_0 E\left(1-\nu^2\right)\sqrt{2al-l^2}}\frac{F}{V}\left(\xi^2 + 2R\xi - 2R - 1\right)\left(3\cos\frac{\theta}{2} + \cos\frac{3\theta}{2}\right)\right). \qquad (5.22)$$

5.5.3 Multiply deflected cracks

For the case where overload plasticity is of a similar scale to the crack deflection (as in Figure 5.16) a different approach must be taken. Following the application of the overload on a section of a multiply deflected crack, a hump of material will be left in the crack wake as described above. However, a residual shear deformation of the fracture surfaces will also occur, due to the local mode II component of the overload. As such, the effective opening of the fatigue crack will be reduced, as illustrated in Figure 5.27. It can be seen that the origin of this additional reduction in crack opening is a global shear of the deflected crack surfaces, analogous to the conventional description of constant amplitude RICC. However, whereas the origin of the global shear of the fracture surfaces under constant amplitude loading is questionable (see the discussion in Chapter 3), under variable amplitude loading the offset can originate from the shear component of the load transient. The reduction of crack opening through this mechanism was investigated by Suresh & Ritchie [1982] for constant amplitude fatigue, and a similar analysis can be combined with that presented above to give an approximation to the crack closure behaviour of multiply deflected cracks (i.e. the reductions in crack opening due to the global shear offset of the fracture surfaces and the presence of the overload-induced hump can be combined, as illustrated in Figure 5.18. From Figure 5.27 the ratio of the reduced crack opening displacement, δ^*, due to the mode II displacement of the fracture surfaces, u_x, to the nominal (mode II displacement free) opening δ, can be seen to be,

$$\frac{\delta^*}{\delta} = 1 - \frac{u_x \tan\theta}{\delta} . \tag{5.23}$$

Hence, by combining Equations 5.22 and 5.23, we obtain:

$$U = \frac{1}{1-R}\left(1 - \frac{\beta K_{max(BL)}\sqrt{\pi a}}{16\sigma_0 E\left(1-\nu^2\right)\sqrt{2al-l^2}} \frac{F}{V}\left(\xi^2 + 2R\xi - 2R - 1\right)\left(3\cos\frac{\theta}{2} + \cos\frac{3\theta}{2}\right)\left(\frac{\delta}{\delta + u_x \tan\theta}\right)\right) \tag{5.24}$$

which is a description of the post-overload crack closure behaviour of a multiply deflected plane strain fatigue crack in terms of the baseline loading, the size of the overload, the specimen geometry, the material properties, the distance through which the crack has propagated subsequent to the overload, crack deflection angle and the extent of the mismatch of the fracture surfaces. The residual shear offset of the fracture surfaces can be approximated as,

$$u_x = CTSD_{res} \tag{5.25}$$

where $CTSD_{res}$ is the residual crack tip sliding displacement due to the overload. Using the expression for $CTSD_{res}$ given in Equation 4.14, with K_{Imax} taken as $K_{max(OL)}$, with $\Delta K_{(BL)}$ = 12

MPa$\sqrt{m}$, $R = 0.1$, 100% overload, $\theta = 45°$, $E = 74$ GPa, $\sigma_0 = 370$ MPa, $\nu = 0.33$, gives $CTSD_{res} = 2.5$ μm. The nominal (mode II displacement free) opening δ, is given by

$$\delta = 2(u_y - h) \tag{5.26}$$

i.e. it is the distance between the crack flanks at maximum load when the reduction due to the overload has been taken into account. For similar loading as above, and $l = 680$ μm ($\sim 1 r_{p(OL)}$) i.e. at a distance away from the crack tip such that this simple analytical model based on linear elastic fracture mechanics assumptions may be expected to have some validity, Equations 5.15 and 5.17 give $h = 5$ μm, and $u_y = 6.5$ μm respectively, i.e. $\delta = 3$μm. As such u_y/δ can be expected to be of the order of 0.8.

5.5.4 Verification of model assumptions

There are three main assumptions in the analytical model of overload effects presented above. These assumptions are (1) that the equation for the elastic stress field displacements (Equation 5.11) is a suitable description of a plane strain fatigue crack (previously addressed in Chapter 4), (2) that the height of the wedge in the crack wake arising from overload plasticity can be approximated through the concept of a residual *CTOD* (Equation 5.15), and (3) that a residual mode II displacement occurs due to the overload, and that it can be approximated as a residual *CTSD* (Equation 5.25).

The validity of the second assumption can be evaluated by examining the overload induced plastic deformation left in the crack wake in the FE models. To do this, profiles of the undeflected cracks were analysed at the point of closure, after the crack had propagated well away ($3\ r_{p(OL)}$) from the overload deformed region. By examining the zone of overload deformation far from the crack tip in this way, the potential influence of the crack tip strain field on the crack flank displacements is reduced. The deformed crack profile for a 100% overload, $\Delta K_{(BL)} = 12$ MPa$\sqrt{m}$, $R = 0.1$, fatigue crack is shown in Figure 5.28. Also shown is the elastic solution based on Equation 5.11 for $K = K_{cl}$. It can be seen that the deviation of the FE solution from the elastic solution appears to be closely related to the overload (applied when the crack tip was approximately 2000 μm behind its current position). The height of the wedge of plastic deformation h can be estimated by comparison to the elastic solution, as shown in Figure 5.28. Using this process, h was evaluated for the various overload ratios and baseline stress intensity factor ranges used. The results are shown in Table 5.3 (labelled $h_{(FE)}$ along with the values of h which can be calculated from the analytical solution given in Equation 5.15 (labelled $h_{(analytical)}$). It can be seen that the analytical solution for h consistently over-predicts the value that is found in the FE analysis ($h_{(FE)}$ is ~70% of

$h_{(analytical)}$), but the general agreement in terms of $\%OL$ and $\Delta K_{(BL)}$ is good. A possible explanation for the lower values of h in the FE models compared to those predicted by Equation 5.15 is compressive yielding of the overload-induced hump during the portion of the loading cycle $K < K_{cl}$ due to crack face contact. Figure 5.29 specifically illustrates such compressive yielding of the overload-induced hump can be seen. As such, the analytical description of post-overload deformation is clearly a simplification of the actual behaviour in that it doesn't take into account the possibility of compressive yielding. However, as a tool to gain further insight into aspects of the functional dependence of overload-induced crack closure the simplification would appear reasonable.

The third assumption, (that the overload leads to a residual mode II displacement which can be approximated as a residual *CTSD*), can also be considered in comparison to the FE results. In Figure 5.30 the profile of the fracture surfaces at the point of first contact is plotted, focussing on the material just ahead of the overload location. The data is taken from the 45° deflected crack with a projected length of the deflected sections of 37.5 μm with the crack having propagated approximately 300 μm (~0.5 $r_{p(OL)}$) subsequent to the application of the overload. The displacements in the plot have been magnified by 30 times. It can be seen that the initial crack face contact has occurred at two locations near the tips of the asperities on the upper fracture surface. However, no contact can be seen to have occurred at the tips of the asperities on the lower fracture surface (e.g. there is no contact at the point labelled A in Figure 5.30, which would be expected under constant amplitude loading, c.f. Figure 3.12). This is consistent with a 'global' shear of the upper fracture surface towards the crack tip relative to the lower fracture surface, due to the overload as assumed in the model formulation.

5.5.5 Predictions of the analytical model

The predictions of the analytical models can be compared to those of the FE models. In Figure 5.31 the predicted effect of overloads of 100% and 150% on $U = \Delta K_{eff}/\Delta K_{app}$ is shown for both the analytical and the FE model. It can be seen that for $\Delta a/r_{p(OL)} < 0.5$ the analytical model clearly overpredicts the closure level compared to that found in the FE model, with a prediction of $U = 0$ for some distance subsequent to the application of the overload. This prediction arises because the predicted size of the overload-induced hump is greater than the predicted crack opening at the specific distance behind the crack tip. In fact, for closure to occur the crack has to grow some distance into the overload plastic zone before the residual deformation will lead to crack closure, and the instant onset of closure implied by the

analytical model is unrealistic. Furthermore, from Figure 5.3 it can be seen that when the overload induced hump is near to the crack tip, the residual blunting of the crack by the overload effectively increases the crack opening. After further crack propagation the opening becomes dominated by the elastic displacements, and the blunting becomes less important. As this feature is not included in the model formulation the overprediction of the crack closure level immediately following the application of the overload is understandable. As such the analytical expression can only be considered to represent the situation where a significant amount of crack growth has occurred subsequent to the overload. For $\Delta a/r_{p(OL)} >$ 0.5 it can be seen that the general agreement between the two models is reasonable with the magnitude of increasing closure with increasing overload ratio exhibited by the FE results being well reproduced by the analytical model.

In Figure 5.32 the predictions of the analytical model are compared to the FE model for a 100% overload from a baseline stress intensity factor range of 12, 8 and 4 MPa$\sqrt{m}$. It can be seen that when normalised by the overload plastic zone size the analytical model predicts no dependence of closure on the baseline ΔK. Apart from a small dependence of closure on $\Delta K_{(BL)}$ in the FE models (discussed previously) the quantitative agreement between the two models is apparent. The lack of baseline dependence in the analytical model is consistent with the notion that the relevant deformations (i.e. the wedge of the plastically deformed material due to the overload and the opening of the crack) should scale with the loading (c.f. the model of constant amplitude PICC of Budiansky & Hutchinson [1978] discussed in section 2.4.1).

In Figure 5.33 the response of the analytical and FE models to changes in the overload ratio are shown for a deflected crack (length of the deflected section L is 150 μm). Given that the deflected section is relatively large compared to the wedge induced by overload plasticity, the analytical solution used is that given in Equation 5.22. An obvious difference between the two solutions is the lack of any constant amplitude RICC effects in the analytical expression which clearly exist in the FE solution. In terms of the overload-induced closure response, the FE models do not exhibit any reduction in closure levels with deflection, whilst some influence is seen in the analytical models (i.e. the closure levels found in the FE models of the deflected and undeflected cracks were similar for this particular crack geometry, whereas the analytical models show a reduction in closure level due to crack deflection). As such the quantitative agreement between the models is not good in this case. A better quantitative agreement would be attained if the approach associated with Equation 5.24 was included, i.e. if a reduction in opening due to an overload induced mode II offset was modelled. For

example, by considering Figure 5.34 which shows a comparison of the post-overload behaviour predicted by the different analytical model solutions, it can be seen that the 'large' and 'small' deflection solutions cover a relatively large range of possible closure responses. Further work would be worthwhile to pursue a further understanding of the transition in behaviour from one case to the other with changing fracture surface morphology.

In Figure 5.35 the effect of the length of the deflected section on the closure level is shown. The FE results are for the large and small (150 and 37.5 μm) deflections, with a 100% overload from $\Delta K_{(BL)}$ 12 MPa$\sqrt{m}$. The analytical solutions are based on Equation 5.22 for the large deflection (i.e. mode II offset not considered) and Equation 5.24 for the small deflection (i.e. mode II offset considered with a value of u_r/δ of 0.6). The general trend in the solutions of increasing closure with deflections of a size, such that residual mode II displacements become important in enhancing crack closure, is well represented. The quantitative agreement between the FE and analytical solutions for the crack with the smaller deflected sections is reasonable, supporting the proposed mechanism of the enhancement of overload effects through crack roughness.

5.6 Comparison with previous results

5.6.1 Modelling results

The general behaviour of the undeflected crack FE model can be compared to a similar FE modelling study of Fleck & Shercliff [1989], shown in Figure 5.36. In both studies cracks in CCP specimens are considered under plane strain, small scale yielding conditions, with the application of a single 100% overload, ($R = 0$ in the Fleck & Shercliff model compared to 0.1 in the present study). In general, the comparison between the two studies is close, with two main differences apparent: (1) The Fleck & Shercliff model exhibits a baseline (pre-overload) closure level, whereas the present results are closure free, and (2) the values of U are approximately 0.15 lower in the Fleck & Shercliff study than in the present results. The first discrepancy can be explained by the definition of the closure point used in the two studies. In the present study, closure is based on contact at the second node or further behind the crack tip in order to avoid the potentially spurious behaviour of the near-tip node, as discussed in Chapter 3. However the Fleck & Shercliff model does consider closure at the first node behind the tip, giving rise to a potentially questionable baseline closure level. The second discrepancy may also be influenced by this factor, with post-overload closure occurring slightly earlier at the first node behind the crack tip, but may also be related to the hardening behaviour assumed in the two studies. In the Fleck & Shercliff model, elastic-perfectly plastic behaviour was assumed, whereas in the present model kinematic hardening was implemented. Thus the higher closure levels exhibited by the Fleck & Shercliff model are consistent with the trend of increasing post-overload closure level with decreasing hardening modulus exhibited by the present model.

A comparison to U values predicted for the same specimen geometry and loading variable can be made between the present FE results and the analytical results of Xu [2000] (Figure 5.37). These analytical results come from a discretised strip yield model similar to the approach of the FASTRAN programme [Newman, 1992], and utilise a constraint factor in a similar manner to account for the stress state at the crack tip. For the results presented the constraint factor has a value of 3, representing plane strain conditions. It can be seen that the values of U following the overload are similar for both values of the overload ratio for both modelling methods, and that the relative increase in shielding with increasing overload ratio is consistent. There is some discrepancy in the occurrence of the maximum shielding, which the analytical model predicts to occur at $\Delta a/r_{p(OL)} \approx 0.5$, compared to 0.2. for the FE results. Also, the analytical model predicts a faster return to baseline closure levels, with retardation

lasting approximately two overload plastic zones. This apparent over-prediction of the retardation distances in the FE model is again consistent with the notion that closure away from the immediate crack tip region will not entirely isolate the crack tip material in the FE model.

Although a direct comparison cannot be made, the predicted effects of the hardening modulus on the closure behaviour in the present FE results (as shown in Figure 5.6) can be seen to be consistent with the FE modelling results of Pommier & Bompard [2000], which show decreased post-overload closure levels with increasing hardening modulus, when using a kinematic hardening rule. This behaviour is physically reasonable in that the extent of crack tip plastic deformation, and hence the reduction of crack opening in the wake, will diminish with increasing hardening modulus, resulting in reduced crack tip shielding.

5.6.2 Experimental results

The response of the FE model to an increase in overload ratio can be compared to experimental data which has been reported for 100% and 150% overloads, with baseline loading of ΔK = 8 MPa$\sqrt{}$m, R = 0.1, in 2124-T351 [Venkateswara Rao & Ritchie, 1988]. Under these loading conditions, the constant amplitude fatigue fracture surfaces in 2124-T351 were observed to be fairly planar, without extensive crack deflection, and, as such, the material may provide a reasonable comparison to the present undeflected crack FE models. The experimental data was presented in terms of *da/dN* rather than U, and hence the model data must be transformed to allow comparison. However, by making some simplifying assumptions, a relationship between the normalised growth rates and the value of U in the FE models can be found. Specifically, if a constant value of the Paris exponent m is assumed across the range of ΔK which will operate, then from the Paris law, the normalised fatigue crack growth rate is,

$$\frac{\frac{da}{dN}}{\frac{da}{dN}(BL)} = \frac{C(U_{OL}\Delta K)^m}{C(U_{BL}\Delta K)^m} = \left(\frac{U_{OL}}{U_{BL}}\right)^m, \qquad (5.27)$$

where U_{OL} and U_{BL} are the values of U for the overload and baseline tests. In the present undeflected crack models U_{BL} = 1, hence the normalised crack growth rate is simply $(U_{OL})^m$, and comparison to the experimental results can be effected. This is shown in Figure 5.38 with m = 2.5. The gradient of the constant amplitude log *da/dN* vs log ΔK_{app} curve for 2124-T351 presented by Venkateswara Rao & Ritchie [1988] does in fact vary somewhat over the range of applied ΔK, from approximately 2.5 for ΔK in the range 4 - 6.5 MPa$\sqrt{}$m, to approximately 5 for ΔK in the range 6.5 to 8 MPa$\sqrt{}$m, for R = 0.1. However, for the purpose

of a qualitative comparison this approximation will suffice. Furthermore, in the experimental results a baseline closure level does exist, hence even if the actual post-overload closure levels were identical in the experimental and FE results, the normalised crack growth rates would be different. As such, it must be stressed that the purpose of presenting the FE and experimental results in this way is to allow a first order comparison of the post-overload fatigue crack growth rate behaviour, and not to effect an accurate quantitative comparison. It can be seen in Figure 5.38 that the relative change in the growth rate predicted by the FE models on going from a 100% to a 150% overload is of the correct order of magnitude, when compared to the experimental results. Furthermore the predicted normalised distance from the point of the overload to the point at which the minimum growth rate occurs compares well to that found experimentally. It can seen that the total affected distance is greater in the present modelling results than for the experimental results, where the baseline growth rate is restored after the crack has grown through approximately 2 overload plastic zones. This is consistent with the overprediction of crack tip shielding by the contact based closure definition for instances where closure occurs far from the tip, as discussed previously.

In Figure 5.39 the response of 2024-T351 to 100% overloads at R = 0.1, $\Delta K_{(BL)}$ = 12 and 8 MPa$\sqrt{m}$, from plain (i.e. non-side-grooved) 12 mm thick specimens sized for nominally plane strain conditions, is shown. The data have been taken from a test programme in which closure assessment is made via non-subjective measurement techniques [Xu *et al*, 1999]. The results are again presented in terms of normalised crack growth rate, as described above. For $\Delta K_{(BL)}$ = 8 MPa$\sqrt{m}$, post-overload *da/dN* drops to approximately 10% of the baseline value, whereas for $\Delta K_{(BL)}$ = 12 MPa$\sqrt{m}$ it drops to approximately 2%. This behaviour is clearly not seen in the FE results, where little effect of baseline ΔK is found. These results could indicate that the experimental post-overload retardation is strongly influenced by factors not represented by the FE models. As discussed in Chapter 2, experimental investigations of the effects of baseline stress intensity factor have revealed complex behaviour. As $\Delta K_{(BL)}$ decreases, oxide and roughness induced crack closure mechanisms may become increasingly significant in enhancing post-overload retardation [Venkateswara Rao & Ritchie, 1988, Ward-Close & Ritchie, 1988], with *da/dN* also being highly sensitive to small changes in ΔK_{eff} [McEvily & Yang, 1990]. At higher $\Delta K_{(BL)}$ post-overload PICC effects may increase with increasing $\Delta K_{(BL)}$ as the crack tip stress state becomes more plane stress in nature (with associated increase in plastic closure effects). Indeed, although the specimens used in the experimental investigation were sized for nominally plane strain conditions, there will be a region at the surfaces where plane stress conditions will exist. These plane stress regions may be relatively small but can have a significant effect on the resulting closure. A similar

comparison to experimental results using side-grooved specimens (Figure 5.40, [Xu *et al*, 1999]) in which the plane stress regions are effectively removed show a much better agreement with the present modelling results in terms of the distance to minimum growth rate as well as the rate of return to baseline behaviour, indicating that the plane stress regions do have a significant effect. There is still a discrepancy in that a greater reduction in normalised growth rate is found to occur for $\Delta K_{(BL)}$ = 12 MPa$\sqrt{m}$ compared to $\Delta K_{(BL)}$ = 8 MPa$\sqrt{m}$, as for the standard specimens. It should be noted however that there is a degree of experimental uncertainty in measuring the minimum growth rates. In particular, due to the higher baseline growth rates, the test performed at $\Delta K_{(BL)}$ = 12 MPa$\sqrt{m}$ is more sensitive to a given relative reduction in da/dN compared to the $\Delta K_{(BL)}$ = 8 MPa$\sqrt{m}$ test. This may explain in part the apparently greater retardation at higher baseline level.

A qualitative comparison of the effects of crack deflection predicted by the FE model to experimental data is shown in Figure 5.41. The experimental data shows the variation in normalised growth rate with increasing crack length for 150% overloads from baseline loading of $\Delta K_{(BL)}$ = 8 MPa$\sqrt{m}$, R = 0.1 for centre cracked panels, sized for plane strain conditions (but without side-grooves), of 2090-T8E41 and 2124-T351. Fatigue crack paths in 2090-T8E41 were found to be significantly deflected, whereas the crack paths in 2124-T351 were found to be much more planar [Venkateswara Rao & Ritchie, 1988]. The FE data is for 100% overloads from baseline loading of $\Delta K_{(BL)}$ = 12 MPa$\sqrt{m}$, R = 0.1, for an undeflected crack, and for the small asperity size deflected crack, with the closure data being transformed to growth rate data as detailed above. It can be seen that the alloy which exhibits significant crack deflections shows greater sensitivity to the overload than the alloy which does not. The basic trends compare well to those exhibited by the FE models with analogous fracture surface morphologies.

5.7 Summary and conclusions

The FE modelling approach has been extended to investigate the effect of a single spike overload on the fatigue crack driving force. In particular;

- An initial baseline study of undeflected crack growth has been performed to enhance understanding of the role of loading and material parameters in overload-induced crack closure.
- Comparison of these baseline results to numerical, analytical and experimental results from the literature has demonstrated the physically reasonable behaviour of the model and has established confidence in the results.
- A detailed investigation of near-tip conditions has confirmed that closure does have a significant effect on the near-tip strain field, and that ΔK_{eff} based on crack face contact is a reasonable estimate of crack driving force, at least for situations where closure occurs near to the crack tip.
- An investigation into the overload-induced crack closure behaviour of deflected cracks has shown little effect of crack deflection for the primary crack morphology studied.
- A significant increase in post-overload closure has been found for crack morphologies in which the wedge of overload plasticity extends over many asperities. This result is explained through the reduction in crack opening of a deflected crack that arises when a residual shear displacement of the fracture surfaces exists.
- Analytical modelling which uses LEFM concepts to describe the overload-induced deformation, the opening of the crack and the effect of this shear displacement has been formulated, and shown to exhibit reasonable agreement with the FE results.
- The assumptions used have been verified through comparison to the FE models, and as such the analytical model can be considered to support the proposed mechanisms through which crack roughness can influence the retardation effect of an overload.
- The results of the analytical and FE modelling have been shown to be consistent with various results from the literature.

Model Number	*%OL*	**Hardening modulus**	$\Delta K_{(BL)}$, MPa$\sqrt{m}$
1	0	0.07 *E*	12
2	100	0.07 *E*	12
3	150	0.07 *E*	12
4	100	0.035 *E*	12
5	100	0.07 *E*	8
6	100	0.07 *E*	4

Table 5.1. Model matrix for the FE investigation of single spike overloads on undeflected cracks.

Model Number	*%OL*	**Hardening modulus**	$\Delta K_{(BL)}$, MPa$\sqrt{m}$	*L*, μm	**Location of OL**
7	0	0.07 *E*	12	150	turning point
8	100	0.07 *E*	12	150	turning point
9	150	0.07 *E*	12	150	turning point
10	100	0.035 *E*	12	150	turning point
11	100	0.07 *E*	8	150	turning point
12	100	0.07 *E*	4	150	turning point
13	100	0.07 *E*	12	37.5	turning point
14	100	0.07 *E*	17	150	turning point
14	100	0.07 *E*	12	150	mid-point
15	100	0.07 *E*	12	150	1/4 point
16	100	0.07 *E*	12	150	3/4 point

Table 5.2. Model matrix for the FE investigation of single spike overloads on 45° deflected cracks.

%OL	$\Delta K_{(BL)}$, MPa$\sqrt{m}$	$h_{(FE)}$, μm	$h_{(analytical)}$, μm	$h_{(FE)}/h_{(analytical)}$
100	12	3.0	4.1	0.73
150	12	5.4	7.2	0.75
100	8	1.4	1.8	0.77
100	4	0.28	0.46	0.61

Table 5.3. Comparison of the values of *h*, the height of the wedge in the crack wake due to overload plasticity, evaluated from the FE and analytical models.

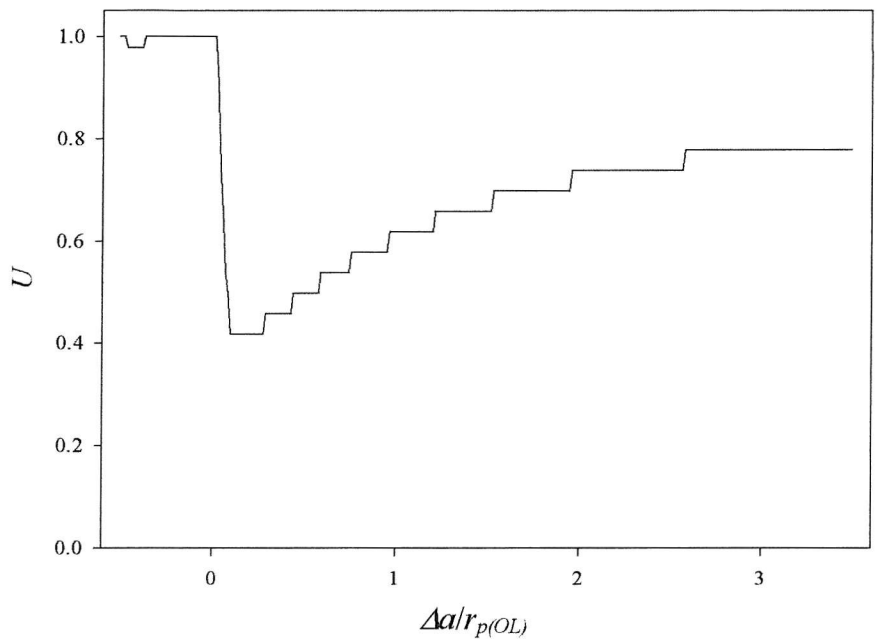

Figure 5.1. General behaviour of the present FE model of an undeflected crack for ΔK = 12 MPa$\sqrt{m}$, R = 0.1, 100% overload (applied at $\Delta a/r_{p(OL)} = 0$).

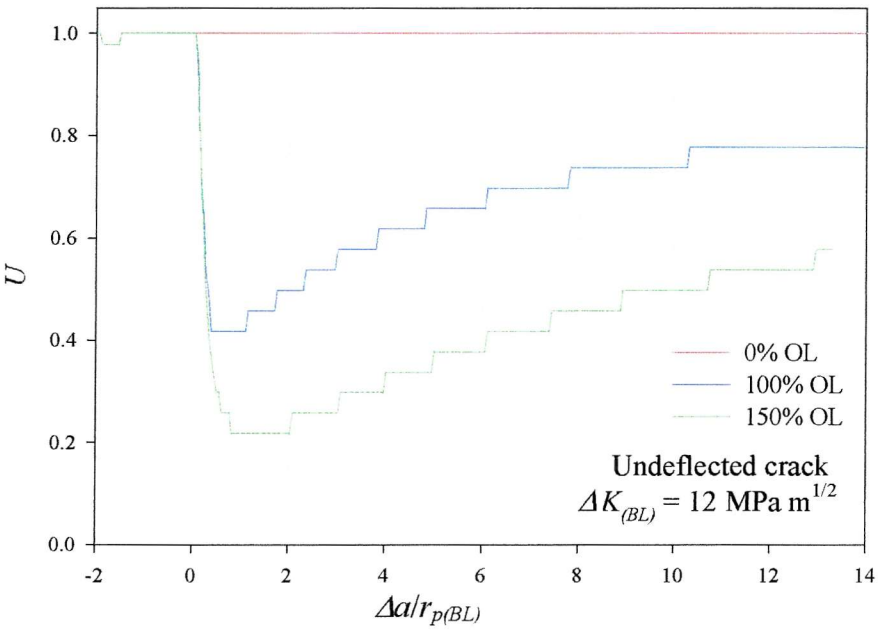

Figure 5.2. Effect of overload ratio on the crack closure behaviour for an undeflected crack.

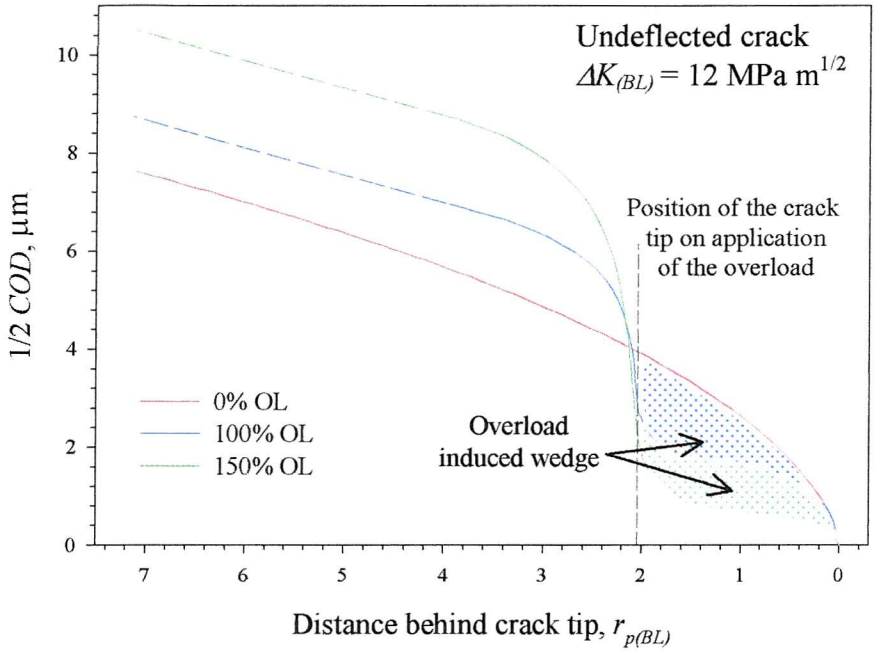

Figure 5.3. Maximum load crack profiles for an undeflected crack, for different overload ratios.

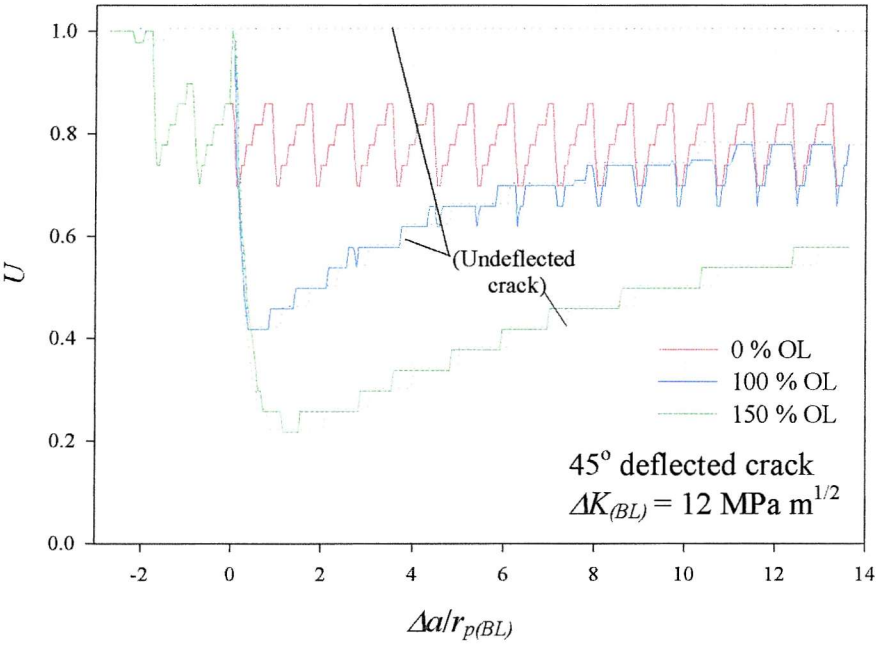

Figure 5.4. Effect of overload ratio on crack closure behaviour of a deflected crack. Dotted lines show undeflected crack behaviour.

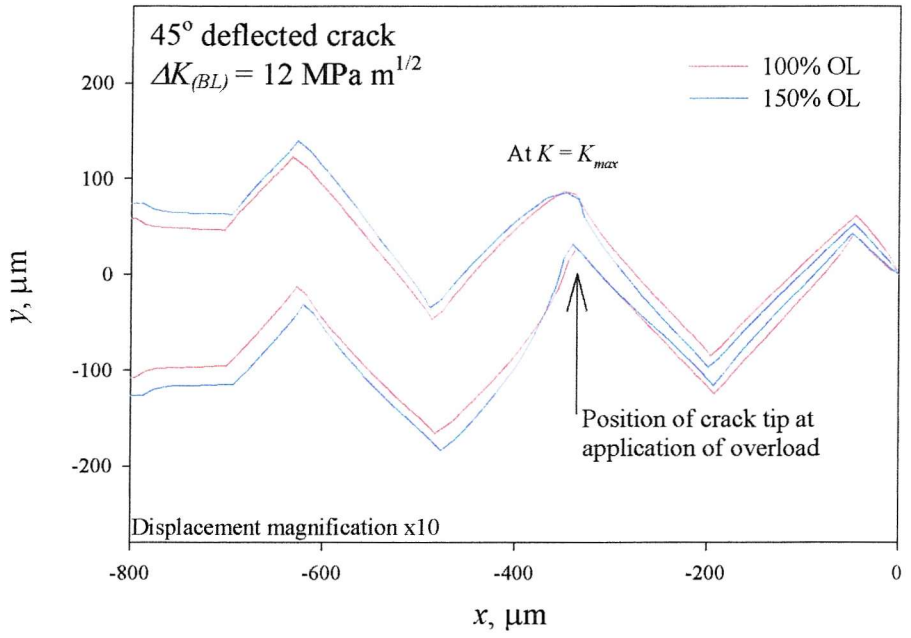

Figure 5.5. Maximum load crack profiles for different overload ratios for a deflected crack.

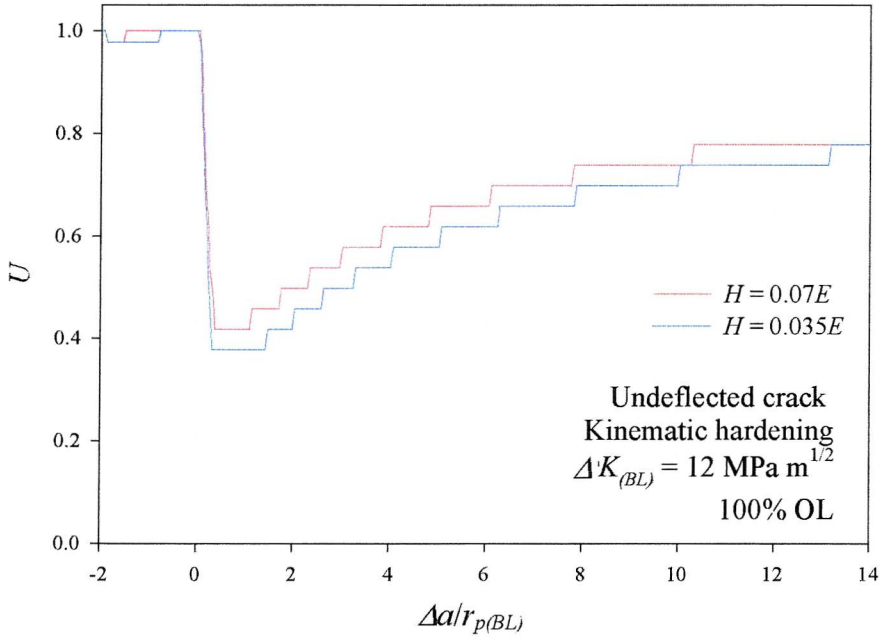

Figure 5.6. Effect of hardening modulus on the crack closure behaviour for an undeflected crack.

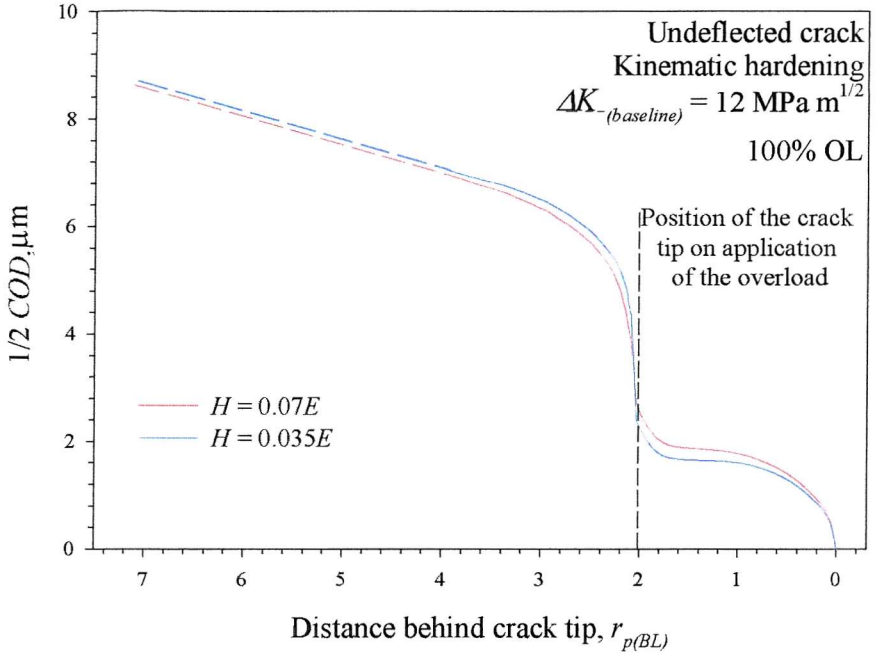

Figure 5.7. Maximum load crack profiles for different hardening moduli for an undeflected crack.

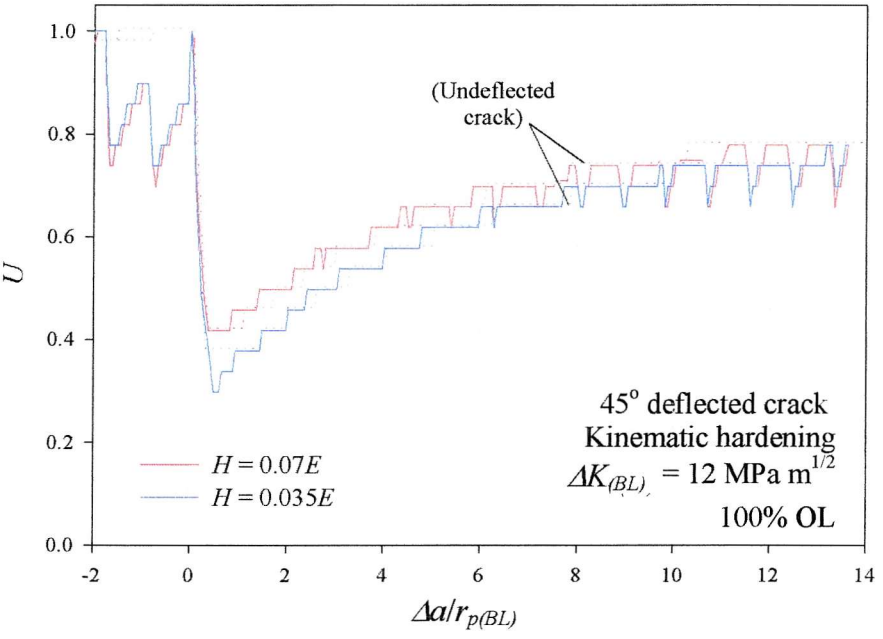

Figure 5.8. Effect of hardening modulus on crack closure behaviour for a deflected crack.

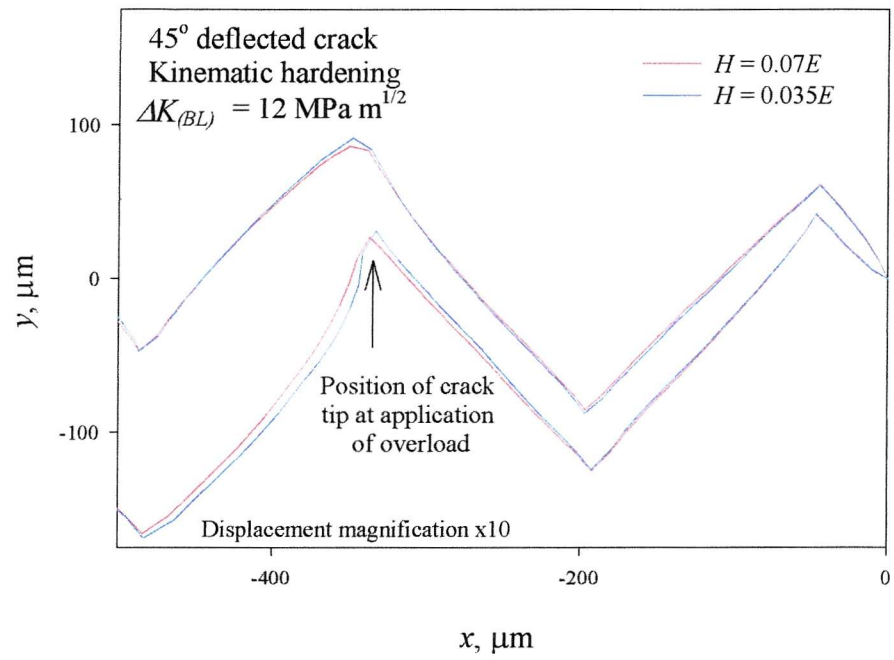

Figure 5.9. Maximum load crack profiles for different hardening moduli for a deflected crack.

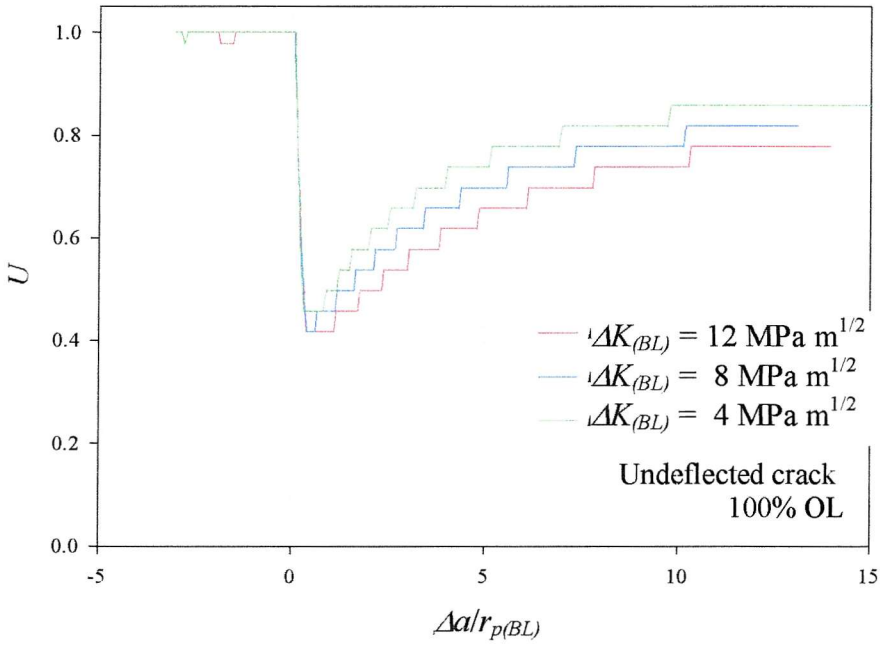

Figure 5.10. Effect of baseline stress intensity factor range on crack closure behaviour, for an undeflected crack.

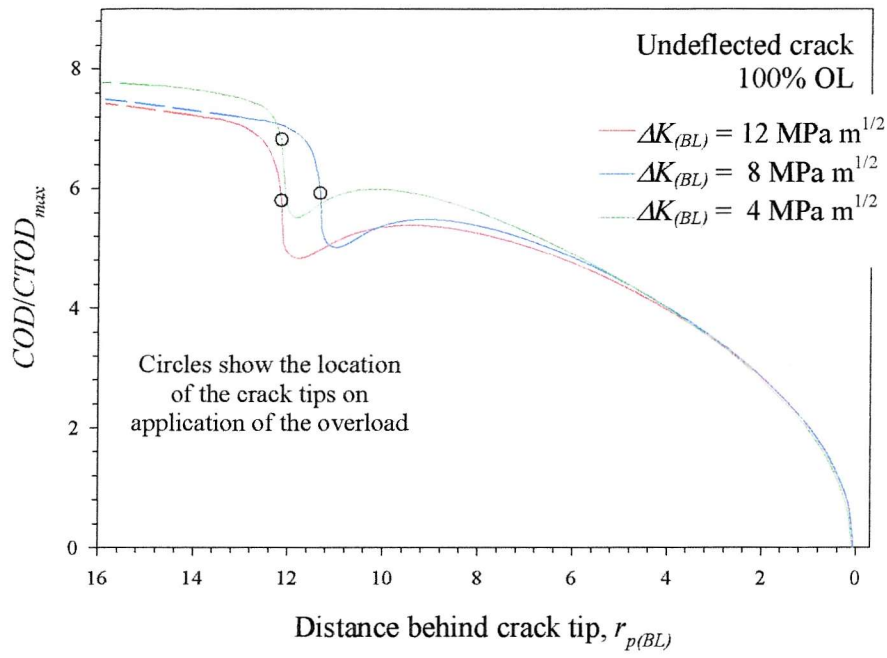

Figure 5.11. Maximum load crack profiles for different baseline stress intensity factor ranges, for an undeflected crack.

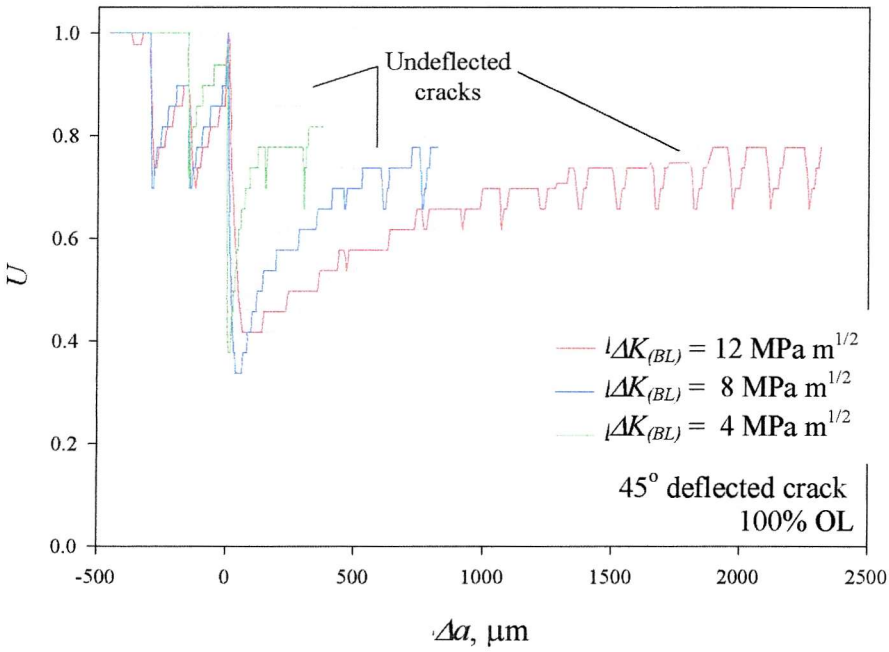

Figure 5.12. Effect of baseline stress intensity factor range on crack closure behaviour for a deflected crack.

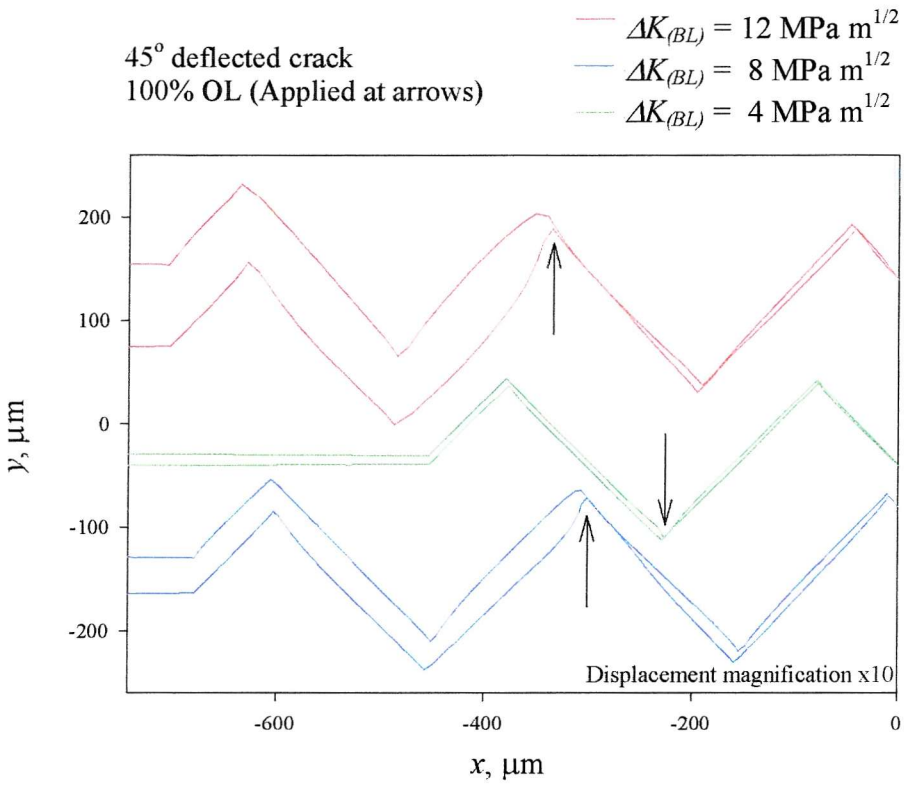

Figure 5.13. Maximum load crack profiles for different baseline stress intensity factor ranges for a deflected crack.

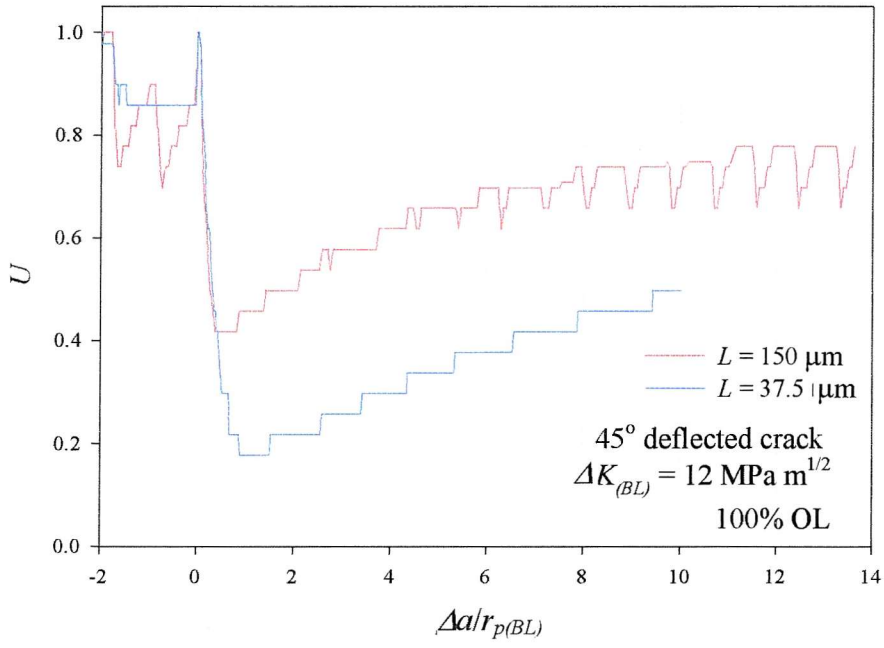

Figure 5.14. Effect of asperity size on crack closure behaviour for a deflected crack.

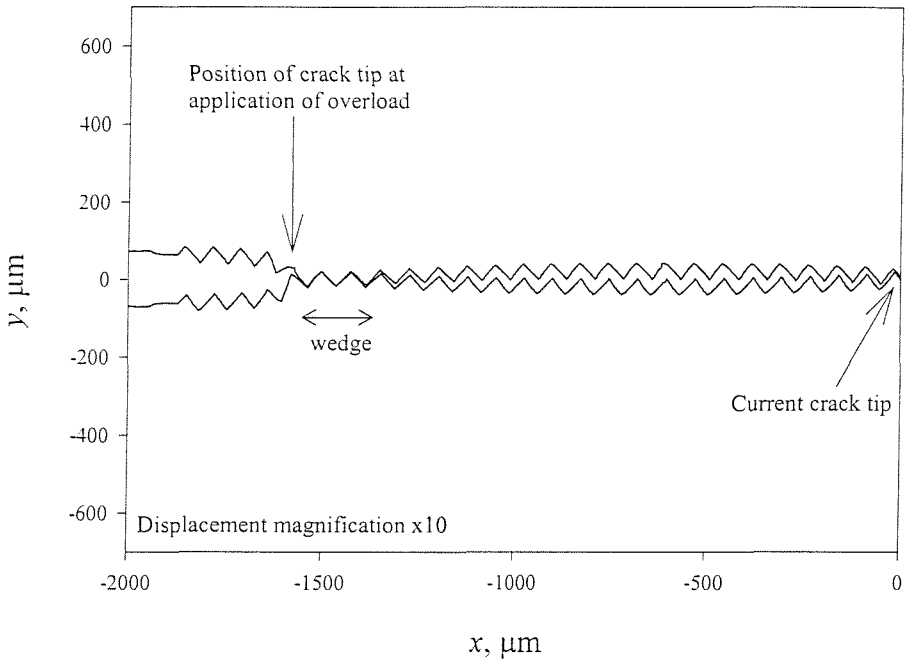

Figure 5.15. Crack profile at the closure point for a deflected crack with $L = 37.5$ μm.

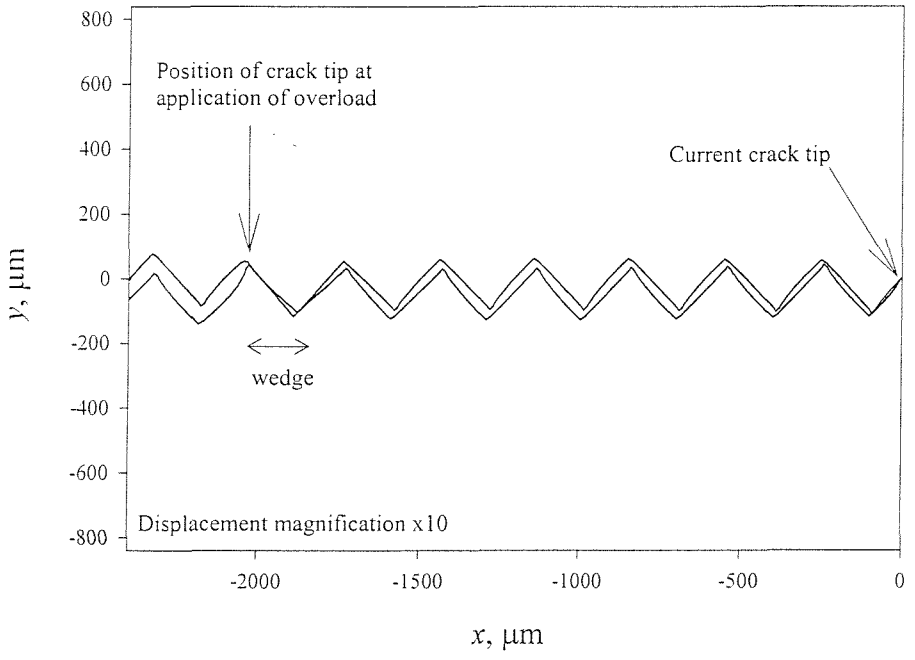

Figure 5.16. Crack profile at the closure point for a deflected crack with $L = 150$ μm.

$h = fn(\Delta k_1^2, R)$

$u_y = fn(\Delta k_1, R)$

$\Delta k_1 = fn(\Delta K, \theta)$

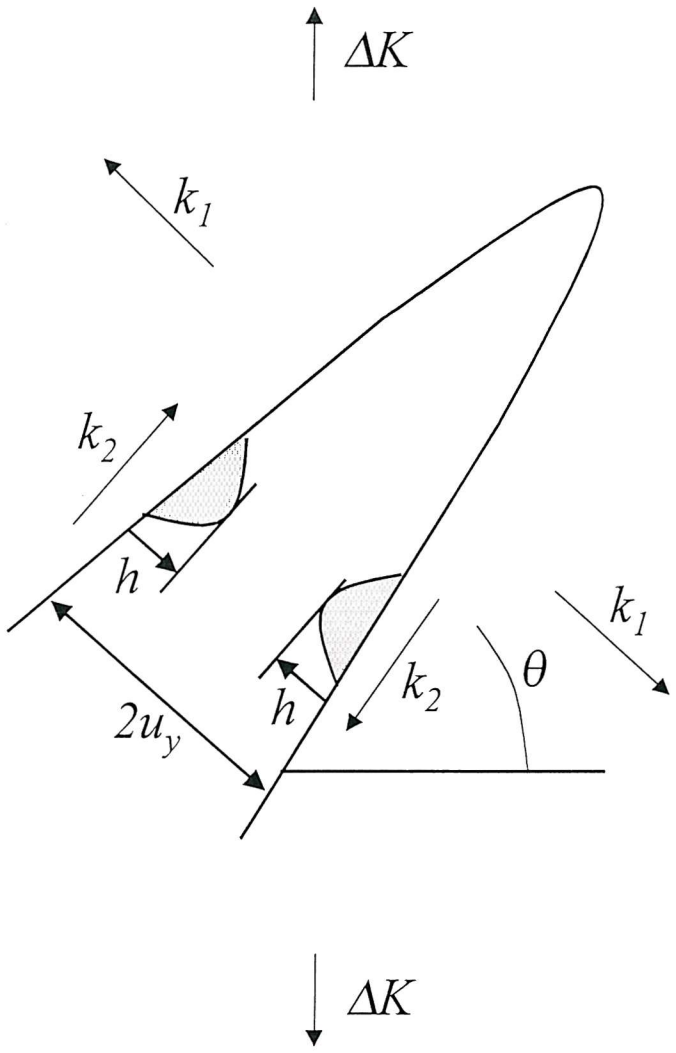

Figure 5.17. Schematic illustration of overload-induced crack closure on a single deflected section. A hump of height *h* (shaded region) exists in the crack wake due to the overload. The hump is small in comparison to the length of the deflected section.

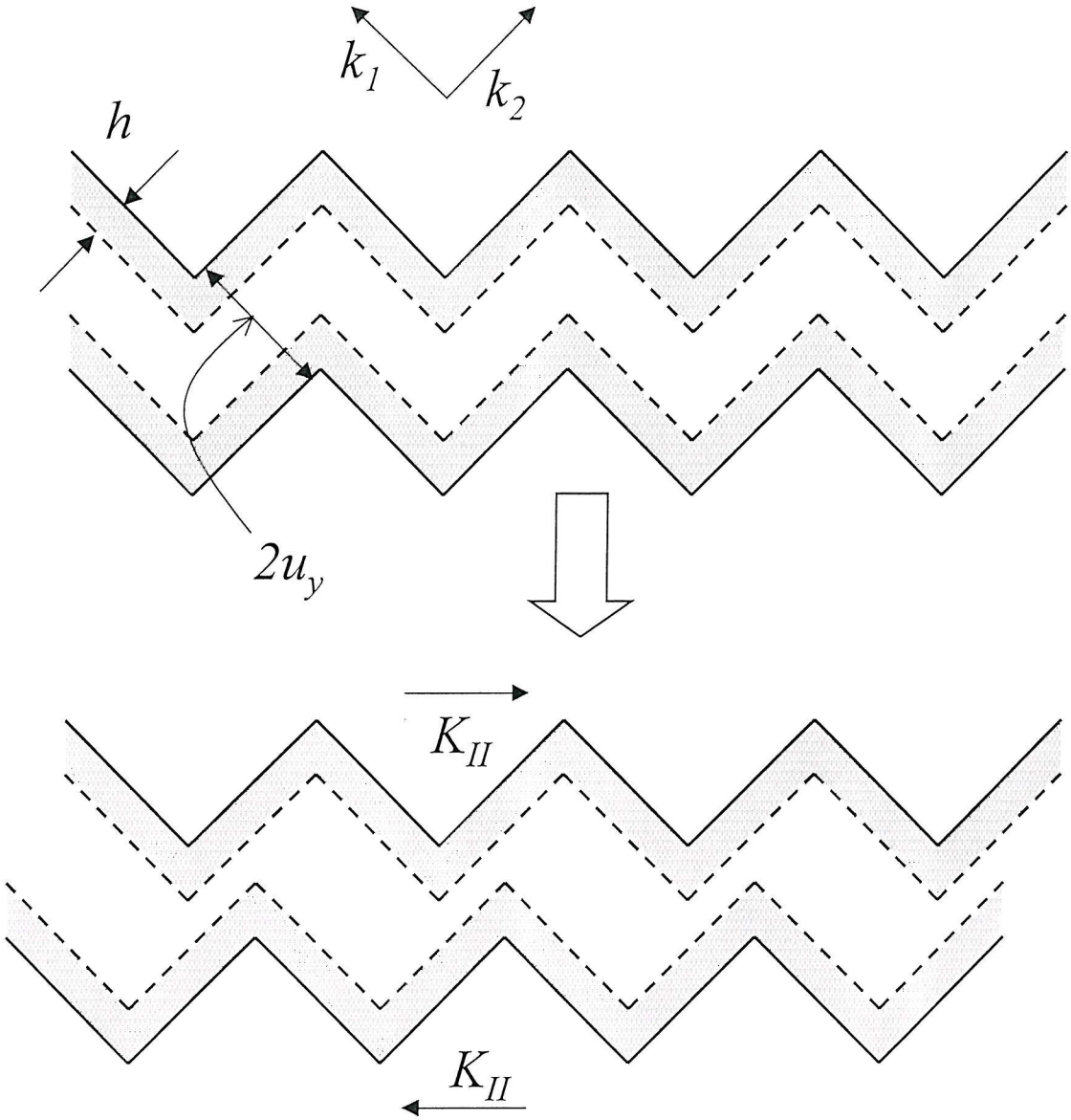

Figure 5.18. Schematic illustration of overload-induced crack closure on a multiply deflected crack. A hump of height h (shaded region) exists in the crack wake due to the overload. The length of the deflected section is small compared to the overload induced hump.

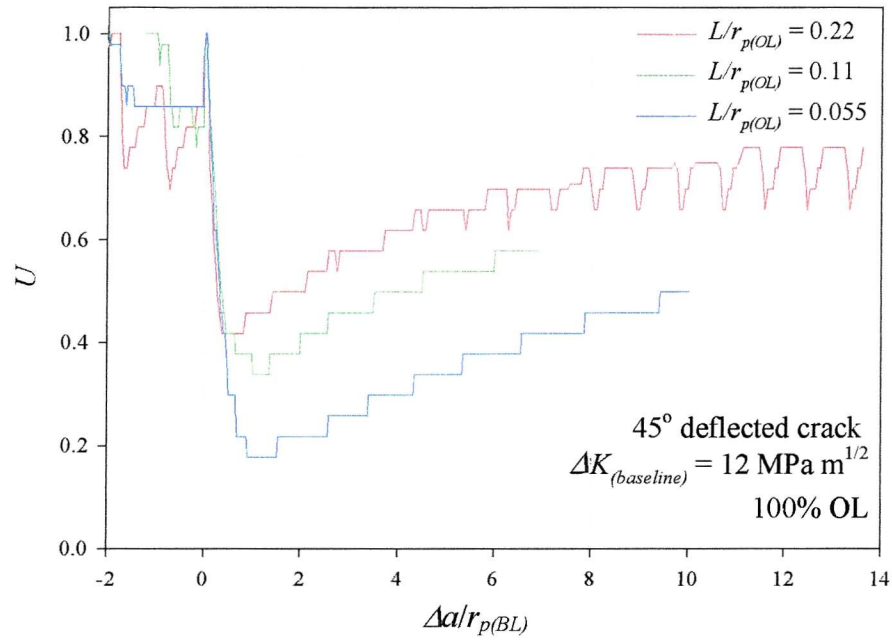

Figure 5.19. Effect of the ratio of asperity size to overload plastic zone size on crack closure behaviour for a deflected crack.

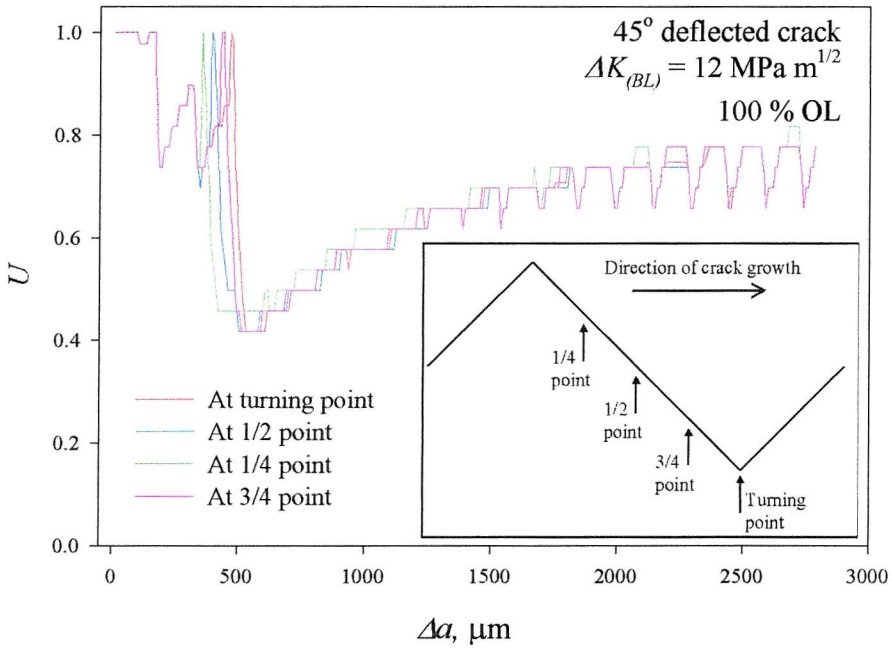

Figure 5.20. Effect of the location of the point of application of the overload relative to the crack deflections on crack closure behaviour.

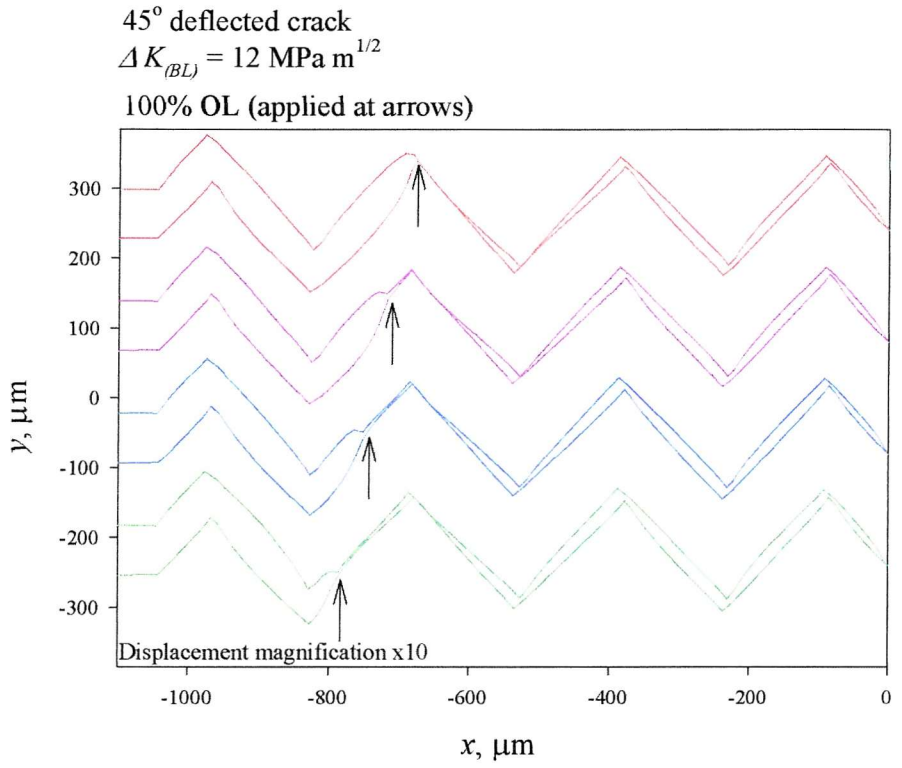

Figure 5.21. Crack profiles at the closure point for a deflected crack with the overloads applied at different positions relative to the crack deflections.

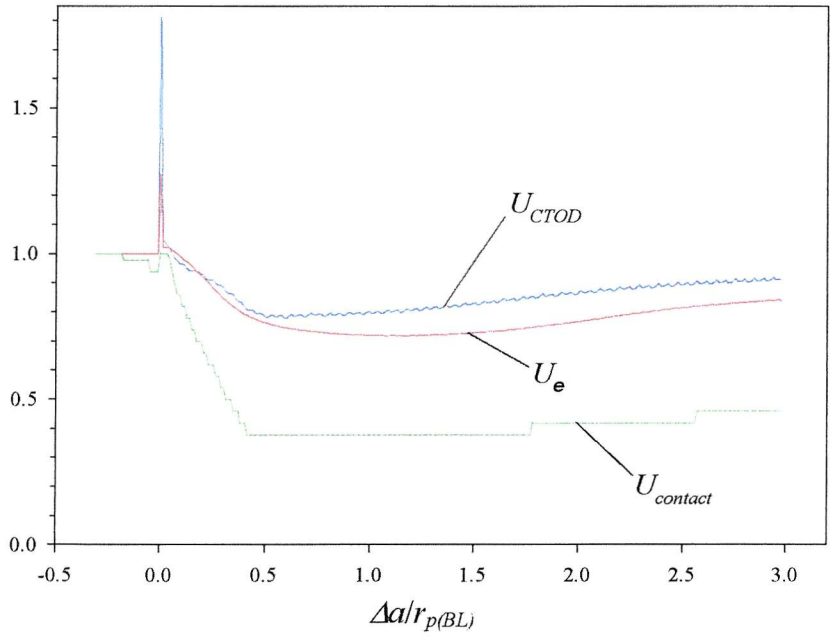

Figure 5.22. Characterisation of closure effects through effective values of $U = \Delta K_{eff}/\Delta K_{app}$ based on contact ($U_{contact}$), cyclic crack tip opening (U_{CTOD}) and cyclic crack tip strain (U_{ε}).

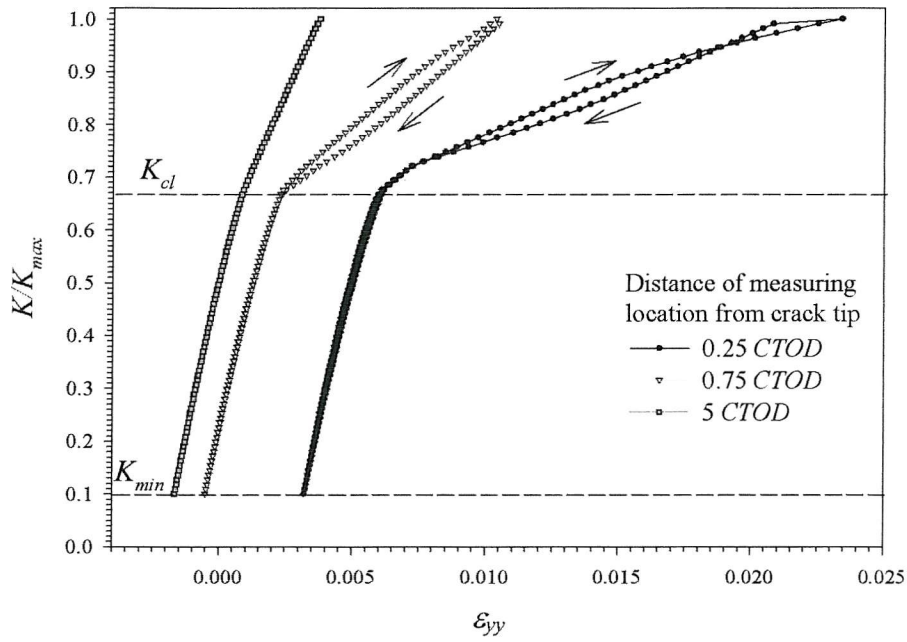

Figure 5.23. Variation of strain normal to the crack face, measured at various locations ahead of the crack tip.

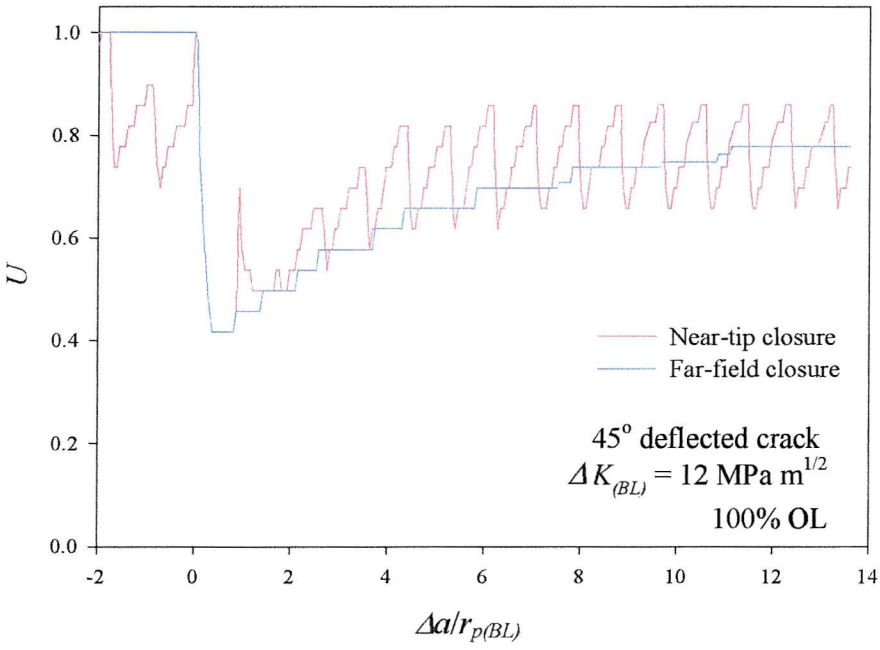

Figure 5.24. Near-tip and far-field crack closure levels for a deflected crack undergoing an overload.

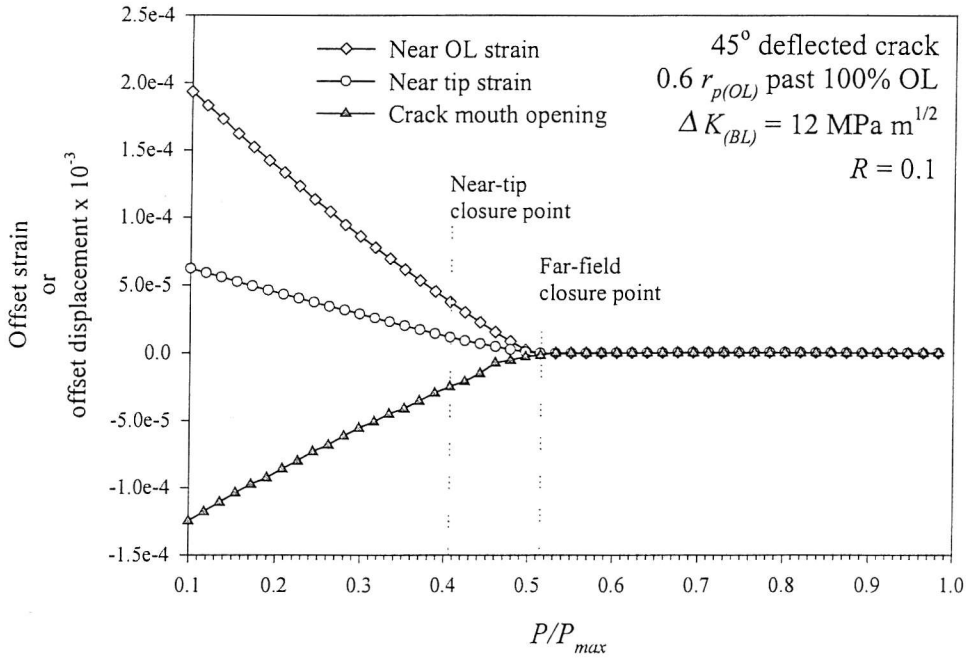

Figure 5.25. Offset strain and displacement plots for strain gauges located near the crack tip and near the location of the overload, and a displacement gauge located at the crack mouth.

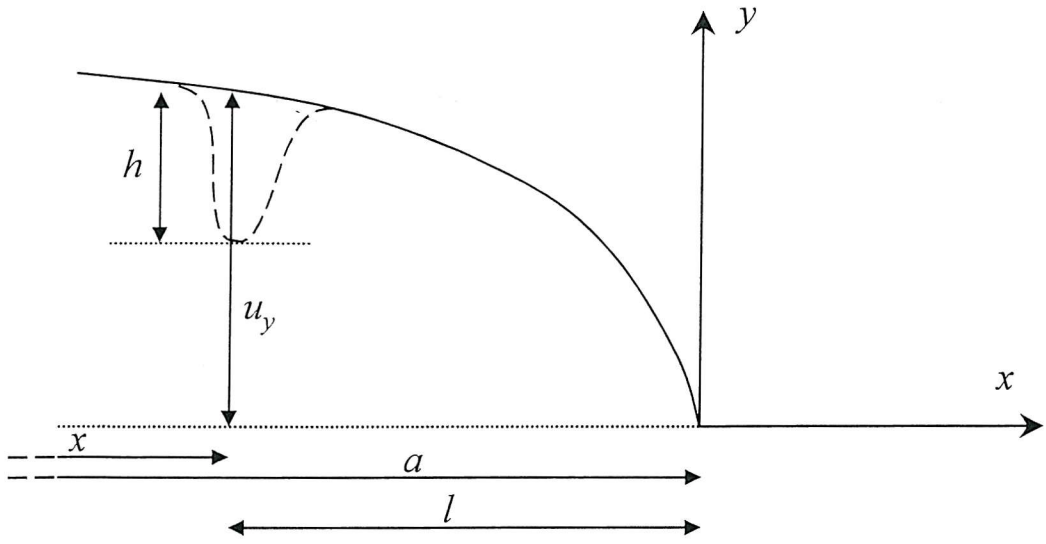

Figure 5.26. Deformed hump of material of height h at a distance l behind the crack tip, where the elastic opening of the crack at maximum load is u_y.

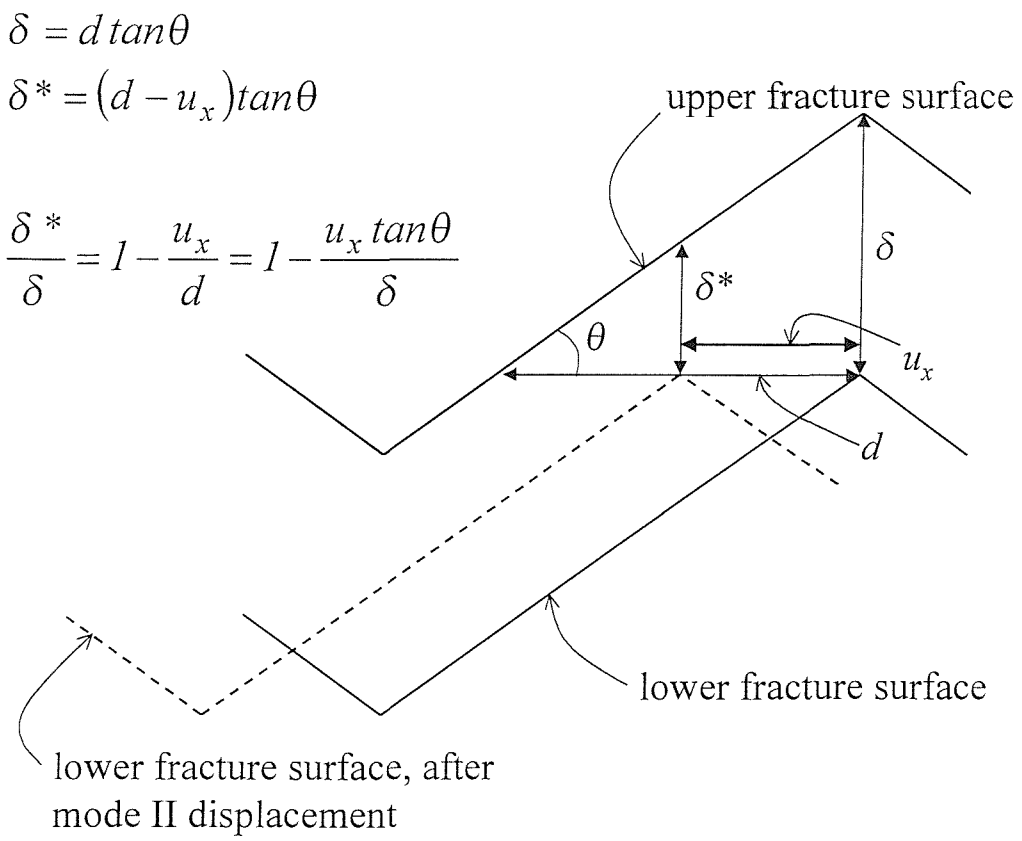

Figure 5.27. Schematic illustration of the reduction of crack opening of a deflected crack due to a residual shear displacement of the fracture surfaces.

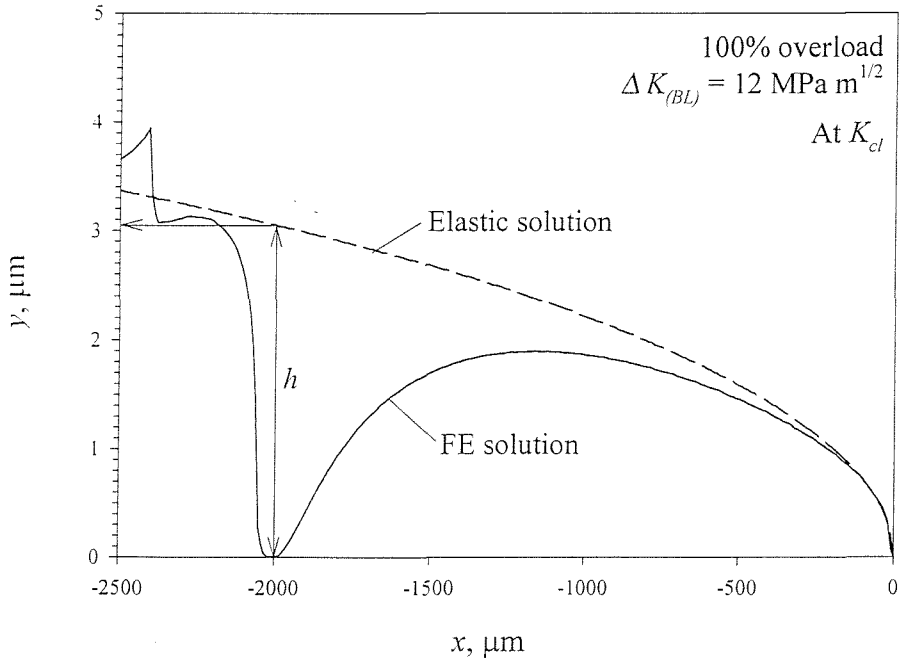

Figure 5.28. Plot of the deformed crack wake at K_{cl}, following a 100% overload (applied when the crack tip was 2000 µm behind its current position. The method of determining h from the FE solution by comparison to the elastic crack opening is illustrated.

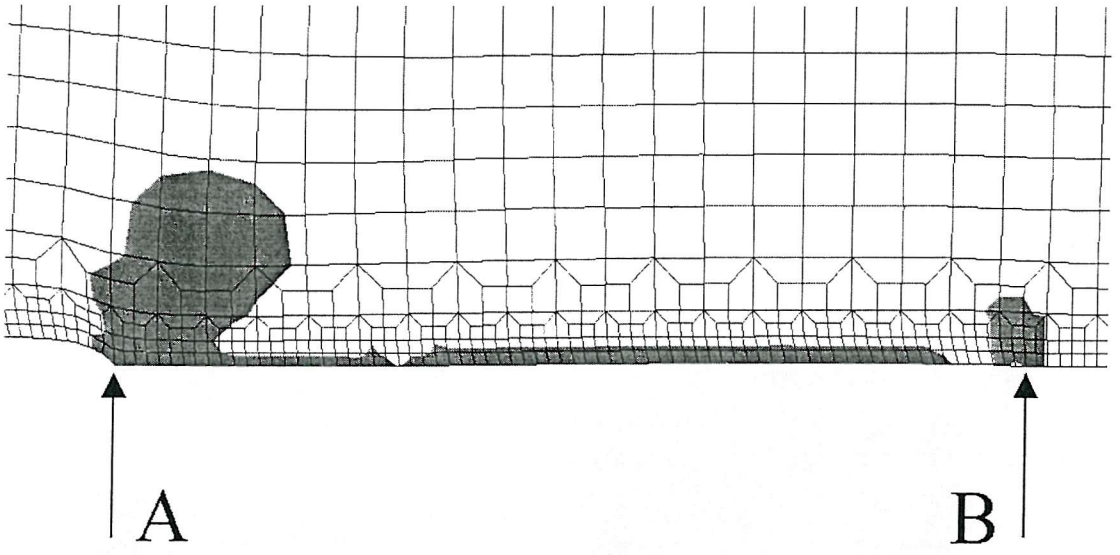

Figure 5.29. Compressive yielding (shaded area shows elements which are actively yielding) of the overload induced hump in the wake of an undeflected crack, shown at minimum load. The overload was applied when the crack tip was at point A, ahead of which a large amount of compressive yielding can be seen. The current crack tip is at point B.

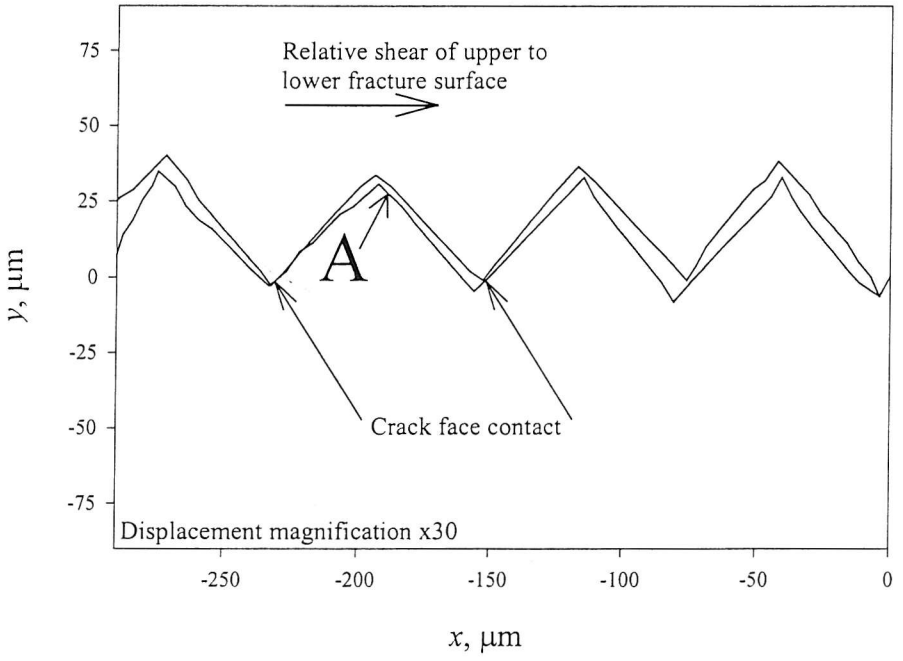

Figure 5.30. Deformed fracture surfaces at the onset of closure of a deflected crack ($L = 37.5$ µm, $\theta = 45°$). The contact of the fracture surfaces is consistent with an overload induced global shear of the fracture surfaces as shown.

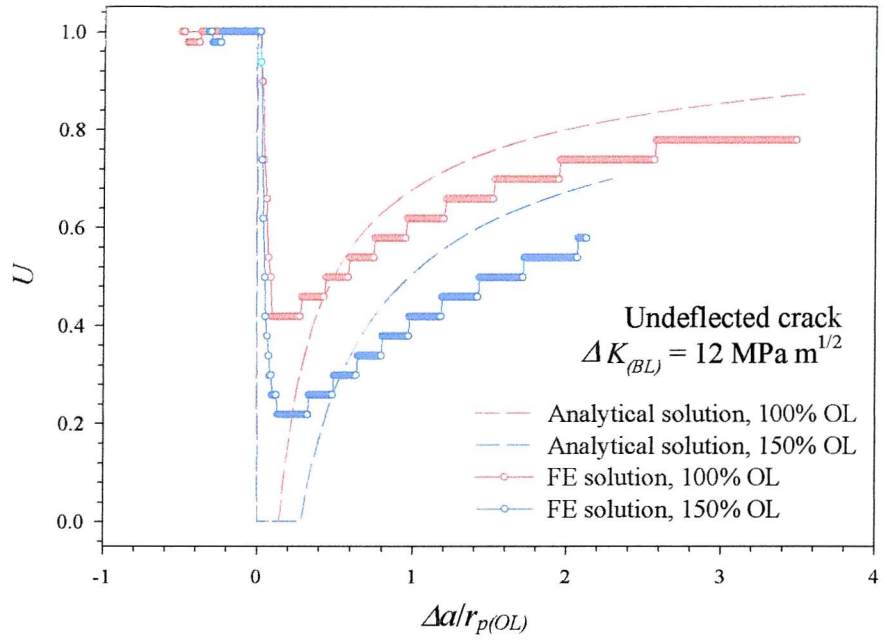

Figure 5.31. Comparison of the analytical and FE element models of the effect of variations in the overload ratio on observed closure response.

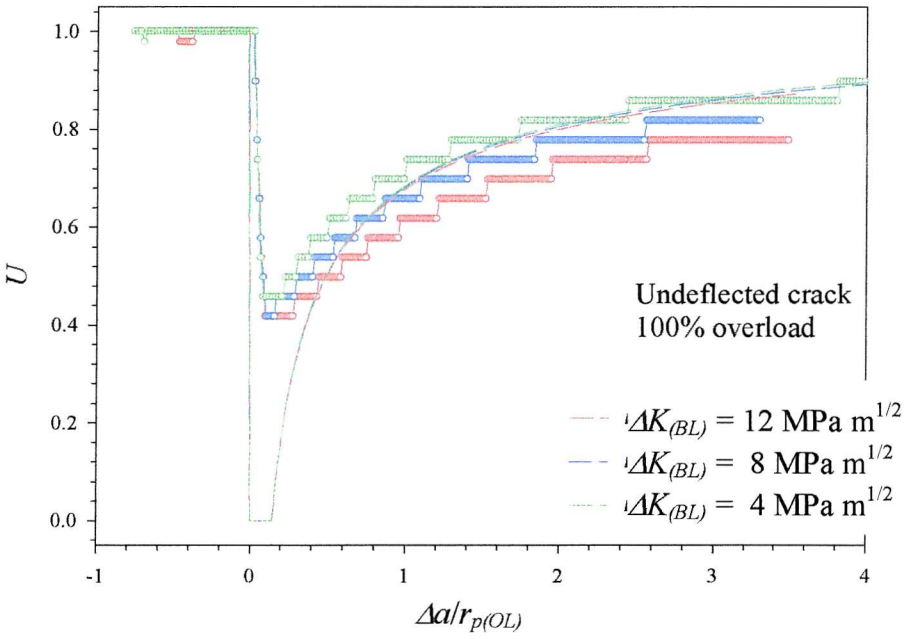

Figure 5.32. Comparison of the analytical and FE element models of the effect of variations in the baseline stress intensity factor range on observed closure response.

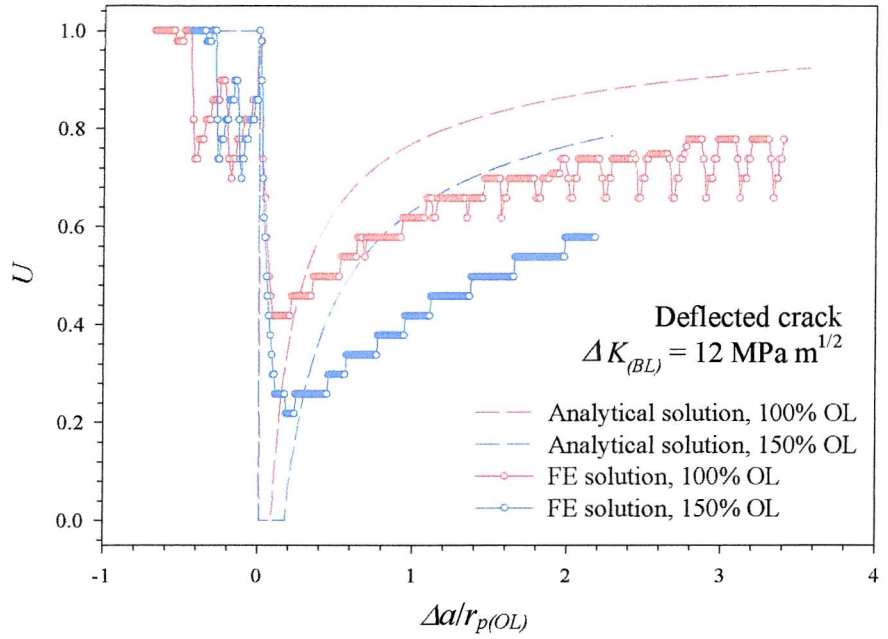

Figure 5.33. Comparison of the analytical and FE element models of the effect of variations in the overload ratio on observed closure response of a deflected crack.

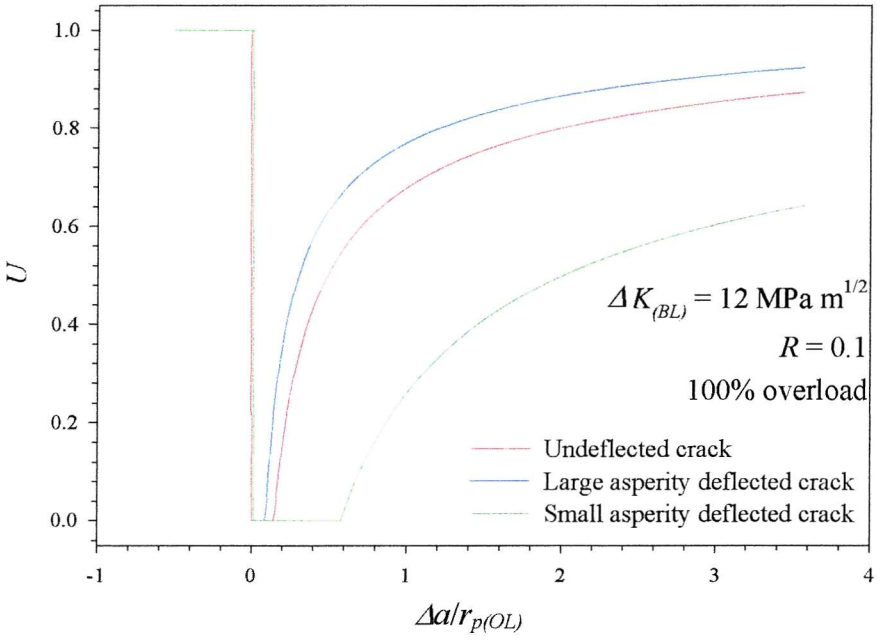

Figure 5.34. Comparison of the various predictions of the analytical model, for an undeflected crack (based on Equation 5.20), a deflected crack where the asperity size is large compared to the overload induced hump (Equation 5.22) and a deflected crack where the asperity size is small compared to the overload induced hump (Equation 5.24).

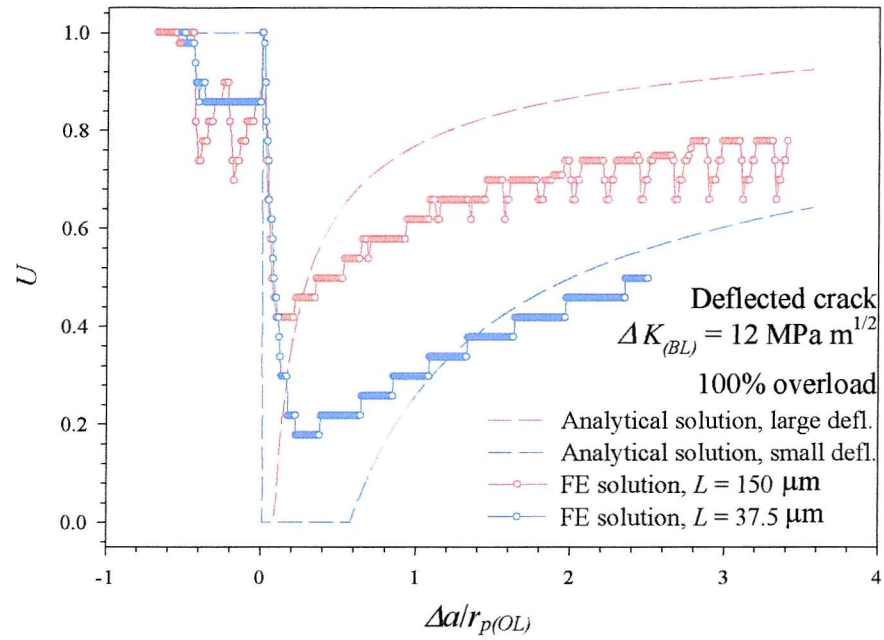

Figure 5.35. Comparison of the analytical and FE element models of the effect of variations in the projected length of the deflected section on observed closure response.

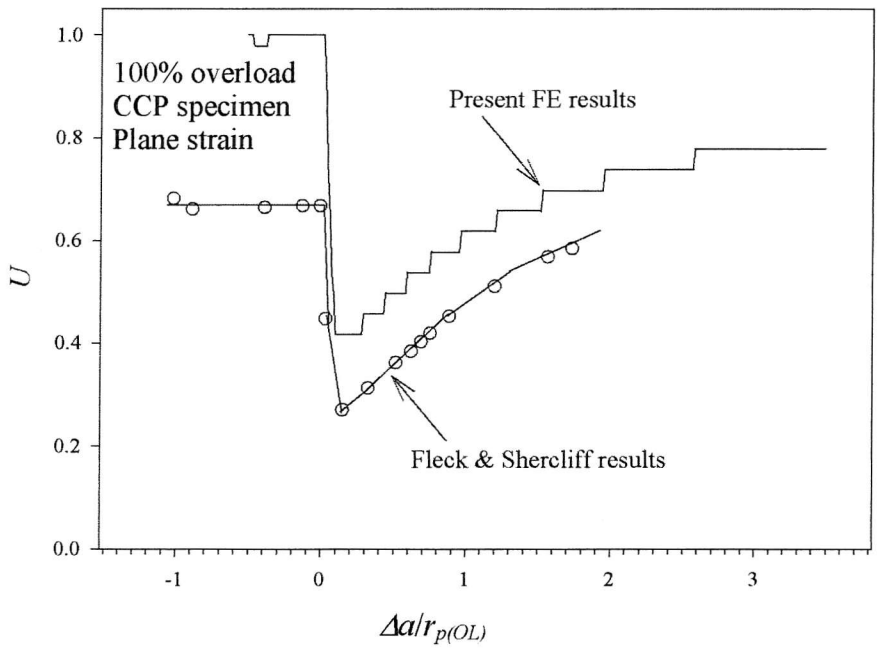

Figure 5.36. Comparison of present FE results to FE results of Fleck & Shercliff [1989] for similar specimen geometry and loading conditions.

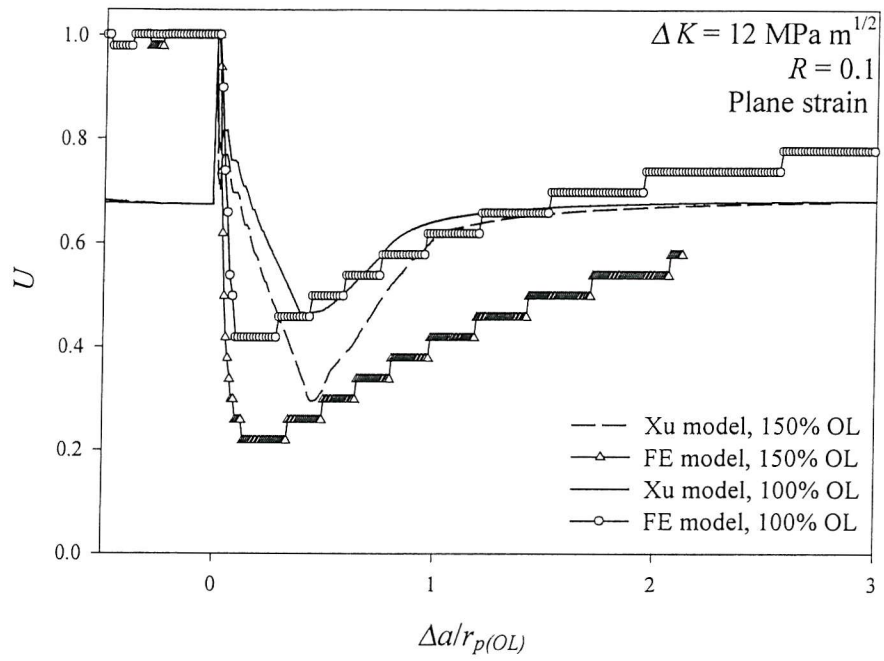

Figure 5.37. Comparison of the effect of changes in overload ratio on shielding predicted by the analytical model of Xu *et al* [2000] and present FE results.

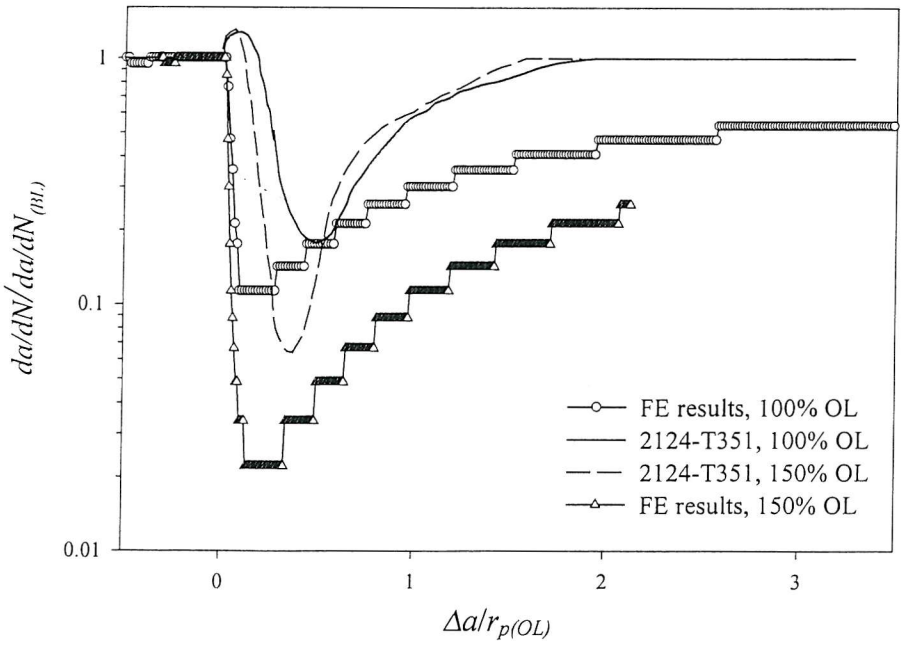

Figure 5.38. Comparison of the effect of changes in overload ratio on normalised growth rate for 2124-T351 [Venkateswara Rao & Ritchie, 1988] and present FE results.

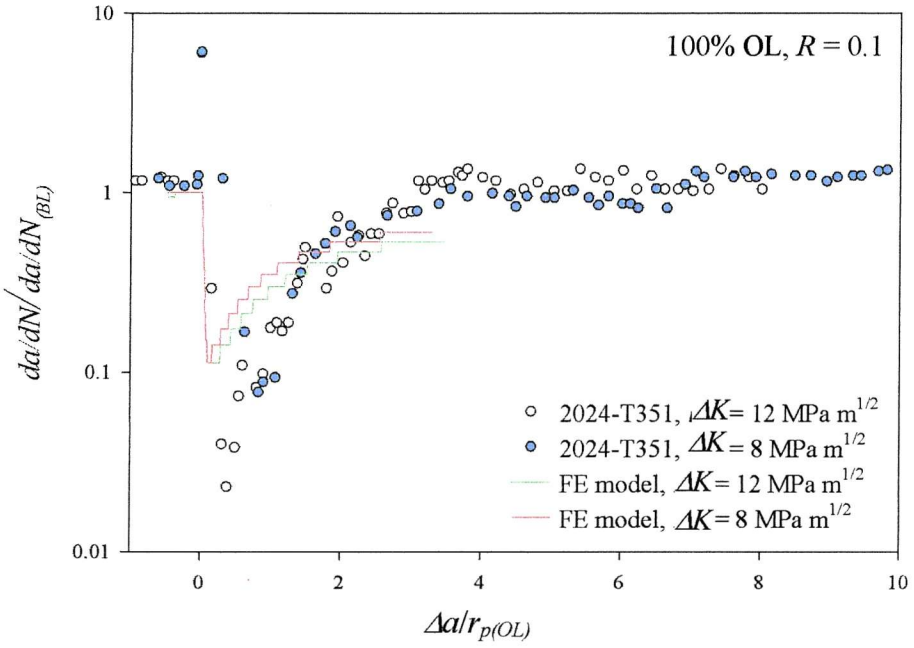

Figure 5.39. Comparison of the effect of changes in baseline stress intensity factor on normalised growth rate for 2024-T351 [Xu *et al*, 1999] and present FE results.

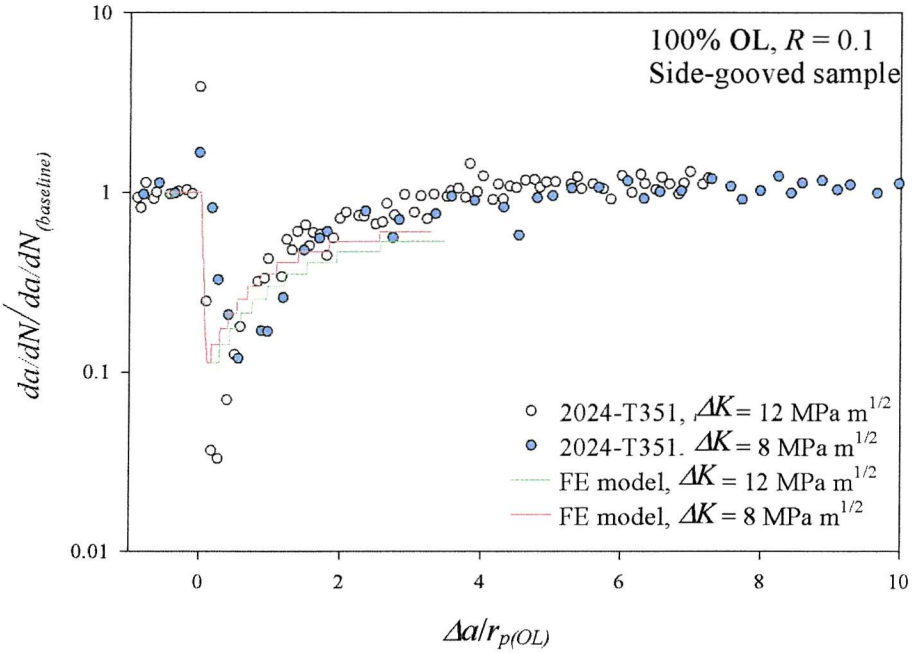

Figure 5.40. Comparison of the effect of changes in baseline stress intensity factor on normalised growth rate for 2024-T351 side-grooved samples [Xu *et al*, 1999] and present FE results.

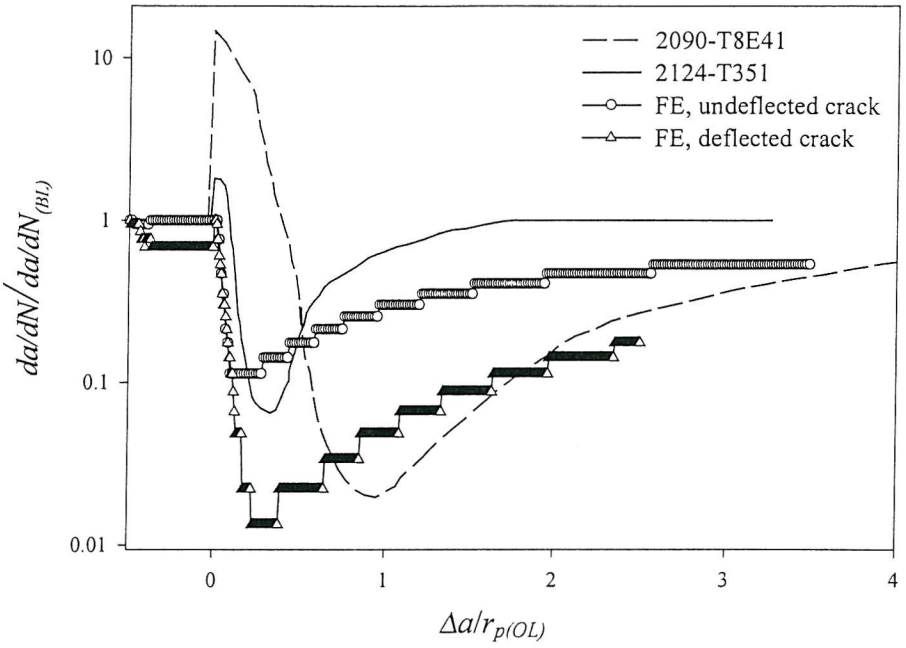

Figure 5.41. Comparison of the effect of changes in crack roughness on normalised growth rate for various aluminium alloys [Venkateswara Rao & Ritchie, 1988] and present FE results.

6 Summary and conclusions

Finite element and analytical models have been constructed to investigate crack closure processes arising from crack deflection, under both constant amplitude and variable amplitude loading conditions. The understanding of underlying mechanisms of roughness induced crack closure, and their relation to plasticity and crack morphology has been substantially increased.

In terms of the finite element modelling of RICC under constant amplitude loading the following conclusions have been drawn:

- The anomalous near-tip behaviour of plane strain FE models of propagating fatigue cracks has been identified, leading to the adoption of a closure definition based on an overall analysis of specimen compliance and crack face contact (excluding the node immediately behind the crack tip).
- Analyses of deflected cracks show an increasing effect of crack path angle on roughness induced closure levels in keeping with the simple analytical model of Suresh & Ritchie, and the general qualitative understanding of RICC.
- The length of the crack deflection (or asperity size) has been shown not to be a critical factor in determining crack closure levels, above a certain threshold deflection length.
- Variation of the crack deflection angle and length along the crack path has been shown to lead to no significant changes in the crack closure behaviour, in contrast to the previously published results of Llorca.
- The mechanism by which closure occurs has been shown to be dependent on residual plastic strains in the wake, and not dependent on the existence of global shear displacements of the fracture surfaces due to the mixed-mode behaviour at the crack tip.
- Various experimental observations from the literature have been shown to be consistent with the proposed RICC mechanism. Weaknesses in the conventional mechanism of RICC have been illustrated, and shown not to affect the newly proposed mechanism.
- The absolute values of the closure levels have been found to be relatively low compared to experimental data, which may be attributed to various simplifications of the modelling process.
- Slip band simulations show a significant increasing effect of inhomogeneous plastic deformation on closure levels, improving the apparent accuracy of the modelling results.

Based on the proposed mechanism of RICC which has arisen from the constant amplitude finite element modelling results, an analytical model of RICC has been formulated. From this model the following conclusions can be made:

- The crack opening behaviour of a propagating plane strain fatigue crack can be reasonably approximated by the expression for elastic crack opening.
- The residual shear deformation of the fracture surfaces can reasonably be expressed as a residual crack tip sliding displacement.
- The predictions of the analytical model agree well with those of the FE models when the crack tip is some fixed fraction of the plastic zone size ahead of the deformed asperity.
- The inability of the analytical model to fully represent the closure behaviour for the situation where the crack tip is close to the deformed asperity can be related to (a) the requirement of a degree of crack growth before closure can occur, and (b) the potential for crack tip blunting which is not fully accounted for in the model formulation.
- The analytical model results show a decreasing roughness induced crack closure level with increasing applied stress intensity factor range, when coupled with a decreasing crack deflection angle, representative of a transition from a crystallographic to ductile mode of crack growth. This behaviour has been shown to be consistent with the experimental crack closure behaviour typically exhibited by damage tolerant aluminium aerospace alloys.
- The simple formulation of the model (based on well accepted fracture mechanics expressions) provides confidence in the new mechanistic description of RICC proposed here.

The finite element and analytical modelling techniques have been extended to investigate the influence of crack deflection on fatigue crack growth under variable amplitude loading, leading to the following conclusions:

- A baseline study of undeflected crack growth has been performed, leading to an enhanced understanding of the role of loading and material parameters in overload-induced crack closure. Comparison of these baseline results to numerical, analytical and experimental results from the literature has demonstrated the physically reasonable behaviour of the model and has established confidence in the results.
- A detailed investigation of near-tip conditions has confirmed that closure does have a significant effect on the near-tip strain field, and that ΔK_{eff} based on crack face contact is a reasonable estimate of crack driving force, when closure occurs close to the crack tip.
- An investigation into the overload-induced crack closure behaviour of deflected cracks has shown little effect of crack deflection for the primary crack morphology studied.

- A significant increase in post-overload closure has been found for crack morphologies in which the wedge of overload plasticity extends over many asperities.
- The dependence on asperity size has been explained through the relative reduction in crack opening of a deflected crack that arises due to a given residual shear displacement of the fracture surfaces.
- An analytical model which uses linear elastic fracture mechanics concepts to describe the overload-induced deformation, the opening of the crack and the effect of this shear displacement has been formulated, and shown to exhibit reasonable agreement with the FE results.
- The assumptions used in the analytical model have been verified through comparison to the FE model, and as such the analytical model can be considered to support the proposed mechanisms through which crack roughness can enhance the retardation effect of an overload.
- The results of the analytical and FE modelling have been shown to be consistent with various results from the literature.

6.1 Recommendations for further work

In terms of the finite element modelling, the following areas in which further work may be beneficial have been identified:

- The implementation of crack surface frictional effects may improve the accuracy of the model, particularly for the assessment of how the near-tip conditions vary during the portion of the loading cycle below K_{cl}.
- Further parametric investigation of the effect of the loading and material parameters, for crack morphologies where crack deflection does have a significant effect on post-overload crack closure, may yield additional significant insights into the RICC mechanism.
- A more explicit quantification of the transition from 'large asperity' behaviour to 'small asperity' behaviour, in terms of variable amplitude fatigue, would be beneficial.

In terms of an extension of the analytical modelling, the following areas have been identified:

- For the constant amplitude RICC model, the deformation of the asperity is R dependent. Feedback of the effect of crack closure on the effective R ratio may yield a more accurate/realistic functional dependence in the model.
- Integration of the constant amplitude model into the variable amplitude model may lead to an improved representation of the overall RICC behaviour.
- In terms of a reflection of the actual material behaviour, the analytical models may benefit from some inclusion of plasticity induced crack closure effects.

Finally, in terms of the overall study of RICC, the work would benefit from an experimental assessment of the proposed mechanisms of RICC under constant and variable amplitude loading. In particular, examination of the residual deformation in the specimen mid-thickness (using modern imaging techniques such as high resolution tomography/ synchotron x-ray microtomography), may help clarify the validity of the closure mechanisms proposed here.

References

ABAQUS (1998). *ABAQUS Theory Manual v5.8*. Pawtucket: Hibbitt, Karlsson & Sorenson, Inc.

Allison, J.E. (1979). Measurement of crack-tip stress distributions by X-ray diffraction. In *Fracture Mechanics*, Special Technical Publication 677, pp. 550-562. Philadelphia: American Society for Testing and Materials.

Allison, J.E., Ku, R.C. & Pompetzki, M.A. (1988). Experimental characterization of fatigue crack closure. In *Mechanics of Fatigue Crack Closure* , Special Technical Publication 982, pp. 165-185. Philadelphia: American Society for Testing and Materials.

Anderson, (1995). *Fracture Mechanics. Fundamentals and Applications*. Boca Raton: CRC Press LLC.

Antolovich, S.D., Saxena, A. & Chanani, G.R. (1975). A model for fatigue crack propagation. *Engineering Fracture Mechanics* **7**, 649-652.

Ashbaugh, N.E., Dattaguru, B., Khobaib, M., Nicholas, T., Prakash, R.V., Ramamurthy, T.S., Seshadri, B.R. & Sunder, R. (1997). Experimental and analytical estimates of fatigue crack closure in an aluminium-copper alloy. Part II: A finite element analysis. *Fatigue and Fracture of Engineering Materials and Structures* **20**, 963-974.

Barlat, F., Miyasato, S.M., Liu, J. & Brem, J.C. (1994). On crystallographic texture and anisotropy in Al-Li sheet. In: *Aluminium Alloys – Their Mechanical & Physical Properties*, (Eds. T.H.Sanders and E.A.Starke), Proc. ICAA4, vol II, pp 389-396, Atlanta, Georgia Institute of Technology.

Beevers, C.J., Bell, K., Carlson, R.L. & Starke, E.A. (1984). A model for fatigue crack closure. *Engineering Fracture Mechanics* **19**, 93-100.

Betegon, C. & Hancock, J.W. (1991). Two parameter characterisation of elastic-plastic crack tip fields. *Journal of Applied Mechanics* **58**, 104-110.

Bilby, B.A., Cardew, G.E. & Howard, I.C. (1977). Stress intensity factors at the tips of kinked and forked cracks. In *Fracture 1977* (Ed. D.M.R. Taplin), vol. 3, pp. 197-200. New York: Pergamon Press.

Bilby, B.A., Cardew, G.E., Goldthorpe, M.R. & Howard, I.C. (1986). A finite element investigation of the effects of specimen geometry on the fields of stress and strain at the tips of stationary cracks. In: *Size Effects in Fracture*, pp 37-46, London: Institute of Mechanical Engineers.

Biner, S.B., Buck, O. & Spitzig, W.A. (1994). Plasticity induced crack closure in single and dual phase materials. *Engineering Fracture Mechanics* **47**, 1-12.

Blom, A., Wang, G. & Chermahini, R.G. (1990). Comparison of crack closure results obtained by 3D elastic-plastic FEM and modified Dugdale model. In: *Localized Damage: Computer-Aided Assessment and Control.* (Eds. M.H. Aliabadi *et al*), pp 57-68. Berlin: Springer-Verlag.

Blom, A.F. & Holm, D.K. (1985). An experimental and numerical study of crack closure. *Engineering Fracture Mechanics* **22**, 997-1011.

Blom, A.F., Hadrboletz, A. & Weiss, B. (1983). Effect of crack closure on near-threshold crack growth behaviour in a high strength Al-alloy up to ultrasonic frequencies. In *Fourth International Conference on Mechanical Behaviour of Materials.* pp. 755-762, Oxford: Pergamon Press Ltd.

Bray, G.H. & Donald, J.K. (1999). Separating the influence of K_{max} from closure-related stress ratio effects using the adjusted compliance ratio technique. In *Advances in Fatigue Crack Closure Measurement and Analysis*, Special Technical Publication 1343, pp. 57-78. West Conshohocken: American Society for Testing and Materials.

Bray, G.H., Reynolds, A.P. & Starke, E.A. (1992). Mechanisms of fatigue crack retardation following single tensile overloads in powder metallurgy aluminum alloys. *Metallurgical Transactions* **23A**, 3055-3066.

Brechet, Y., Louchet, F., Marchionni, C. & Verger-Gaugry, J.L. (1987). Experimental (TEM and STEM) investigation and theoretical approach to the fatigue-induced dissolution of δ' precipitates in a 2.5 wt % Al-Li alloy. *Phil. Mag. A.* **56**, 353-366.

Budiansky, B. & Hutchinson, J.W. (1978). Analysis of closure in fatigue crack growth. *Journal of Applied Mechanics* **45**, 267-276.

Carlson, R.L. & Beevers, C.J. (1985). A mixed mode fatigue crack closure model. *Engineering Fracture Mechanics* **22**, 651-660.

Carter, R.D., Lee, E.-W., Starke, E.A. & Beevers, C.J. (1984). Effect of microstructure and environment on fatigue crack closure in 7475 aluminum alloy. *Metallurgical Transactions* **15A**, 555-563.

Chaki, T.K. & Li, J.C.M. (1984). Overload effect and fatigue crack propagation in amorphous metallic alloys. *Scripta Metallurgica* **18**, 1675-1678

Chen, D.L., Weiss, B. & Stickler, R. (1996). A model for crack closure. *Engineering Fracture Mechanics* **53**, 493-509.

Chermahini, R.G., Shivakumar, K.N. & Newman, J.C. (1988). Three-dimensional finite-element simulation of fatigue crack growth and closure. In *Mechanics of Fatigue Crack Closure* , Special Technical Publication 982, pp. 398-413. Philadelphia: American Society for Testing and Materials.

Christensen, R.H. (1959). *Metal Fatigue*, New York: McGraw-Hill.

Collins, R.C. (1999). Private communication.

Damri, D. & Knott, J.F. (1991). Transient retardations in fatigue crack growth following a single peak overload. *Fatigue and Fracture of Engineering Materials and Structures* **14**, 709-719.

Donahue, R.J., Clark, H.M., Atanmo, P., Kumble, R. & McEvily, A.J. (1972). Crack opening displacement and the rate of fatigue crack growth. *International Journal of Fracture Mechanics* **8**, 209-219.

Donald, J.K. & Paris, P.C. (1999). An evaluation of ΔK_{eff} estimation procedures on 6061-T6 and 2024-T3 aluminum alloys. *International Journal of Fatigue* **21**, S47-S57.

Donald, J.K. & Phillips, E.P. (1999). Analysis of the second ASTM round-robin program on opening-load measurement using the adjusted compliance ratio technique. In *Advances in Fatigue Crack Closure Measurement and Analysis*, Special Technical Publication 1343, pp. 79-93. West Conshohocken: American Society for Testing and Materials.

Donald, J.K. (1997). Introducing the compliance ratio concept for determining effective stress intensity. *International Journal of Fatigue* **19**, S191-S195.

Dougherty, J.D., Padovan, J. & Srivatsan, T.S. (1997). Fatigue crack propagation and closure behavior of modified 1070 steel: finite element study. *Engineering Fracture Mechanics* **56**, 189-212.

Dowling, N.E. & Begley, J.A. (1976). Fatigue crack growth during gross section plasticity and the *J*-integral. In *Mechanics of Crack Growth*, Special Technical Publication 590, pp. 82-103. Philadelphia: American Society for Testing and Materials.

Dugdale, D.S. (1960). Yielding of steel sheets containing slits. *Journal of the Mechanics and Physics of Solids* **8**, 100-8.

Elber, W. (1970). Fatigue crack closure under cyclic tension. *Engineering Fracture Mechanics* **2**, 37-45.

Elber, W. (1971). The significance of fatigue crack closure. In *Damage Tolerance in Aircraft Structures*, Special Technical Publication 486, pp. 230-242. Philadelphia: American Society for Testing and Materials.

Ellyin, F. & Wu, J. (1999). A numerical investigation on the effect of an overload on fatigue crack opening and closure behaviour. *Fatigue and Fracture of Engineering Materials and Structures* **22**, 835-847.

Evans, A.G. & Hutchinson, J.W. (1989). Effects of non-planarity on the mixed mode fracture resistance of bimaterial interfaces. *Acta Metallurgica* **37**, 909-916.

Fitzpatrick, M.E., Bhattacharjee, D., Cree, A.M. & Daykin, C.R.S. (1996). Is fatigue surface roughness a sufficient condition for the generation of crack closure? *Scripta Materialia* **35**, 1335-1340.

Fleck, N.A. & Newman, J.C. (1988). Analysis of crack closure under plane strain conditions. In *Mechanics of Fatigue Crack Closure* , Special Technical Publication 982, pp. 319-341. Philadelphia: American Society for Testing and Materials.

Fleck, N.A. & Shercliff, H.R. (1989). Overload retardation due to plasticity-induced crack closure. In *Proceedings of the 7th International Conference on Fracture ICF7, Houston, Texas, USA, 1989*. pp 1405-1415

Fleck, N.A. & Smith, R.A. (1982). Crack closure - is it just a surface phenomenon? *International Journal of Fatigue* **4**, 157-160.

Fleck, N.A. (1985). Fatigue crack growth due to periodic underloads and overloads. *Acta Metallurgica* **33**, 1339-1354.

Fleck, N.A. (1986). Finite element analysis of plasticity-induced crack closure under plane strain conditions. *Engineering Fracture Mechanics* **25**, 441-449.

Fleck, N.A. (1988). Influence of stress state on crack growth retardation. In *Basic Questions in Fatigue*, Special Technical Publication 924, pp. 157-183. Philadelphia: American Society for Testing and Materials.

Gangloff, R.P., Piascik, R.S., Dicus, D.L. & Newman, J.C. (1994). Fatigue crack propagation in aerospace aluminum alloys. *Journal of Aircraft* **31**, 720-729.

Garcia A.M. & Sehitoglu, H. (1997). Contact of the crack surfaces during fatigue: Part 1. Formulation of the model. *Metallurgical and Materials Transactions* **28A**, 2263-2275.

Geary, W. (1992). A review of some aspects of fatigue crack growth under variable amplitude loading. *International Journal of Fatigue* **14**, 377-386.

Griffith, A.A. (1921). The phenomena of rupture and flow in solids. *Philosophical Transactions of the Royal Society, London* **A221**, 163-197.

Grimes, R., Reynolds, M.A., Titchener, A.P., Greaves, M.S., Strassheim, I. & Warrington, D. (1992). The commercial manufacture of 8090 plate, sheet and extrusions. In: *Aluminium-Lithium*, (Eds. M.Peters & P.J.Winkler), Proc. 6th International Conference on Aluminium–Lithium Alloys, vol 1, pp 3-14, Oberursel: DGM.

Guvenilir, A. & Stock, S.R. (1998). High resolution computed tomography and implications for fatigue crack closure modelling. *Fatigue and Fracture of Engineering Materials and Structures* **21**, 439-450.

Guvenilir, A., Breunig, T.M., Kinney, J.H. & Stock, S.R. (1999). New direct observations of crack closure processes in Al-Li 2090 T8E41. *Philosophical Transactions of the Royal Society of London* **357**, 2755-2775.

Harter, J.A. (1999). Comparison of contemporary FCG life prediction tools. *International Journal of Fatigue* **21**, S181-S185.

Higo, Y., Pickard, A.C. & Knott, J.F. (1981). Effects of grain size and stacking fault energy

on fatigue-crack-propagation thresholds in Cu-Al aluminium alloys. *Metal Science* **15**, 233-240.

Hornbogen, E. & Zum Gahr, K.-H. (1976). Microstructure and fatigue crack growth in a γ-Fe-Ni-Al alloy. *Acta Metallurgica* **24**, 581-592.

Hutchinson, J.W. (1968). Singular behavior at the end of a tensile crack in a hardening material. *Journal of the Mechanics and Physics of Solids* **16**, 13-31.

Irwin, G.R. (1948). Fracture Dynamics. In: *Fracturing of Metals*, pp. 147-166. Cleveland: American Society for Metals.

Irwin, G.R. (1957). Analysis of stresses and strains near the end of a crack traversing a plate. *Journal of Applied Mechanics* **24**, 361-364.

Irwin, G.R. (1960). Plastic zone near a crack and fracture toughness. In *Proceedings of the Seventh Sagamore Ordnance Materials Conference*, vol IV, pp. 63-78. New York: Syracuse University.

James, R.S. (1996). Aluminum-lithium alloys. In: *ASM Handbook Volume 2. Properties and Selection: Non-Ferrous Alloys and Special Purpose Materials*, pp 178-199, Ohio: American Society for Metals.

Jones, R.E. (1973). Fatigue crack growth retardation after single-cycle peak overload in Ti-6Al-4V titanium alloy. *Engineering Fracture Mechanics* **5**, 585-604.

Kim, S.S. & Shin, K.S. (1999). Closure-affected fatigue crack propagation behaviors of powder metallurgy-processed Al-Li alloys in various environments. . *Metallurgical and Materials Transactions* **30A**, 2097-2102.

Kitagawa, H., Yuuki, R. & Ohira, T. (1975). Crack-morphological aspects in fracture mechanics. *Engineering Fracture Mechanics* **7**, 515-529.

Knott, J.F. & Pickard, A.C. (1977). Effects of overloads on fatigue crack propagation: Aluminium alloys. *Metal Science* **11**, 399-404.

Krenn, C.R. & Morris, J.W. (1999). The compatibility of crack closure and K_{max} dependent models of fatigue crack growth. *International Journal of Fatigue* **21**, S147-S155.

Kumai, S. & Higo, Y. (1996). Effects of delamination on fatigue crack growth retardation after single tensile overloads in 8090 Al-Li alloys. *Materials Science and Engineering* **A221**, 154-162.

Lafarie-Frenot, M.C. & Gasc, C. (1983). The influence of age-hardening of fatigue crack propagation behaviour in 7075 aluminium alloy in vacuum. *Fatigue of Engineering Materials and Structures* **6**, 329-344.

Laird, C. (1979). Mechanisms and theories of fatigue. In: *Fatigue and Microstructure*, Papers presented at the 1978 ASM Materials Science Seminar, pp 149-203, Ohio: American Society for Metals.

Lalor P.L. & Sehitoglu, H. (1988). Fatigue crack closure outside a small-scale yielding regime. In *Mechanics of Fatigue Crack Closure* , Special Technical Publication 982, pp. 342-360. Philadelphia: American Society for Testing and Materials.

Landgraf, R.W. (1979). Control of fatigue resistance through microstructure - ferrous alloys. In *Fatigue and Microstructure*, Proceedings of the 1978 ASM Materials Science Seminar, pp. 439-466. Ohio: American Society for Metals.

Lankford, J. & Davidson, D.L. (1976). Fatigue crack tip plasticity associated with overloads and subsequent cycling. *Journal of Engineering Materials and Technology* **98**, 17-23.

Lankford, J., Davidson, D.L. & Chan, K.S. (1984). The influence of crack tip plasticity in the growth of small fatigue cracks. *Metallurgical Transactions* **15A**, 1579-1588.

Larsson, S.G. & Carlsson, A.J. (1973). Influence of non-singular stress terms and specimen geometry on small-scale yielding at the crack tip in elastic-plastic solids. *Journal of the Mechanics and Physics of Solids* **21**, 263-277.

Lawson, L. Chen, E.Y. & Meshii, M. (1999). Near-threshold fatigue: a review. *International Journal of Fatigue* **21**, S15-S34.

Li, C. (1990). Vector CTD analysis for crystallographic crack growth. *Acta Metallurgica et Materialia* **38**, 2129-2134.

Liebowitz, H. & Moyer, E.T. (1989). Finite element methods in fracture mechanics. *Computers and Structures* **31**, 1-9.

Liu, Y., Gregson, P.J. & Sinclair, I. (1998). Unpublished research, School of Engineering Sciences, University of Southampton.

Liu, Y., Sinclair, I. & Gregson, P.J. (1999). Extended slip band mixed-mode fatigue crack growth in an AA8090 Al-Li alloy. In: *Engineering Against Fatigue*, (Eds. J.H.Benyon, M.W.Brown, R.A.Smith, T.C.Lindley, B.Tomkins), Proc. International Conference on the Importance of Understanding the Fundamentals of the Fatigue Process. pp 381-389, Rotterdam: A.A.Balkema.

Llorca, J. & Sanchez-Galvez, V. (1990). Modelling plasticity-induced fatigue crack closure. *Engineering Fracture Mechanics* **37**, 185-196.

Llorca, J. (1992). Roughness-induced fatigue crack closure: A numerical study. *Fatigue and Fracture of Engineering Materials and Structures* **15**, 655-669.

Louat, N., Sadananda, K., Duesbury, M. & Vasudevan, A.K. (1993). Theoretical evaluation of crack closure. *Metallurgical Transactions* **24A**, 2225-2232.

McClung, R.C. & Newman, J.C. (1999). *Advances in fatigue crack closure measurement and analysis, second volume*. Special Technical Publication 1343. West Conshohocken: American Society for Testing and Materials.

McClung, R.C. & Sehitoglu, H. (1989). On the finite element analysis of fatigue crack

closure. 1. Basic modeling issues. 2. Numerical results. *Engineering Fracture Mechanics* **33**, 237-272.

McClung, R.C. (1991). The influence of applied stress, crack length, and stress intensity factor on crack closure. *Metallurgical Transactions* **22A**, 1559-1571.

McClung, R.C. (1994). Finite element analysis of specimen geometry effects on fatigue crack closure. *Fatigue and Fracture of Engineering Materials and Structures* **17**, 861-872.

McClung, R.C. (1999). Overview. In *Advances in Fatigue Crack Closure Measurement and Analysis*, Special Technical Publication 1343, pp. xi-xiv. West Conshohocken: American Society for Testing and Materials.

McClung, R.C., Thacker, B.H. & Roy, S. (1991). Finite element visualization of fatigue crack closure in plane stress and plane strain. *International Journal of Fracture* **50**, 27-49.

McEvily, A.J. & Yang, Z. (1990). The nature of the 2 opening levels following an overload in fatigue crack-growth. *Metallurgical Transactions* **21A**, 2717-2727.

McEvily, A.J. and Ritchie, R.O. (1998). Crack closure and the fatigue-crack propagation threshold as a function of load ratio. *Fatigue and Fracture of Engineering Materials and Structures* **21**, 847-855.

McMeeking, R.M. & Parks, D.M. (1979). On the criteria for J dominance of crack tip fields in large-scale yielding. In *Elastic-Plastic Fracture*, Special Technical Publication 688, pp. 175-94. Philadelphia: American Society for Testing and Materials.

McMeeking, R.M. (1977). Finite deformation analysis of crack tip opening in elastic-plastic materials and implications for fracture initiation. *Journal of the Mechanics and Physics of Solids* **25**, 357-381.

Mendelsohn, D.A., Gross, T.S. & Zhang, Y. (1995). Fracture surface interference in shear-I. A model based on experimental surface characterizations. *Acta Metallurgica et Materialia* **43**, 893-906.

Miller, K.J. (1991). Metal fatigue-past, current and future. *Proceedings of the Institution of Mechanical Engineers* **205**, 291-304.

Miller, K.J. (1993). Materials science perspective of metal fatigue resistance. *Materials Science and Technology* **9**, 453-462.

Minakawa, K. & McEvily, A.J. (1981). On crack closure in the near-threshold region. *Scripta Metallurgica* **15**, 633-636.

Minakawa, K., Levan, G. & McEvily, A.J. (1986). The influence of load ratio on fatigue crack growth in 7090-T6 and IN9021-T4 P/M aluminum alloys. *Metallurgical Transactions* **17A**, 1787-1795.

Miner, M.A. (1945). Cumulative damage in fatigue. *Journal of Applied Mechanics* **12**, 159-

164.

Mitchell, M.R. (1979). Fundamentals of modern fatigue analysis for design. In *Fatigue and Microstructure*, Proceedings of the 1978 ASM Materials Science Seminar, pp. 385-437. Ohio: American Society for Metals.

Nagtegaal, J.C., Parks, D.M. & Rice, J.R. (1974). On numerically accurate finite element solutions in the fully plastic range. *Computer Methods in Applied Mechanics and Engineering* **4**, 153-177.

Nakamura, H., Kobayashi, H., Yanase, S. & Nakazawa, H. (1983). Finite element analysis of fatigue crack closure in compact specimen. In *Mechanical Behaviour of Materials*, Proc. ICM4, Vol 2, pp 817-823.

Nayeb-Hashemi, H., McClintock, F.A. & Ritchie, R.O. (1983). Influence of overloads and block loading on mode III fatigue crack propagation in A469 rotor steel. *Engineering Fracture Mechanics* **18**, 736-743.

Newman, J.C. & Armen, H. (1975). Elastic-plastic analysis of a propagating crack under cyclic loading. *AIAA Journal* **13**, 1017-1023.

Newman, J.C. & Elber W. (1988). *Mechanics of Fatigue Crack Closure*. Special Technical Publication 982. Philadelphia: American Society for Testing and Materials.

Newman, J.C. (1976). A finite-element analysis of fatigue crack closure. In *Mechanics of Crack Growth*, Special Technical Publication 590, pp. 281-301. Philadelphia: American Society for Testing and Materials.

Newman, J.C. (1981). A crack-closure model for predicting fatigue crack growth under aircraft spectrum loading. In *Methods and Models for Predicting Fatigue Crack Growth under Random Loading*, Special Technical Publication 748, pp. 53-84. Philadelphia: American Society for Testing and Materials.

Newman, J.C. (1992). FASTRAN-II - A fatigue crack growth structural analysis program. *NASA Technical Memorandum 104159.*

Newman, J.C. (1997). Prediction of crack growth under variable-amplitude loading in thin-sheet 2024-T3 aluminum alloys. In: *Engineering Against Fatigue*, (Eds. J.H.Benyon, M.W.Brown, R.A.Smith, T.C.Lindley, B.Tomkins), Proc. International Conference on the Importance of Understanding the Fundamentals of the Fatigue Process. pp 261-268, Rotterdam: A.A.Balkema.

Newman, J.C. (1998). An evaluation of the plasticity-induced crack-closure concept and measurement methods. *NASA Technical Memorandum 208430.*

Newman, J.C. (1999). Analyses of fatigue crack growth and closure near threshold conditions for large-crack behavior. *NASA Technical Memorandum 209133.*

Nicholas, T., Palazotto, A.N. & Bednarz, E. (1988). In *Mechanics of Fatigue Crack Closure* ,

Special Technical Publication 982, pp. 361-379. Philadelphia: American Society for Testing and Materials.

Ogura, K., Ohji, K. & Honda, K. (1977). Influence of mechanical factors on the fatigue crack closure. In *Fracture 1977* (Ed. D.M.R. Taplin), vol. 2, pp. 1035-1047. New York: Pergamon Press.

Ohji, K., Ogura, K. & Ohkubo, Y. (1974). On the closure of fatigue cracks under cyclic tensile loading. *International Journal of Fracture* **10**, 123-124.

Ohji, K., Ogura, K. & Ohkubo, Y. (1975). Cyclic analysis of a propagating crack and its correlation with fatigue crack growth. *Engineering Fracture Mechanics* **7**, 457-464

Palmgren, A. (1924). Die Lebensdauer von Kugellagern. *Zeitschrift des Vereins Deutscher Ingenieure* **68**, 339-341.

Paris, P.C. & Hermann, L. (1982). In *Fatigue Thresholds* (Eds. J.Backlund, A.F.Blom & C.J.Beevers), vol 1, pp. 11-33. Warley: EMAS Ltd.

Paris, P.C. (1998). Fracture mechanics and fatigue: a historical perspective. *Fatigue and Fracture of Engineering Materials and Structures* **21**, 535-540.

Paris, P.C., Gomez, M.P. & Anderson, W.P. (1961). A rational analytic theory of fatigue. *The Trend in Engineering* **13**, 9-14.

Petit, J, Tintillier, R., Ranganathan, N., Ait Abdedaim, M. & Chalant, G. (1988). Influence of microstructure and environment on fatigue crack propagation affected by single or repeated overloads. In *Fatigue crack growth under variable amplitude loading*, pp.162-179, London: Elsevier Applied Science.

Phillips, E.P. (1989). Results of the round robin on opening-load measurement conducted by ASTM task group E24.04.04 on crack closure measurement and analysis. *NASA Technical Memorandum 101601.*

Phillips, E.P. (1993). Results of the second round robin on opening-load measurement conducted by ASTM task group E24.04.04 on crack closure measurement and analysis. *NASA Technical Memorandum 109032.*

Pippan, R. & Riemelmoser, F.O. (1998). Visualization of the plasticity-induced crack closure under plane strain conditions. . *Engineering Fracture Mechanics* **60**, 315-322.

Pippan, R., Kolednik, O. & Lang, M. (1994). A mechanism for plasticity-induced crack closure under plane strain conditions. *Fatigue and Fracture of Engineering Materials and Structures* **17**, 721-726.

Polmear, I. (1995). *Light Alloys*, Third Edition, London: Arnold.

Pommier, S. & Bompard, Ph. (2000). Bauschinger effect of alloys and plasticity-induced crack closure: a finite element analysis. . *Fatigue and Fracture of Engineering Materials and Structures* **23**, 129-139.

Ravichandran, K.S. (1990). A theoretical model for roughness induced crack closure. *International Journal of Fracture* **44**, 97-110.

Reed, P.A.S. (1999). Unpublished research. School of Engineering Sciences, University of Southampton.

Reynolds, A.P. (1992). Constant amplitude and post-overload fatigue crack growth behavior in PM aluminum alloy AA 8009. *Fatigue and Fracture of Engineering Materials and Structures* **15**, 551-562.

Rice, J.R. & Rosengren G.F. (1968). Plane strain deformation near a crack tip in a power law hardening material. *Journal of the Mechanics and Physics of Solids* **16**, 1-12.

Rice, J.R. & Tracey, D.M. (1973). Computational fracture mechanics. In: *Numerical and Computer Methods In Structural Mechanics* (Eds. Fenues *et al*), pp 585-623, New York: Academic Press.

Rice, J.R. (1967). Mechanics of crack tip deformation and extension by fatigue. In *Fatigue Crack Propagation*, Special Technical Publication 415, pp. 247-309. Philadelphia: American Society for Testing and Materials.

Rice, J.R. (1968). A path independent integral and the approximate analysis of strain concentrations by notches and cracks. *Journal of Applied Mechanics* **35**, 379-386.

Rice, J.R. (1973). Paper I-441. In *Proceedings of the Third International Conference on Fracture,* Vol. II. Dusseldorf: Verein Deutscher Eisenhuttenleute.

Riemelmoser, F.O. & Pippan, R. (1998). Mechanical reasons for plasticity-induced crack closure under plane strain conditions. *Fatigue and Fracture of Engineering Materials and Structures* **21**, 1425-1433.

Riemelmoser, F.O. & Pippan, R. (1999*a*). On the ΔK_{eff} concept: An investigation by means of a discrete dislocation model. In *Advances in Fatigue Crack Closure Measurement and Analysis*, Special Technical Publication 1343, pp. 1-13. West Conshohocken: American Society for Testing and Materials.

Riemelmoser, F.O. & Pippan, R. (1999*b*). Discussion of "Reconsideration of error in the analysis of the wake dislocation problem" by K.Sadananda & A.K.Vasudevan. *Metallurgical and Materials Transactions* **30A**, 1452-1457.

Ritchie, R.O. & Suresh, S. (1982). Some considerations on fatigue crack closure at near-threshold stress intensities due to fracture surface morphology. *Metallurgical Transactions* **13A**, 937-940.

Ritchie, R.O. (1988). Mechanisms of fatigue crack propagation in metals, ceramics and composites: Role of crack tip shielding. *Materials Science and Engineering* **A103**, 15-28.

Ritchie, R.O., Yu, W., Blom, A.F. & Holm, D.K. (1987). An analysis of crack tip shielding in aluminium alloy 2124: A comparison of large, small, through-thickness and surface

fatigue cracks. *Fatigue and Fracture of Engineering Materials and Structures* **10**, 343-363.

Ritchie, R.O., Yu, W., Blom, A.F. & Holm, D.K. (1989). Response to a discussion by A.J. McEvily. *Fatigue and Fracture of Engineering Materials and Structures* **12**, 73-75.

Robin, C., Louah, M. & Pluvinage, G. (1983). Influence of the overload on the fatigue crack growth in steels. *Fatigue of Engineering Materials and Structures* **6**, 1-13.

Sadananda, K. & Vasudevan, A.K. (1998). Reply to "Discussion of error in the analysis of the wake dislocation problem" by F.O.Riemelmoser & R.Pippan. *Metallurgical and Materials Transactions* **29A**, 1359-1360.

Sadananda, K., Vasudevan, A.K., Holtz, R.L. & Lee, E.U. (1999). Analysis of overload effects and related phenomena. *International Journal of Fatigue* **21**, S233-S246.

Schijve, J. & Broek, D. (1962). The result of a test programme based on a gust spectrum with variable amplitude loading. *Aircraft Engineering* **34**, 314-316.

Schutz, W. (1996). A history of fatigue. *Engineering Fracture Mechanics* **54**, 263-300.

Sehitoglu, H. & Sun, W. (1991). Modeling of plane strain fatigue crack closure. *Transactions of the ASME. Journal of Engineering Materials and Technology* **113**, 31-40.

Shih, C.F. (1974). Small-scale yielding analysis of mixed-mode plane strain crack problems. In *Fracture Analysis*, Special Technical Publication 560, pp. 187-210. Philadelphia: American Society for Testing and Materials.

Shih, C.F. (1981). Relationships between the *J*-integral and the crack opening displacement for stationary and extending cracks. *Journal of the Mechanics and Physics of Solids* **29**, 305-326.

Shin, C.S. & Hsu, S.H. (1993). On the mechanisms and behaviour of overload retardation in AISI 304 stainless steel. *International Journal of Fatigue* **15**, 181-192.

Shuter, D.M. & Geary, W. (1996). Some aspects of fatigue crack growth retardation behaviour following tensile overloads in a structural steel. *Fatigue and Fracture of Engineering Materials and Structures* **19**, 185-199.

Sinclair, I. & Buffiere, J.Y. (2000). Private communication.

Sinclair, I. & Gregson, P.J. (1994). Microstructural and micromechanical influences on fatigue crack path behaviour in Al-Li alloy AA8090. In: *Aluminium Alloys – Their Mechanical & Physical Properties*, (Eds. T.H.Sanders and E.A.Starke), Proc. ICAA4, vol II, pp 436-443, Atlanta, Georgia Institute of Technology.

Skorupa, M. (1998). Load interaction effects during fatigue crack growth under variable amplitude loading - a literature review. Part I: empirical trends. *Fatigue and Fracture of Engineering Materials and Structures* **21**, 987-1006.

Skorupa, M. (1999). Load interaction effects during fatigue crack growth under variable

amplitude loading - a literature review. Part II: qualitative interpretation. *Fatigue and Fracture of Engineering Materials and Structures* **22**, 905-926.

Slavik, D.C. & Gangloff, R.P. (1996). Environment and microstructure effects on fatigue crack facet orientation in an Al-Li-Cu-Zr alloy. *Acta Materialia.*, **44**, 3515-3534

Socie, D.F. (1977). Prediction of fatigue crack growth in notched members under variable amplitude loading histories. *Engineering Fracture Mechanics* **9**, 849-865.

Suresh, S. & Ritchie, R.O. (1982). A geometric model for fatigue crack closure induced by fracture surface roughness. *Metallurgical Transactions* **13A**, 1627-1631.

Suresh, S. (1983). Micromechanisms of fatigue crack growth retardation following overloads. *Engineering Fracture Mechanics* **18**, 577-593.

Suresh, S. (1985*a*). Crack initiation in cyclic compression and its applications. *Engineering Fracture Mechanics* **21**, 453-463.

Suresh, S. (1985*b*). Fatigue crack deflection and fracture surface contact: Micromechanical models. *Metallurgical Transactions* **16A**, 249-260.

Suresh, S. (1991). *Fatigue of Materials*, Cambridge, Cambridge University Press.

Suresh, S., Vasudevan, A.K. & Bretz, P.E. (1984). Mechanisms of slow fatigue crack growth in high strength aluminum alloys: Role of microstructure and environment. *Metallurgical Transactions* **15A**, 369-379.

Swift, T. (1996). Damage tolerance certification of commercial aircraft. In: *ASM Handbook volume 19 : Fatigue and fracture*, pp 566-576. Ohio: American Society for Metals.

Tada, H., Paris, P.C. & Irwin, G.R. (1973). *Stress Analysis of Cracks Handbook*, Hellertown: Del Research Corporation

Topper, T.H. & Yu, M.T. (1985). The effects of overloads on threshold and crack closure. *International Journal of Fatigue* **3**, 159-164.

Tsukuda, H., Ogiyama, H. & Shiraishi, T. (1995). Transient fatigue crack growth behaviour following single overloads at high stress ratios. *Fatigue and Fracture of Engineering Materials and Structures* **19**, 879-891.

Vasudevan, A.K. & Sadananda, K. (1999). Application of unified fatigue damage approach to compression-tension region. *International Journal of Fatigue* **21**, S263-S273.

Vasudevan, A.K. & Suresh, S. (1985). Lithium-containing aluminum alloys: cyclic fracture. *Metallurgical Transactions*, **16A**, 475-477.

Vasudevan, A.K., Sadananda, K. & Louat, N. (1992). Reconsideration of fatigue crack closure. *Scripta Metallurgica et Materialia* **27**, 1673-1678.

Vasudevan, A.K., Sadananda, K. & Louat, N. (1994). A review of crack closure, fatigue crack threshold and related phenomena. *Materials Science and Engineering* **A188**, 1-22.

Venkateswara Rao, K.T. & Ritchie, R.O. (1988). Mechanisms for the retardation of fatigue

cracks following single tensile overloads: Behavior in aluminum-lithium alloys. *Acta Metallurgica* **36**, 2849-2862

Venkateswara Rao, K.T. & Ritchie, R.O. (1992). Fatigue of aluminum-lithium alloys. *International Materials Reviews* **37**, 153-185.

Venkateswara Rao, K.T., Yu, W. & Ritchie, R.O. (1988). Fatigue crack propagation in aluminum-lithium alloy 2090: Part 1. Long crack behavior. *Metallurgical Transactions*, **19A**, 549-561.

Walker, N. & Beevers, C.J. (1979). A fatigue crack closure mechanism in titanium. *Fatigue of Engineering Materials and Structures* **1**, 135-148.

Wang, S.-H., Muller, C. & Exner, H.E. (1998). A model for roughness-induced fatigue crack closure. *Metallurgical and Materials Transactions*, **29A**, 1933-1939.

Ward-Close, C.M. & Ritchie, R.O. (1988). On the role of crack closure mechanisms in influencing fatigue crack growth following tensile overloads in a titanium alloy: Near threshold versus higher ΔK behaviour. In *Mechanics of Fatigue Crack Closure* , Special Technical Publication 982, pp. 93-111. Philadelphia: American Society for Testing and Materials.

Wasen, J., Hamberg, K. & Karlsson, B. (1988). The influence of grain size and fracture surface geometry on the near-threshold fatigue crack growth in ferritic steels. *Materials Science and Engineering* **A102**, 217-226.

Weertman J (1992). Why a complete solution has not been found of a mode-I crack in an elastic plastic solid, *Physica Status Solidi* **B172**, 27-40

Wei, L.W. & James, M.N. (2000). A study of fatigue crack closure in polycarbonate CT specimens. *Engineering Fracture Mechanics* **66**, 223-242.

Westergaard, H.M. (1939). Bearing pressures and cracks. *Journal of Applied Mechanics* **61**, A49-53.

Wheeler, O.E. (1972). Spectrum loading and crack growth. *Journal of Basic Engineering* **94**, 181-186.

Willenborg, J., Engle, R.M. & Wood, H. (1971). A crack growth retardation model using an effective stress intensity concept. *Technical Report TFR 71-701*. Los Angeles: North American Rockwell.

Xu, Y. (2000). Ph.D Thesis. School of Engineering Sciences, University of Southampton.

Xu, Y., Gregson, P.J. & Sinclair, I. (2000*a*). Dispersoid and grain size effects on fatigue crack growth in AA2024-type alloys. In: *Aluminium Alloys – Their Mechanical & Physical Properties*, (Eds. E.A.Starke, T.H.Sanders and W.A.Cassada), Proc. ICAA7, Materials Science Forum Vols. 331-337, pp 1525-1530.

Xu, Y., Gregson, P.J. & Sinclair, I. (2000*b*). Systematic assessment and validation of

compliance-based crack closure measurements in fatigue. *Materials Science and Engineering* **A284**, 114-125.

Zapatero, J., Moreno, B. & Dominguez, J. (1997). On the use of the strip-yield model to predict fatigue crack growth under irregular loading. *Fatigue and Fracture of Engineering Materials and Structures* **20**, 759-770.

Zhang, J.Z., Halliday, M.D., Bowen, P. & Poole, P. (1999). Three dimensional elastic-plastic finite element modelling of small fatigue crack growth under a single tensile overload. *Engineering Fracture Mechanics* **63**, 229-251.

Zhang, S., Marissen, R., Schulte, K., Trautmann, K.H. & Schijve, J. (1987). Crack-propagation studies on Al-7475 on the basis of constant amplitude and selective variable amplitude loading histories. *Fatigue and Fracture of Engineering Materials and Structures* **10**, 315-332.

Zhang, X., Chan, A.S.L. & Davies, G.A.O. (1992). Numerical simulation of fatigue crack growth under complex loading sequences. *Engineering Fracture Mechanics* **42**, 305-321.

Appendix A Implementation of the FE model

In this work FE models of deflected and undeflected fatigue cracks under constant and variable loading histories have been designed and studied. The majority of the information on the implementation of these models is detailed in Chapter 3. In this appendix some supplementary details concerning the model implementation is presented.

A.1 Loads and boundary conditions

In the models the loads were applied to the specimen along the top and bottom faces. For the loading and crack geometry as above, the common solution for K in a CCP gives

$$\sigma = \frac{K_I}{C\sqrt{\pi a}} = \frac{4\times 10^6}{1.02\times\sqrt{\pi}\times 0.0076} = 25.6\,MPa \qquad \text{(A.1)}$$

where the shape factor C is,

$$C = \frac{1}{\sqrt{1-\left(\frac{2a}{W}\right)^2}} = \frac{1}{\sqrt{1-\left(\frac{2\times 0.0076}{0.075}\right)^2}} = 1.02 \qquad \text{(A.2)}$$

Hence the applied load P is given by

$$P = \sigma BW = 25.6\times 10^6 \times 0.0075\times 0.075 = 14.4kN \qquad \text{(A.3)}$$

The load was distributed over 36 elements an each face, hence the applied load per element was 14.4 kN ÷ 36 = 400 N. This load was actually applied at the nodes, hence the load for each element was split between its two surface nodes. Thus at each surface node, there was a contribution of 200 N from each adjacent element. In total then, the load at each node, P_n, was 400 N except for the nodes at the corners (and on the line of symmetry) where it is 200 N (½ P_n) . As one half of the specimen was modelled (one quarter for the undeflected crack) symmetry boundary conditions are enforced. One node on the back face is also constrained to prevent any free body motion.

A.2 Material properties

Material properties analogous to a high strength aluminium alloy were chosen. i.e. σ_0 = 370 MPa, E = 74 GPa, H = 0.07E, ν = 0.33. These were implemented in a linear kinematic hardening model. In the models, the mesh unit was 1 μm, and the material properties must be defined likewise, i.e. the values that were inputted to the model were, σ_0 = 0.00037 N(μm)^2, E = 0.074 N(μm)^2, H = 0.00518 N(μm)^2, ν = 0.33.

A.3 Properties of the elements

Several different types of elements were used within the analysis. To model the plate itself, first order, fully integrated isoparametric quadrilateral elements under conditions of plane strain were used (CPE4 in the ABAQUS notation). To enforce the changing boundary conditions due to crack propagation and crack face contact, line spring elements were used. In the undeflected crack model, SPRING1 elements were used to tie the nodes ahead of the crack tip and to prevent interpenetration behind the tip. These elements act between a node and ground, in a fixed direction. The relative displacement across the SPRING1 element is the *ith* component of the displacement of the node attached to the spring, i.e. $\Delta u = u_i$. The variation of force in the spring with displacement is specified by the user and can be linear or non-linear. In the models of the deflected cracks SPRING2 and SPRINGA elements were used. These elements act between two nodes, with the line of action of the elements being in a fixed direction, and being the line joining the two nodes (which is allowed to rotate). That is, for the SPRING2 element, the relative displacement is the difference between the *ith* component of displacement at the first node of the spring and the *jth* component of displacement of the second node of the spring, i.e. $\Delta u = u_i^1 - u_j^2$. For the SPRINGA elements, in a geometrically non-linear analysis, the relative displacement is change in length of the element between the initial and current configurations, i.e. $\Delta u = l - l_0$, where $l = \sqrt{\left(x^1 - x^2\right)^2}$ and l_0 is the value of l in the initial configuration, and x^1 and x^2 are the current nodal positions. It should be noted that using this formulation it is possible for large strains to develop in the spring elements (i.e. displacements of the order of, or greater than, the element size) which may affect the accuracy of the model response. Again, the dependence of the force in the spring on the displacement could be non-linear. To prevent interpenetration of the crack faces SPRING2 elements were used acting normal to the crack surface, such that the elements were stiff in compression. In the standard models, the nodes ahead of the crack tip were constrained using SPRINGA elements, acting to restrain the nodes in all directions. In the slip band models the nodes ahead of the crack tip were constrained using SPRING2 elements acting normal to the fracture surface, with the elements being stiff in tension. Additional truss elements were used to restrain the motion of nodes ahead of the crack tip. The elements used were 2-node linear displacement truss elements (T2D2 in ABAQUS notation). The strain in the truss element in a geometrically non-linear analysis is calculated as $\varepsilon = ln(dl/dL)$ where dl is the length of the truss in the current configuration and dL is the length in the original configuration.

A.4 Annotated extracts from typical ABAQUS input files

```
*HEADING
s/s0=0.081, R=0, CCP specimen, truss psb model
**
*PREPRINT,CONTACT=NO,ECHO=NO,HISTORY=NO,MODEL=NO                    (Suppress output to the data file)
*INCLUDE, INPUT=45truss.inp                                         (Read mesh data)
*MATERIAL, NAME=DTAALLOY                                            (Matrix material properties)
*ELASTIC
 0.074,0.33                                                         (Young's modulus, Poisson Ratio)
*PLASTIC,HARDENING=KINEMATIC
 0.00037, 0                                                         (Yield stress 0, plastic strain 0)
 0.0004218, 0.01                                                    (Yield stress 1, plastic strain 1)
*SOLID SECTION, ELSET=QUADS, MATERIAL=DTAALLOY                      (element thickness)
 7500
*MATERIAL, NAME=TRUSS                                               (Truss properties)
*ELASTIC
 0.1,0.3
*PLASTIC
 4.75E-6                                                            (Yield stress, no hardening)
*SOLID SECTION, ELSET=PSB, MATERIAL=TRUSS                           (Truss cross section)
 7500
*BOUNDARY
 SUPP1,1                                                            (apply boundary conditions to previously defined node sets)
 SUPP2,2
**********************************************************************
*****************  Loading Step  *****************************
**********************************************************************
*STEP,INC=1000,NLGEOM                                               (max no. of increments, specify non-linear strain displacement relationship)
*STATIC                                                             (static load step)
0.1, 1, 0.0001, 0.1                                                 (initial, total, min, max time incs)
*OUTPUT,HISTORY,FREQUENCY=0                                         (Suppress output to the odb file)
*CLOAD                                                             (Apply loads to previously defined node sets)
 LOADTOP,   2, 468.28125
 HALFTOP,   2, 234.140625
 LOADBOTT, 2,-468.28125
 HALFBOTT, 2,-234.140625
*EL FILE,FREQUENCY=1                                               (Request element output to .fil file)
S, E, PE                                                           (Stress, strain, plastic strain)
*EL PRINT,FREQUENCY=0                                              (Request results in text format)
*NODE FILE,FREQUENCY=1                                             (Request nodal results)
U                                                                  (Displacement)
*NODE PRINT,FREQUENCY=0
*END STEP
**********************************************************************
*****************  Debonding Step *****************************
```

```
**************************************************************
*STEP,INC=1000
*STATIC
0.1, 1, 0.0001, 0.1
*MODEL CHANGE,REMOVE                                    (Remove tensile spring element at crack tip, to propagate crack)
9978
*EL FILE,FREQUENCY=0
*EL PRINT,FREQUENCY=0
*NODE FILE,FREQUENCY=0
*NODE PRINT,FREQUENCY=0
*END STEP
**************************************************************
*****************  Unloading Step  ***************************
**************************************************************
*STEP,INC=1000
*STATIC
0.1, 0.5, 0.0001, 0.1
*CLOAD
 LOADTOP,   2, 234.140625                               (Unload to P/Pmax=0.5, in a minimum of 5 increments)
 HALFTOP,   2, 117.0703125
 LOADBOTT,  2,-234.140625
 HALFBOTT,  2,-117.0703125
*EL FILE,FREQUENCY=0
*EL PRINT,FREQUENCY=1,ELSET=CRACK
S11
*NODE FILE,FREQUENCY=0
*NODE PRINT,FREQUENCY=0
*END STEP
**
**
*STEP,INC=1000
*STATIC
0.025, 0.5, 0.0001, 0.025
*CLOAD
 LOADTOP,   2, 0                                        (Unload to P/Pmax =0, in a minimum of 20 increments)
 HALFTOP,   2, 0
 LOADBOTT,  2, 0
 HALFBOTT,  2, 0
*EL FILE,FREQUENCY=0
*EL PRINT,FREQUENCY=1,ELSET=CRACK                       (Write the forces in the compressive spring elements to the data file)
S11
*NODE FILE,FREQUENCY=0
*NODE PRINT,FREQUENCY=1,NSET=GAUGES                     (Write the displacement at the gauges to the data file at each increment)
U
*END STEP

                                                        (This process is typically repeated for 100-300 crack growth increments)
```

```
(extract from file containing mesh data)

*NODE
       1,       -4.83537,        1.27246
       2,       -1.20885,       0.318116
       3,       -2.41769,       0.636231
        .
        .
        .
*ELEMENT, TYPE=CPE4 , ELSET=QUADS                          (Q4 elements, plane strain)
       1,       18,       22,       20,    16000
       2,       20,       21,    16001,    16000
       3,        6,    15000,        9,       10
        .
        .
        .
*SPRING,ELSET=CRACK1,NONLINEAR                             (Tensile spring elements)
2,2                                                        (dof at 1st and 2nd node from which force is calculated)
0,0                                                        (force 0, relative displacement 0)
7.4E5,1000                                                 (force 1, relative displacement 1)
*ELEMENT, TYPE=SPRING2,ELSET=CRACK1
 9978,15100,16100
 9979,15101,16101
 9980,15102,16102
        .
        .
        .
*ORIENTATION,NAME=PLUS45                                   (Define local orientations)
1,1,0,-1,1,0
*ORIENTATION,NAME=MINUS45
1,-1,0,1,1,0
*SPRING,ELSET=CRACK3,NONLINEAR,ORIENTATION=PLUS45          (Compressive spring elements)
2,2
-7.4E5,-1000
0,0
*ELEMENT, TYPE=SPRING2,ELSET=CRACK3
10197,15110,16110
10198,15111,16111
10199,15112,16112
        .
        .
        .
*ELEMENT, TYPE=T2D2,ELSET=PSB                              (Plastic truss elements)
10301,15183,16183
10302,15184,16184
10303,15185,16185
        .
        .
```